5-18-2007

Thermal and transport properties of layered silicate nanomaterials subjected to extreme thermal cycling

Vilarino Sofia Martinez
University of New Orleans

Thermal and transport properties of layered silicate nanomaterials subjected to extreme thermal cycling

A Dissertation

Submitted to the Graduate Faculty of the
University of New Orleans
in partial fulfillment of the
requirements for the degree of

Doctor of Philosophy
in
The Engineering and Applied Science Program

by

Sofía Martínez Vilariño

M.S. Industrial Engineering, 2002

May, 2007

ACKNOWLEDGEMENTS

No dissertation is ever the product of one person's efforts, and certainly this one was no different. It would never have become reality without the help and suggestions of many supportive friends, colleagues and family.

First I must acknowledge my family, the constant support and love of my parents, Ramón and Purificación, and their belief that I could achieve anything in life has pushed me through all these years of work. Of course, I cannot forget my sisters, Puri, Eva and Fani, who shared with me many moments of friendship and love even if it was just by phone.

I would like to thank the group of Materials Science at the Escuela Politécnica de Ferrol, Spain. Especially to Dr. Ramon Artiaga who was the first person that spoke to me about this lifetime opportunity, without their help I wouldn't be at this point today. To Dr. Salvador Naya thanks for his friendship and vast knowledge in statistics.

This work would not be possible without the help of Ms. Sandi G. Miller, at NASA John H. Glenn Research Center, I am truly grateful to her for supplying all the samples and assisting me with her collaboration in this work.

My thanks must go also to my supervisor Dr. David Hui and his caring wife Ms. Shun-Ying Hui for being involved in our lives beyond the duty as a supervisor. My gratitude goes as well to the committee members for their knowledgeable suggestions.

Numerous people had contributed in many different ways to this dissertation; special thanks go to all my classmates and to the faculty members and staff at the Mechanical Engineering Department at University of New Orleans. Particularly, my gratitude goes to Dr. Carl A. Ventrice, from Physics' Department, without him the tests would not be possible, to Dr. Leonard Daniel for trying to keep us in track, to Mr. Claude Zeringue for helping me to retrieve all my samples after hurricane Katrina and to Ms. Deborah B. Duzac for her valuable help handling the administrative nightmare involved in the graduation process.

After relocation due to Katrina, I was warmly welcomed at Prairie View A&M University, TX where I received an incredible support from all the people at the Department of Mechanical Engineering. In particular I want to thank Dr. Jianren Zhou who made possible for me to continue with this dissertation at PVAMU. Special thanks must go also to Dr. Paul O. Biney and Dr. Richard Wilkins for their financial support and to the students for their friendship.

It would not have been possible to obtain some of the results without the precious help of Dr. C. A. Quarles and Dr. Yuri M. Strzhemechny, from the Department of Physics and Astronomy at Texas Christian University. In addition, I need to express my deepest appreciation to Dr. Andrey Beyle from Pittsburg State University for sharing his expertise with me and his knowledgeable suggestions and ideas.

Last but definitely not least I would like to thank my fiancé Robert Chan whose continuous joking, encouragement and support in countless different ways has got me through this experience. Hopefully now you'll get to see the flower growing!

Thank you all.

This work was funded by the NASA-Marshall SBIR (Grant # NNM05AA26C) and partially funded by the Office of Naval Research, Solid Mechanics division, under grant N00014-05-1-0532, subcontract from Pittsburg State University, Kansas, monitored by Dr. Yapa Rajapakse.

TABLE OF CONTENTS

LIST OF FIGURES

LIST OF TABLES

LIST OF NOMENCLATURE AND ABBREVIATIONS

A	Area
ASE	Average squared error
atm.	Atmosphere
ANOVA	Analysis of Variance
BMI	Bismaleimide
C	Gradient of the Gas Concentration
°C	Degree Celsius
cc	Cubic Centimeter
CFRP	Carbon Fiber Reinforced Plastics
CLTE	Coefficient of Linear Thermal Expansion
COD	Crack Opening Displacement
COV	Crack Opening Volume
CTE	Coefficient of Thermal Expansion
CNT	Carbon Nanotube
cm	Centimeter
D	Diffusion
DGEBA	Diglycidylether of Bisphenol A
DMONT	Dodecyl-Montmorillonite
DMA	Dynamic Mechanical Analysis
DSC	Differential Scanning Calorimetry
DTG	Derivative of the Thermogravimetric curve
E_a	Activation Energy
°F	Degree Fahrenheit
$\bar{F}$	Mass flux
F_v	Relative Fractional Free Volume
FEA	Finite Element Analysis
FMLDS	Flexible Micro-Leak Detection System
GENOA	General Optimizer Analysis Code
Gr/Ep	Graphite-Epoxy
HDT	Heat Deflection Temperature
Hz	Hertz
J	Flux of Gas in the Polymer Matrix
IM	Intermediate Modulus
in.	Inches
K	Degree Kelvin
kV	Kilovolts
L	Average Length of Platelets
LC	Logistic Component
LHe	Liquid Helium
LH_2	Liquid Hydrogen
LN_2	Liquid Nitrogen
nm	Nanometer

μm	Micrometer
m	Mass
MD	Molecular Dynamics
MeV	Megaelectron Volt
mL	Milliliter
min	Minute
mm	Millimeter
MMT	Montmorillonite
NASP	National Aerospace Plane
O	Octahedral
OMMT	Organically Modified Montmorillonite
o-Ps	Ortho-positroniums
p	Pressure
P	Permeability
PAS	Positron Annihilation Spectroscopy
PALS	Positron Annihilation Lifetime Spectroscopy
PCN	Polymer-Clay Nanocomposites
phr	Parts Per Hundred Resin
PETI	Phenylethynyl Terminated Imide
PI	Polyimide
PLS	Polymer Layered Silicate
PMC	Polymer Matrix Composites
ppm	Parts per Million
psi.	Pounds per Square Inch
RT	Room Temperature
RLV	Reusable Launch Vehicles
S	Solubility
s	Second
SBR	Styrene Butadiene Rubber
STP	Standard Temperature and Pressure
t	Time
T	Tetrahedral
TEM	Transmission Electron Microscopy
T_g	Glass Transition Temperature
TGA	Thermogravimetric Analysis
TPS	Thermal Protection System
V_f	Average Size Free Volume Holes
V.I.F.	Variance Inflation Factor
W	Thickness of platelets
wt.	Weight
XRD	X-ray diffraction
α	Aspect ratio
Ψ	Porosity
Φ_f	Volume Fraction of Filler
μ	Viscosity

ABSTRACT

There is a raising need to design a safe and efficient cryogenic fuel tank for the new generation of reusable launch vehicles. The new tank design focuses on composite materials that can achieve the drastic reduction of empty/non-payload and structural weight.

In addition to the materials to be compatible with cryogenic temperatures, interior components of the vehicle may be subjected to significantly elevated temperatures due to heat conduction from the vehicle surfaces during and after atmospheric re-entry. Therefore, there is the need to understand the performance of the composites after experiencing extreme thermal environments.

Polymer-layered nanocomposites were studied to determine if they can reduce the permeation to the liquid nitrogen used as fuel in the next generation of space vehicles. Due to the non-permeable nature of the silicates and the exfoliated structure they adopt into the polymer matrix the addition of nanoclays into a polymer is expected to reduce the permeation to several gases without sacrificing the mechanical strength of the nanocomposite as well as providing additional improvements such as increase of thermal stability of the nanocomposite.

Several types of matrixes modified with different types and content of nanoclays were tested and their permeability coefficient was calculated. The permeability values obtained for the different formulations assisted to understand the transport properties of nanoclay modified composites. In addition to this, thermal characterization was performed with the help of dynamic mechanical analysis, thermogravimetric analyses and differential scanning calorimetry studies.

To determine if the nanoclay modified nanocomposites were affected by extreme temperatures the samples were subjected to thermal cycling. Comparison of the transport and thermal properties before and after cycling helped to analyze the effect of the addition of the nanoclays in the nanocomposites. Positron annihilation spectroscopy (PAS) was utilized to comprehend how the distribution of the free volume was affected by the presence of the nanoclays and by the thermal cycling applied.

Different permeability models were utilized in an attempt to validate the experimental results of the different nanocomposite structures. This analysis was used to provide additional insight into many aspects of the experimental results obtained in this study.

Keywords: Polymer-layered nanocomposites, nanoclays, thermal stability

CHAPTER 1

INTRODUCTION

The development of the available technologies for synthesis, characterization and modeling of new materials during the past years, has contributed enormously to the growth of nanotechnology research. This growing interest in nanotechnology resides in the prosperous future that nanostructures anticipate. The main idea on the development of new nanostructures lays on the fact that 'size matters'. The properties imparted to nanostructures when they are built with particle sizes on the nanometer range differ from those of materials with macroscopic modifiers. When modifiers are smaller than the characteristic length of a particular phenomenon, they display new chemistry and physics leading to a unique synergism between materials.

The geometry of the nanomaterials varies depending on how many dimensions are in the nanoscale range. There are nanoparticles where all three dimensions belong to the nanoscale range; elongated structures such as nanotubes, where two dimensions are in the nanometer scale and lastly there are layered-like particles where only one dimension is on the nanometer scale.

Nanoclays belong to this last group; they are particles with a sheet-like structure. They are extensively used as reinforcements due to their availability and the materials that are reinforced with these nanoparticles are known as polymer-layered nanocomposites.

The advantage of nanoclays resides in their platelet-like shape with thicknesses of one nanometer and diameters in the range of a few hundred nanometers. Due to this high aspect ratio, even a small weight percent dispersed in the matrix achieves a high surface area for a great polymer-filler interaction.

The applications of these materials are numerous, ranging from food packaging to electrical applications, automotive and aerospace.

Polymer-layered nanocomposites have different properties and applications depending on the type of resin and nanoclay used in the system. This study is focused on epoxy resins modified with different types of nanoclays derived from montmorillonite.

The aim of this investigation is to analyze if the modification of epoxy matrixes with nanoclays affects the permeability to helium when the nanocomposites are subjected to extreme thermal conditions. It is well known that the addition of nanoclays have positive effects on

properties of the materials such as flame retardance, thermal stability, mechanical properties and permeability, but does this behavior hold for extreme temperatures? When nanoclays are properly dispersed in the matrix they provide excellent barrier properties, as they increase the path for the permeant to travel through the resin. But cryogenic cycling can cause significant changes in a nanocomposite material and the permeation performance can be affected.

The influence of the composition of the materials in the permeability performance it is studied in order to increase the understanding of how the nanoparticles modify the properties of the nanocomposite structure.

1.1. Background

The next generation of reusable launch vehicles (RLV) will require new and innovative materials capable of solving one of the most critical issues in the design of this new vehicle, which is the development of durable, lightweight, cryogenic propellant tanks. The development and fabrication of reusable cryogenic tanks is one of the significant technical challenges to be overcome to develop an operable RLV. Large expendable cryogenic tanks have been made for launch vehicles, but the durability of flight-weight reusable cryogenic propellant tanks has not been demonstrated. Cryogenic tank development is critical for an RLV because the tanks may comprise as much as 70 to 80 percent of the volume of the vehicle. The cryogenic tanks of an RLV must not only function as pressure vessels at cryogenic temperatures, but they also must carry primary structural loads and support the Thermal Protection System (TPS). The cryogenic tanks, along with the TPS, must be easy to maintain, easy to repair, and reusable for the life of the vehicle [1, 2].

The cryogenic tanks are the dominating components of the vehicle structure. Thus, the application of lightweight carbon fiber reinforced plastics (CFRP) to these components is one of the most promising but challenging technologies for achieving the drastic reduction of empty/non-payload and structural weight.

Despite the lack of long-term flight data, there is some history of design and testing of polymer matrix composites (PMC) cryogenic tanks that includes the National Aerospace Plane (NASP), DCX-A, X-33, and other launch vehicle applications. These programs have considered several tank wall design concepts including externally stiffened shells of PMC material or thin-walled sandwich shells constructed with a lightweight core and PMC facesheets.

Regardless of the design, the next generation of polymer matrix composites-based tanks will be required to safely carry pressure and flight loads and to operate over temperatures that may range from –250 °C to +120 °C. From a durability perspective, the primary performance criteria of the PMC material is to retain mechanical properties within allowable limits over the life-time of the tank while minimizing loss of cryogenic fuel because of permeation or leakage through the tank wall [3].

Polymer matrix composites are lightweight, strong and stiff; therefore they are the ideal choice to obtain the desired reduction of weight. The main disadvantage arises from the fact that the resin used as matrix usually has higher gas permeability than metals, increasing the risk of hydrogen loss through the body of the tank.

These composite structures also develop microcracks at cryogenic temperatures due to the mismatch of the coefficient of thermal expansion (CTE) between matrix and fiber of the composite and among the different plies of the laminate. This microcracking increases the probability of permeation of the liquid hydrogen through the structure leading to the failure of the tank [4].

But even if the greatest contributor to leakage is believed to be microcracks forming leak paths that allow gases to pass through the material, this is not the only factor that causes the failure of polymeric matrix composites. Porosity, manufacturing flaws, internal damage and environmental conditions each contribute to the permeability of a material.

It can be observed that the use of composite materials brings some technical barriers that need to be studied in order to suggest efficient and safe designs for composite hydrogen storage systems.

Several approaches can be used to solve these problems. One solution is to build composite tanks with thin metal liners. This option reduces the hydrogen permeability but it also introduces new problems due to the substantial mismatch in the coefficient of thermal expansion. Another possibility involves introducing one or more thin layers of polymeric film interleaved or as a coating in the composite inner skin that will act as a barrier and contain the liquid hydrogen (LH_2) fuel in the presence of microcracks. And a third option is to modify the matrix of the polymer composite with nanocomposites to reduce the hydrogen permeability through the composite, without introducing a CTE mismatch, offering the potential for the development of linerless PMC tanks.

No matter the approach considered, it would need to comply with the following requirements:

- Low permeability of cryogen being stored
- Good adhesion to the structure to avoid delamination failure
- Modulus match to structure to prevent cracking
- Resistance to harsh environmental conditions
- Feasibility of manufacturing
- Low weight and low cost

The increased incorporation of polymeric materials into aerospace applications is credited to their contribution to weight savings in spacecraft construction. The modification of polymeric materials with particulate fillers to make composites expands the range of applications as the properties of the composite overcome those of the neat polymer. Nevertheless, it is necessary to ensure that in the effort of enhancing certain properties in the composite others also required for the application are not diminished.

Through the use of various kinds of fillers the mechanical and thermal properties of polymers and composites structures can be modified. The dimensions of the fillers typically fall on the macroscopic length scale, but these types of fillers usually cause decreases in the mechanical properties of the composite. A new area of composites research has emerged in the last two decades that utilizes nanoparticles as fillers to modify the properties of polymers. Trends show that when processed properly small amounts ($\leq$ 5 wt. %) of nanoparticle fillers can increase the modulus, strength, toughness, resistance to chemical attack, gas impermeability, resistance to thermal degradation, and dimensional stability of polymeric materials [5].

1.2. Objectives, scope and approach of research

The aim of the work is:

1. Study the permeability to helium of different systems of nanocomposites
2. Correlate the type of polymer and nanoclays with their effects on the permeability
3. Analyze the effect of extreme thermal cycling on the nanocomposites
4. Examine the influence of the different compositions of the nanocomposites in the thermal properties

The experimental phase of the work includes acquire information on how the permeability properties of the materials studied evolve with the different contents of nanoclays.

The permeation performance of several composite structures is measured before and after damage caused by extreme thermal cycling (between –196 °C and 177 °C).

The need of testing the composite structure under extreme thermal environment is conditioned by the type of application in which the material will perform. The materials will be exposed to a wide range of temperatures, they will be not only in contact with the cryogen but also they may be subjected to elevated temperatures due to heat conduction from the vehicle surfaces during and after atmospheric re-entry. The critical materials issues for these applications are focused on preventing micro-crack distributions that produce continuous through-thickness gas leakage paths [6].

An experimental approach is used in this research to achieve empirical information related to the above-mentioned issues. As a secondary approach, a mathematical analysis will be used in an attempt to provide additional insight into many aspects of the experimental results obtained in this study.

1.3. Organization of the dissertation

The need to find a material that withstands mechanical loads, supports cryogenic and high temperatures and has good permeation to hydrogen has lead to new designs on composites structures. These structures merge the strength, lightweight and stiffness of composites with the ability of nanoparticles of reducing permeability to gases. The state of the art on this field it is presented on Chapter 2. The performance of these new composite structures is evaluated to obtain a thorough analysis on how the nanoparticles influence the thermal and mechanical behavior of the composite.

The experimental phase of this work is detailed in Chapter 3. From the design of the permeability fixture to the thermal cycling of the samples and the permeation measurements, every experimental procedure needed to achieve the main goal of this work is described here.

Chapter 4 deals with the permeability theory and mathematical models and Chapter 5 discusses the results of all the experimental tests as well as the models analyzed.

Finally, on Chapter 6 the results' discussion and the conclusions that can be inferred are listed, as well as the future work.

1.4. References

[1] H.K. Rivers, J.G. Sikora, S.N. Sankaran. Detection of micro-leaks trough complex geometries under mechanical load at cryogenic temperature. AIAA-1218-2001

[2] B. W. Grimsley, R. J. Cano, N.J. Johnston, A. C. Loos, William M. MacMahon. Hybrid composites for LH_2 fuel tank structure. NASA, 2001

[3] T. S. Gates, K. S. Whitley, R. W. Grenoble, T. Bandorawalla. Thermal/Mechanical durability of polymer-matrix composites in cryogenic environments. AIAA-2003-7408

[4] B. Sankar, P. Ifju. Fiber reinforced composites for hydrogen storage systems. University of Florida

[5] J. F. Timmerman, B. S.Hayes, J. C. Seferis. Composites Science and Technology 2002; 62: 1249–1258

[6] V. T. Bechel, J. D. Camping, R. Y. Kim. Composites Part B: Engineering 2005; 36: 2

CHAPTER 2

LITERATURE REVIEW

One of the major drivers in the research of composite materials is the aerospace industry. The need to comply with the demanding requirements needed to undergo any of the spatial missions motivates the quest of new materials. Composite materials, with their specific characteristics are able to achieve great mechanical performance while they offer an outstanding advantage over metals, reduction of structural weight. Nevertheless, this reduction in structural weight must be tempered against the safety and reliability criteria associated with damage tolerance, and lifetime durability [1].

The actual trend in materials research is the introduction of nanomodifiers into conventional composite materials. This modification will further improve the outstanding characteristics of the traditional composites. But before full advantage can be taken out of this modification, the characteristics and properties of the nanomodifiers need to be understood.

It is the purpose of this work to help in the understanding of the barrier properties of polymer clay nanocomposites and their behavior after being subjected to extreme temperatures. This research would be the first stage before the nanoclay particles are included in traditional composite laminates to further improve their performance.

First a review of composites structures is given in order to understand the requirements needed to improve their properties. And then, the state-of-the-art in the field of nanoclay-modified composites is summarized as well as their properties, applications and advantages. One of the main applications of these materials, and the one of interest in this work, is as barrier materials and therefore their permeation properties are also explored here.

2.1. Composites structures in cryogenic applications

There are several factors to deal with when composites structures are the choice considered for fuel tanks. These structures will function as pressure vessels; they need to support the Thermal Protection System (TPS) and in addition carry primary structural loads. The cryogenic tanks must be easy to maintain, easy to repair, and reusable for the life of the vehicle. The structure must support harsh environmental conditions and avoid leakage of the cryogen fuel during the life of the vehicle [2].

The model used as a reference on the investigation of fuel tanks is the Lockheed-Martin X-33 vehicle design that incorporated two polymer matrix composites liquid hydrogen tanks (PMC/LH_2). These tanks were quad-lobed tanks with honeycomb core sandwich wall construction [3]. Both face-sheets of the sandwich were graphite-epoxy (IM7/977-2) and the core material was Korex™ 3-pcf, unvented, aramid-phenolic honeycomb. Even though this design failed, the failure gave a new understanding of the factors to consider when designing a composite fuel tank. The X-33 hydrogen tank program and the following incident investigation [3] did give understanding into many complex interactions and provided several lessons learned. New insights were obtained into the phenomenon and significance of microcracking of cryogenic tanks under thermal and mechanical loads. The results of the investigation did not invalidate the use of composite materials for cryogenic tanks. As mentioned in the final report of the X-33 liquid hydrogen tank [3], the lessons learned, if applied to composite cryogenic tank technology, should advance the technology and aid in the successful use of composites for cryogenic tanks.

During preflight proof testing the first X-33 LH_2 tank failed when pressure increased in the core of the sandwich tank wall causing the face-sheets to separate from the core material. The failure of the X-33 composite fuel tank occurred in part due to microcracking of the polymer matrix, which allowed cryogen to permeate through the inner skin to the honeycomb core.

When the polymer experiences the extremely low temperatures associated with the cryogenic propellant, the material shrinks. The polymer matrix has a higher coefficient of thermal expansion (CTE) than the carbon fiber reinforcement and, therefore, will shrink or strain more upon cooling. The fiber with a near zero CTE acts to resist this strain and internal stresses build up in the matrix. If the stress is sufficiently high, it causes microscopic cracks to form within the composite. The microcracking in the matrix creates a sort of maze for the pressurized LH_2 to traverse and enter the honeycomb core [4].

The failure occurred after the tank had been emptied and had heated to -73°C. At this temperature, the microcracks closed due to expansion of the polymer matrix. Then, the gas created by evaporation of the LH_2, having no free volume to expand, built up pressure in the core causing the inner composite skin to rupture [4]. This process is called cryopumping, and occurs when a void in a material or structure is at a low enough temperature to densify a contained volume of gases. As the gases are condensed, a vacuum is created. If there is a pathway to the surface or other voids, additional gases are pulled or pumped into the void. When the material or

structure is heated, the densified gases expand and are expelled or pumped from the void. During this expansion phase of cryopumping, the most damage in the material can be incurred [5].

As noted in the report the causes of failure were a combination of the following: microcracking of the inner face-sheet with subsequent gaseous hydrogen infiltration, cryopumping of the exterior nitrogen purge gas, reduced bondline strength and toughness, and manufacturing flaws and defects. It can be observed that there are few factors that need to be considered when a PMC material is selected to design a cryogenic tank. It is believed that the greatest contributor to leakage in PMCs is microcracking [5].. Microcracks form leak paths that allow gases to pass through the material and the loading conditions to which the tank is subjected to, will not only generate new microcracks but also will cause existing ones to open. This will increase the rate of leakage through the material. Consequently, leakage should be studied while the material is at operational temperature and under mechanical load [6].

The construction of the tank with composites materials was innovative and opened up new possibilities in the designs of fuel tanks. The honeycomb core sandwich wall construction used on the X-33 tank had an inner and outer facesheets made of graphite-epoxy (IM7/977-2) and the core material was Korex™ 3-pcf, unvented, aramid-phenolic honeycomb [3]. This combination of materials is the base for the new projects of tanks. There are multiple investigations on systems that combine different graphite/epoxy (Gr/Ep) laminates and new sandwich structures. The main idea on these investigations is the study of the performance of these systems under conditions similar to those suffered on the space. Therefore there are environments that consider cryogenic temperatures, thermal loads, or a combination of both thermal and mechanical loads. Some works focused in the microcracking of the composites and others concentrate on the permeation performance of the system.

Another possibility being investigated after these results is the introduction of a liner or thin film into the structure of the cryogenic tank that will act as a barrier containing the LH_2 if microcracks are formed and therefore avoiding the cryogen to reach the honeycomb core [4].

This introduction of a layer or layers of polymeric/metallic film has some disadvantages due to the different CTE of the film and the composite, which can lead to delamination or debonding failure. Some studies carried out on permeability and thermal cycling of thin films [7]. showed the influence of the thickness on the mechanical properties of the system and the delamination problem.

The modification of the polymeric matrix of the composite is the next step followed. The addition of particulate fillers into thin polymer films to make composites greatly improves the properties over that of the neat polymer film. However, it needs to be ensured that in the effort to enhance certain properties in the composite, others that are also necessary to the application are not diminished.

2.1.1. Induced stresses

Fiber reinforced composites have been used in many different applications. In the past the understanding of the behavior of these materials under high temperatures was the focus but recent applications of composites in aerospace have focused the interest of the study in the performance under cryogenic temperatures [9]. In order to increase the reliability of the next generation of space transportation systems, the mechanical behavior of fiber reinforced polymeric composites materials at cryogenic temperatures must be investigated [13].

The main cause of microcracking in composites at cryogenic temperatures is the increased thermal stresses. Residual stresses develop in composite materials during cure and after cure as the temperature of the material falls below its stress free temperature. The stress free temperature is the temperature at which no residual stresses exist in the laminate. During the curing process there are dimensional changes in the matrix that usually drive the stress free temperature above the maximum processing temperature. When the residual stresses in the material become large enough they are relieved through physical processes such as potholing, delamination and/or microcracking [8].

Additional stresses are also developed within each ply and at the fiber-matrix interface due to the mismatch in CTE between the fibers and the matrix, Poisson's effects and cure shrinkage. See Figure 2.1. When there is a decrease in temperature the matrix shrinks more than the fibers and generates a compressive hoop stress around the fiber, while the fibers expand axially and cause the matrix to be in tension [9]. All these factors combine together and therefore there is a complex stress state in fiber reinforced composites when they are subjected to cryogenic temperatures.

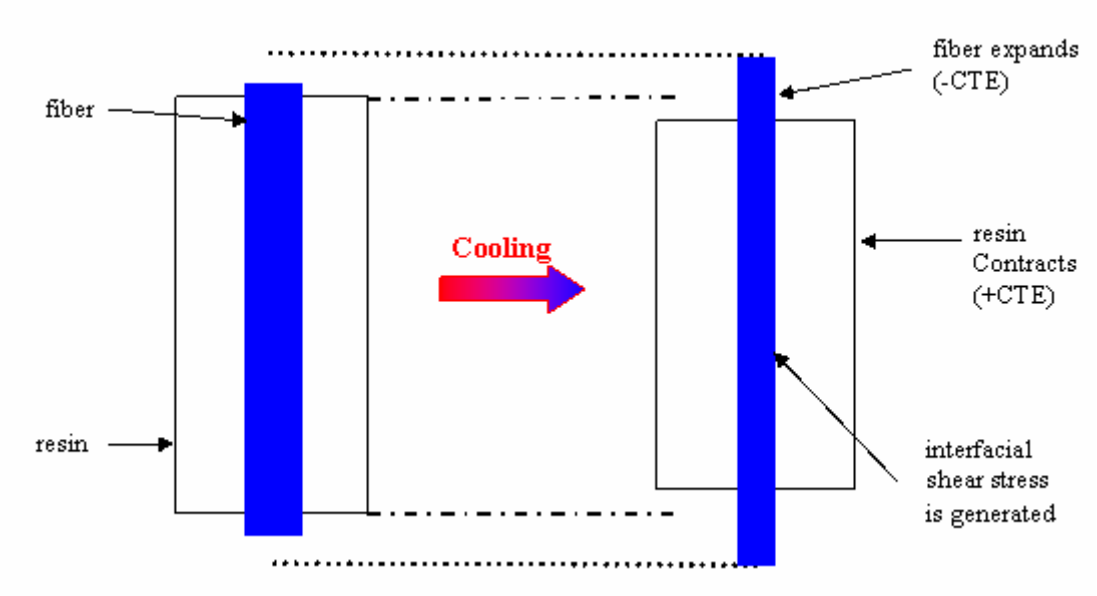

Figure 2.1. Induced stress generated by CTE's mismatch [10]

When the internal stresses in fiber reinforced composites under cryogenic temperatures is large enough it originates the failure of the material. In a transverse tensile loading mode the fibers behave like inclusions and points of stress concentrations. The stresses originated in the end result in debonding or matrix failure that forms transverse cracks that propagate through the composite [9].

Microcracks create a path for the permeation of the liquid fuel, as shown in Figure 2.2. Liquid hydrogen and helium have a very small molecular size and they easily diffuse through small flaws. The release of the liquids can cause condensation of liquid water and air on the tank or in the interior of sandwich tanks. Then emptying and filling of the tank results in solid/liquid and solid/gas transformations than can originate catastrophic failure [9].

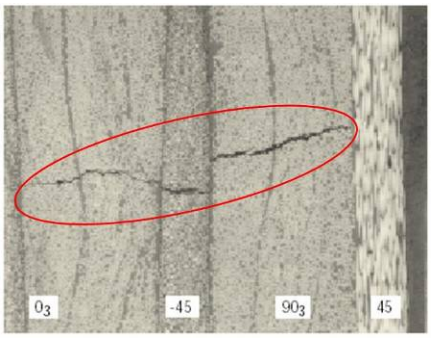

Figure 2.2. Microcracks path in a CFRP laminate [3]

Several studies have been performed on microcracking of composites structures under cryogenic temperatures. Yokozeki et al. [11] mentioned that the damage mode in composite laminates that first takes place after loading is usually transverse cracking. Although this damage mode is not critical from a final fracture point of view, it reduces the laminate mechanical performance, and it is the cause of more severe damages and leakage of contained liquid or gas. Transverse cracking in laminates subjected to static and fatigue loadings are one of the important factors that affect the component design [11]. In order to study transverse cracking a system of cross-ply and quasi-isotropic CFRP laminates (IM600/Q133) was exposed to fatigue loading at room temperature (RT) and detailed observations of both crack density and crack length were conducted. An analytical two-dimensional model including both mechanical and thermal stresses of full-width transverse cracks was applied to inward crack propagation, and fatigue crack propagation was expressed in terms of energy release rates associated with crack propagation [11].

The resin used in this study was a tough resin system. It was observed that with this type of resin the crack saturation densities were relatively low and crack spaces were about three or four times the thickness of cracked layers. Under this condition, crack densities have little effect on fatigue growth of individual cracks as the nearby cracks have little influence to each other. It was also noted that stable crack propagation without traversing the entire width of the specimens was characteristic in this system. The average crack lengths were measured and were used for evaluation of fatigue crack growth. Then a power-type propagation law was adopted and the relationship between crack growth rates and calculated energy release rates was found [11].

Yokozeki et al. concluded that two-dimensional analytical models could be used to evaluate inward crack propagation. There was also another important issue addressed in this investigation related with the difference that exists when a coupon specimen or the whole structure itself are chosen to evaluate microcracks. The structure has different free edge boundaries from the samples and this will lead to different damage process. When a laminate is being use in a structure, free edge stress fields may considerably influence the cracking behavior. Therefore, it is necessary a propagation controlled criterion for practical structures [11].

One of the multiple choices considered among the polymeric matrix composites systems is IM7/PETI-5. This PMC consisted of a continuous, high-strength, intermediate-modulus carbon fiber in a thermoplastic polyimide matrix. This system has unique characteristics and potential

for use under high compressive loads at varying temperature conditions [12]. Graphite/epoxy laminates can develop significant residual stresses in a laminate due to curing. The IM7/PETI5 laminates have a glass transition temperature, T_g, of 238°C, which is much higher than the T_g of 177°C for graphite/epoxy. Consequently, IM7/PETI5 laminates may develop more significant residual stresses, for that reason, since there is no enough data on advanced composites for cryogenic applications these studies focused on the evaluation of the thermal/mechanical durability of IM7/PETI-5 at cryogenic temperatures, and provided insights into the effects of temperature and aging on mechanical performance [12].

Gates et al. [13, 14] measured tension modulus and strength at room temperature, –196°C, and –269°C on five different IM7/PETI5 ply lay-ups. The test conditions represented a range of exposure times, loads and temperatures similar to those experienced during the lifetime of a cryogenic, hydrogen fuel tank.

Three different preconditioning sets were done. One set of the samples was isothermally aged for 576 hours at –184°C, in an unloaded state. On another set a constant uniaxial strain was applied to the specimens for 576 hours at –184°C. A third set was mechanically cycled in tension at –184°C. The experimental data on the residual mechanical properties of IM7/PETI-5 were given as a function of temperature and aging [13, 14].

The measured properties indicated that the temperature, aging, and loading mode can all have significant influence on performance. Results obtained for the basic lamina properties such as strength and stiffness in the longitudinal, transverse, and shear directions indicated that cryogenic temperatures can significantly influence performance [13]. Tension loading, longitudinal and transverse stiffness and strength decreased as the test temperature decreased. Conversely, the tensile shear modulus and strength increased as the temperature decreased. It was concluded on this research that aging or long-term exposure to cryogenic temperature while under load could significantly alter the as-received mechanical properties, implying that design criteria should take into account thermal/mechanical exposure over the duration of the structure [14].

Su and Abdi [15] presented a comparison of analytical life prediction methodology and experimentally observed test data on the residual mechanical properties of IM7/PETI-5, both before and after aging. They intended to provide a validated analytical design tool for cryogenic tank applications.

They observed that the strengths, including both damage initiation strength and final failure strength, of the laminate at -196°C and -253°C are lower than those at room temperature due to the induced thermal stress in the laminate at cryogenic temperature. It was also noted that the damage initiation strength of the laminate depends on the matrix properties because damage initiates as matrix failure and that final failure strength of the laminate is determined mainly by fiber properties [15].

Depending on the type of materials chosen the mechanical properties and CTE will differ and the behavior will be a function of the temperature use on the tests. There is a considerable variation in the mechanical properties and CTE's in PMCs as a function of decreasing temperature; consequently, the damage accumulation trends from cycling at one temperature may not adequately simulate trends from cycling at a much lower temperature [16]. In addition, microcrack initiation can be delayed for many cycles and still reach significant densities after additional cycles. Consequently, for many materials projecting trends from tens of cycles to hundreds of cycles is not appropriate. This is why there is the necessity of study the system under similar conditions to those experienced during the lifetime of a cryogenic fuel tank.

During thermal cycling, usually, thermal stresses appear in the laminates at two levels: first, at a microscopic level, due to both matrix and fibers deformations, according to their thermal expansion coefficient and secondly at the ply level due to adjacent plies stacked with different orientations in the laminate. These cyclic thermal stresses may induce damage similar to that observed under mechanical fatigue: transverse matrix cracks, debonding and delaminations [17].

The damage tendencies of carbon polymer composites under different cycling conditions have been widely studied. Bechel et al. [18] analyzed samples of IM7/977-2 carbon/epoxy, IM7/5250-4 carbon/bismaleimide, and IM7/3K carbon/epoxy that were cryogenically cycled by repeated submersion in liquid nitrogen (LN_2) tested for up to 1000 cycles [18]. The materials and lay-ups were chosen to study the density of ply-level micro-cracks that formed as a function of number of cycles, prepreg thickness, residual stresses, and the orientation of adjacent plies.

The cycling apparatus consisted of an aluminum frame used to support and guide a sample container in vertical movement between positions inside a dewar of LN_2 and in ambient air. The sample container was attached to a hollow aluminum bar that was actuated at 6 cm/s by a motor. The mesh sample container had a capacity of up to eighteen 50.8 mm long by 50.8 mm

wide samples. To reduce the time required for the samples to return to ambient temperature, a fan was used to force ambient air across the sample container during periods when the samples were held outside the LN_2 [18]. To determine the minimum hold time necessary, a thermocouple was bonded in the center of the laminate. The times necessary for the center ply of this sample to reach the required temperatures were recorded when the sample was submerged in LN_2 and warmed up to room temperature. Based on these measurements, a cycle of 2 min in the LN_2 followed by 5 min at RT was used. Micro-cracks were counted after different numbers of cycles up to 1000 cycles. The results obtained after these tests concluded that reducing the ply thickness by 30% in the IM7/5250-4 delayed surface ply microcracking by up to 200 cycles, but by 1000 cycles the densities were approximately equal again. The thinner-ply laminates had significantly greater microcrack densities in some of the inner plies. Sectioning showed micro-crack densities in the sample interiors that were equal to or greater than those measured on the sample edges once damage became relatively persistent in a ply. The IM7/977-2 samples when compared to IM7/5250-4 had no microcracks or two orders of magnitude fewer microcracks in each ply. But this doesn't imply that this material would be preferred over the IM7/5250-4. The two systems have different maximum service temperature, so the structures on which the material will perform would determine the election. For the e-beam cured IM7/3K there were significant microcrack densities in all plies due to trapped voids that masked its inherent microcrack resistance advantage [18].

It was concluded in this investigation that there is the need of finding a more predictive analysis that captures the different parameters (single ply versus multiple ply, processing induced residual stresses, composite maximum service temperature versus minimizing the number of damaged plies) that influences damage accumulation from cryogenic cycling. The complex interaction of these variables and their effects on whether leakage paths will develop emphasizes the need for accurate methods for predicting damage due to cryogenic cycling [18].

The system IM7/977-2 was found to be extremely resistant to microcracking even after 1000 cycles from LN_2 to RT [18]. But in order to choose the proper composite it would need to be considered which type of thermal cycling it would be applied and the final service temperature.

Rouquié [17] studied IM7/977-2 with a different thermal cycle profile. The thermal cycles imposed in this work were triangular, with the maximum and minimum temperatures

being respectively of 180°C and -50°C with constant cooling and heating rates of 4°C/min and the test were conducted under vacuum and during 300 cycles. On this case the material was also found to resist the thermal cycling and no signs of matrix shrinkage were found [17].

The properties of IM7/977-2 have been studied in depth; this material is referred as one of the best choices for cryogenic tanks. And the results obtained by Kessler et al. [19] sustain this finding. The degradation of the composite's mechanical properties due to cryocycling was studied. The properties used for this investigation were the Young's Modulus, Poisson's ratio and ultimate stress, as well as the material's general response to tension and compression. Groups of samples were thermally cycled pre-specified numbers of times in a custom-built cryogenic dewar, and then tested for strength and stiffness. A customized thermal cycling chamber was designed to simulate the operating environment of the X-33 fuel tank. A single cycle consisted of a cool-down from 27°C to -253°C, a heat-up to 127°C, and then back to 27°C, thereby simulating one flight cycle of the X-33. Both the heating and cooling rates were fixed at -259°C/min and the target temperatures were held for 5 minutes to guarantee that the samples had reached the same temperature as their environment [19].

After being cycled, the groups of samples were mechanically tested in tension until destruction in order to determine their material properties. The samples were mounted vertically in a MTS servo-hydraulic testing machine. From this test, the tensile stiffness and Poisson's ratio was calculated. When the specimen failed, the ultimate strength was also recorded. Microscopic analyses were done as well as permeability measurements, since permeability testing is a useful method to determine the relative porosity of a material. The permeability of a material correlates with the crack density since a high number of cracks will produce a larger flow path through the thickness of the material. The tests showed no significant change in pressure in both the control and the test specimens over time periods of as high as two week. These results indicated that there was no through-thickness crack damage due to thermal cycling in IM7, qualifying it as suitable selection for a fuel tank material [19].

These results for the permeation agreed with the values obtained for Poisson's ratio and Young's modulus. There were no changes observed in these values. If the material presented microcracks it would be reflected in the Poisson's ratio and Young's modulus values. When thermal cycling is introduced to the laminate the value of Young's modulus would be expected to decrease if cracks were forming, since the bonds holding the material together are breaking

apart effectively making it less stiff. The same reasoning holds for Poisson's ratio, if cracks were to propagate due to thermal stress, one would expect the value of Poisson's ratio to increase as the fibers are able to move around more freely without having to strain the matrix as well [19]. When the crack density was measured it was confirmed that there were no microcracks after 10 cycles of the X-33 vehicle, and therefore the material was suitable for cryogenic tanks.

The problem arises when the results need to be compared. We can conclude that IM7/977-2 does not microcrack after thermal cycling but it wouldn't be true. As mention before, the damage accumulation trends from cycling at one temperature may not adequately simulate trends from cycling at a much lower temperature [16]. And the number of cycles is another important factor, maybe for 10 or 300 cycles the material does not show any microcrack initiation but after few more cycles it can reach significant densities. Therefore the results obtained need to be understood within the testing conditions that have been carried out.

2.1.2. Matrix modification

The composition of PMCs can be chosen in such a way that the resistance to microcracking at cryogenic temperatures will be improved. The curing agent, the matrix backbone flexibility, toughening agents and longitudinal CTE of the reinforcing fibers can be altered to study their part in the microcracking behavior [8].

Timmerman et al. [8] combined a set of different resins, (Epon828, Epon836, Epon871 and D.E.R.661) with two different curing agents (HT976, CG1400) and three different types of carbon fibers with low, intermediate and high tensile moduli (T300, T800H, M35J). A toughening agent was also added in some of the formulations. The different systems of laminates were equilibrated at 22 ^{o}C and then placed in a LN_2 bath for ten minutes. After that the samples were placed in a dessicator and returned to room temperature (RT). Each sample was exposed to a minimum of 5 cycles until no further microcracking was observed.

The resin formulation was chosen to provide a balance between strength and flexibility. The same way, the curing agents selected provided varying degrees of regularity of the network and different crosslink morphologies.

The conclusions of this work were linked to the structure of the resin. It was observed that the choice of the curing agent had a significant effect on the final morphology of the polymeric matrix. Increasing the backbone flexibility altered the response of the matrix to temperature changes [8]. Flexible matrix segments are more mobile and occupy a greater

effective volume, which increases the CTE of the matrix. When the curing agent creates a more irregular and flexible network, the ability of the matrix to accommodate thermal stresses decreases and this contributes to the increase in the microcracking density of the laminate. These results are also linked to the glass transition temperature (T_g) of the matrix. The higher backbone flexibility, the lower is the T_g observed and the higher is the microcracking detected [8].

It has been observed in [8] that the tensile modulus of the fibers influences the microcrack morphology as well as the crack density. Microcracks usually become wider and more tortuous when fibers with higher modulus are used. Therefore if the composite contains higher modulus fibers it will tend to microcrack easily. Higher tensile modulus corresponds to elevated crystallinity and orientation of the crystallographic basal planes parallel to the fiber axis; this increases the negative longitudinal CTE of the fibers. When the temperature is decreased the fibers contracted in the radial direction and expanded along the longitudinal axis while the matrix contracted in all directions. Larger differences in the CTE between fibers and matrix increase the thermal stresses at low temperatures and cause a corresponding raise in microcracking. In relation to the rubber-toughening agent it was detected that when it was included in the formulation it prevented the formation of microcracks [8].

Ueki, Nishijima and Izumi [20] give another example of matrix modification in their work. The mechanical and thermal properties of several types of epoxy systems were designed based on the chemical structure, network structure and morphology aiming at cryogenic application. In this study, di-epoxies or multifunctional epoxies were cured by several kinds of hardeners such as anhydride, amine or phenol and were blended with polycarbonate, carboxyl-terminated butadiene acrylonitrile copolymer or phenoxy. The mechanical properties and thermal properties of these cured epoxies were measured at room and liquid nitrogen temperature, and it was observed that chemical structure as well as network structure and morphology were highly connected with improvements on the fracture toughness at cryogenic temperatures. Therefore, it is very important to control the structures in order to optimize epoxy systems for cryogenic application.

Overall, it is noticed that fiber and matrix play an important part in determining the response to cryogenic cycling by altering the thermal stresses present in a material as well as the ability of the material to resist thermal stresses.

2.1.3. Thin films

The increased incorporation of thin polymer films into aerospace applications can be credited to their contribution to weight savings in spacecraft construction [22]. The addition of particulate fillers to thin polymer films to make composites would improve the properties of the composite over that of the neat polymer film.

The choice of liner should be a function of the environment conditions, loads and the application in which is going to perform. For cryogenic applications if a metallic liner is considered, coefficient of thermal expansion (CTE) compatibility between metal and composite is a major barrier for their use. CTE mismatch exacerbates the problem of strain compatibility and it becomes critical for cryogenic applications where the temperature excursions could be as wide as 250°C and a temperature drop to cryogenic operation temperature would cause the liner to pull away from the composite. Furthermore, the thermal strain would cause yield of the metallic liner.

If the option chosen is about polymeric liners, they offer some advantages [21]:

- Significant weight advantage over metal liner
- Lower cost for "conformable" (non-cylindrical) geometries
- Liner serves as a mandrel for winding composite wrap

But there are also some disadvantages

- High permeability for stored hydrogen
- Loss of hydrogen & possible damage to structure
- Limited permeability data available

When thin films are being considered as materials for space applications it needs to be evaluated not only their mechanical properties but also their manufacturing, since it could affect the future performance of the material.

Manufacturing of thin film polymer nanocomposites can be achieved in several ways and the choice of the processing method would influence the final behavior of the film. Herring [22] and Herring et al. [23] manufactured thin film polymer nanocomposites by two distinct methods as combinations of two different polymers and three separate metal oxides. They were evaluated to determine the storage modulus and degree of dispersion of nanoparticles, respectively. It was

observed that changes in the storage modulus for the TOR-NC-[1]based nanocomposites were dependent on the method of manufacture. The first method, where the particles were added to a prepared polyimide, produced samples with a higher storage modulus than the clean polymer. The second method, where the polymer and particles were prepared together, produced samples of decreased storage modulus compared to the clean polymer. However, in the case of the LaRC^{TM} CP-2[2]-based nanocomposites, storage modulus for most of the polymer/particulate systems was diminished by the addition of the metal oxide particles. The dispersion of the metal oxide particles within both polymers was shown to be poor with clumps of the particles non-uniformly distributed throughout each film. While this did not appear to adversely affect the storage modulus of the TOR-NC-based films, it seemed to have been a contributor to the diminished storage modulus for the LaRC^{TM} CP-2 samples.

For most cases, the use of nano-scale additives resulted in films with comparable or lower strengths and elongations and higher stiffness as compared to the baseline polymer. Nevertheless, the use of nanoscale metal oxide additives lowered the storage modulus for both polymer types. Processing of the nanocomposite films also influenced the storage modulus over a wide temperature range. It was observed a drop in strength and decreased elongation to break that suggested that the dispersion of the fillers was not achieved.

Delamination of the thin film from the composite is another issue to consider when composites-thin film systems are exposed to thermal loads. Humpenoder [7] applied thin films to a CFRP. The samples of CFRP were exposed to thermal and mechanical cycling, with temperatures ranges from 52°C to -196°C and then permeability to helium was measured. Some of the liners used were Kapton, amorphous hydrogenous carbon, titanium nitride and several metals such as, copper, aluminum and silver. The thickness was observed to be a problem since very thin films do not improve the permeability of the composite and if the thickness was increased the system was mechanically unstable. A different possibility studied was embedded thicker metallic films within the composite. Results showed that the composite with embedded metal foil did not permeate but delamination occurred under thermal and mechanical cycling [7].

[1] Polyimide prepared from stoichiometric amounts of oxydiphthalic dianhydride and 1, 3-bis(3-aminophenoxy)benzene.

[2] Polyimide prepared at Langley Research Center from stoichiometric amounts of 4,4´-perfluoroisopropylidiene dianhydride and 1,3-bis(3-aminophenoxy)benzene

Thin films could be placed in the outer surface of the composite or they could be embedded into the laminate. Grimsley et al. [4] introduced thin film as a layer into a composite to form an interleaved composite. These films were tested to determine the permeability of argon at room temperature and then several of these films were introduced as a layer in the composite to form an interleaved, or hybrid, composite to determine the effects on permeability. The effects of the interleaved layer thickness, number, and location on the mechanical properties of the composite laminate were investigated. The hybrid composite coupons and related films were evaluated as viable barriers to gaseous argon permeation at room temperature. Some examples of the films evaluated were Aluminized Mylar^{TM}, Self-Metallized Polyimide film, Vectra^{TM} film, Inorganic-Organic films, Polyimide-Nanoclay films, Phenylethynyl-Containing Imide Silanes [4]. Several hybrid composite panels were prepared; one control panel for barrier property characterization and three more panels were fabricated using the same ply stacking sequence and processing cycle as the control, but with a layer of film placed at the center of the lay-up. After testing several configurations, it was concluded that the lowest overall permeability was found for Mylar^{TM} sample having aluminum on both sides but after a mechanical testing was completed the aluminum coating separated from the film during the test. These results indicated that the aluminum-to-Mylar^{TM} bond was weaker than the aluminum-to-composite bond [4]. Therefore in order for the Mylar^{TM} to be used as an interleaved barrier material the bonding strength would have to be improved.

Nanoparticles could be introduced in the carbon fiber reinforced composites as modifiers into the matrix or as separated modified thin films that could be interleaved with the layers of the laminates. In either case, the election of the materials, the synthesis process, compatibility and final operational conditions are factors that need to be considered in the designing procedure.

2.1.4. Permeability measurements

The measurement of the permeability of the materials that will be used in containment applications is of vital importance. Their gas permeation properties will determine their validity as barrier materials. After the X-33 failure, new test methods and apparatus to measure leakage through complex structures under several loads were developed.

In the screening process for new materials for cryogenic tanks there are several issues to be considered, what would be the temperature used to perform the test, what type of gas it will be

chosen, if there will be any kind of preconditioning of the samples or the type of loads applied to the material.

Rivers et al. [6] designed the Flexible Micro-Leak Detection System (FMLDS) a new method to measure the leakage through a geometrically complex structure at cryogenic temperature and under mechanical load. In this study was measured hydrogen leakage through a piece of the X-33 tank structure while it was under mechanical load and at cryogenic temperature. The FMLDS consisted of a flexible aluminized Mylar™ vacuum membrane, sealed to the test specimen with a vacuum seal material, and a micro-leak collection and measurement system. Gases that leak through the test specimen were captured in a space maintained by a cloth under the vacuum membrane and were vented through a capillary tube to an evacuated control volume. The capillary tube was connected to the control volume and any pressure rise and temperature change in the evacuated control volume would be monitored and converted to mass flow rates giving the leak measurement [6]. A mass spectrometer used to determine the gas species leaking into the system verified that the leak being measured was not from a source other than the test panel. Because the vacuum membrane and the sealing material were very flexible, they could be applied to complex geometric shapes. This system was applied to specimens cut from the scrapped lobe 4, LH_2 tank 1 of the X-33. Test articles were evaluated for liquid helium (LHe) and LH_2 leakage [6] In these tests, an in-plane tensile load was introduced to the inner face-sheet by loading the specimen in 4 point bending. The specimens were maintained at cryogenic temperatures and the two test articles were subjected to thermal and thermo-mechanical conditioning to ensure that thermal and mechanical load history of the test articles was as close to the X-33 tank structure as possible [6].

Stokes [24] performed permeability testing under tetra-axial strain on a Bismaleimide (BMI) based graphite fiber composite material at LH_2 and noted that permeability was dependent on the material's strain level and temperature as well as time. The cycling was done at LH_2 temperatures. The RT gas permeability was measured on the specimen in the thickness direction. A circular gage at the center of each specimen was employed to measure the material's permeability under strain. A sealing gasket was placed on the downstream and upstream halves of the setting and the two halves were paired. A compressive force was applied to the two halves that ensured the alignment and even distribution of force on the specimen seals. A dynamic vacuum was applied to the upstream, downstream, and edges of the specimen overnight or until

the specimen ceased to outgas. The downstream valve between the vacuum pump and transducer was then closed. After a sufficient record was obtained at these settings, hydrogen gas at a fixed pressure was applied to the upstream surface from a high pressure, high purity hydrogen gas source. To convert the increase in pressure as a function of time into mass flow rate the ideal gas equation was used.

To measure the samples under tetra-axial strain, strain gages were placed on the specimen and the specimen was placed in the loading facility. All permeability testing of specimens was done at uniform levels of strain in the eight in-plane directions within the material.

From the permeability testing it was observed that the failure initiation for the BMI material under uniform in-plane strain begun from the exposed surfaces and progressed toward the center of the material. It was also noted that for 1500 micro-strain at RT with uniform tetra-axial in-plane strain, there were localize failures in surface plies and when the strain was between 2500 and 3000 micro-strain there was widespread microcracking of the surface plies [24]. When the level of strain rose to values between 3500 and 4000 micro-strain, a contiguous through thickness crack system begun to generate in the material. When the level of strain was above 4600 micro-strain catastrophic failure of the material was noticed. When the material was not initially microcracked, permeability was affected mainly by the strain applied while for materials that already had a well-developed crack system; the main factor that affected permeability was the temperature.

Bechel et al. [16] chose a set of materials as IM7/977-2, IM7/5250-4, and IM7/3K which were submersed in LN_2. They investigated the density of ply-level micro-cracks that formed as a function of number of cycles, prepreg thickness, residual stresses, and the orientation of adjacent plies. Choi and Sankar [26] developed a based micro-mechanical analysis method to compute the detailed stresses in the fiber and matrix phases of IM7/977-2 composite laminate subjected to thermo-mechanical loading. Yokozeki et al. [25] measured the diffusion controlled gas permeability through a CFRP laminate at RT. It was observed that the existence of matrix cracks and loads affects the gas permeability. A diffusion model was applied based on thermodynamics and continuum damage mechanics and revealed that gas permeability including the combined effects of damages and loads could be evaluated with this model.

2.1.5. Mathematical approach

In the investigation process of new materials, the experimental approach is mostly used to analyze the behavior of composites at different loads and thermal conditions. But to develop an experimental method for every existing composite system under all possible environmental conditions involves a great effort. In order to reduced the experimental work it is needed to develop a method where all the different parameters are considered and the results can be extrapolated to different scenarios.

One approach used to study microcracking without involving testing every type of materials and cycles is using finite element analysis (FEA). As noted by Choi and Sankar [26] developing a finite element analysis can help to obtain results for different sets of materials under thermo mechanical loads. In this study a based micro-mechanical analysis method was developed to compute the detailed stresses in the fiber and matrix phases of IM7/977-2 composite laminate subjected to thermo-mechanical loading. The longitudinal and transverse strains at the laminate level at cryogenic temperatures were calculated using the laminate theory. The failure of a laminate could be predicted by using the maximum strength criterion. If the maximum principal stresses in the matrix exceed the allowable stresses of the material properties would indicate that matrix cracking is quite possible under cryogenic conditions. It is important to take into consideration that even the FEA gives results on the behavior of the samples, an experimental confirmation is needed to accurate predict microcracking.

There are some commercially available life prediction software "GENOA" used to predict permeation (leak rate) versus strain, critical damage events, and the contributing failure mechanisms associated with permeation [27]. This prediction model attempts to reduce the required amount of testing by predicting the permeability at any given point in the tank life cycle. GENOA simulations are used to show the damage initiation, propagation, fracture initiation, final failure, surface crack length, and vertical or through-the-thickness crack.

The prediction of the crack density in the composite matrix with this software includes the onset of cracks in the matrix, which is predicted by the transverse tensile failure criterion. Also includes the propagation of cracks in the matrix, which is defined by the progressively increasing crack density and predicted by the assumption that the energy released due to the damage in the matrix forms new crack areas and finally, the degradation of composite properties due to the existence of cracks.

Several materials were evaluated with this software, IM7/977-2, IM7/8552 and IM7/5250. After the comparison done of GENOA predicted results with permeability tests, was observed that there was a good match and therefore the analysis algorithm was validated. This software gives a good example on how the computer simulation can help to decrease the number of tests needed to assure the viability of a determined material [27].

Smeltzer and Waters [28] used the computational effort to help in the decision process of choosing a material. The finite element code ABAQUS was used to conduct a thermal evaluation of a composite tank wall design for a liquid hydrogen tank. The design of the tank wall consisted on IM7/977-2 facesheets and a Korex honeycomb core sandwich insulated with Airex cryogenic foam and an Alumina Enhanced Thermal Barrier (AETB-12). The aim of the investigation was to perform a thermal analysis to determine the temperature profiles through the thickness of the tank wall. This evaluation could help to identify weak points on the design that would lead to a future failure of the tank. The performance of the tank wall was evaluated for different vehicle flight conditions: cold-soak (ground-hold), ascent, and re-entry.

The objective for Smeltzer and Waters [28] was to ensure that ABAQUS is a tool of confidence that can be used for thermo-structural evaluations of cryogenic fuel tanks. To accomplish this task the thermal response of the tank wall was evaluated and the results were compared to previous analysis. It was concluded that ABAQUS is a useful tool that can help to perform nonlinear, thermal analysis and it was established that the temperatures calculated through the thickness of the tank wall were within the limitations of the materials being used. This evaluation could be use to improve future tank wall designs guaranteeing that operational temperature limits of the materials used are not exceeded.

Abdi et al. [27] used the finite-element method to predict permeation versus strain, critical damage events, and the contributing failure mechanisms associated with permeation. Crack opening displacement (COD) was found to be critical in the permeation trough laminates and there are many researchers who have analytically derived solutions for finding the COD displacement.

Roy and Benjamin [29, 30, 31] developed a mathematical model for predicting opening displacement of a transverse crack. Analytical studies were done in order to relate failure of an IM6/3501-6 composite with crack opening displacement. Since the amount of leakage increases with evolving damage it was necessary to determine various factors like loading conditions,

crack density and laminate orientation on COD in order to understand and quantify the influence of damage on cryogenic fuel permeation. In this study, an expression for predicting opening displacement of a transverse crack was derived based on shear lag analysis and verified using FEA. Using this expression, the COD can be calculated for any symmetric laminate lay-up for any given crack density and loading conditions. It was observed that when the crack density increases, COD tend to be constant and then starts to decrease rapidly when the crack density is very high. This is due to the fact that as the crack density increases the transverse ply loses its ability to carry much tensile load and therefore the COD decrease. As the crack density increases, the crack opening volume increases linearly, but then the rate of increase starts to slow down. It is supposed that for very high crack densities crack opening volume may reach saturation resulting in constant permeation through laminates irrespective of the increase in the number of cracks. This investigation was carried on one type of composite structure IM6/3501-6 and the results cannot be extrapolated to other systems but the analytical model could be applied to different materials under several loads to study permeation [29].

Whitcomb [32] calculated the opening displacement for various damage configurations with transverse matrix cracks and delaminations and developed a simple expression for calculating the crack opening volume (COV) based on changes in the effective moduli of a cracked ply and studied the effect of various parameters such as adjacent ply orientation, material properties of adjacent plies, initial properties of the cracked ply and cracks in adjacent ply on COV.

Composite structures subjected to harsh thermal environments build up internal stresses due to the differences in the CTE of matrix and fiber. Even if a thermoplastic or a thermoset matrix forms the composite, when the materials are tested between cryogenic and room temperature, the principal problem is the microcracking creation and the subsequent formation of a leakage path that leads to the failure of the structure.

Efforts are being made to overcome this problem. Testing the materials with different temperature cycles, loading samples with different strains are steps needed to study the performance of the composites. Modification of the matrix with several curing agents, studies on the T_g and toughening agents are also possible solutions to the problem. The inclusion of nanomodifiers into the composite laminate in order to take advantage of the synergistic effect caused by the combination of these materials is the next step in the modification of matrixes. But

in order to take full advantage of these materials the nanoparticle-modified matrix needs to be studied first and then the manufacturing of the laminates can be accomplished.

2.2. Nanoparticle-modified composites

Nanomaterials are part of an extensive and growing area of research known as nanotechnology. Nanostructured materials may be classified in three areas: nanoparticles (the building blocks), nano-intermediates, and nanocomposites [33].

There are various classes of nanoparticles that serve as the building blocks of nanomaterials and devices. They include nanocrystalline materials such as ceramic, metal and metal oxide nanoparticles; fullerenes, carbon nanotubes; nanofibers and wires, and organic as well as hybrid organic-inorganic nanoarchitectures such as dendrimers and polyhedral silsesquioxanes, respectively. Nanocomposites are materials with a nanoscale structure that improve the macroscopic properties of products. Nanocomposites, materials with nanoscale separation of phases can generally be divided into two types: multilayer structures and inorganic/organic composites. Multilayer structures are typically formed by gas phase deposition or from the self-assembly of monolayers. Inorganic/organic composites can be formed by sol-gel techniques, bridging between clusters, or by coating nanoparticles [33].

Traditional fillers usually are in the range of microns but new technologies are reducing the size of fillers to the order of a few nanometers. This decrease in the size of the fillers brings new possibilities of materials with enhanced properties. When the dimensions of these fillers fall on a macroscopic length scale, the properties of the material are affected. The stiffness and heat distortion temperature of the polymer are increased but strength, impact resistance, and processability usually decreases [34]. Polymers modified with nanoparticles are able to provide value-added properties not present in the neat resin, without sacrificing its inherent processability and mechanical properties. Trends show that when processed properly small amounts ($\leq$ 5 wt%) of nanoparticles fillers can increase the modulus, strength, toughness, resistance to chemical attack, gas impermeability, resistance to thermal degradation, and dimensional stability of polymeric materials [34].

2.2.1. Layered silicate clays

Usually, two types of sheets, tetrahedral (T) and octahedral (O), form the structure of clay minerals. The T sheets are arranged in such a way that the silicon atoms are surrounded by four

oxygen atoms, with the silicon cations linked via covalent bonding through shared oxygen. The O sheets have cations, aluminum or magnesium, organized with six oxygens or hydroxyls covalently linked into a sheet structure. The two layers are also linked with covalent bonds through the top tetrahedral oxygens. There are different groups and subgroups of phyllosilicate clay minerals depending on their structure type. The structure of the clays is classified depending on the layer type. There are two predominant types, 1:1 (TO), and 2:1 (TOT). Smectite minerals belong to the 2:1 group; they have a charge per unit cell in the range of 0.5-1.2. Smectites are the most interesting clays from a chemical point of view, due to their possibilities of modification and application. In the smectite group is found beidellite, montmorillonite, nontronite, saponite and hectorite [35].

Most clay minerals are capable of incorporating species into their structures. For layer silicates, the term used is intercalation. The 2:1 layer silicates have a very varied propensity for intercalation, which depends on their layer charge. In the case of smectites the interlayer forces are lower and intercalation is achieved through chemistry, involving cation exchange or the intercalation of polar molecules that can coordinate around interlayer cations [36].

Under most conditions, clay minerals have hydrophilic, charged surfaces and will not intercalate nonpolar or low-polarity molecules. However, clays can be converted to more hydrophobic materials that are known as organoclays by two methods, by replacing the intercalate cations with long-chain alkylammonium ions or by directly grafting functionalized nonpolar groups onto the clay surfaces. Such organophilic clays are then capable of intercalating nonpolar organic guest molecules [37].

The clays used in this study are montmorillonite clays, which have an ideal formula of $[(Al_{3.5\text{-}2.8}Mg_{0.5\text{-}1.2})(Si_8)O_{20}(OH)_4]Ex_{0.5\text{-}1.2}$ where the exchange cation (Ex) can be K, Ma, Ca and Mg. The thickness of the three layer clay is about 1nm, while the lateral dimensions can range anywhere from 100-500 nm. The aspect ratio of the layered silicates is very high and therefore when a few weight percent of layered silicates are properly dispersed throughout the polymer matrix creates much higher surface area for polymer/filler interaction as compared to conventional composites. Their structure can be observed in Figure 2.3.

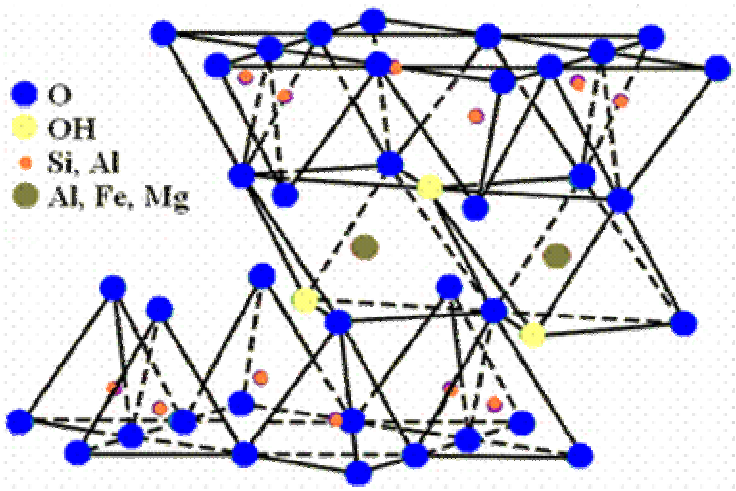

Figure 2.3. Structure of Montmorillonite [38]

2.2.2. Polymer-clay nanocomposites

Polymer-clay nanocomposites (PCN) are one of the most attractive materials nowadays. This new family of composite materials frequently exhibits remarkable improvements of material properties when compared with the matrix polymers alone or conventional micro- and macro-composite materials.

Modification of polymeric matrixes with minerals is very common but the challenge is to achieve the desired exfoliation in order to take full advantage of the properties that the introduction of nanoscale clays brings.

Depending on the strength of interfacial interactions between the polymer matrix and layered silicates there are mainly two different types of PCN's that are achievable [39].

1. Intercalated nanocomposites: in intercalated nanocomposites, the insertion of a polymer matrix into the layered silicate structure occurs in a crystallographically regular fashion, regardless of the clay to polymer ratio. Intercalated nanocomposites are normally interlayer by a few molecular layers of polymer. Properties of the composites typically resemble those of ceramic materials.
2. Exfoliated nanocomposites: sometimes also called delaminated, here, the individual clay layers are separated in a continuous polymer matrix by an average distances that depends on clay loading. Usually, the clay content of an exfoliated nanocomposite is much lower than that of an intercalated nanocomposite.

The exfoliated PCN's are the best option when it is sought an improvement in the material properties, Figure 2.4. When the polymer matrix has exfoliated nanoclays the improvement in properties can be manifested as an increase in tensile properties, as well as enhanced barrier properties; decreased solvent uptake, increased thermal stability and flame retardance [40].

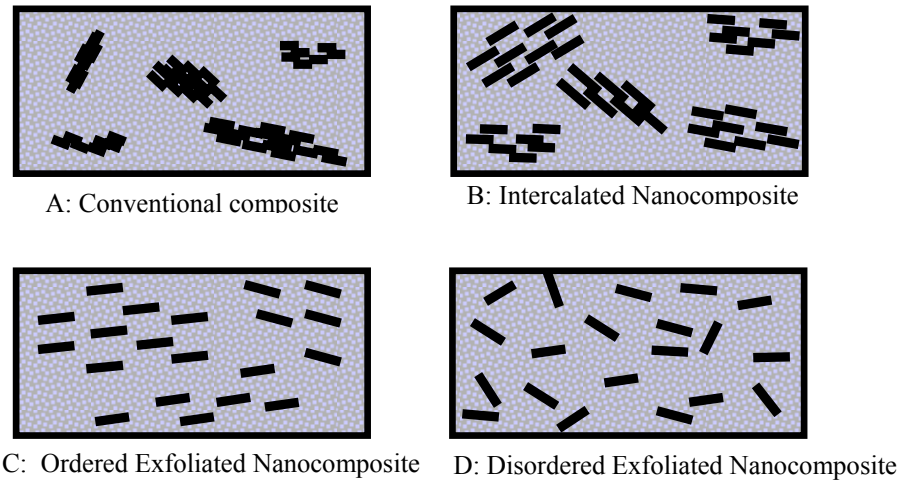

Figure 2.4. Schematic illustrations of polymer –clay nanocomposites [40]

The improvements in tensile and toughening properties of the composite are achieved thanks to the coupling between the surface area of the clay and the matrix facilitating the stress transfer to the reinforcement phase [40].

There are mainly two methods used to prepare intercalated PCN's. They are direct intercalation and *in situ* polymerization of preintercalated monomers. Direct intercalation is limited due to the fact that not all the polymers can be directly intercalated; *in situ* polymerization is more universal but results in a loss of control over the molecular weight of the final polymer. Another way to intercalate polymers directly is through a melt method, where the polymers are heated with preexfoliated clays. This method depends on the thermodynamic interaction between polymer chains and layers, usually for hydrophobic polymers the clays need to be modified into more organophilic to improve their compatibility [41].

The methods to produce exfoliated PCN's are basically the same as mentioned above. The success on the exfoliation depends on the polymer clay system that is used. Some success has been shown using the melt method but one of the most successful processes is through the polymerization of monomers that are in the presence of clay minerals. In this case the conditions

are such that the polymerization is promoted and causes uniform dispersion of the silicate layers within the polymer matrix [41].

It is clear that the introduction of nanoclays into polymeric matrixes improves the performance of the polymer but not only are they used in polymer matrixes. The effect of the addition of nanoclays into conventional composites has been also investigated.

There are some results reported on fiber-reinforced polymeric material where the fillers are layered nanoclays. Timmerman et al. [34] altered epoxy matrices of CFRP with both nanoclays and a traditional filler to determine the effects of particle reinforcement on cryogenic cycling. A mixture of two commercial epoxy resins (Epon828 and Araldite MY 9512) was used as the base resin for the polymeric matrix. The particles used to modify the matrix were Cloisite®25A and 5 μm alumina particles. The concentration of the particles was 2, 5 and 8 parts per hundred resin (phr) for the 25A material and 5 phr for the alumina particles.

The fibers used were T300YC50C carbon fibers and they were prepared as unidirectional prepregs with the modified resin. The samples after being at RT were placed in a LN_2 bath for 10 min. Then they were desiccated and brought back to RT. Each sample was exposed to a minimum of five cycles until optical microscopy revealed no further microcracking [34].

It was found that transverse cracking in symmetric carbon fiber/epoxy laminates as a response to cryogenic cycling was significantly reduced when nanoparticle fillers were used at concentrations much lower than those used for traditional fillers. It was observed that the concentration and distribution of the particles also played an important role in order to maximize the benefits of the reinforcement [34]. Large concentrations exhibited a typical, macro-scale filler effect and low concentrations showed little or no effect. When the structures were exfoliated and disordered intercalated type of structures the reinforcement was better than more ordered intercalated structures. The mechanical properties and processing characteristics were not negatively affected by the nanoparticles presence and the thermal expansion characteristics were improved. Overall it was seen that nanoclays could be easily used to modify traditional fiber-reinforced composite materials and enhance their resistance to thermal cycling induced stresses [34].

One of the important parameters to be controlled when designing a polymer clay nanocomposite is the amount of nanoclays added, increasing the content will not necessarily improve the properties of the composite as the clays will agglomerate and lose the exfoliated

characteristic structure that yields the specific properties of these materials. Magaraphan et al. [42] also observed that the clay content significantly influences thermal behavior of the nanocomposite films, such as CTE, glass transition and yielding temperatures. The system studied was constituted by polyimide/montmorillonite nanocomposites with different clay contents, ranging from 0.5 to 11wt% of dodecyl-montmorillonite (DMONT). X-ray diffraction tests showed that for a content of clays of 0.5 wt% the silicate layers were randomly dispersed in the matrix, and when the amount of clay increased to 9 wt% there was a dense pack of layers and aggregates were formed. The higher the content of clays the more rigid is the polyimide matrix and rigid matrix are found to give a superior thermal behavior; i.e. lower CTE, higher glass transition and yielding temperatures than the flexible ones, (lower content of clay). Changes in the polymer with the content of nanoclays were observed even in the color density, which increased as montmorillonite content increased [42].

Mechanical properties were also affected by the content of clays in the nanocomposite. The system showed an increase in brittle characteristics due to the rigidity of the inorganic filler as the amount of silica increased. The addition of clay improved the tensile modulus and strength at break of the polyimide-clay nanocomposite films. The clay can act as a reinforcing material for a polyimide film, as long as the amount of clays is under the limit where the aggregates are formed [42].

Agag, Koga and Takeichi [43] used a type of nanoclays organically modified montmorillonite (OMMT) and observed that the improvement in the tensile modulus was also enhanced by the inclusion of the clay nanolayers into the polyimide films, accompanied with a decrease in the elongation at break. For this system the best balance in properties concerning the modulus, T_g, CTE and thermal stability was at 2wt% of clay loading due to the homogeneous dispersion of the clay.

With the actual developments in spacecraft technologies, new applications for polymer nanoclays composites are been investigated and cryogenic properties are of much interest. Cryogenic mechanical behaviors of materials are generally very different from those at room temperature [44]. The results about the mechanical properties obtained from room temperature cannot simply be transferred to the cryogenic case. Zhang et al. [44] investigated the cryogenic mechanical properties of polyamide/montmorillonite (PI/MMT) hybrid films at cryogenic temperature, -196°C, and compared them with the mechanical properties at RT.

It was observed that the tensile strength at cryogenic temperature was generally higher than that at room temperature except at 20wt%. Zhang et al. [44] attributed this behavior to the arrangement of the molecules of the polymer matrix at cryogenic temperatures which are tightly frozen resulting in a higher strength than that at room temperature. The clay and polymer matrix interface adhesion was stronger at cryogenic temperature than that at room temperature due to the shrinkage of the polyimide matrix that acted as a clamp on the layered clays giving a higher composite strength. When the MMT content was 20wt%, the tensile strength at cryogenic temperature was lower than that at RT because the layer of clays aggregated and increased the stress concentration at the interfaces of the polymer and the clay.

The mechanical properties of the composite were improved when the nanoclay content was between 1-3 wt%. The strength and ductility of PI hybrid films could be simultaneously increased by the incorporation of exfoliated or intercalated MMT when contents were 1–3 wt%. The enhancement in the tensile strength of hybrid films resulted from the exfoliation and intercalation as well as the good dispersion into the matrix [44].

Regarding the fracture behavior, when the content of nanoclays in the matrix was about 10wt% or more, the adhesion between the nanoclays and matrix become weaker because of the increasing agglomeration degree of nanolayers. This would lead to the propagation of the cracks along the clay-matrix interface giving a coarse fracture surface. The fracture surfaces of the hybrid composite films were rougher at room temperature than those at cryogenic temperature, indicating that the fractures at cryogenic temperature are more brittle than those at room temperature, leading to a reduction in ductility of hybrid films comparing with those at room temperature. As an important conclusion it was noted that the strength, modulus and ductility at both room and cryogenic temperature were simultaneously enhanced by incorporation of organo-montmorillonite into polyimide matrix when the content of nanoclays was between 1 and 3wt% [44].

Other advantages that layered nanoclays offer is the improvement on the barrier properties to gas permeation, which is one of the reasons why they are candidate materials to be used in the design of the cryogenic fuel tank. When the nanoclays are exfoliated throughout the matrix, the composites not only show improvements in rigidity without sacrificing strength, elongation and toughness, but there are also improvements in the gas permeation of the composite because the impermeable clay layers act as an intricate pathway for a permeant to go

through the composite. Figure 2.5 shows the model proposed for the diffusion path in an exfoliated polymer clay nanocomposite when used as a gas barrier [45]. The enhanced barrier characteristics, chemical resistance, reduced solvent uptake and flame retardance of clay–polymer nanocomposites all benefit from the hindered diffusion pathways through the nanocomposite [40].

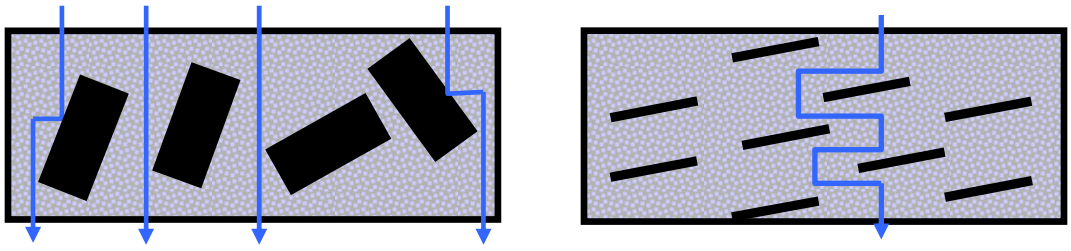

Conventional composite [39]

Proposed model for the intricate diffusion path in an exfoliated polymer–clay nanocomposite when used as a gas barrier [45]

Figure 2.5 Diffusion paths in nanocomposites

Campbell et al. [46] found that the distribution of low concentrations of layered nanoclays improved the barrier properties of the polymer. The barrier properties of a system with montmorillonite clay organically modified and dispersed into a thermoplastic and a thermosetting polyimide matrix were measured and noticed that the gas permeability through the thermoplastic matrix was greatly decreased in the presence of carbon fabric reinforcement. A carbon fabric reinforced composite was prepared with nanoclays dispersed into the matrix and it was measured the helium permeability. It was found that dispersion of 2wt% of nanoclays reduces the gas permeability by up to 70%, compared to that of the neat resin matrix composite. This large decrease in the permeability of the nanocomposite matrix composite suggested that the carbon fibers may align the silicate layers; thereby increasing the path a diffusing gas must travel. A measurement of the mechanical properties of these composites was also performed and it was found that there was an increase in modulus, but no change in flexural strength or interlaminar shear strength. It can be observed in Figure 2.6 the results of the helium permeability measurements for the carbon fiber polyimide composite with and without nanoclays.

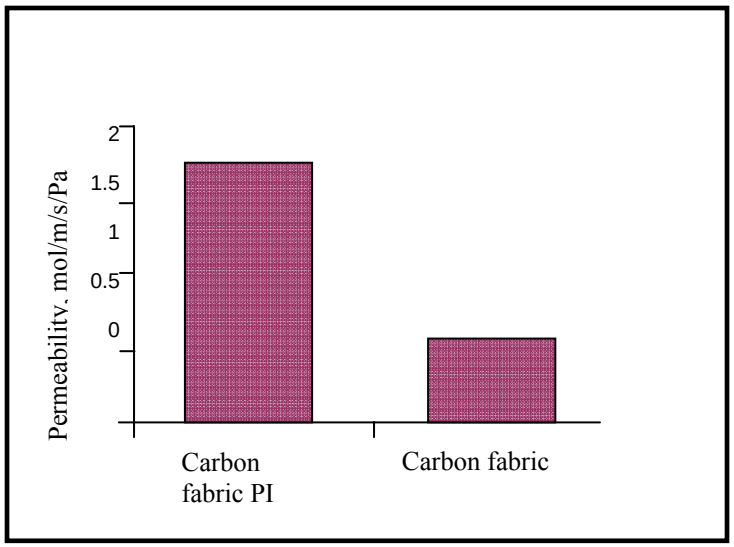

Figure 2.6. Helium permeability of carbon fabric reinforced composites with and without nanoclays [46]

Osman at el. [47] studied the barrier properties of an epoxy layered modified nanocomposite to oxygen and water vapor. They observed that the incorporation of small volume fractions of the platelike MMT nanoparticles in the polymer matrix decreased its permeability coefficient when the interface between the two heterogeneous phases was properly designed. The permeability coefficient of the epoxy matrix was reduced to one-fourth at 5vol % of the nanoclay loading, and the reduction was attributed to the tortuous pathway the gas molecules have to cover during their random walk to penetrate the composite. The transmission rate of water vapor through the composites was more influenced by the permeant-composite interactions but it was also observed that at 5vol % of the modified MMT, the relative vapor transmission rate was reduced to half.

2.2.3. Epoxy-clay nanocomposites

The focus of this work is on epoxy-modified nanocomposites and therefore the properties reported on this type of materials are of high interest.

Epoxy resins have a wide range of applicability and thanks to their modification with nanoclays the properties of the neat epoxy are further enhanced. The first question that arises when epoxy resins are modified with nanoclays is if the curing kinetic of the resin would be affected by the nanofillers. Depending on the type of curing agent and curing conditions, the structure of the crosslinked molecular network formed can vary significantly and greatly influence the properties and performance of the cured epoxy. Ton-That et al. [48] studied the effect of the addition of an organo-nanoclay (Nanomer®I30E) on the cure mechanism and

kinetics of epoxy nanocomposites based on Epon828 and Epicure3046. They studied the curing kinetics with the help of differential scanning calorimetry (DSC) tests and calculated the activation energy. It was noted that the activation energy of the epoxy nanocomposite was similar to that of the epoxy-amine system in the early stages of dynamic DSC cure, but was lower at higher temperature. It was noticed that the presence of nanoclays facilitated the curing reaction and also lowered the final glass transition temperature by about 4°C.

Xu et al. [49] also reported data on the curing kinetics of DGEBA at different amounts of organic montmorillonite. The activation energy was obtained with DSC measurements and it was observed little changes in the activation energy during the curing process.

In the work reported by Nigam et al. [50] the cure rate of the pristine diglycidyl ether of bisphenol A (DGEBA) resin was enhanced by the addition of organoclay MMT and the rate was also progressively increased with increasing clay content. The mechanical properties of the nanocomposite attained maximum value at 6wt % loading of the exfoliated organoclay. Beyond that level it was observed a fall in the mechanical properties attributed to improper filler dispersion and agglomeration of the clays. The thermal stability of the organocomposite was less than that of the inorganic composite but a substantial increase of 100% in modulus was observed.

In another study performed by Miyagawa et al. [51] the processing of nanocomposite materials composed of amine-cured DGEBA reinforced with organomontmorillonite clay was reported. They achieved a well disperse nanocomposite with mixed exfoliation and intercalation and they found that the glass transition temperature linearly increased with an increased weight ratio of the nanoclay. The same authors reported in a different publication [52] based on the same material that there was also increase in the mechanical properties of the material with the addition of the nanoclays. The storage modulus at 100 °C, which was above the glass-transition temperature, increased approximately 350% with the addition of 10wt % of clay. Below the T_g, the storage modulus at 30 °C increased 50% relative to the value of unfilled epoxy. The tensile modulus of epoxy at room temperature increased approximately 50% with the addition of 10wt% of clay.

The enhancement on the properties of the epoxy nanoclay materials depends highly on the exfoliation of the nanoclays and consequently, the process utilized on their synthesis is very important. Chen and Yang [53] utilized in their work different methods to produce the intercalation of clay layers with acid onium ions in order to synthesize an epoxy–

montmorillonite nanocomposite. The nanocomposite was characterized by different techniques and TEM photographs showed that the spacing between the clay layers was further enlarged to about 50 Å and no segregation between the clay particle and the polymer was observed. The glass transition temperature of one of the nanocomposite synthesized increased 38°C.

Feng et al. [54] used polymerization compounding in order to produce intercalated nanocomposites of a modified nanoclay in epoxy resin Epon828. Dynamic mechanical analysis (DMA) was used to evaluate the interfacial interaction between layered silicate and epoxy matrix. Modified organoclay composites were found to have enhanced storage moduli, particularly at temperatures higher than the glass transition temperature of the matrix. The storage modulus was increased 3-fold in rubbery state with addition of 10wt% modified organoclay, compared to 1.8-fold for unmodified organoclay with the same loading. Glass transition temperatures were found to be slightly higher for modified organoclay nanocomposites, indicating enhanced interactions between the modified organoclay and the epoxy matrix.

Zerda et al. [55] analyzed the mechanics and fracture behavior of intercalated modified montmorillonite clays in a glassy epoxy resin. The macroscopic compressive behavior was unchanged, although the failure mechanisms in compression varied from the unmodified samples. The fracture energy of the composites was increased by 100% at clay concentrations of 5wt %. It was observed in this study that the morphology of the system played an important role in the toughening mechanism because the spacing of regions of intercalated clay is important to toughening.

The mechanical and thermoviscoelastic properties in the glassy regime of epoxy-clay nanocomposites were studied by Abot et al. [56] in intercalated systems prepared by direct mixing of epoxy resin and two types of MMT. The elastic modulus of the nanocomposites was found to improve with respect to the pure epoxy modulus at the expense of both tensile strength and ductility regardless of clay content. The glass transition temperature was found to decrease with the increase of clay loading.

The tensile strength and moduli of an epoxy-MMT system in the rubbery state were analyzed by Lan and Pinnavaia [57]. They observed that the presence of the organoclay substantially increased both the tensile strength and the modulus relative to the pristine polymer and that the mechanical properties increased with increasing clay exfoliation. More than a 10-

fold increase in strength and modulus was realized by the addition of 15wt % of the exfoliated organoclay. It was also noticed that the strain at break for all the epoxy-clay composites was essentially the same as the pristine matrix, suggesting that the exfoliated clay particles did not disrupt matrix continuity.

The system of resin Epon862/curing agent W was modified with montmorillonite clay at different loadings in the study performed by Chen and Curliss [58]. It was not detected any modification of the glass transition with the addition of the clays but the storage modulus increased by 30% in the glassy state and 90% in the rubbery state with only 3% loading.

A different type of filler was analyzed in the work of Messersmith et al. [59]; they analyzed the effect of a mica type silicate in a DGEBA epoxy resin. The nanocomposite exhibited a broadened T_g at slightly higher temperature than the unmodified epoxy. And the dynamic storage modulus of the nanocomposite containing 4 vol. % silicates was approximately 58% higher in the glassy region and 450% higher in the rubbery plateau region compared to the unmodified epoxy.

Thermal stability data is normally obtained with the help of thermogravimetric analysis (TGA). The data obtained for different systems of epoxy-clay nanocomposites is contradictory. It is said that is dependent on the dispersion achieved of the MMT. Guo et al. [60] noticed this in their results. A modified MMT was dispersed in an epoxy matrix and the thermal stability of the epoxy nanocomposite was shown to be dependent upon the dispersion state of the nanoclay in the matrix although all the epoxy nanocomposites had enhanced thermal stability compared with the neat epoxy resin.

Not only the dispersion plays an important role in the thermal stability properties of epoxy-clay nanocomposites but also the loading and nature of the purge gas used in the TGA analyses. Gu and Liang [61] proved these results in their work, showing that in both nitrogen and air, the epoxy modified with 10 phr MMT had the lowest initial degradation temperature, while the nanocomposite modified with 2 phr of clay had the highest values. The activation energy values were also investigated and found that samples in air had far smaller values than those in nitrogen, indicating that the thermal degradation mechanism was different in the two gases.

It was reported above [51, 53] that in general, T_g increases with the addition of nanoclays, but in the particular case studied by Xu et al. [62] the glass transition decreased with the increase of MMT content. Dynamic mechanical analysis was performed and indicated that the glass

transition temperature of the exfoliated nanocomposite decreased with the increase of the montmorillonite content. The storage modulus in the rubbery region increased with the increase of the montmorillonite content, as it also did the amplitude of the storage modulus of the intercalated nanocomposite in the rubbery plateau.

It has been shown that nanoclays enhance the thermal and mechanical properties of the polymer to where they are added. The properties' improvement depends greatly on the exfoliation and dispersion of the nanoclays as well as on the synthesis process and amount of clays. Each system needs to be studied under its own particular conditions and extrapolation of the results to different systems needs to be done with caution. The positive effects of the reinforcement of polymers with nanoclays on properties such as flame retardance, thermal stability, mechanical properties and permeability have been reported [39-40, 43, 63-64]. But how the nanoclay-modified composite will behave at extreme temperatures is not yet fully understood. When nanoclays are properly dispersed in the matrix, they provide excellent properties' improvements but extreme temperatures can cause significant changes in a nanocomposite affecting the material's performance. In order to understand how the properties of the materials are affected, this work was focused in the study of the thermal properties of epoxy-nanoclay composites subjected to extreme thermal cycling.

2.2.4. Glass transition, free volume and permeability

It has been noticed from the literature available in PCN's that the thermal properties and values obtained for the glass transition vary from one system to another but in general, it was reported an increase of the T_g with the increasing clay content. This increase of the glass transition with the nanoclay content is often related to the decrease on the mobility of the polymeric chains. When the nanoclays are added into the matrix the chains of the polymer are confined to galleries between clay platelets, as a consequence, the stiffness increases with the subsequent augment of the glass transition temperature [65]. This increase of the stiffness of the polymer is connected with the decrease of the free volume in the nanocomposite.

The free volume is also related with the diffusion properties of the material. According to the free volume concept [66], an elementary mass-transport event is rationalized as follows. At some instant, *t*, a small penetrant molecule in a host polymer is at rest waiting for creation of a micro-hole nearby. When a hole with a sufficient size is formed (due to thermal motion of chains), the penetrant molecule hops into the hole, and remains in the new position until a new

hole arises in its neighborhood. According to this theory mass transport is strongly influenced by mobility of chains.

Therefore, any decrease in the free volume is connected to an increase of the glass transition and a decrease in the permeability as well.

One of the present methods used to study the free volume is Positron Annihilation Spectroscopy (PAS). When a positron is injected into a solid from a radioactive source such as ^{22}Na, it becomes thermalized within a few picoseconds by a succession of ionizing collisions, plasmon and electron hole excitations, and phonon interactions. This results in a positron with its highest density in the interstitial regions because the positron is repelled from the positively charged ion cores of the atoms. If there are lattice defects such as vacancies, vacancy clusters, or dislocations in the material in sufficient concentration, the positron can subsequently be trapped in a bound state in such a defect. In this bound state the positron may be highly localized [67]. A schematic of the process for lifetime tests is shown below.

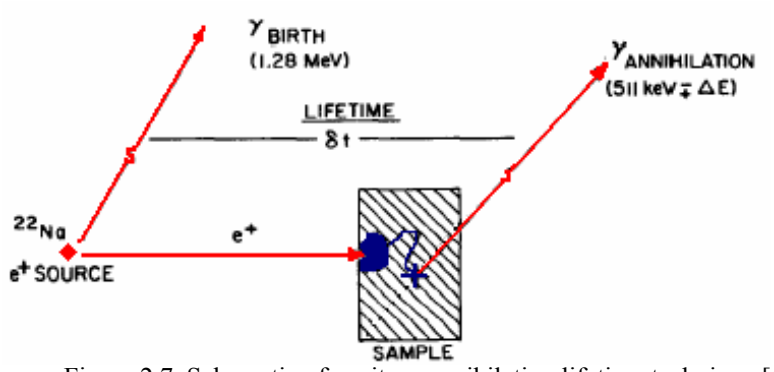

Figure 2.7. Schematic of positron annihilation lifetime technique [67]

The most commonly used experimental methods for observing the positron annihilation in matter are based on measuring the positron mean lifetime, observing the angular correlation of the annihilation photons, and determining the rate of three-photon annihilation of positrons.

Measuring the positron lifetime in matter involves using the ^{22}Na nuclide. The essence of the method of determining the positron lifetime amounts to measuring the delayed coincidence counting rate between the nuclear gamma quantum with an energy of 1.28 MeV and one of the 0.511-MeV photons emitted in the annihilation of the positron (stop signal) [68].

There are reported data on the relationship of the free volume measured by the PAS technique and the transport properties of MMT filled nanocomposites. Wang et al. [69] measured the free-volume hole property by positron annihilation lifetime spectroscopy (PALS) on a polymer clay nanocomposite material that consisted of styrene–butadiene rubber (SBR) and layered silicate clay of rectorite and conventional composite materials. The free-volume void fraction in rectorite/SBR was lower compared to pure SBR. The gas barrier of rectorite/SBR exhibited a 68.8% reduction in permeability compared to pure SBR, which was attributed to the tortuous diffusional path and lower fractional free volume.

PAS studies are also used to understand the effects of the distribution of the nanoclays in the material. Wang et al. [70] analyzed the PAS lifetimes for an epoxy MMT modified nanocomposite. They found that the ortho-positronium (o-Ps) intensity decreased with increasing MMT content, which indicated that the interaction between the host and nanofillers restrained the segmental motion, resulting in a decrease of the free volume. On the other hand, they also observed a good correlation between the interfacial interaction and mechanical properties, suggesting that the dispersion states of MMT and interfacial property between clay layers and matrix played an important role in determining the mechanical properties. When the MMT content was $\leq$ 2wt%, nanoscale layered MMT were well dispersed in the epoxy matrix. For MMT content > 2 wt%, the exfoliation and intercalation structures coexisted, the interfacial interaction between MMT and matrix was reduced and this resulted in poorer mechanical properties.

The study of the glass transition in the current work will allow us to determine the effect of the addition of the nanoclays in the molecular mobility of the polymeric chains. As seen above, this is related to the variation of the free volume in the nanocomposite, which, in turn is related to the diffusion properties.

2.3. References

[1] K. S. Whitley, T. S. Gates. Mechanical properties and damage mechanisms for polymeric matrix composites subjected to cryogenic environments. NASA LaRC, 2001

[2] T. F. Johnson, R. Natividad, H. Kevin Rivers, R. Smith. Thermal structures technology development for reusable launch vehicle cryogenic propellant tanks. NASA, LaRC, 1998

[3] Final Report of the X-33 Liquid Hydrogen Tank Test Investigation Team, George C. Marshall Space Flight Center, Huntsville, NASA Report, May, 2000

[4] B. W. Grimsley, R. J. Cano, N.J. Johnston, A. C. Loos, W. M. MacMahon Hybrid composites for LH2 fuel tank structure. NASA, 2001

[5] T. Johnson, E. S. Weiser, B. W. Grimsley, B. J. Jensen. Cryopumping in cryogenic insulations for a reusable launch vehicle. NASA, LaRC, 2003

[6] H.K. Rivers, J.G. Sikora, S.N. Sankaran. Detection of micro-leaks trough complex geometries under mechanical load at cryogenic temperature. AIAA-2001-1218

[7] J. Humpenoder. Cryogenics 1998; 38: 143–147

[8] J. F. Timmerman, M. S. Tillman, B. S. Hayes, J. C. Seferis. Composites: part A 2002; 33

[9] J.C. Seferis. Cryogenic cycling behavior of polymeric composite materials. AFOSR Technical report, 2003

[10] C. Pittman, L. Wang, R. Patton, J. Lee, J. Schneider, J. Ragsdale. CFRP micro-cracking at cryogenic temperatures. PPT Mississippi State University.

[11] T. Yokozeki, T. Aoki, T. Ishikawa. Composites Science and Technology 2002;62:1223–1229

[12] S. Polesky Walter. Thermal effects on the compressive behavior of IM7/PETI5 laminates. NASA, LaRC, 2003

[13] T. S.Gates, K. S.Whitley, R. W.Grenoble, T. Bandorawalla. Thermal/Mechanical durability of polymer-matrix composites in cryogenic environments. AIAA-2003-7408

[14] K. S. Whitley, T. S. Gates. Thermal/mechanical response of a polymer matrix composite at cryogenic temperatures. NASA/TM-2003-212171

[15] X. Su, F. Abdi. Progressive failure analysis of RLV laminates of IM7/PETI-5 at high, room, and cryogenic temperatures. AIAA-2003-1430

[16] V. T. Bechel, J. D. Camping, R. Y. Kim. Composites Part B: Engineering 2005; 36, 2

[17] S. Rouquié. Microcracking and weight loss of composite laminates subjected to vacuum thermal cycling. Measurements of moisture diffusion and expansion coefficients. AMTT, 1999

[18] V. T. Bechel, R. Y. Kim. Composites Science and Technology 2004; 64: 1773–1784

[19] S. S. Kessler, T. Matuszeski, H. McManus. Cryocycling and mechanical testing of CFRP for X-33 liquid H2 fuel tank structure. Massachusetts Institute of Technology

[20] T. Ueki, S. Nishijima, Y. Izumi. Cryogenics 2005; 45:141–148

[21] P. A. Lessing, Y. Yang, N. Sirosh. Low permeation liner for H2 gas storage tanks. INEEL, 2003

[22] H. Herring. Dynamic mechanical characterization of thin film polymer nanocomposites. NASA/CR-212147, 2003

[23] H. M. Herring, C. M. Thompson, T. S. Gates, J. W. Connell. Composites Science and Technology 2003; 63, 11

[24] E. H. Stokes. Hydrogen permeability of polymer based composite tank material under tetra-axial strain. 5th Conference on Aerospace Materials, Processes, and Environmental Technology (AMPET), September 2002

[25] T. Yokozeki, T. Aoki, T .Ishikawa. Adv. Composite Materials 2004; 13: 3-4: 227-236

[26] S. Choi, B. V. Sankar. A micromechanics method to predict the microcracking of the LH2 composite tank at cryogenic temperature. University of Florida, 2003

[27] F.Abdi, L. Israel, S. Johnson, P Aggarwal , J. Rayburn, D. Fox. Composite tank permeation prediction and verification. AIAA 2003-1760

[28] S. S. Smeltzer III, W. A. Waters Jr. Nonlinear thermal analyses of a liquid hydrogen tank wall. NASA LaRC, 2003

[29] S. Roy, M. Benjamin. Composites Science and Technology 2004; 64: 2051–2065

[30] S. Roy, M. Benjamin. Modeling of opening displacement of transverse cracks in graphite-epoxy laminates using shear lag analysis. Oklahoma State University, 2002

[31] S. Roy, M. Benjamin. Modeling of crack opening displacement due to delamination using first-order shear laminate theory. AIAA 2003-1603

[32] J. Whitcomb, D.Lagoudas, V. Kinra. Prediction of microcracking induced permeability of cryogenic composite tanks. NCAM and UNO, 2003

[33] http://www.sigmaaldrich.com/Area_of_Interest/Chemistry/Materials_Science/Nanomaterials/Tutorial.html

[34] J. F. Timmerman, B. S. Hayes, J. C. Seferis. Composites Science and Technology 2002; 62: 1249–1258

[35] S.M. Auerbach, K.A.Carrado, P.K. Dutta. Handbook of layered materials. CRC 2004

[36] J. M. Adams and J. J. Hooper. Encyclopedia of Materials: Science and Technology. Clays; 2006: 1236-1242

[37] C. O. Oriakhi, Michael M. Lerner. Encyclopedia of Physical Science and Technology. Nanocomposites and Intercalation Compounds, 269-283

[38] U.S.Geological Survey Open-File Report 01-041.http://pubs.usgs.gov/of/of01-041/htmldocs/clays/smc.htm

[39] S. Sinha Ray, M. Okamoto. Prog. Polym. Sci. 2003; 28: 1539–1641

[40] P. C. LeBaron, Z. Wang, T. J. Pinnavaia. Applied Clay Science 1999; 15: 11–29

[41] G.O. Shonaike, S.G. Advani. Advanced polymeric materials. CRC 2003

[42] R.Magaraphan, W. Lilayuthalert, A.Sirivat, J. W. Schwank. Composites Science and Technology 2001; 61: 1253–1264

[43] T. Agag, T. Koga, T. Takeichi. Polymer 2001; 42: 3399-3408

[44] Y-H. Zhang, J-T. Wu, S-Y. Fu, S-Y. Yang, Y. Li, L. Fan, R. K.-Y. Li, L-F. Li, Q. Yan. Polymer 2004; 45: 7579–7587

[45] K. Yano, A. Usuki, A. Okada, T. Kurauchi, O. Kamigaito. Journal of Polymer Science, part A: Polymer chemistry 1993; 31: 2493-2498

[46] S. Campbell, J. C. Johnston, L. Inghram, L. McCorkle, E. Silverman. Analysis of the barrier properties of polyimide-silicate nanocomposites. NASA/TM—2003-212221

[47] M. A. Osman, V. Mittal, M. Morbidelli, U. W. Suter. Macromolecules 2004; 37: 7250-7257

[48] M.-T. Ton-that, T.-D. Ngo, P. Ding, G. Fang, K. C. Cole, D. V. Hoa. Polymer engineering and science 2004; 44: 6: 1132-1141

[49] W. Xu, S. Bao, S. Shen, W. Wang, G. Hang, P. He. Journal of Polymer Science: Part B: Polymer Physics 2003; 41: 378–386

[50] V. Nigam, D. K. Setua, G. N. Mathur, K.K. Kar. Journal of Applied Polymer Science, 2004; 93: 2201–2210

[51] H. Miyagawa, M. J. Rich, L.T. Drzal. Journal of Polymer Science: Part B: Polymer Physics 2004; 42: 4384–4390

[52] H. Miyagawa, M. J. Rich, L.T. Drzal. Journal of Polymer Science: Part B: Polymer Physics 2004; 42: 4391–4400

[53] K. H. Chen, S. M. Yang. Journal of Applied Polymer Science 2002; 86: 414–421

[54] W. Feng, A. Ait-Kadi, B. Riedl. Polymer engineering and science 2002; 42: 9: 1827-1835

[55] A. S. Zerda, A. J. Lesser. Journal of Polymer Science: Part B: Polymer Physics 2001; 39: 1137–1146

[56] J. L. Abot, A.Yasmin, I. M. Daniel. Materials Research Society, Symposium Proceedings Vol. 740, 2003

[57] T. Lan, T. J. Pinnavaia. Chem. Mater. 1994; 6: 2216-2219

[58] C. Chen, D. Curliss. Nanotechnology 2003; 14: 643–648

[59] P. B. Messersmith, E. P. Giannelis. Chem. Mater. 1994; 6: 1719-1725

[60] B. Guo, D. Jia, C. Cai. European Polymer Journal 2004 ; 40 : 1743–1748

[61] A. Gu, G. Liang . Polymer Degradation and Stability 2003; 80: 383–391

[62] W. -B. Xu, S.-P. Bao, P.-S. He. Journal of Applied Polymer Science 2002; 84: 842–849

[63] D. Schmidt, D. Shah, E.P. Giannelis. Current Opinion in Solid State and Materials Science 2002; 6: 205–212

[64] M. Alexandre, P. Dubois. Materials Science and Engineering 2000; 28: 1-63

[65] A.D. Drozdov, J. deC. Christiansen, K. Gupta, A.P. Shah. Journal of Polymer Science, Part B: Polymer Physics 2003; 41: 5: 476-492

[66] M.H. Cohen, D. J Turnbull. Chem Phys 1959; 31: 1164

[67] R. W. Siegel. Ann. Rev. Mater. Sci. 1980; 10: 393-425

[68] V I Grafutin, E P Prokop'ev. Physics- Uspekhi 2002; 45: 1: 59 - 74

[69] Z.F. Wang, B. Wang, N. Qi, H.F. Zhang, L.Q. Zhang. Polymer 2005; 46: 719–724

[70] B. Wang, N. Qi, W. Gong, X.W. Li, Y.P. Zhen. Radiation Physics and Chemistry 2007; 76: 146–149

CHAPTER 3

EXPERIMENTAL PLAN

The goal of the experimental effort is to characterize the permeability under severe thermal conditions and measure the amount of helium gas that permeates in different nanoparticle-modified composite structures. The glass transition temperature will be studied as a function of the amount of modifiers and type of resin with Differential Scanning Calorimetry (DSC). Dynamic Mechanical Analysis (DMA) and Thermogravimetric Analysis (TGA) are also used in order to understand the thermal properties of the different combinations of polymeric nanocomposites.

3.1. Materials

The nanoparticle-modified resin samples were supplied by NASA Glenn Research Center. The specimens provided were from 6 different resins modified each of them with different percentage of nanoclays.

3.1.1. Resins

Epoxy resins are a class of cross-linkable polymers made from monomers containing at least two strained-ring groups called oxiranes. These rings contain one oxygen and two carbon atoms and are attached to a large variety of other aliphatic or aromatic organic molecules. This group is shown in Figure 3.1 [1].

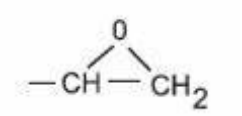

Figure 3.1. Oxirane [1]

They are used in applications ranging from high strength adhesives and specialty coatings to advanced composites. In all of these applications the final resin formulations also contain a variety of fillers, hardeners, pigments, and accelerators but the major component is usually the epoxy-containing molecule. The most important commercial epoxy resins are formed by the reaction of polyphenolic compounds or other active hydrogen molecules (amines, aliphatic alcohols, etc.) with epichlorohydrin under basic conditions. One of the most common phenols

used is bisphenol A and it provides the basis of a whole family of epoxy resins of general structure showed in Figure 3.2 [2].

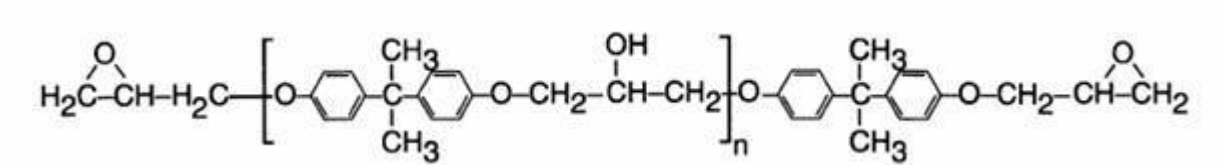

Figure 3.2. Diglycidylether of bisphenol A (DGEBA) [2]

Improvement of the performance properties can be obtained by cross-linking the epoxy resins into a three-dimensional and infusible network. The choice of curing agent depends on processing method, curing conditions, i.e., curing temperature and time, physical and chemical properties desired, toxicological and environmental limitations, and cost. The epoxy group, because of its three-membered ring structure, is highly reactive and it can be opened up by a variety of nucleophilic and electrophilic reagents. Curing agents are either correactive or catalytic. A catalytic curing agent functions as an initiator for epoxy resin homopolymerization, whereas the co-reactive curing agent acts as comonomer in the polymerization process. A variety of curing agents containing active hydrogen atom such as aliphatic and aromatic amines, polyamide amines, polyamides, anhydrides, dicyandiamide, isocyanate, polysulphides, mercaptans, melamine-formaldehyde, urea formaldehyde, etc. have been used [1].

The different resins used in the manufacturing of the samples are listed below.

Epon™826:

This system is a light colored liquid bisphenol-A based epoxy resin. It has high elongation (10%), low viscosity, low color, low ionic contamination, it reacts with a full range of curing agents and it produces high-strength cured systems resistant to chemical attack. It is especially useful in applications when high fatigue and microcracking resistance are required [3].

Epon™862:

This system is based on a bisphenol-F epoxy resin and an aromatic amine hardener. It provides low viscosity, long working life, high elongation, and it is a very versatile processing system for fabricating composite parts using filament winding or resin transfer molding. When it is cross-linked with appropriate curing agents, it offers superior mechanical, adhesive, electrical and chemical resistance properties [3].

Hexcel® 8552, Hexcel®8552-1:

Hexcel®8552 and 8552-1 are amine cured, toughened epoxy resin systems. It is a high performance tough epoxy matrix for use in primary aerospace structures that exhibits good impact resistance and damage tolerance for a wide range of applications [4].

Cycom®977-2

This material is a toughened epoxy resin with a curing temperature of 177ºC. It has a 127-138 ºC dry and 104 ºC wet service capability. It is used in aircraft primary and secondary structures, space structures, ballistics, cryogenic tanks or any application where impact resistance and light weight is required [5].

Hexcel M72

This material is a 177°C curing toughened resin with 177°C dry and 132°C wet service capabilities. It is used in aircraft primary and secondary structures, space structures and any application where impact resistance and lightweight use are required [4].

3.1.2. Nanoparticles

One of the type of nanoclays used on this research is known as Cloisite® which is a high aspect ratio additive designed and manufactured by *Southern Clay Products, Inc*. Benefits from Cloisite® technology result in part from the very high surface area of montmorillonite clay - which is in excess of 750 m^2/gram - and high aspect ratio (about 70 to 150). In dry form, Cloisite® exists in clusters or aggregates of montmorillonite platelets and very little surface area of the montmorillonite is exposed, causing very low aspect ratios but with the necessary modifications it can be obtained a good exfoliation and dispersion of the nanoclays into the resin matrix, necessary to realize the performance benefits [6].

There are several types of Cloisite®, the one used in the manufacturing of the samples is Cloisite®30B, which is a natural montmorillonite modified with a quaternary ammonium salt, observed in Figure 3.3. These nanoclays are used as an additive for plastics to improve heat deflection temperature (HDT), to improve the coefficient of linear thermal expansion (CLTE), to act as reinforcement, and to act as a barrier [6].

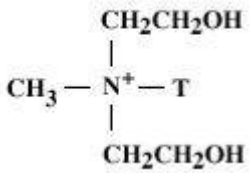

Figure 3.3. Quaternary ammonium salt used in the modification of Cloisite®30B.
T is Tallow (~65% C18; ~30% C16; ~5% C14). Anion: Chloride [6]

The other nanoclays used in the modification of the epoxy resins are referred as B18 and they are nanoclays that have been modified with protonated octadecylamine or protonated dodecylamine through an ion-exchange procedure. These nanoclays were provided by Michigan State University, which did the nanoclays modification themselves, and the modifier is proprietary.

3.2. Experimental procedure

3.2.1. Sample fabrication

The samples were manufactured by Ms. Sandi Miller at the Polymers Branch, Materials Division from NASA John H. Glenn Research Center.

The Epon™826 and Epon™862 were two part epoxies. For these resins, the epoxy portion was heated to liquid state on a hotplate, the nanoclay was stirred with it for 2 hours and the epoxy was cooled. The hardener used in the case of resin Epon™826 is a Jeffamine®D230, and in the case of Epon™862 is *W* curing agent, a non- methylene dianiline aromatic amine curing agent. The molecular structure of the resins Epon™826 and Epon™862 and their respective curing agents used in the samples' manufacturing are plotted below.

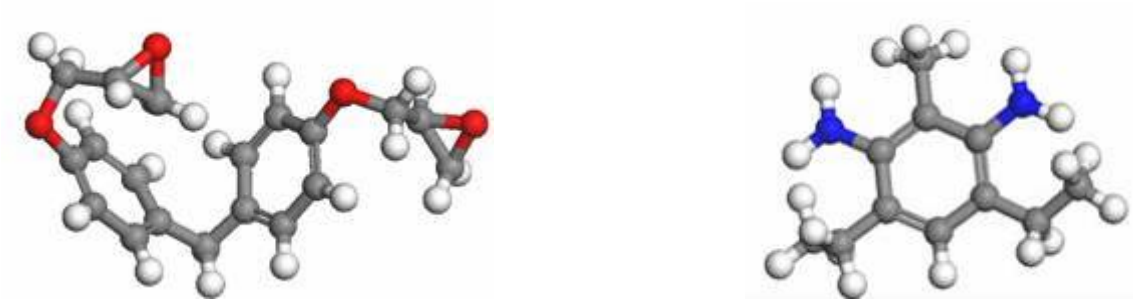

(a) (b)

Figure 3.4. (a) Epon™862 (b) curing agent *W*.
Carbon: grey, Hydrogen: white, Oxygen: red, Nitrogen: blue

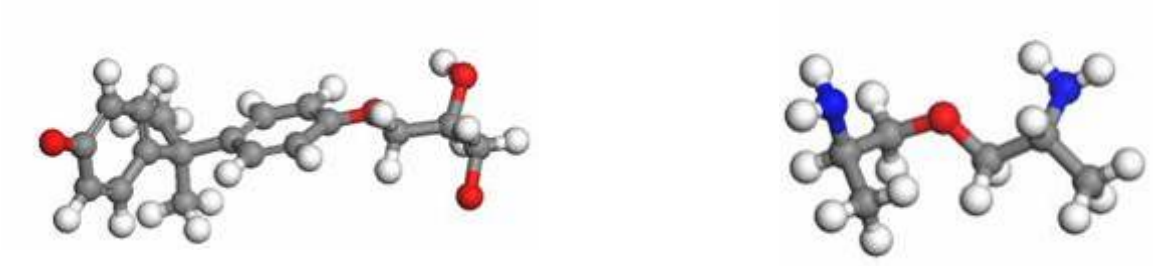

(a) (b)

Figure 3.5. (a) Epon™826 (b) curing agent J*effamine®D230*
Carbon: grey, Hydrogen: white, Oxygen: red, Nitrogen: blue

After cooling down of the resin with the nanoclays, the hardener was added, and the resin was placed in a vacuum oven to degas for about 2 hours, at 60°C. Then the resin was cured for two hours at 24°C and 2 more hours at 52°C.

The other set of resins, M72, Hexcel®8552, Hexcel®8552-1, and CYCOM®977-2 were received with the epoxy, hardener, and toughener premixed.

The sample was put in a beaker, with about 50 mL of methanol. The beaker was heated, keeping it below the boiling point of methanol. Clay was added, and the melted epoxy mixture was stirred with the clay, in solution, for two hours.

The solvent and epoxy mixture were poured into an aluminum pan, where the solvent was allowed to evaporate at room temperature overnight. The sample was placed in a vacuum oven at 60°C to degas for approximately 5 hours. The resin was then cured for 2 hours at 177°C.

The content of nanoclays added to the set of resins was 2wt% and 5wt%.

For each sample, a 10.16 x 10.16 cm (4 x 4 inch) plaque was made and was cut into smaller disk samples of 2.54 cm (1 in) diameter each. The disks were cut from the resin plaque using a water jet cutter. An example of the specimens is shown below.

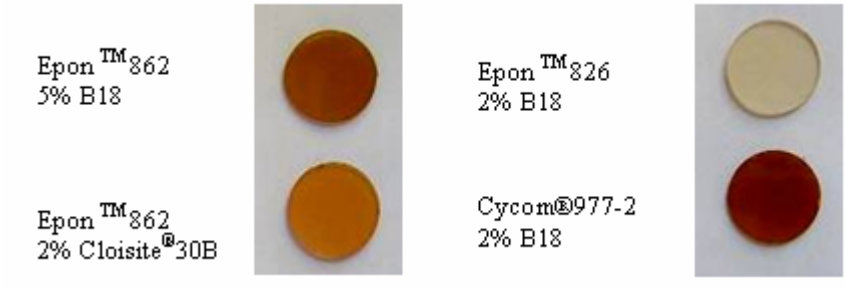

Figure 3.6. Samples of epoxy-nanoclay modified resin

The total of samples provided is listed below.

Table 3.1. List of samples

Sample	number	Sample	number
9772-B18-2/1	1	826-30B-5/2	19
85521-0/3	2	862-0/3	20
826-30B-2/3	3	826-B18-2/2	21
862-30B-2/1	4	85521-0/2	22
862-0/2	5	826-30B-2/2	23
862-B18-2/1	6	826-B18-2/3	24
826-30B-5/1	7	M72-0/3	25
826-0/1	8	862-30B-2/2	26
826-30B-2/1	9	862-B18-2/2	27
8552-0/2	10	862-30B-2/3	28
M72-0/2	11	826-B18-2/1	29
M72-0/1	12	862-B18-5/2	30
826-B18-5/1	13	862-30B-5/2	31
85521-0/1	14	862-0/1	32
8552-0/1	15	862-B18-5/1	33
862-30B-5/1	16	9772-B18-2/2	34
826-0/2	17	9772-0/1	35
862-B18-2/3	18	9772-0/2	36

The samples were given a number but they are mainly referred throughout the document with the following format: type of resin-type of nanoclay-percentage of nanoclay/number of sample. For example, 862-30B-2/1 refers to the sample number one of Epon^{TM}862 modified with 2wt% of Cloisite$^{®}$30B.

After the first screening of the samples, from the six different types of resins received, three types were further analyzed, Epon^{TM}826, Epon^{TM}862 and Cycom$^{®}$977-2, since they were the resins modified with 2wt% and 5wt% of the two types of nanoclays.

3.2.2. Permeability test

Helium permeability tests were carried out in a Varian 979 leak detector with a fixture specially manufactured for these experiments. The fixture consisted of two custom made steel flanges with an o-ring groove where the Viton o-ring is placed to seal the edges. The specimen was placed between the o-rings and the bolts were securely tightened. See Figure 3.7 for reference. The fixture was then connected to the leak detector port and to the hose that goes to the Helium cylinder respectively.

The Varian 979 leak detector is an automated portable leak detector with a minimum detectable leak at 1000 ppm ambient helium of $5x10^{-11}$ atm-cc/s helium. It can be operated with

single or dual pumps and it allows gross-leak testing to atmospheric pressure as well as high test-port pressure tolerances.

(a) (b)

Figure 3.7 (a) Permeability set up (b) fixture with sample sandwiched between o-rings

The helium was pressurized on the upper part of the specimen at a constant pressure of $1.38 \cdot 10^5$ Pa (20 psi). During each test any Helium which permeated through-the-thickness of the sample was recorded every 30 seconds by an automatic data acquisition system using a computer. All the measurements were performed at an average temperature of 23.8°C±0.5°C.

3.2.3. Thermal analysis

3.2.3.1. DMA measurements

The viscoelastic properties of the polymers are related with the transport of particles in the material. When nanoclays are added into the matrix there is a reduction in the mobility of the polymeric chains and therefore it is believed that the diffusivity is affected [7].

A 2980 DMA from TA Instruments was used in order to measure the storage and loss modulus and their ratio, tangent delta. The tests were performed using the DMA Multi-frequency-Single Cantilever test. The samples were cut into rectangular shape with average dimensions of 17.43 x 12.61 x 2.05 mm. The frequency of the test was set at 1Hz, with amplitude of 0.020 mm.

The temperature of the storage modulus is related with the crystallinity of the polymer under study. See Figure 3.8 for reference. It can be observed in (b) that when an amorphous polymer increases the molecular weight there is an increase of the plateau of the storage modulus curve. The plateau of a thermoset polymer is stable and drops at higher temperatures but there is

no change in the Tg values. For crystalline polymers if there is an increase in the crystallinity the storage modulus will increase its value.

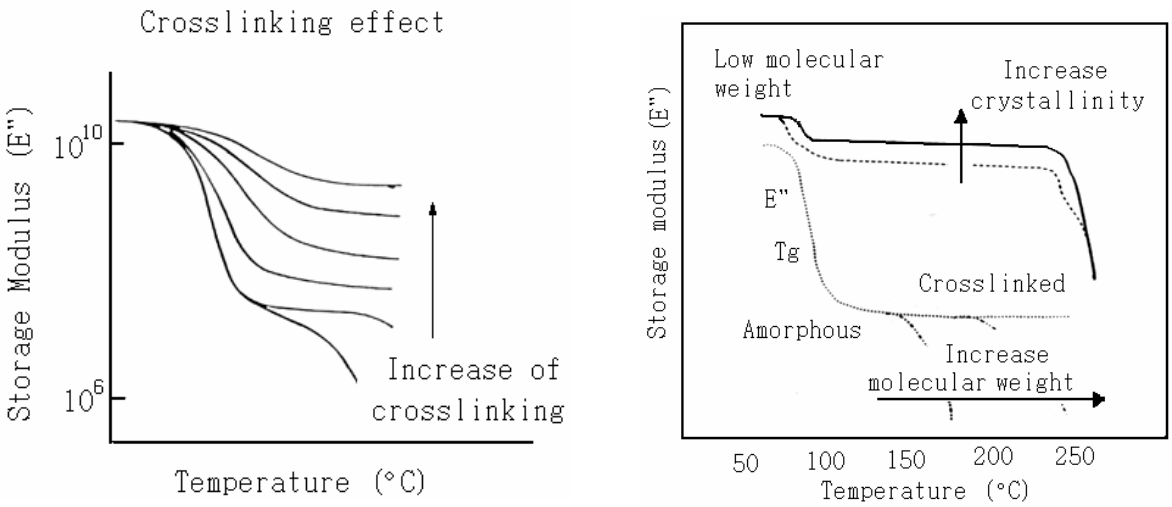

Figure 3.8. (a) crosslinking effect on storage modulus (b) crystallinity effect on storage modulus

In the case of the crosslinking increase (a) it is noted that the modulus drop is smaller when the crosslinking increases and the onset of the curve starts at higher temperatures. Therefore it is observed an increase in the T_g with the crosslinking.

An image of the DMA equipment used is shown below.

Figure 3.9. 2980 DMA from TA Instruments

Since three different matrixes were evaluated the methods used had different range of temperatures. In the case of Epon™826 samples, they were subjected to an equilibrium stage at 50˚C followed by a ramp at 5˚C/min up to 125˚C. The same method was followed for Epon™862 samples but increasing the temperature up to 150˚C. And finally for samples of Cycom®977-2 the temperature reached was 250˚C.

The values obtained for each run were the loss modulus, storage modulus and tangent delta.

3.2.3.2. TGA tests

Thermogravimetric analyses were performed in order to know the degradation temperature of the samples and if the addition of nanoclays would modify this value.

The samples were tested in a 2050 TGA from TA Instruments. The samples were cut from the original disks into pieces of about 24 milligrams. Open platinum pans were used in all the experiments. The tests were performed under airflow at a rate of 100 mL/min, running from room temperature up to 600˚C with a heating rate of 10˚C/min followed by an isothermal period of 10 minutes at 600˚C.

The degradation temperature can be measured as the onset temperature of the weight change curve, but sometimes this onset is not too clear, instead the first derivate of the curve was plotted (DTG) and the peak of the derivative was used as the indicator for the degradation temperature of the material. The residue after thermal degradation was also calculated at the end of each run. A detail of the sample holder and the furnace is shown in the figure below.

Figure 3.10. 2050TGA from TA Instruments

3.2.3.3. DSC measurements

Glass transition temperatures were obtained using a differential scanning calorimeter model 2910 MDSC from TA Instruments.

The samples were cut from the original disks into pieces of about 8-10 milligrams and placed in a closed aluminum pan. The tests were performed under air flow at a rate of 100 cc. /min, running from room temperature up to 600˚C with a heating rate of 10˚C/min followed by an isothermal period of 10 minutes at 600˚C.

The glass transition was calculated as the inflection point of the change of slope in the DSC trace using the help of the Universal Analysis Software.

An image of the sample pans in the DSC machine is shown below.

Figure 3.11. Sample pan in 2910 MDSC from TA instruments

3.2.4. Thermal cycling

Thermal cycling experiments were done in a cycling machine with data acquisition system which were designed and built at Prairie View, Texas A&M University FAST Center. The specimen holder is suspended on a steel rope moved by a stepper compute controlled motor/pulley transport system. Two pneumatic doors are controlled by a computer to open and close at predetermined times to allow the specimen to enter and exit the cryogenic chamber, air space and the convection oven. The setting can be observed in Figure 3.12. It is set to automatically cycle between an oven which will heat at a predetermine temperature and a LN_2 bath. The test temperatures run from -196^{o}C to 177^{o}C. The cycle profile can be observed in Figure 3.13.

Figure 3.12. Thermal cycling machine, Prairie View, Texas A&M University

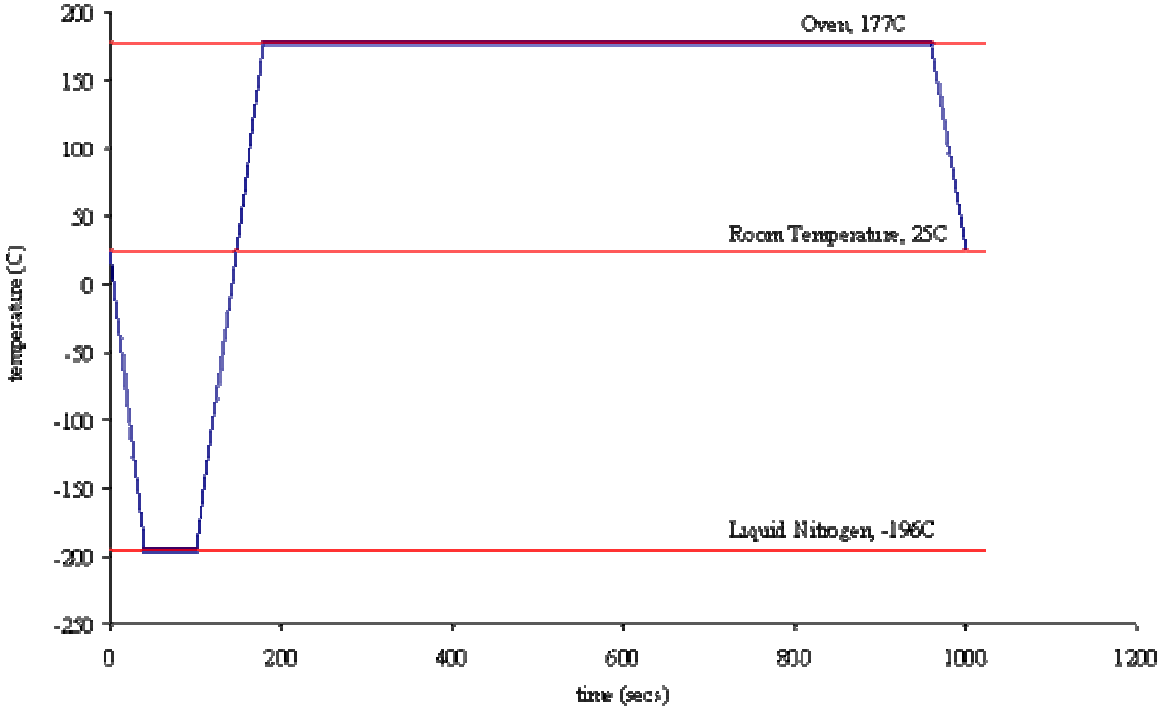

Figure 3.13. Thermal cycle profile

The samples were cycled 140 times until some cracks were observed in three of the samples. Two samples from the Epon™862 resin (862-0 and 862-B18-5) and one from the Cycom®977-2 resin (9772-B18-2) were affected.

3.2.5. Positron Annihilation Spectroscopy

Dr. Yuri M. Strzhemechny and Dr. C. A. Quarles at the department of Physics and Astronomy at Texas Christian University performed the measurements of the free volume in the specimens using positron annihilation spectroscopy (PAS).

Positron spectroscopy is a well-developed tool for investigating nanostructures in materials. In this case positron annihilation lifetime spectroscopy (PALS), which is sensitive to the electron density in the samples, was used to investigate atomic scale structure and to measure nano-scale free volume in the nanocomposite samples.

The PALS spectra were measured at room temperature with a conventional lifetime spectrometer where a Na-22 radioactive source was used as the source of positrons.

3.2.6. Microscopic evaluation

The damage produced in the samples after thermal cycling was observed with the help of a Buehler Versamet©3 Metallograph with an optical magnification of 200X.

3.2.7. X-Ray diffraction and TEM analysis

X-ray diffraction (XRD) and transmission electron microscopy (TEM) measurements were obtained by Ms. Sandi G. Miller at the Polymers Branch, Materials Division at NASA John H. Glenn Research Center. To obtain the XRD patterns it was used a Philips XRG 3100 X-ray diffractometer with Ni-filtered CuKα radiation. TEM specimens were prepared by microtoming sections of the nanocomposites, 70 to 80 nm thick, and floating the sections onto Cu grids. Micrographs were obtained with a Philips CM 200, using an acceleration voltage of 200 kV.

3.2.8. Density measurements

Density of all samples was determined using the Archimedes' principle. The rule of mixtures was applied and compared to the experimental values. Differences between the theoretical value and the experimental one were used to understand the void's concentration on the samples.

3.2.9. Activation energy calculation

The different degradation processes observed in the TGA results and their activation energy (E_a) were studied with the help of the software Polysolver®. This software is intended to separate complex TGA curves into single parallel processes optimizing the fitting of the TGA curves to a mixture of logistic functions.

3.2.10. Statistical studies

In this work some of the statistical tools used in experiments design with nanocomposite materials were discussed and the application of reliability techniques was proposed. With the help of the statistical methods and the software Statgraphics®, it was possible to assess the influence that nanoclays had on the permeability coefficients. With the application of the response surface method, the dependent variable, permeability, was studied with respect to the types of resin and nanoclays. The novel methodology proposed allows continuous and discrete factors to be considered simultaneously. Main effects were evaluated and the selection of key factors was based on design and material criteria.

For many scientific investigations the interest lies in the study of the effects of two or more factors simultaneously and factorial designs are most commonly used for this type of investigation. A special case of three factors with several levels is discussed in the next chapter.

3.3. References

[1] I. K. Varma and V. B. Gupta. Comprehensive Composite Materials. Thermosetting Resin-Properties, 1-56

[2] J. Hodgkin. Encyclopedia of Materials: Science and Technology. Thermosets: Epoxies and Polyesters : 9215-9221

[3] Resolution Performance Products, http://www.resins.com/resins/am/products/epon/EPON_Liquid_Blends.html

[4] Hexcel Corporation, www.hexcelcomposites.com

[5] Cytec Engineered Materials, http://www.cytec.com/business/EngineeredMaterials/Cycom%20977-2.shtm

[6] Southern Clay Products, Inc. http://www.nanoclay.com

[7] A.D. Drozdov, J. deC. Christiansen, R.K. Gupta. Journal of Polymer Science, Part B: Polymer Physics 2003; 41: 5: 476-492

CHAPTER 4

THEORY AND MODELS OF GAS PERMEABILITY

Gas permeation in a polymer is described as the property of the material to be penetrated and crossed by the gas molecules. It is described usually with help of the linear law of permeation:

$$\vec{F} = -P(\nabla \vec{p}) \tag{1}$$

Where $\vec{F}$ is the mass flux (or density of the mass flow), i.e. it is the mass (m) per unit area (A) of the cross section (with respect to the direction of the flow) per unit of time (t)

$$\vec{F} = \frac{\partial^2 m}{\partial t \partial A_n} \vec{n} \tag{2}$$

Here p is the pressure and P is an empirical permeability coefficient (measured in seconds in the SI system). The cause of the mass flow is the gradient of the pressure. By substituting the permeation law into the differential form of the mass conservation law

$$\frac{\partial C}{\partial t} + \nabla \cdot \vec{F} = 0 \tag{3}$$

gives

$$\frac{\partial C}{\partial t} = P\Delta p = P\left(\frac{\partial^2 p}{\partial x^2} + \frac{\partial^2 p}{\partial y^2} + \frac{\partial^2 p}{\partial z^2} \right) \tag{4}$$

or in the case of the proportionality of concentration ($C=m/V$) to the pressure (Henry law)

$$C = Sp \tag{5}$$

where S is the empirical coefficient of solubility, the diffusion equation can be obtained

$$\frac{\partial C}{\partial t} = D\Delta C \tag{6}$$

where

$$D = \frac{P}{S} \tag{7}$$

is the diffusion coefficient

or

$$P = SD \tag{8}$$

Thus, the linear permeability law can be described as the sequence of two linear laws: Henry law of solubility and Fick's law of diffusion

$$\vec{F} = -D\left(\nabla \vec{C}\right) \tag{9}$$

Permeability is not necessary only due to diffusion but also due to other mechanisms, for example, due to hydrodynamic flow through a system of micro-channels in a porous medium. In the case of non-diffusion permeability, the following equation can be derived

$$\frac{\partial p}{\partial t} = P_{(pV)}\Delta p = P_{(pV)}\left(\frac{\partial^2 p}{\partial x^2} + \frac{\partial^2 p}{\partial y^2} + \frac{\partial^2 p}{\partial z^2}\right) \tag{10}$$

Here the permeability coefficient $P_{(pV)}$ is measured in m^2/sec and it describes not mass flow but flow of the gas' pressure*volume product through the medium.

In both cases of diffusion or non-diffusion mechanism of permeability, equations (6) and (10), the stationary flow is described with the help of Laplace's equation.

$$\Delta C = 0 \tag{11}$$

This allows the use of analogy with electromagnetic, thermal, and other problems, especially in the analysis of permeability in heterogeneous media.

For polymers, the diffusion interpretation of permeability is the most popular. The general transport of gases through a homogeneous polymer membrane is usually separated in five phases [1]:

- diffusion through the limit layer of the side corresponding to the higher partial pressure (upstream side)
- absorption of the gas by the polymer, either by chemical affinity or by solubility
- diffusion of the gas inside the membrane polymer
- desorption of the gas at the side of lower partial pressure
- diffusion through the limit layer of the downstream side

Permeability is then identified as the product of two different coefficients, the diffusion coefficient, D and the solubility coefficient, S, as mentioned in equation (8). The diffusion coefficient accounts for the kinetic term that reflects the mobility of the penetrating gas in the polymer phase. The solubility coefficient has a thermodynamic origin and depends on the penetrant–polymer interactions as well as on the gas condensability. It is related to the

concentration C of the gas dissolved in the polymer and on the gas pressure p through equation (5).

As mentioned above the permeation process is broken down into five steps although the first and fifth processes are usually negligible since the formation of a limit layer is generally not observed [2]. In order to understand equation (8) and the three steps of the transport of gases in polymeric membranes it is assumed that the diffusion coefficient describes the flux of a certain volume of gas (in cc at STP) in response to a drop in the concentration (c_2-c_1) of the gas across the membrane of thickness d and area A, which is Fick's law, equation (9). That is, the diffusion is the response of the system to the gas concentration difference at the two opposite surface layers of the membrane. It is further assumed that the uptake and release of penetrant from and into the gas phase is much faster than the diffusion across the membrane, so that the latter becomes the rate-limiting step for the permeation process [3]. In turn, the gas concentration in the surface layer is linked to its partial pressure in the gas phase by the solubility, as shown in equation (5). If it is considered that the two partial pressures p_1 and p_2 are different but similar in magnitude, then the dependence of the solubility on the pressure can be neglected and these two equations are combined to yield equation (8).

4.1. Mechanisms of diffusion

On the microscopic level the mechanisms of diffusion are affected by the polymer-solute interactions and therefore it is necessary to understand these interactions to interpret the diffusion mechanisms.

Polymeric segmental mobility is affected by changes in size, shape, concentration, component interactions, temperature, etc. and diffusive motions will be affected by relative mobilities of the penetrant molecules and the polymeric chain segments. The overall transport process in a polymer depends on two major factors, polymer chain mobility and defect structures, such as voids, microcracks and other non-thermodynamic variations in polymer structure and morphology. These two factors are at the same time governed by a variety of other elements related to composition, fabrication and experimental conditions [4].

One of the important parameters to take into consideration is the polymer structure because the transport process will vary whether it occurs in a glassy or in a rubbery polymer. Depending on the relative mobilities of the penetrant and the polymer the diffusion in a polymeric matrix is classified into three categories [5]:

- Case I or Fickian: the diffusion process has a rate much smaller than that of the relaxation modes of the polymeric matrix. The sorption equilibrium is quickly reached and the boundary conditions are independent of time and swelling kinetics
- Case II, or non-Fickian behavior, refers to a fast diffusion process compared with the simultaneous relaxation processes of the polymer. The sorption phenomena are complicated by a strong dependence with the swelling kinetics
- Anomalous diffusion, which refers to a process where the diffusion and the polymer relaxation rates are comparable. The sorption and the transport of molecules are affected by the presence of pre-existing microvoids in the matrix; the penetrant motion is influenced by the geometrical structure of the polymer

4.2. Sorption

Sorption is a term used to describe the penetration and dispersal of penetrant molecules in a polymeric matrix to form a mixture. The sorption process is described as the distribution of the penetrant between two or more phases to include adsorption, absorption, incorporation into micro-voids, cluster formation, solvation-shell formation and other modes of mixing [4]. In the same polymer matrix, several modes of sorption can occur and the distribution of penetrant between different modes of sorption may change with changes in temperature, sorbed concentration, swelling of the matrix, time, etc.

In a polymer, under given conditions, the equilibrium amount of penetrant molecules sorbed and its sorption mode distribution are governed by the thermodynamics of the system. There are five characteristic modes of sorption: Henry's law, Langmuir, Flory-Huggins, BET and dual-mode sorption.

The first mode of sorption is that of and ideal solution behavior with sorbed penetrant randomly dispersed within the polymer. There is a linear relation between the penetrant concentration in the membrane and its partial pressure. This mode is observed essentially for low pressures when the penetrant-penetrant and the penetrant-polymer interactions are weak in front of the polymer-polymer interactions.

The Langmuir mode corresponds to a predominance of the penetrant polymer interactions. Diffusing molecules occupy specific sites in the polymer, for example, pre-existing microvoids or high-area inorganic fillers.

The Flory-Huggins mode represents the preference for penetrant-penetrant pairs to be formed such that the solubility coefficient increases continuously with pressure.

The BET mode is the combination of the Langmuir and Flory-Huggins models.

Finally, the dual-mode of sorption, or dual-sorption model, was proposed to describe curves observed in the case of sorption of low-activity gases in glassy polymers. It postulates the existence of two populations of diffusing molecules. This situation corresponds to the combination of Henry's law mode and Langmuir mode.

4.3. Theories on gas diffusion

There are different theories trying to explain the transport phenomena of diffusion of penetrant molecules in polymeric matrixes. These models formulate the diffusion coefficient and permeability from free volume theories and energetic and structural considerations. The difficulty resides in the fact that the transport process differs depending if the polymeric matrix is above (rubbery polymers) or below (glassy polymers) the glass transition temperature. Also the degree of crystallinity, the interaction with sorbed molecules and the thermal history are crucial [2].

Glassy polymers are characterized by a low intrasegmental mobility and long relaxation times, whereas rubbery polymers exhibit the opposite characteristics. The morphology of glassy polymers is considered as inhomogeneous with respect to the transport of small penetrant molecules, even if the polymers are completely amorphous [6]. For these reasons, the molecular transport mechanisms in glassy polymers are very different from those in rubbery polymers. Thus, the solubility of gases with low critical temperatures (e.g., H_2, He, N_2, CH_4, CO_2) is very low in rubbery polymers. As a result, the gas solubility, diffusion, and permeability coefficients are then normally independent of the gas pressure or concentration, provided that the polymers are not significantly plasticized (swelled) by the penetrant gases. By contrast, the solubility, diffusion, and permeability coefficients for such gases in unplasticized glassy polymers are strong functions of the penetrant gas pressure or concentration in the polymers. These differences in the gas solubility and transport behavior of rubbery and glassy polymers are due to the fact that glassy polymers are not commonly in a state of true thermodynamic equilibrium. As a result, characterization of gas transport and separation properties of glassy polymers is limited by the time dependent changes of the polymer's physical properties. These changes are important in evaluating the performance of the polymer during its anticipated service life [6].

4.4. Dual-sorption model

This model is the most widely used for glassy polymer systems. It postulates that the penetrant dissolves by two component processes: an ordinary dissolution similar to the one observed above the glass transition and a filling of a number of pre-existing microcavities [4]. The concentration of the dissolved penetrant, C_D, is usually represented by Henry's law. The concentration, C_H, of penetrant involved in hole-filling is represented by the Langmuir equation.

$$C = C_D + C_H = k_D p + \frac{C_H' bp}{1 + bp} \tag{12}$$

C_H' is the hole saturation constant and b the hole affinity constant which represents the ratio of rate constants for adsorption and desorption in microcavities.

In this model the solubility coefficient is expressed as:

$$S = \frac{C}{p} = k_D + \frac{C_H' b}{1 + bp} \tag{13}$$

And the diffusion process is:

$$J = -D_D(\partial C_D/\partial x) - D_H(\partial C_H/\partial x) \tag{14}$$

where D_D and D_H are the diffusion coefficients that characterize the mobility of the penetrant in the two sorption modes. By using some mathematical transformations it is defined the effective diffusion coefficient,

$$D_{eff} = D(C) = D_D\left[1 + \frac{KF}{(1 + \alpha C_D)^2}\right]\left[1 + \frac{K}{(1 + \alpha C_D)^2}\right]^{-1} \tag{15}$$

with:

$$K = \frac{C_H' b}{k_D} \qquad F = \frac{D_H}{D_D} \qquad \alpha = \frac{b}{k_D} \tag{16}$$

Using these parameters the permeability coefficient is then defined as:

$$P = k_D D_D\left[1 + \frac{KF}{1 + bp}\right] \tag{17}$$

This model has represented good the solubility and transport in glassy polymers but it is based on a simplified physical picture and it needs to be pointed that the nature and distribution of the microcavities is not really known, they are described as domains of lower density. In addition, the interactions between polymer-penetrant and penetrant-penetrant in those regions of

lower density must differ from those in the matrix to account for the difference in penetrant mobilities, but it is not known how.

4.5. Free volume theory

Most theories that describe the barrier properties of polymeric materials are based on the free-volume approach. The packing of the polymer chains leaves holes or microvoids, the so-called hole free volume, which may be occupied by the penetrant molecules. Since the chains are in constant motion the free-volume is continuously redistributed in the system, and the penetrants can move with it. According to this model, transport proceeds by a three step mechanism: By motion of segments of the polymer chains, the so-called jumping units, a void opens up adjacent to a penetrant molecule. The penetrant performs a quick move from its original position into the new void, leaving a void of similar size behind. The latter is then filled by other polymer segments in a process similar to the first step. From this model it is expected that amorphous regions of a polymer show much higher penetrant diffusion rates than crystalline regions, since they contain more free volume and it is redistributed more easily [7].

Following the free volume theory [8-9], the specific volume of a polymer-penetrant mixture is assumed to be composed of three components. The volume of the equilibrium liquid at 0 K is the occupied volume, and the remainder of the volume is taken to be free volume. The energy for redistribution of part of this free volume (the interstitial free volume) is large, and it is assumed that this part of the free volume is distributed uniformly among the molecules of a given species. The remainder of the free volume is denoted as the hole free volume, and it is accepted that this volume can be redistributed without an increase in energy. For diffusional transport the volume available is the hole free volume and this volume is the one generally utilized for the analysis of diffusion in polymer-penetrant systems [10].

There are several models that relate diffusivity of polymers with the free volume (V_f). In the model proposed by Cohen and Turnbull [11], the diffusion coefficients D are proportional to the probability of finding a microcavity the size of which is greater than the molecular size of B_D of the diffusant, hence,

$$D = A \exp(-\gamma B_D / V_f) \tag{18}$$

where $1 > \gamma > 0$ accounts for partial overlapping of microcavities. There is no variation of the free volume with the temperature taken into consideration in this equation, it is the model suggested by Fujita [12] that introduces this parameter,

$$D = A_d RT \exp(-B_D/V_f) \tag{19}$$

Vrentas and Duda [13] proposed including an energy term into the preexponent accounting for energy needed for the diffusant molecule to jump into the opened microcavity.

$$D_1 = \overline{D}_O \exp\left(-\frac{E^*}{RT}\right)\exp\left(-\frac{\omega_1 \hat{V}_1^* + \omega_2 \xi \hat{V}_2^*}{\hat{V}_{FH}/\gamma}\right) \tag{20}$$

In this equation, the solvent is component 1 and the polymer is component 2. D_0 represents an effectively constant preexponential factor, T is the temperature, $\hat{V}_I^*$ is the specific hole free volume of component I required for a jump, ω_I is the mass fraction of component I, ξ is the ratio of the critical molar volume of the solvent jumping unit to the critical molar volume of the polymer jumping unit, V_{FH} is the average hole free volume per gram of mixture, and γ represents an average overlap factor for the mixture. E^* represents the effective energy per mole that a molecule needs to overcome attractive forces that hold it to its neighbors. The first exponential term can be considered as the energy factor, and the second exponential term is the free-volume factor [14].

Considering the relationship given by equation (8) the permeability can be calculated according to the same exponential formula as the diffusion coefficient explained in equations (18) to (20) and therefore, the connection between permeability and free volume is established.

4.6. Influence of fillers in the diffusion process

The rate of diffusion in amorphous polymers is influenced by the coupling of the penetrant motion to local or segmental polymer motion. Penetrant motion exhibits a region of anomalous diffusion between short time ballistic and long-time Fickian diffusion. This region is attributed to the tortuous pathway topology and correlated motion in the polymeric structure in which the penetrants diffuse. Polymer motion is known to aid penetrant diffusion in the dynamic formation of cavities between which jump events occur, leading to a diffusion mechanism that is generally thought of to be an activated process. The polymer structure determines the local structure of activation barriers as well as the available pathways for diffusion. Transition state theory simulations have shown that the majority of penetrant jump events occur in the vicinity of the polymer side groups, due to the relative mobility of the side groups compared to the chain backbone [15].

The diffusion process is therefore affected by the polymer structure, the type of penetrant and it is also greatly influenced by other parameters such as fillers and modifiers.

It is known that the addition of well exfoliated sheets of layered minerals such as mica or clay into a polymer can improve the barrier properties of the material. The improvement levels can, however, vary rather strongly, depending on a number of factors, such as the mineral loading fraction and platelet aspect ratios, the degree of platelet exfoliation, platelet orientation distribution and the possible molecular level transformations in the matrix and/or at the platelet–matrix interfaces induced by the presence of the atomic-thickness high aspect ratio platelets [16].

When platelet-like particles are embedded into the polymer there are mainly two factors that can influence gas barrier property [17]. One is the geometric factor that favors the reduction in permeability by forcing diffusing molecules to take a long way around the platelets and hence depends only on the size of clay nanoparticles. There are many models based on the idea of the tortuous path and geometric considerations. The model developed by Nielsen depicts the effect of size on the barrier performance of polymer composites containing platelet particles, and can be written by the following equation:

$$P = P_0\left(\frac{1-\Phi_f}{1+\alpha\Phi_f/2}\right) \tag{21}$$

P and P_0 are the permeability of the filled polymer and the neat polymer, respectively. Φ_f is the volume fraction of filler and $\alpha = L/W$ is the aspect ratio of the platelets; L is the average length of the clay platelets and W being the thickness.

In this model the tortuosity factor is defined as the ratio of the actual distance that a penetrant must travel to the shortest distance that it would have traveled in the absence of the layered silicate. Figure 4.1 shows the additional distance a permeant travels in a particle filled system. The total path of a diffusing gas is given as [18]:

$$d' = d + d\frac{L}{2W}\phi_F = d\left(1+\frac{L}{2W}\phi_F\right) = d\cdot\tau \tag{22}$$

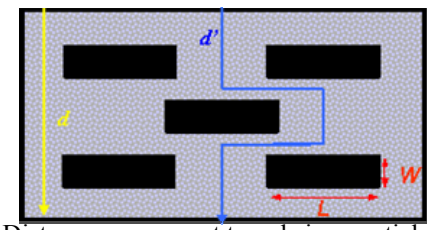

Figure 4.1. Distance a permeant travels in a particle filled material [18]

The second factor that can influence the barrier properties is related to the molecular level interaction of the matrix polymer with the filler, which in turn results in changes in the fractional free volume. Physically, reduced permeation in filled polymers is attributed to the increase in diffusion path length and decrease in effective cross-sectional area available for transport.

For nanocomposite materials, the two factors should be considered in the free volume theory: the tortuosity factor and the constraining effect of the nanoparticles on the amorphous chain segments (β) [17]. After taking account of these two factors, equation (18) should be modified as:

$$D = \frac{A}{1 + \alpha\Phi_f / 2} \exp\left(-B / V_f\right) \tag{23}$$

Any change in factor β can be reflected in changes in the free volume, $V_{\text{f.}}$

Many different models have been developed taking into consideration the tortuosity factor and geometric considerations, Nielsen formula, given in equation (21) is widely used but there are modifications to the formula taking other factors in account.

On the model developed by Fredrickson and Bicerano [19] the diffusion coefficient of composites containing randomly placed, impermeable, oriented disks of high aspect ratio was studied. The model includes the effects of disordered platelets and also introduces the idea that there are three regimes relevant for an understanding of the barrier properties of composites, depending on the platelet aspect ratio, α, and the platelet volume fraction, Φ_f, the dilute regime, corresponding to $x = \alpha\Phi_f << 1$, the semi-dilute regime, with $x >> 1$ but $\Phi_{\text{f}} << 1$, and the concentrated regime, with Φ_f no longer negligible compared with unity. The expression that relates the permeability of the filled and unfilled polymer is:

$$\frac{P}{P_0} = \left[\frac{1}{2 + a_1\kappa x} + \frac{1}{2 + a_2\kappa x}\right]^2 \tag{24}$$

With the following parameters:

$$a_1 = \frac{2 - \sqrt{2}}{4} \qquad a_2 = \frac{2 + \sqrt{2}}{4} \qquad \kappa = \frac{\pi}{\ln\left(\alpha / 2\right)} \tag{25}$$

In this model the platelets are circular in shape with radius R and thickness $2a$, the aspect ratio α is the disk radius to thickness aspect.

Cussler et al. [20] modified the formula derived by Nielsen by a geometric factor when they studied the variation of permeability with the concentration and the aspect ratio of the flakes. In their formula they introduced the factor μ, a combined geometric factor characteristic of the random porous media. Their model is formulated as:

$$\frac{P}{P_0} = \frac{1}{1 + \mu x^2} \tag{26}$$

Where the geometric factor is

$$\mu = \frac{\pi^2}{\left(8 \ln(a/2)\right)^2} \tag{27}$$

Gusev and Lusti [21] developed a model using direct finite-element permeability calculations with multi-inclusion of a random dispersion of non-overlapping platelets. With this model they tried to establish the role of geometric factors alone and to provide the understanding of the contribution of molecular-level transformations occurring in the matrices of nanocomposites.

They developed the following relationship where the permeability reduction is governed by the product $x = \alpha\Phi_f$, where $\alpha = L/W$ is the platelet aspect ratio and Φ_f is the volume fraction.

$$P/P_0 = \exp[-(x/x_0)^{\beta}] \tag{28}$$

Where the least square parameters values are $\beta = 0.71$ and $x_0 = 3.47$.

In their work, Gusev and Lusti compared the numerical predictions obtained in their work with those of Fredrickson and Bicerano, Nielsen and Cusler-Aris mentioned above. They found that the Nielsen formula gives quite accurate predictions for $x = \alpha\Phi_f < 10$. However, for values where $x > 10$, all the models underestimate the improvement attainable in barrier properties.

Following the same approach of considering geometric factors and using as the starting point Nielsen's formula, Bharadwaj [22] took into consideration on his model the effect of the orientation of the silicate layers. He introduced as a parameter the normal of the silicate layers (***p***) and the angle (θ) between the direction of preferred orientation (***n***) and the sheets normal. The order parameter was then defined as

$$S = \frac{1}{2}\left\langle 3\cos^2\theta - 1 \right\rangle \tag{29}$$

This function can range from 1 ($\theta = 0$), which indicates perfect orientation of the sheet normal unit vectors ***p*** with ***n***, to -1/2 ($\theta = \pi/2$), indicating perpendicular or orthogonal

orientation, and a value of 0, indicating random orientation of the sheets. The tortuosity factor is then modified to:

$$\frac{P}{P_0} = \frac{1-\Phi_f}{1+\frac{L}{2W}\Phi_f\left(\frac{2}{3}\right)\left(S+\frac{1}{2}\right)} \tag{30}$$

In this model is expected that the barrier property is enhanced when $S = 1$ and decays in a continuous fashion to nearly that of the pure polymer when S = -1/2 where the sheets are arranged such that there is negligible increase in the tortuosity.

It is necessary to mention that the models based on the concept of tortuosity are not rigorous ones: the gradients of concentrations in horizontal and vertical directions (on Figure 4.2) has to be different and has to be obtained in the process of the solution; several hypotheses are used instead of such finding.

Another approach used to model the permeability and the effect of inclusions is based on the rigorous solution of the problem of individual inclusion in the matrix. For spherical inclusions is used Maxwell's formula [23]:

$$\langle P \rangle = P_0 \frac{2P_0 + P_I - 2\Phi_f(P_0 - P_I)}{2P_0 + P_I + \Phi_f(P_0 - P_I)} \tag{31}$$

Here, P is the permeability, P_0 stands for the matrix permeability, index I denotes inclusion, and Φ_f is the volume concentration of inclusions ($0 < \Phi_f < 1$), the angular brackets denote effective property.

This formula is valid for two cases:

a) When the concentration of inclusions is small $\Phi_f << 1$ and inclusions have spherical shape; ratio of permeability of phases can be arbitrary, (original Maxwell's derivation).
b) When the concentration of inclusions is arbitrary, their shapes and orientations are arbitrary, but the difference of permeabilities of the phases is small in comparison with their sum: $\left|\frac{P_0 - P_I}{P_0 + P_I}\right| << 1$ (Lifshitz's derivation using correlation functions).

Nanoclays are more impermeable to gas than the polymer; therefore $P_I << P_0$. According to this relationship, Maxwell's formula degenerates into the expression:

$$\langle P \rangle = P_0 \frac{1-\Phi_f}{1+\frac{1}{2}\Phi_f} \approx P_0\left(1-\frac{3}{2}\Phi_f\right) \tag{32}$$

This formula will be used to verify the experimental results obtained in this work.

A modified version of this formula was derived by Beyle [24]. The analysis of Fricke's work [25] gave results close to Maxwell's formula. In his work, Fricke derived an expression for the electric conductivity of a suspension of homogeneous spheroids. He made several simplifications that were used by Beyle to derive a modified formula for the permeability.

a) Use of the partial solution of the problem, which is valid for single inclusion in infinitely big region
b) Do angular averaging of the randomly oriented inclusions
c) Neglected interaction between inclusions
d) Neglected the spatial lattice of the centers of inclusions

According to this last simplification in the schematic shown below, the three model versions a, b, and c are equivalent with respect to the permeability in the direction perpendicular to the platelets.

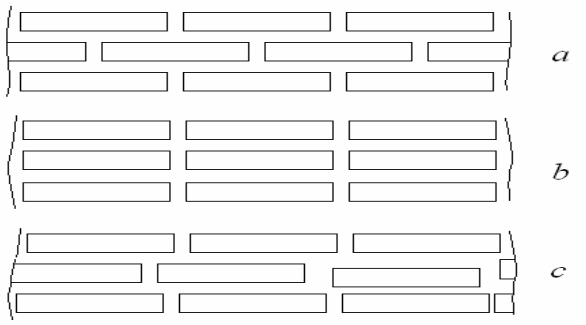

Figure 4.2. Different possibilities of platelet distribution [26]

In the case of small concentrations of oblate spheroid inclusions the calculated relative decrease with volume concentration Φ_f of the permeability for the case of impermeable inclusions is shown on the graph below for the different ratios of aspect ratio L/W.

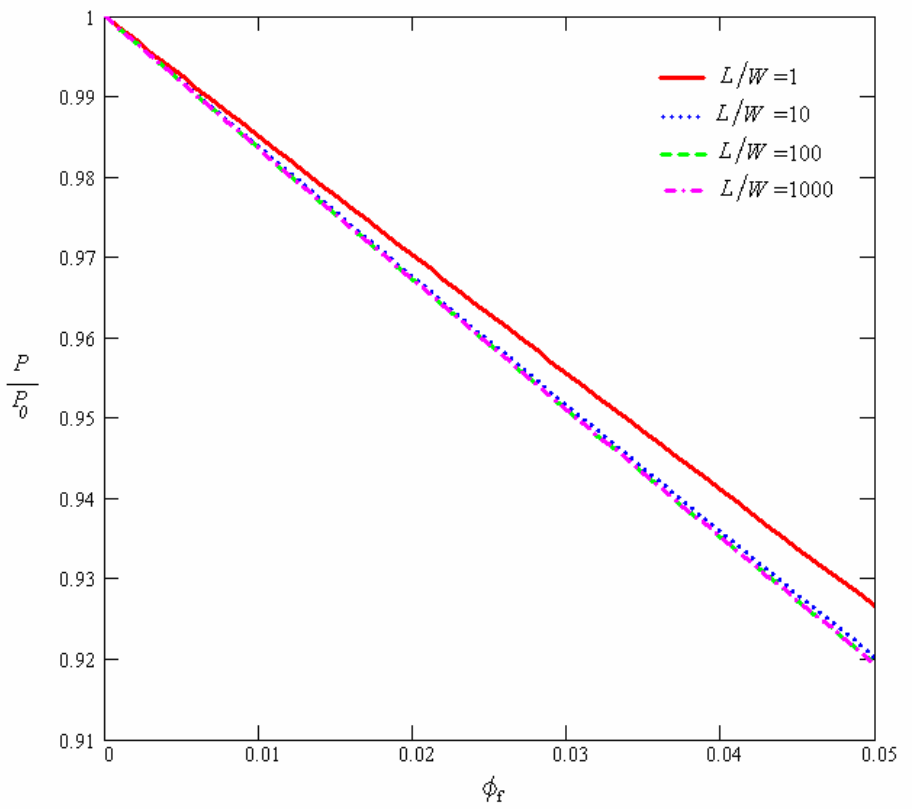

Figure 4.3. Relative permeability for different concentration and aspect ratio of inclusions

The results obtained in the case of higher values of the aspect ratio, which corresponds to platelet shape inclusions, such as nanoclays, are close to the formula:

$$\langle P \rangle \approx P_0 \left(1 - 1.6\Phi_f\right) \tag{33}$$

As it is noted this is very close to the Maxwell's degenerated formula given in equation (32).

Usually, in the case of nanocomposites the system is considered as non-permeable inclusions in small volume concentrations, and in this case it is possible to use a formula similar to (32) and (33).

$$\langle P \rangle \approx P_0 \left(1 - \alpha\Phi_f\right) \tag{34}$$

where α is a numerical coefficient depending on the shape of inclusions, their orientation, and on their type of the spatial lattice. Normally, the role of spatial lattice is less studied but it is known that it is important in the cases of high concentrations and platelet shaped inclusions. The values of the coefficient α for different shapes and orientations of nanoinclusions are collected in Table 4.1.

Table 4.1. Values of the coefficient α in formula (34) for different shapes of inclusions and their orientations with respect to the flow

Shape	Orientation	α
Spherical		1.5
Platelets	Random	1.6
Platelets	Parallel to flow	1.0
Platelets	Perpendicular to flow	3.0
Fibers	Parallel to flow	1.0
Fibers	Perpendicular to flow	2.0

The role of the orientation of the platelets is shown also on the Figure 4.4. As it is observed when the platelets are oriented perpendicular to the flow, the decrease in permeability is more effective.

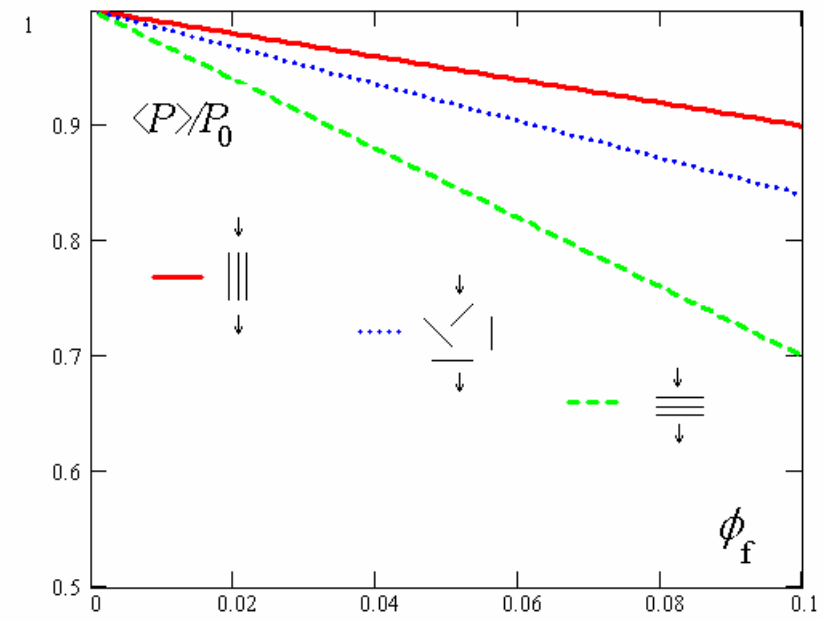

Figure 4.4. Role of the orientation of the platelets in the permeability

When the permeability is studied in thin films, the orientation of the platelets is not random; a big percentage of them are parallel to the film's plane. Experimental results are more close to the case of platelets orientation perpendicular to the flow. The equation showed in formula (34) corresponds to the random lattice, such as on the Fig. 4.2. (c).

There are other factors playing some role in the permeability of nanocomposites. The nucleation ability of the particles could create small layers of modified matrix near the surface of the particles where the ability of the segments of polymeric molecules to move is restricted. These layers having different properties (including permeability) than the remaining matrix would contribute to the total permeability of the system. Also pores, concentration of which is usually increased with the number of inclusions per volume unit and with the total volume concentration of inclusions, also contribute to the total permeability.

4.7. Effect of the interface clay-polymer in the permeability

The fact that the clay and polymer may interact and the existence of an interface were considered in the conceptual model proposed by G. W. Beall [27]. In this model there are three distinctive regions defined around the nanoclays. The first region of 1-2 nm is near the surface of the nanoclay and is occupied by the surface modifier used to make the clay compatible to the polymer. The second region was called the constrained polymer region and is about 50-100 nm wide. The width of this area would depend on the type of bonding between the surface modifier and the polymer, the strength interaction between polymer molecules and the extent of nucleation imparted by the clay. The third region is the unconstrained polymer with properties like those of the neat polymer.

The permeability in each of the regions varies and several cases were studied by Beall. One of the most interesting cases is when the permeability of the surface area (P_s) and the constrained polymer (P_c) is lower than that of the neat polymer. When this happens, the constrained polymer area will become a barrier and the permeant will go preferably through the polymer.

In this particular case of an interface with smaller permeability than that of the pristine polymer, the actual aspect ratio of the nanoclay would be affected. It would not be considered anymore as a thin layer, but the thickness would actually increase to have almost an aspect ratio of 1. The schematic for this system is presented below. In this system the length of the clay is L, and the total width is $W_T = W_c + W + W_s$. Where W_c is the thickness of the constrained polymer area, W_s the thickness of the surface modifier area and W is the clay thickness.

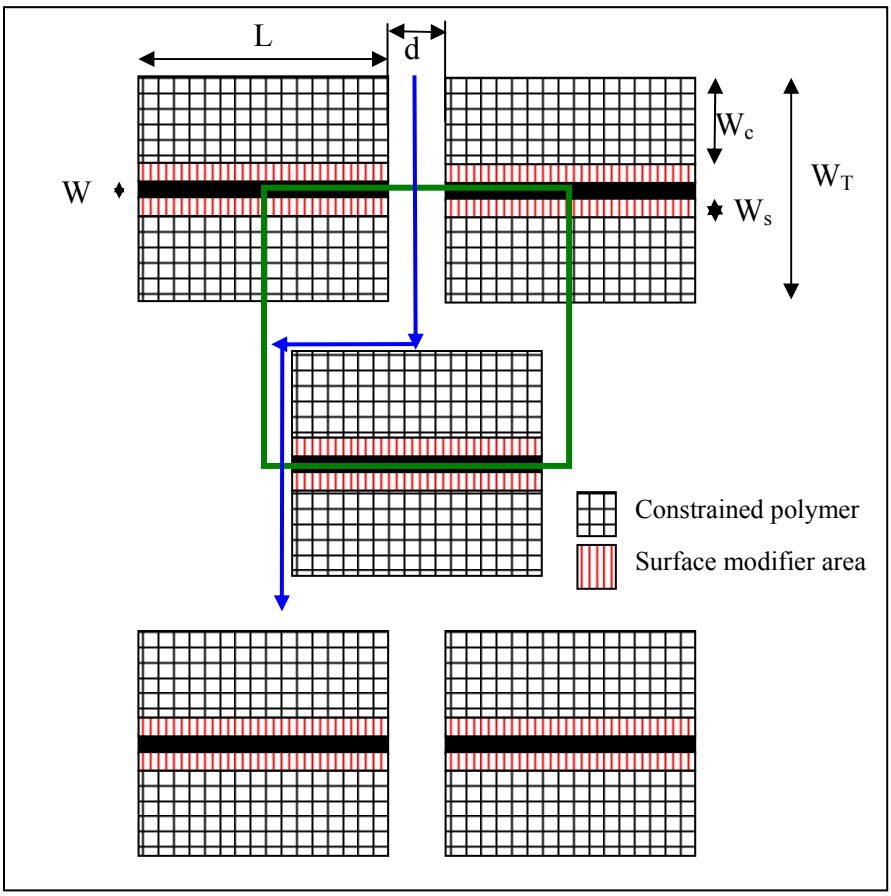

Figure 4.5. Effect of the interface in the tortuous path

Using this geometric model that accounts for the interface of clay-polymer, an approximation of the permeability was obtained. Yu [28] studied the tortuosity factor of this specific geometric consideration, obtaining the value of τ for a set of particles in a porous media.

This case would correspond to a set of un-overlapped particles; the path followed by the permeant in the unit cell, marked in green, is shown in the schematic above. The actual length of the flow is shown in blue and the definition of tortuosity is given as the ratio of the actual length of the flow path and the straight length or thickness of a unit cell ($\tau = L_e/L$). According to the calculation done by Yu, the tortuosity in this configuration was defined as:

$$\tau = 1 + \frac{1}{2}\sqrt{1 - \Psi} \tag{35}$$

Where Ψ, is the porosity, defined as the ratio between the volume of the pores and the volume of the unit cell.

Taking this definition of the tortuosity into the formula (21) it was obtained a new relationship for the permeability that accounts for a higher aspect ratio of the clays.

$$\frac{P}{P_0} = \frac{1 - \Phi_f}{1 + \frac{1}{2}\sqrt{1 - \Psi}} \tag{36}$$

The values obtained with this model are shown in the next chapter.

4.8. References

[1] J. Crank, G.S. Park. Diffusion in polymers. Academic Press, London 1968

[2] M.H. Klopffer, B. Flaconnèche. Oil & Gas Science and Technology 2001; 56: 3: 223-244

[3] F. Muller-Plathe. Acta Polymer 1994; 45: 259-293

[4] C. E. Rogers. Permeation of gases and vapours in polymers. In: J. Comyn. Polymer permeability. Elsevier; 1985: 11-73

[5] J. Crank. The mathematics of diffusion. 2nd Ed. Clarendon Press, Oxford 1975

[6] S. Alexander Stern. Polymers for gas separations: the next decade. Journal of Membrane Science 1994; 94: l-65

[7] F. Muller-Plathe. J.Chem.Phys. 1991; 94 :4:1

[8] J.S. Vrentas, J.L. Duda, H.-C. Ling. J. Polym. Sci., Polym. Phys. Ed.1985; 23: 275

[9] J.S. Vrentas, J.L. Duda, H.-C. Ling, A.-C. Hou. J. Polym. Sci., Polym. Phys. Ed. 1985; 23: 289

[10] J.S. Vrentas, J.L. Duda, H.-C. Ling. Journal of Membrane Science 1989; 40: 101-107

[11] M. Cohen, D Turnbull. The Journal of Chemical Physics 1959; 31: 5

[12] Fujita, H. Fortschr Hochpolym Forsch 1961, 3, 1

[13] J. S. Vrentas, J. L. Duda. Macromolecules 1976; 9: 785

[14] J. S. Vrentas, C. M. Vrentas. Journal of Polymer Science: Part B: Polymer Physics 2003; 41: 501–507

[15] J. H. D. Boshoff, R. F. Lobo, N. J. Wagner. Macromolecules 2001; 34: 6107-6116

[16] H. R. Lusti, A. A Gusev, O. Guseva. Modelling Simul. Mater. Sci. Eng. 2004; 12: 1201–1207

[17] Z.F. Wang, B. Wang, N. Qi, H.F. Zhang, L.Q. Zhang. Polymer 2005; 46: 719–724

[18] K. Yano, A. Usuki, A. Okada, T. Kurauchi, O. Kamigaito. Journal of Polymer Science, part A: Polymer chemistry 1993; 31: 2493-2498

[19] G. H. Fredrickson, J. Bicerano. Journal of Chemical Physics 1999; 110: 4

[20] E.L. Cussler, S.E. Hughes, W. J. Ward, III, R. Aris. Journal of Membrane Science 1988; 38: 161-174

[21] A. A. Gusev, H.R. Lusti. Adv. Mater. 2001; 13: 21

[22] R. K. Bharadwaj. Macromolecules 2001; 34: 26

[23] J.C. Maxwell. Treatise on electricity and magnetism, 1873

[24] A. Beyle. Role of the lattice of inclusions in physical properties of composites and nanocomposites. Journal of Composite Materials. (Prepared for submission in 2007)

[25] H. Fricke. Phys. Rev., 1924; 24: 575-587

[26] A. Beyle, D.L. Cocke. Nanoeffect in different types of nanocomposites: possible explanations. ICCE-10 Tenth Annual International conference on composites/nano engineering. New Orleans, 2003: 56

[27] G.W. Beall Conceptual model for interpreting nanocomposite behavior, in Polymer clay-nanocomposites. T. J. Pinnavaia, G. W. Beall. Wiley 2000; 267-279

[28] B-M. Yu, J.-H. Li. Chin

CHAPTER 5

EXPERIMENTAL RESULTS

In this chapter the results of the experimental part are presented. First the selection of the duration of the permeability test was done. After the parameters of the permeability test were selected the leak rate was measured and the permeability coefficient calculated. The samples were characterized with the help of the DMA, DSC and TGA machines. Morphology of the samples was observed with XRD and TEM. Calculations of the free volume were done with the results obtained from the PAS test. The specimens were subjected to severe thermal cycling and the effects of this environmental change were analyzed in the leak detector and compared with all the measurements performed before thermal aging.

5.1. Permeability tests

The values obtained from the helium leak detector were given as flow rate values (atm-cc/s). The area of flow was taken into consideration and then the permeability coefficient was calculated in square meters for each specimen using Darcy's law. The surface area specific volume flow rate was calculated in cubic meter of gas per square meter of exposed material per second at $1.38 \cdot 10^5$ Pa (20 psi) differential pressure across the specimen.

The formula used in the calculation is:

$$K_P = \frac{Q \cdot \mu \cdot L}{\Delta p} \qquad (1)$$

Where Q is the flow rate obtained from the tests after it is reached a steady state value per area of the sample. The units are in m/s.

The viscosity for He is $\mu = 1.78 \cdot 10^{-5}$ Pa·s. L is the thickness in meter of the specimens, measured in 5 different points of the samples with a calibrated dial gage and then averaged. See Table 5.1 for values. The differential pressure is $\Delta p = 20$ psi which was converted to Pascal to be consistent with the units chosen.

Table 5.1. Thickness of specimens

number	Sample	thickness (m)	number	Sample	thickness (m)
32	862-0/1	0.00078	19	826-30B-5/2	0.00247
5	862-0/2	0.00105	29	826-B18-2/1	0.00212
20	862-0/3	0.00067	21	826-B18-2/2	0.00234
4	862-30B-2/1	0.00228	24	826-B18-2/3	0.00238
26	862-30B-2/2	0.00228	13	826-B18-5/1	0.00145
28	862-30B-2/3	0.00231	x	826-B18-5/2	0.00155
16	862-30B-5/1	0.00255	15	8552-0/1	0.00108
31	862-30B-5/2	0.00180	10	8552-0/2	0.00095
6	862-B18-2/1	0.00216	14	85521-0/1	0.00198
27	862-B18-2/2	0.00202	22	85521-0/2	0.00202
18	862-B18-2/3	0.00210	2	85521-0/3	0.00207
33	862-B18-5/1	0.00188	12	M72-0/1	0.00133
30	862-B18-5/2	0.00125	11	M72-0/2	0.00138
8	826-0/1	0.00244	25	M72-0/3	0.00122
17	826-0/2	0.00140	1	9772-B18-2/1	0.00195
9	826-30B-2/1	0.00256	34	9772-B18-2/2	0.00171
23	826-30B-2/2	0.00237	35	9772-0/1	0.00132
3	826-30B-2/3	0.00183	36	9772-0/2	0.00129
7	826-30B-5/1	0.00233			

It is necessary to mention that permeability measurements are dependant of the procedure used to calculate it. Agreement with other methods is material dependant and the conditions of the test must be specified.

Permeability can be reported as flow values in std. $cc/s/in^2$ which is useful to understand the rate of loss of gas per unit area; however it must be specified the gas used in the measurements, the temperature of the observed flow, the pressure differential across the leaking surface and the thickness of the material tested [1].

In order to select the appropriate duration of the permeability test some trial measurements were done. Some of the samples were selected randomly and run for 20 hours period. After observing the data for the leak rate it was determined that the stable value is reached approximately after 400-450 minutes. The steady-state region can be observed in Figure 5.1.

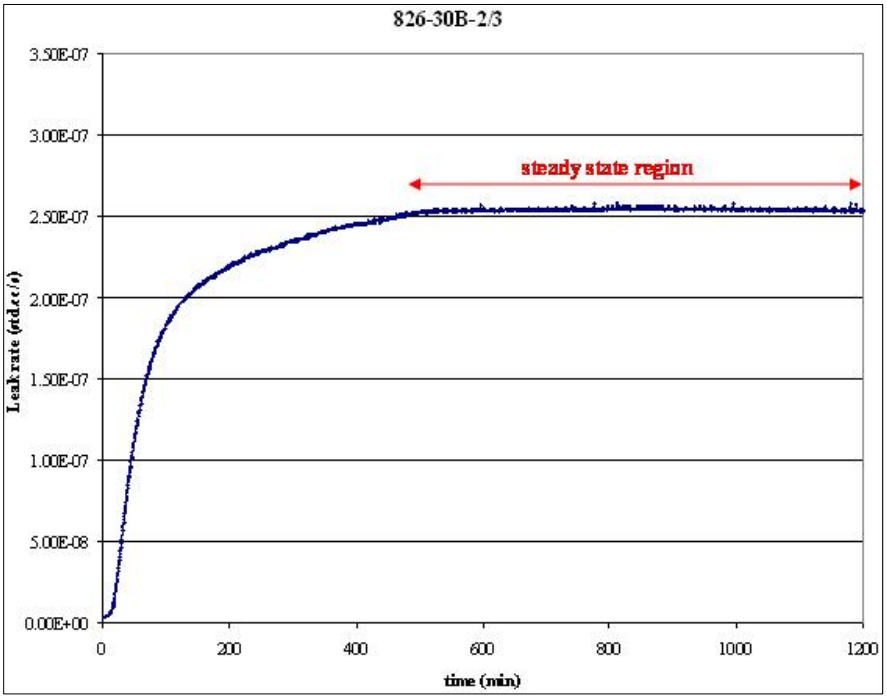

Figure 5.1. Leak rate graph for 20 hours test

The values of the permeability coefficient were calculated with the data from 20 hours and the data for 12 hours tests. The values obtained are plotted in figure 5.2.

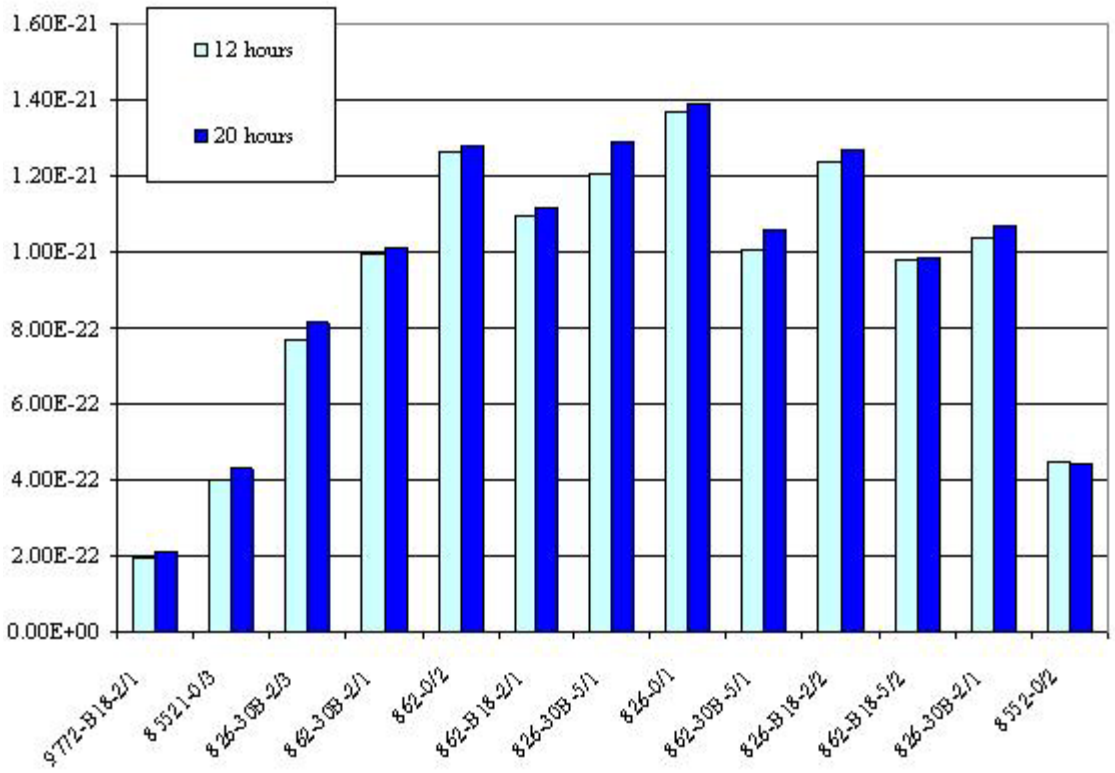

Figure 5.2. Comparison of the permeability coefficient for 12 and 20 hours tests

These coefficients were statistically compared to study the error of taking 12 hours data instead of 20 hours data.

The statistical analyses done are summarized below.

Box-plot analysis:

The box-plot summarizes the following statistical measures: median, upper and lower quartiles and minimum and maximum data values. Box-plots have the following strengths [2]:

- Graphically display a variable's location and spread at a glance.
- Provide some indication of the data's symmetry and skewness.
- Unlike many other methods of data display, box-plots show outliers.
- By using a box-plot for each categorical variable side-by-side on the same graph, one quickly can compare data sets.

It can be observed in Figure 5.3 that the data for the permeability coefficients are very similar, there is symmetry and the two populations are not skewed.

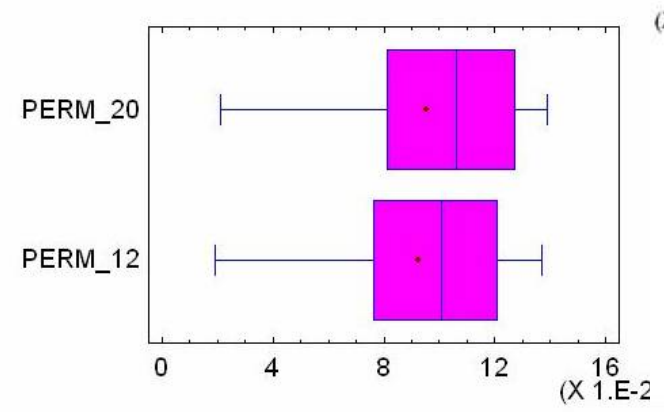

Figure 5.3. Box-plot for the permeability coefficients

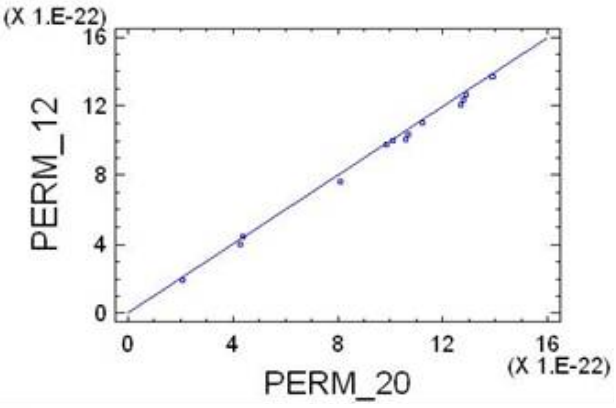

Figure 5.4. Quantile-quantile plot

Quantile-Quantile Plot:

The quantile-quantile (q-q) plot is a graphical technique for determining if two data sets come from populations with a common distribution.

A q-q plot is a plot of the quantiles of the 12 hours run against the quantiles of the20 hours run. By a quantile, it is meant the fraction of points below the given value. That is, the 0.3 (or 30%) quantile is the point at which 30% percent of the data fall below and 70% fall above that value. A 45-degree reference line is plotted and if the two sets come from a population with the same distribution, the points should fall approximately along this reference line. The greater the departure from this reference line, the greater the evidence for the conclusion that the two data sets have come from populations with different distributions [3].

It can be observed in the Figure 5.4 that the data are very close to the 45 degree reference line and therefore we can assume that the two sets of data come from populations with the same distribution.

The distribution of both populations and the density has also been calculated and the results are shown in Figure 5.5 and 5.6. It can be observed that the results are quite similar and therefore we can assume that there is no significant error when we consider samples tested for 12 hours instead of 20 hours.

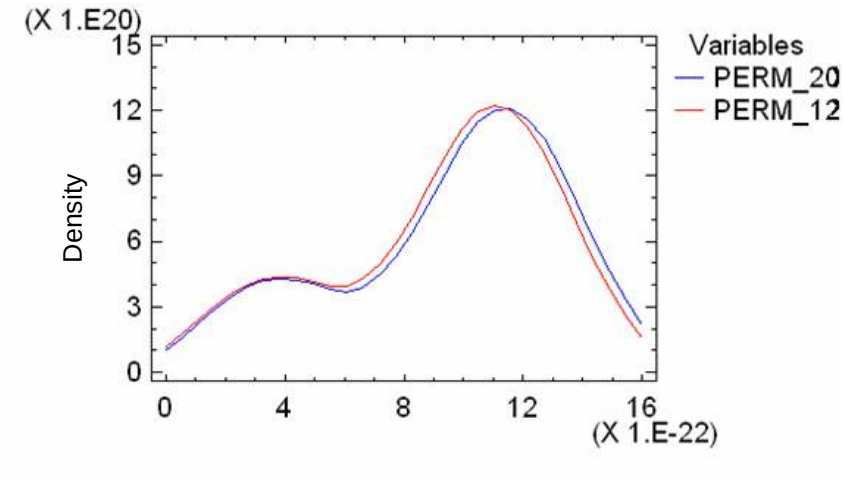

Figure 5.5. Density function

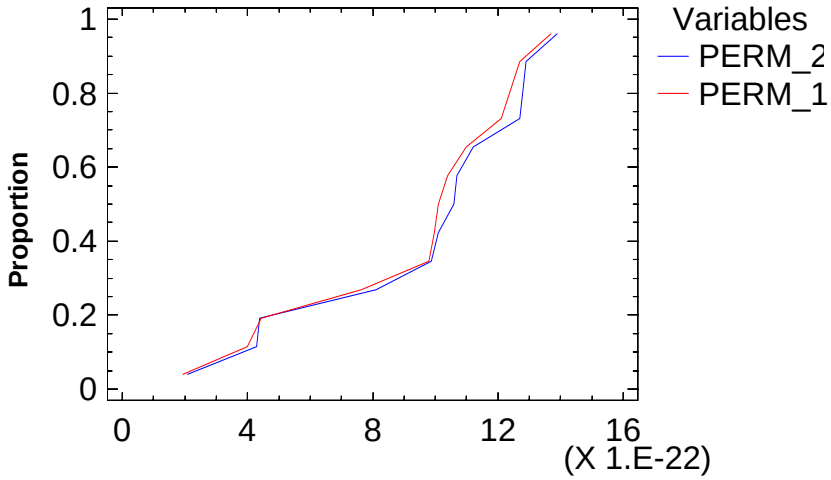

Figure 5.6. Empirical distribution of samples

An important analysis done to compare the permeability coefficients for 12 and 20 hours was the hypothesis test. Three different hypotheses were considered. First the mean for the coefficients for 12 and 20 hours were compared and determined if there was any significant difference in their values. A second hypothesis tests studied the difference between the variance of the two populations and a third analysis would confirm if the medians were similar or not.

Mean analysis The following null hypothesis was considered:

$$H_0 : PERM\_12 = PERM\_20$$

The alternative hypothesis was:

$$H_1 : PERM\_12 \neq PERM\_20$$

A t-test is performed to contrast the means from the two populations. The value obtained was t = 0.586155 and P-Value = 0.563244.

It is of particular interest to see that the confidence interval for the difference between the means ranged from -2.12547E-22 to 3.81162E-22. Since the interval included the value 0, then it can be concluded that there was no statistically significant difference between the means of the two populations at a confidence level of 95%.

A hypothesis test was performed to determine if the difference between the two means is equal to zero (null hypothesis) against the alternative hypothesis that the difference was not zero. Since the P-value was bigger than 0.05, the null hypothesis can be accepted, and therefore it was concluded that the permeability coefficient for the two populations is not statistically different.

Variance analysis The previous results assumed that the variance of the two sample population was equal, therefore a new hypothesis contrast is needed to verify this assumption.

To compare variances, an F contrast test was carried out. The null hypothesis was as follows:

$$H_0 : \sigma_1 = \sigma_2$$

And the alternative hypothesis was:

$$H_1 : \sigma_1 \neq \sigma_2$$

The results of the F-test performed to compare the variance of the samples were F = 1.09833 and a P-Value = 0.873613. The confidence interval for the ratio of the variance ranged from 0.335134 to 3.59952. Since the interval included the value 1, it is concluded that there was no statistically significant difference between the variance of the two populations at a confidence level of 95%. The F-test also determined if the standard deviations were equal against the alternative hypothesis of being different. Since the P-value is bigger than 0.05, the null hypothesis was accepted.

Median analysis In order to compare the medians, a Mann-Whitney (Wilcoxon) W-test was performed. The null hypothesis was the following:

$$H_0 : median_1 = median_2$$

And the alternative hypothesis was:

$$H_1 : \ median_1 \neq median_2$$

The average rank of the samples from population 1 was 14.6923. For the samples from population 2, it was 12.3077. The Mann-Whitney W test had a value of W= 69.0 and the P-Value = 0.441598. This test combined the two populations, organized the data from the smaller to the bigger values and then compared the average ranks of the two populations of the combined data. Since the P-value was bigger than 0.05, it is concluded that there was no statistically significant difference between the medians at a confidence level of 95%.

After examining the results of the statistical calculation it was determined that the permeability test would run for 12 hours. The leak rate was measured four times for each sample, the permeability coefficient was calculated following the procedure outlined before and the results averaged. Some of the most representative leak rate graphs are displayed in Figures 5.7 to 5.14. A summary of the permeability coefficient results is shown if the following table.

Table 5.2. Permeability coefficient values (m^2)

Sample	number	thickness (m)	differential pressure (Pa)	steady state leak rate/ area (m/s)	Permeability coefficient (m^2)*10^{-22}	standard dev.*10^{-22}
826-0	17	0.00140	$1.38*10^5$	$8.59*10^{-9}$	16.93	1.05
826-30B-2	23	0.00237	$1.38*10^5$	$4.69*10^{-9}$	14.25	0.1
826-30B-5	19	0.00247	$1.38*10^5$	$3.90*10^{-9}$	11.9	1.16
826-B18-2	21	0.00234	$1.38*10^5$	$4.23*10^{-9}$	13.58	0.79
826-B18-5	13	0.00145	$1.38*10^5$	$6.49*10^{-9}$	12.68	0.6
862-0	5	0.00105	$1.38*10^5$	$9.32*10^{-9}$	13.28	0.57
862-30B-2	26	0.00228	$1.38*10^5$	$3.45*10^{-9}$	11.18	0.75
862-30B-5	31	0.00180	$1.38*10^5$	$4.65*10^{-9}$	11.55	0.56
862-B18-2	27	0.00202	$1.38*10^5$	$4.25*10^{-9}$	12.03	0.65
862-B18-5	30	0.00125	$1.38*10^5$	$6.48*10^{-9}$	10.72	0.82
9772-0	36	0.00129	$1.38*10^5$	$4.68*10^{-9}$	8.03	0.55
9772-B18-2	34	0.00171	$1.38*10^5$	$3.58*10^{-9}$	8.76	0.62

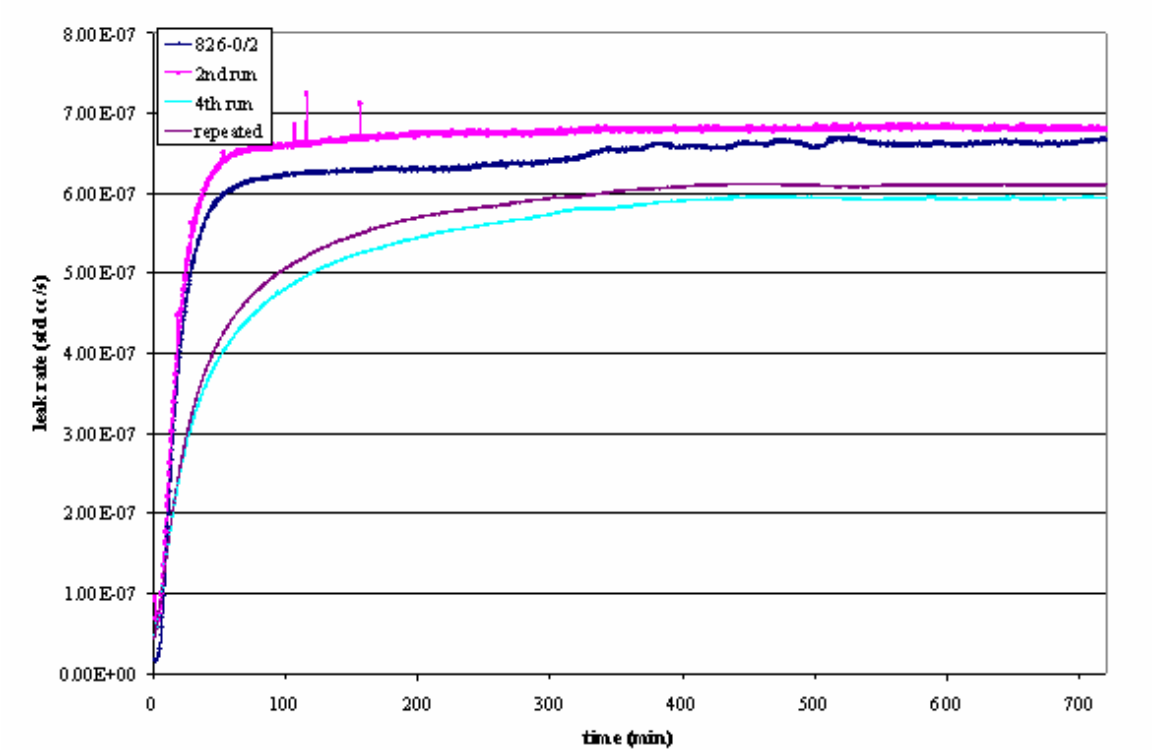

Figure 5.7. Leak rate of Epon™826 non-modified

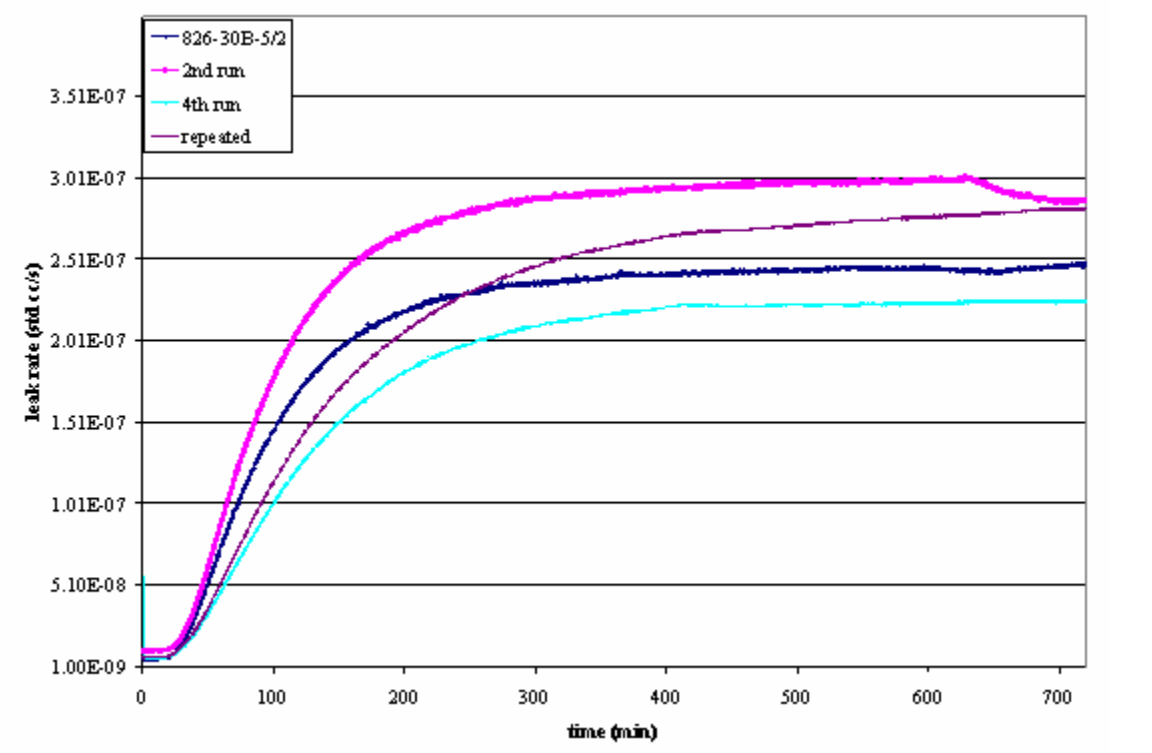

Figure 5.8. Leak rate of Epon™826 modified with 5wt% of Cloisite®30B

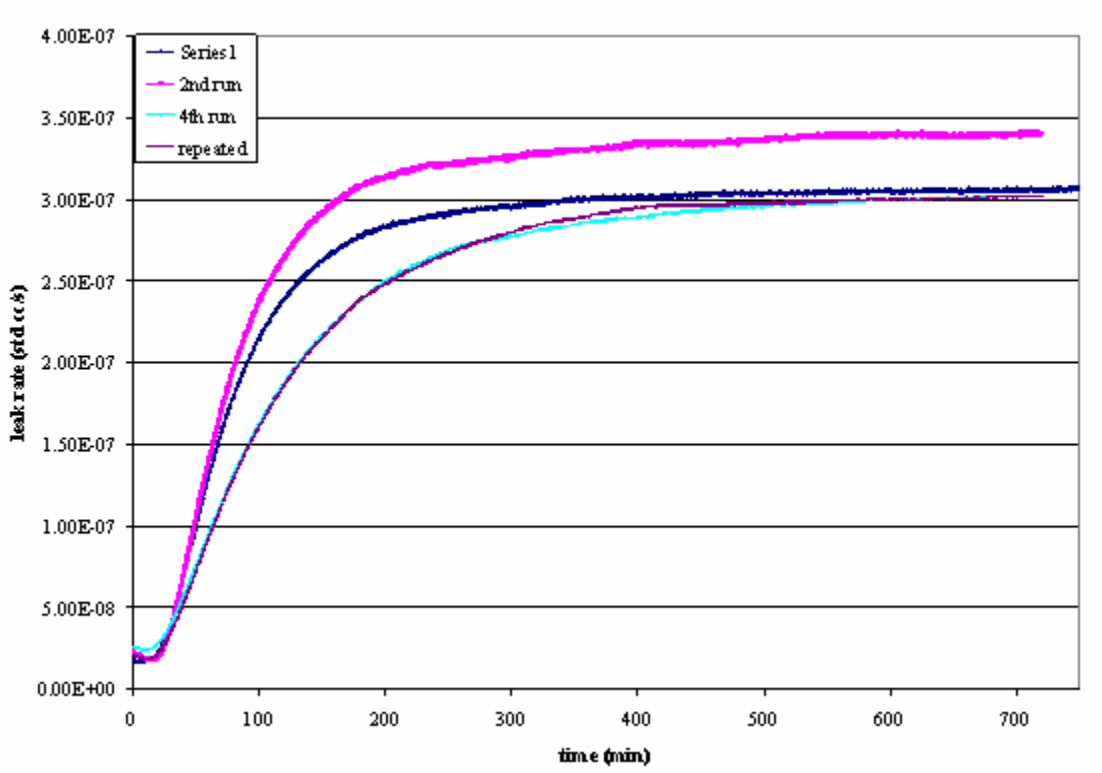

Figure 5.9. Leak rate of Epon^{TM}826 modified with 2wt% of nanoclay B18

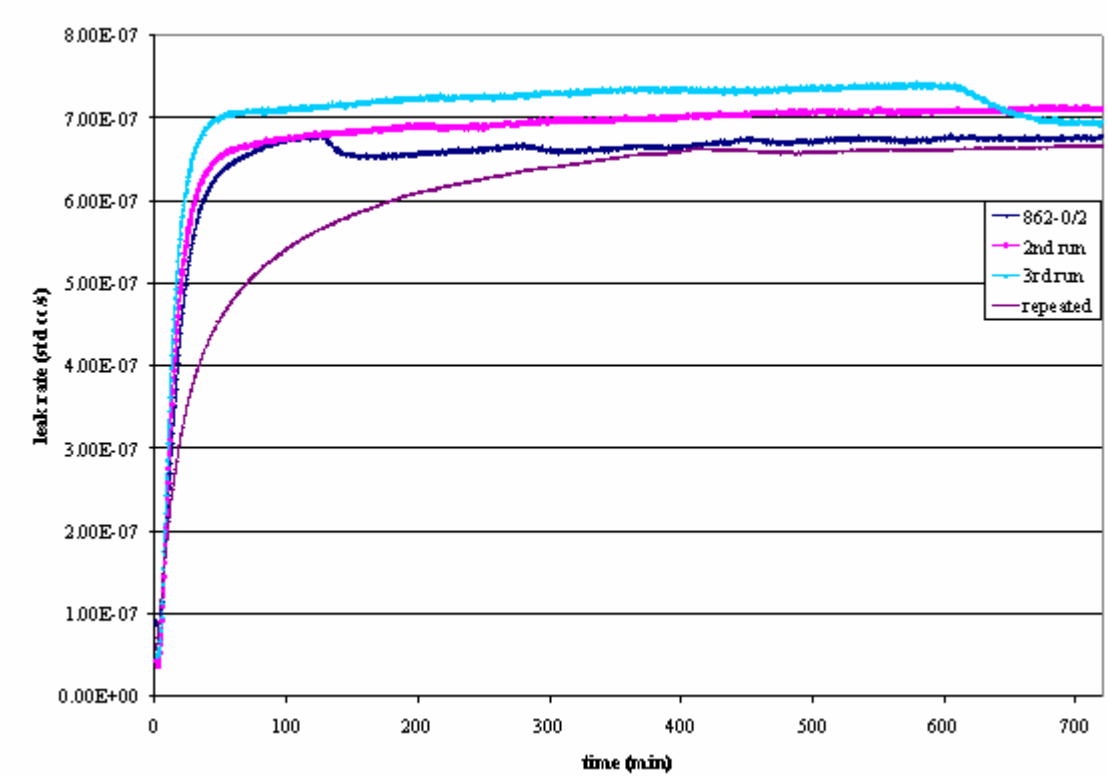

Figure 5.10. Leak rate of Epon^{TM}862 non-modified

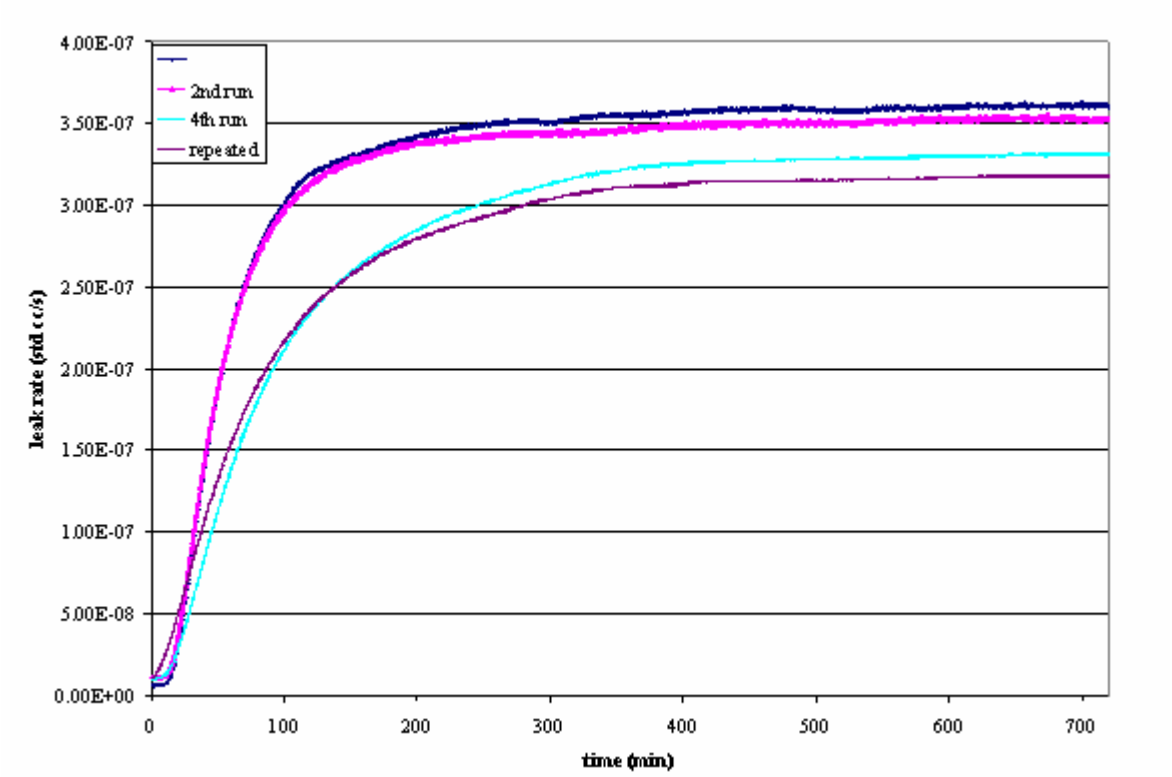

Figure 5.11. Leak rate of Epon™862 modified with 5wt% of Cloisite®30B

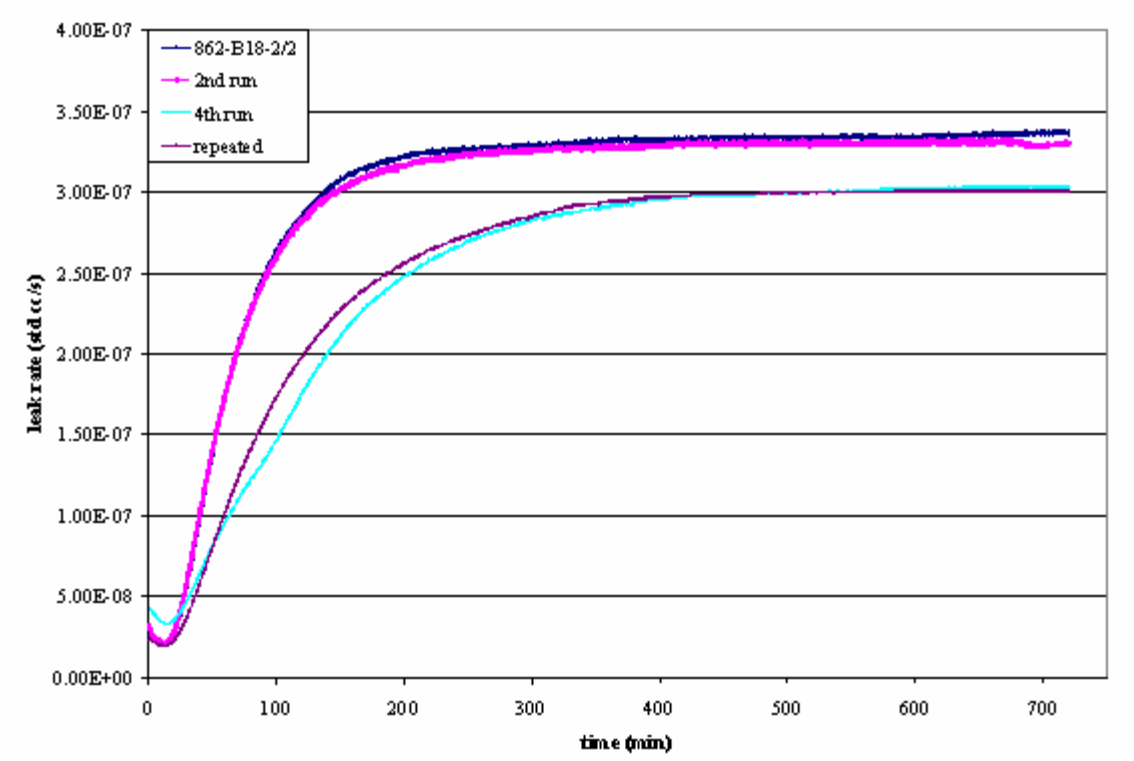

Figure 5.12. Leak rate of Epon™862 modified with 2wt% of nanoclay B18

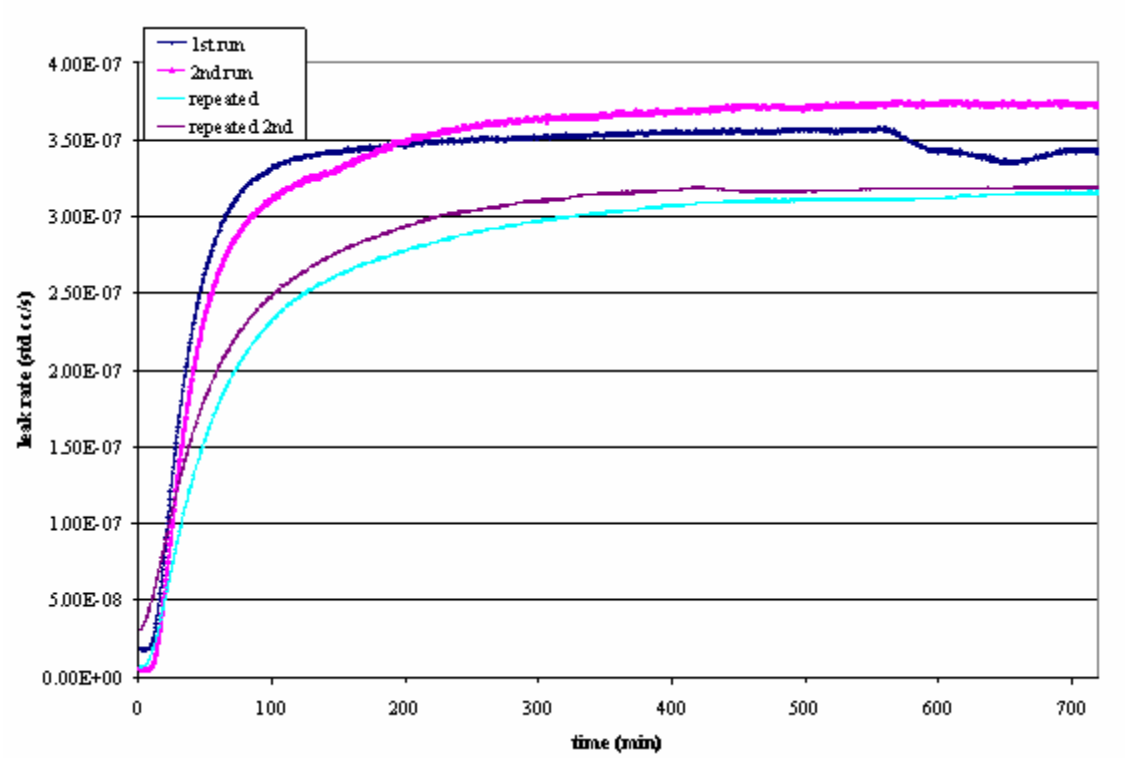

Figure 5.13. Leak rate of Cycom®977-2 non-modified

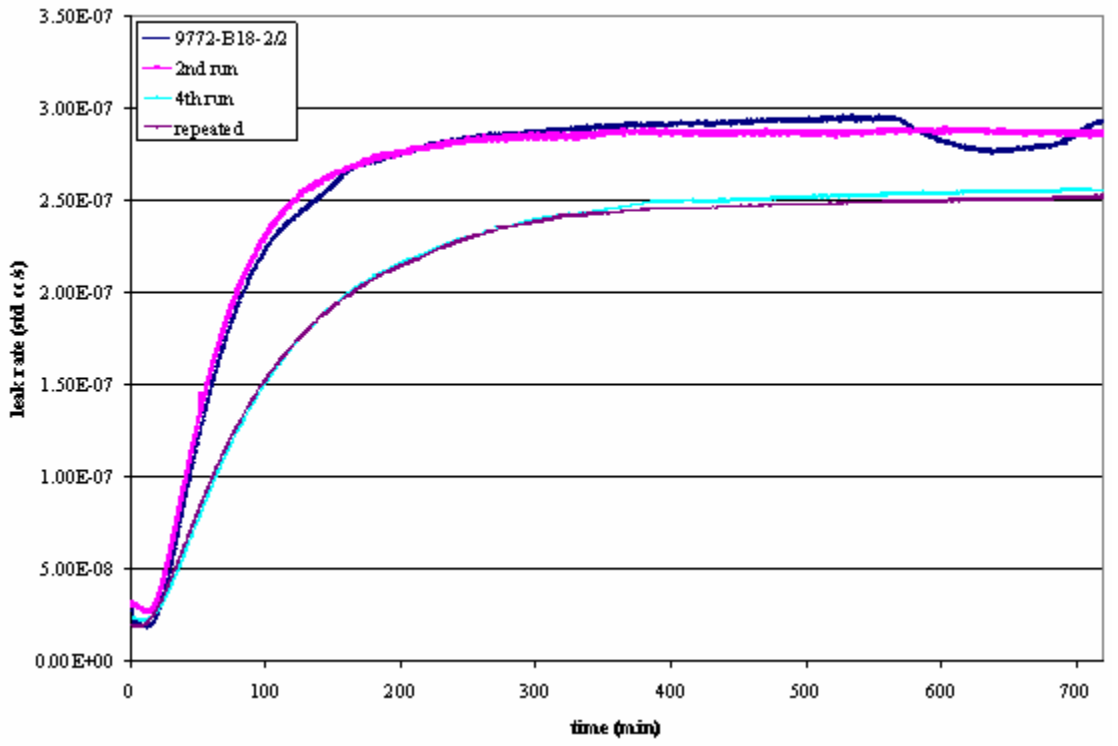

Figure 5.14. Leak rate of Cycom®977-2 modified with 2wt% of nanoclay B18

A summary of the values of the permeability coefficient are represented in Figure 5.15.

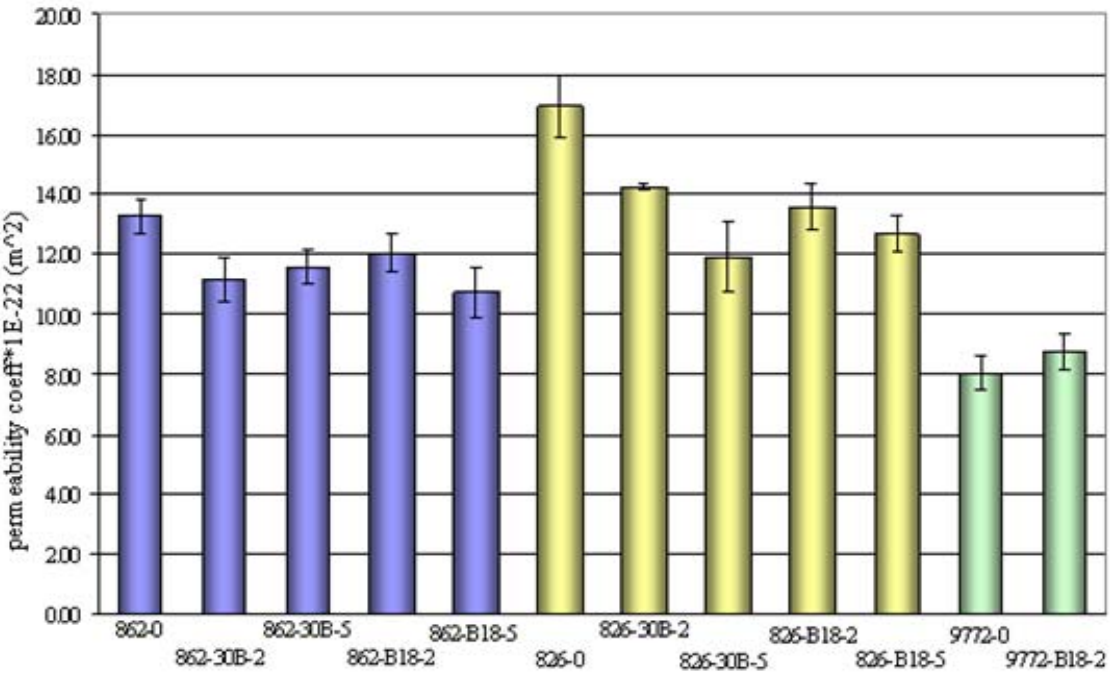

Figure 5.15. Permeability coefficient (m^2) values

As it is observed in the above figure, the addition of nanoclays decreased the permeability of helium when compared to non-modified samples in the mentioned conditions of room temperature and an applied differential pressure of $1.38*10^5$ Pa.

Samples manufactured from Epon™826 showed in general higher reduction of the permeability to helium than samples from Epon™862. The highest decrease in the permeability when compared to the neat resin Epon™826 was observed in samples modified with 5wt% of Cloisite®30B where a decrease of 29% on the permeability coefficient was noticed. It is observed in general that the addition of 5wt% of nanoclays is more effective in the reduction of the permeability than the addition of 2wt%. It is usually assumed that the random arrangement of the nanoclays in the polymeric matrix increases the path of the diffusing gas into the sample and therefore decreases the permeability. The good dispersion/exfoliation of the nanoclays is vital in achieving the desired improvements. The amount of nanoclays plays an important role as well, when the amount of nanoclays is too high the particles start to agglomerate and the benefits of their addition are not longer observed.

5.2. DMA results

The purpose of the DMA tests was to observe the loss modulus and storage modulus of the neat resin and compared them with the nano-modified resins in order to understand the effect of the addition of nanoclays in the microscopic mechanical behavior.

The DMA tests can also be used to evaluate the glass transition temperature (T_g) but in this work the T_g was evaluated with DSC tests instead.

The graphs obtained are shown in Figures 5.16 to 5.21.

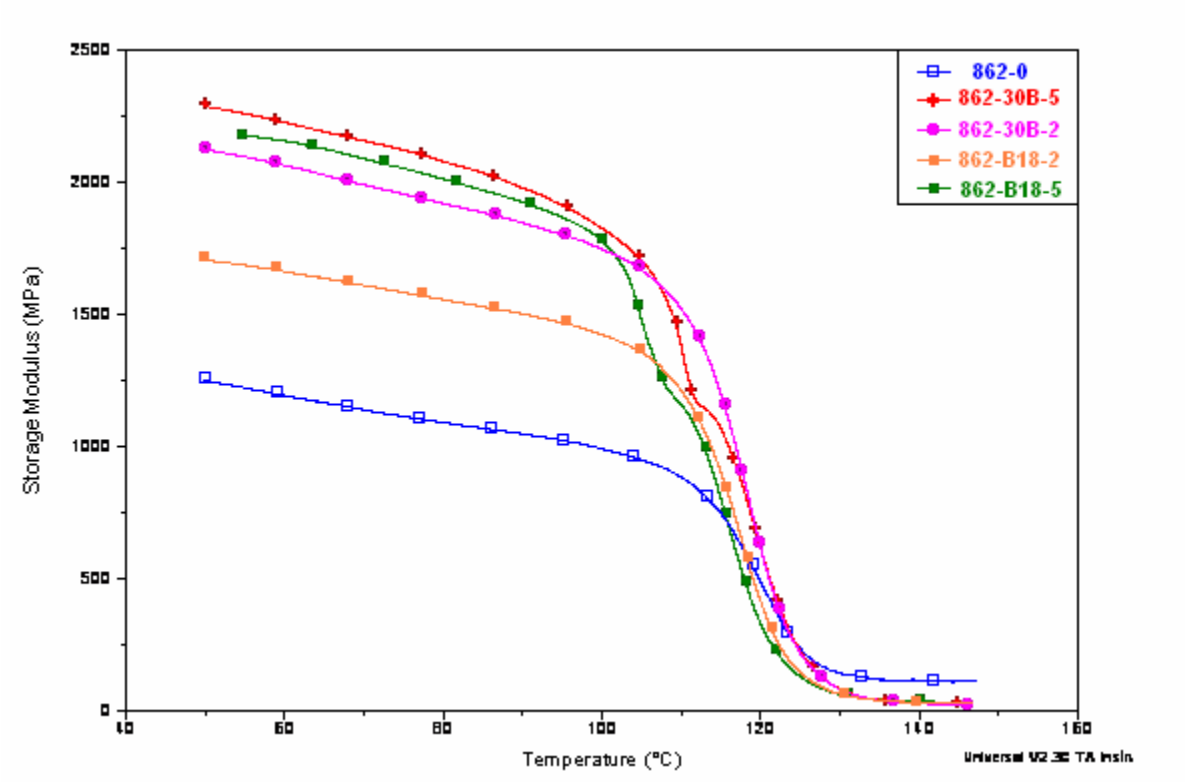

Figure 5.16. Comparison of storage modulus for Epon™862 samples

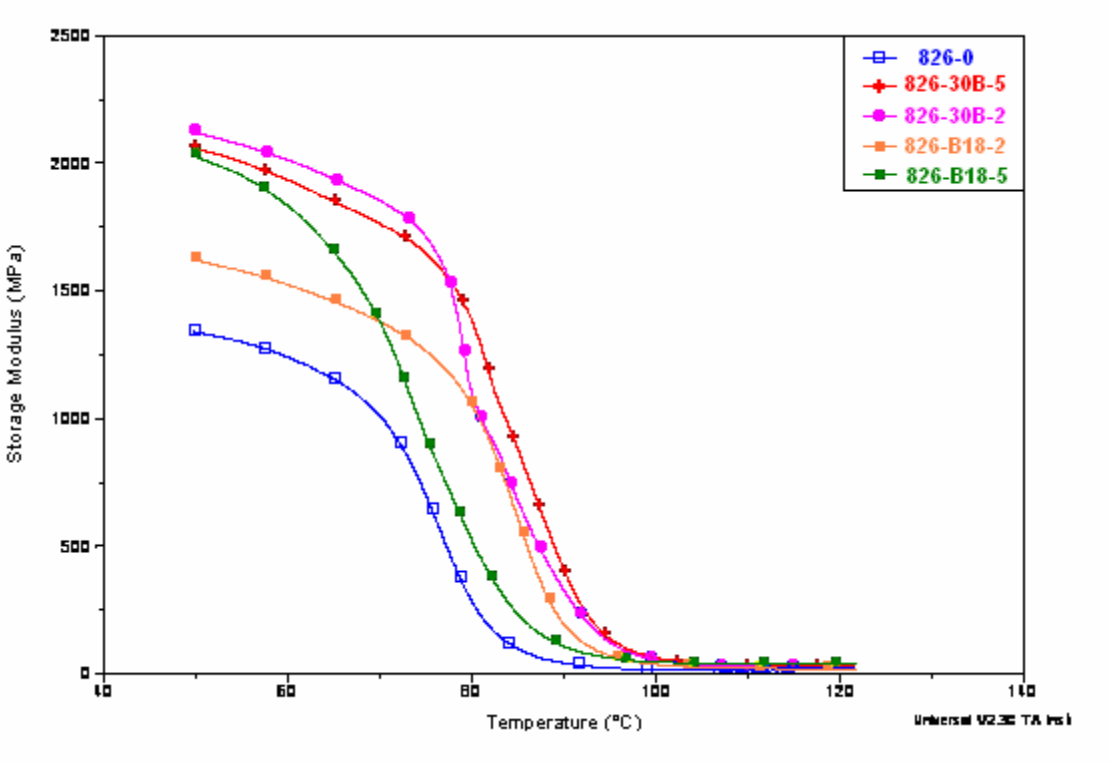

Figure 5.17. Comparison of storage modulus for Epon^{TM}826 samples

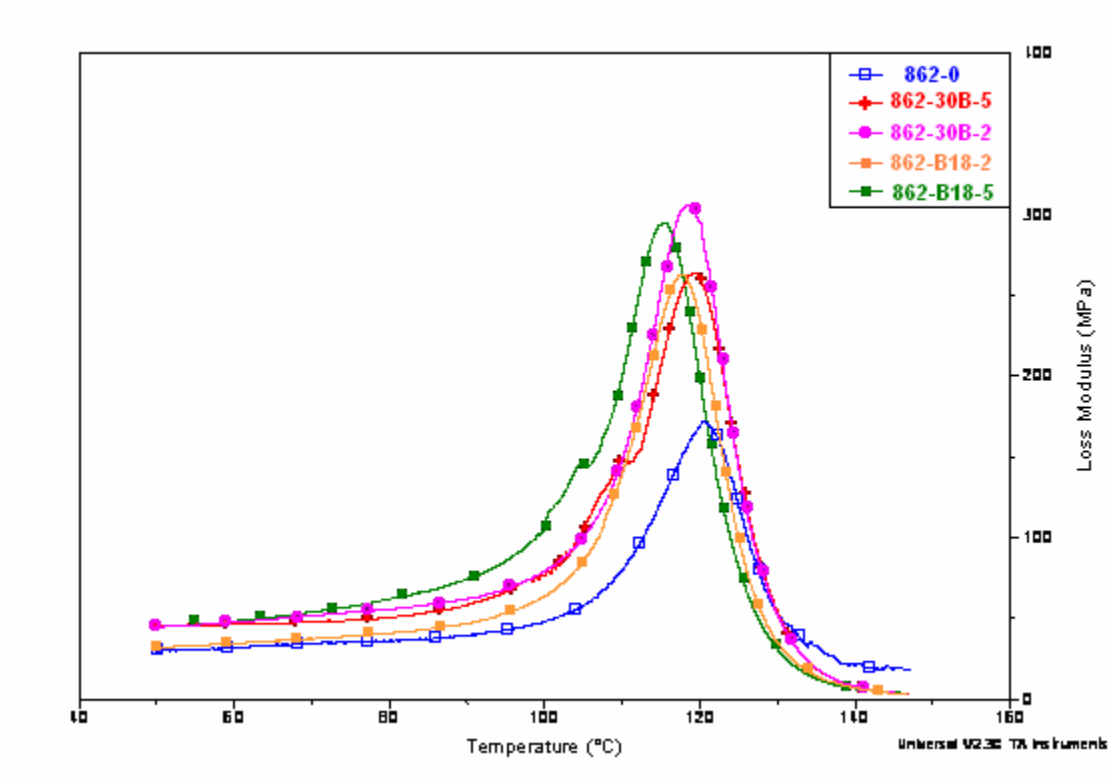

Figure 5.18. Comparison of loss modulus for Epon^{TM}862 samples

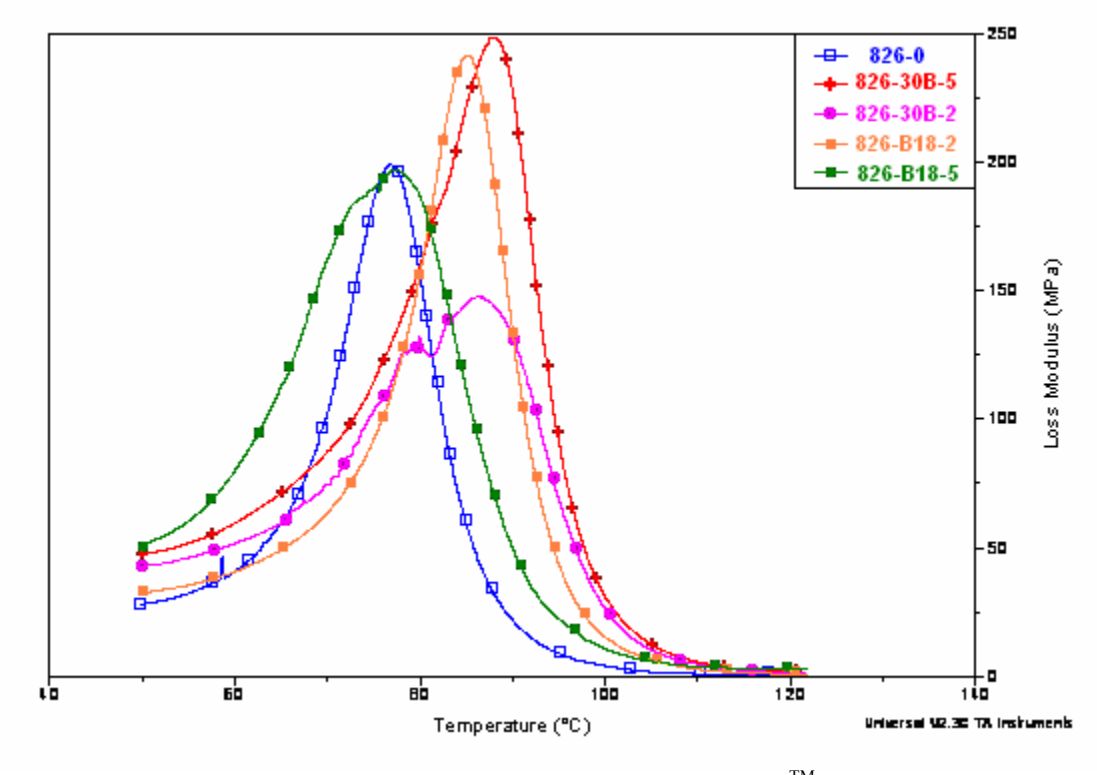

Figure 5.19. Comparison of loss modulus for Epon™826 samples

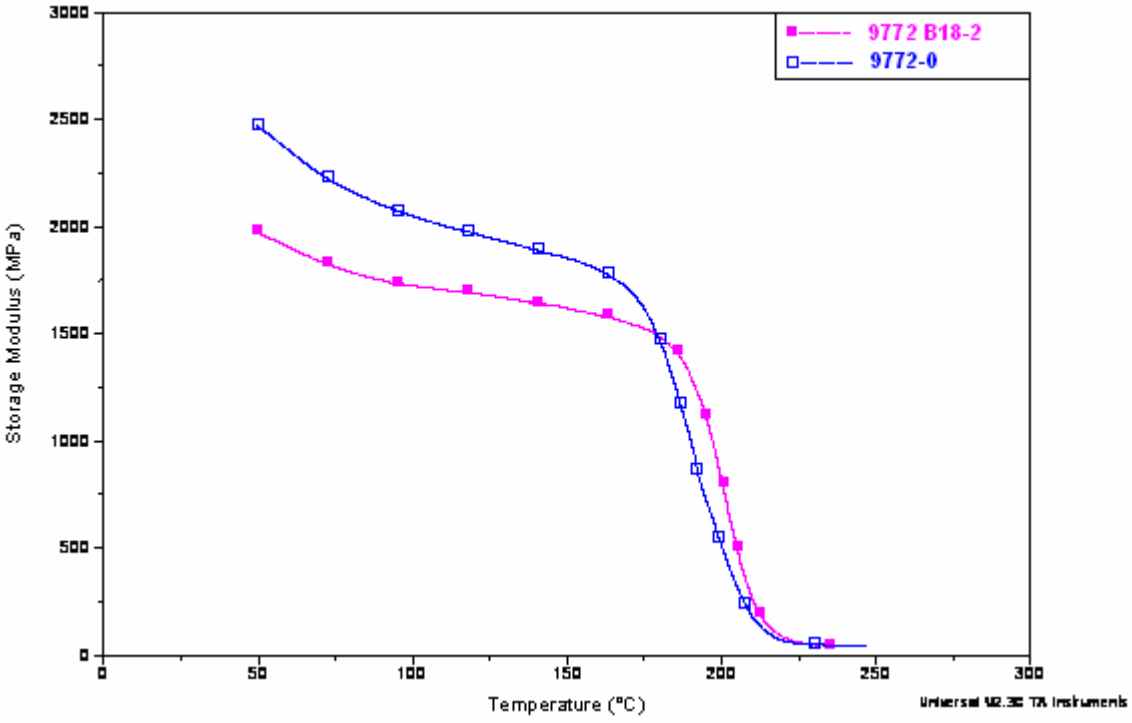

Figure 5.20. Comparison of storage modulus for Cycom®977-2 samples

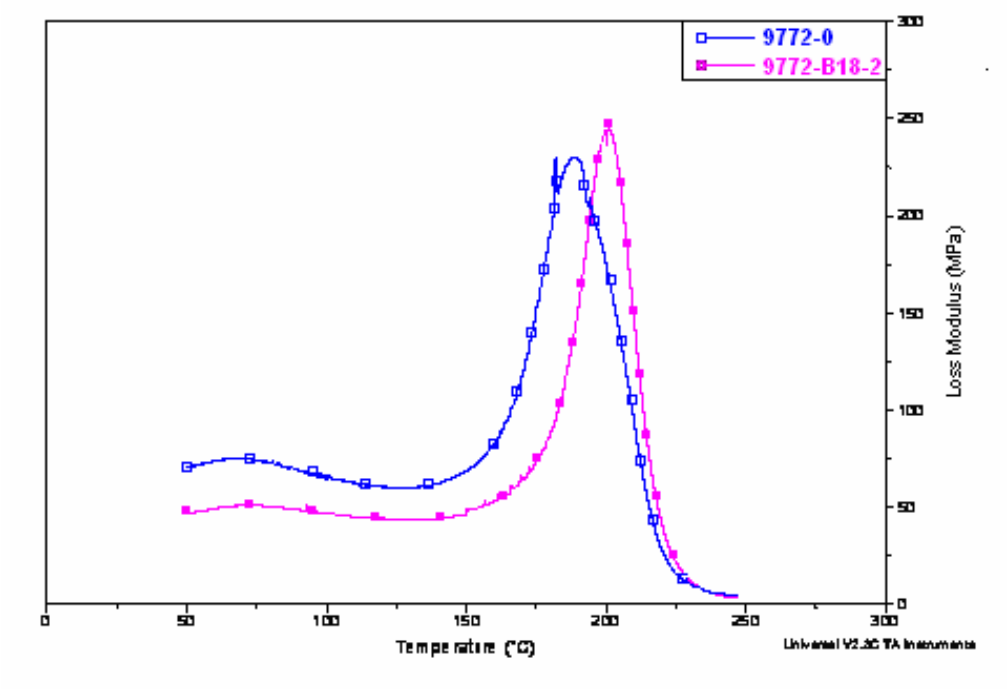

Figure 5.21. Comparison of loss modulus for Cycom®977-2 samples

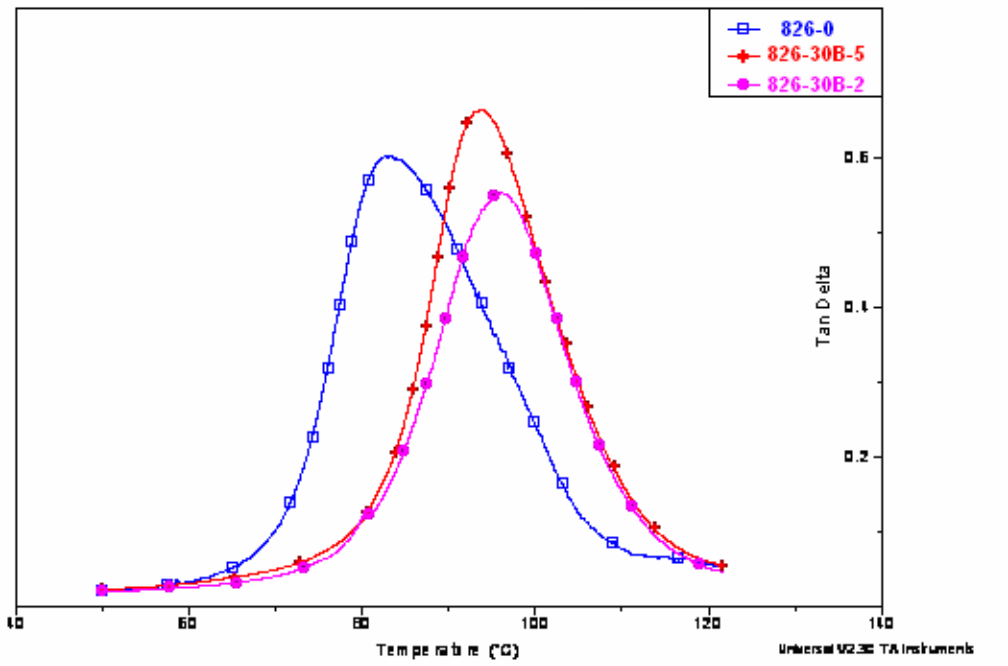

Figure 5.22. Comparison of tan delta for samples of Epon™826 modified with Cloisite®30B

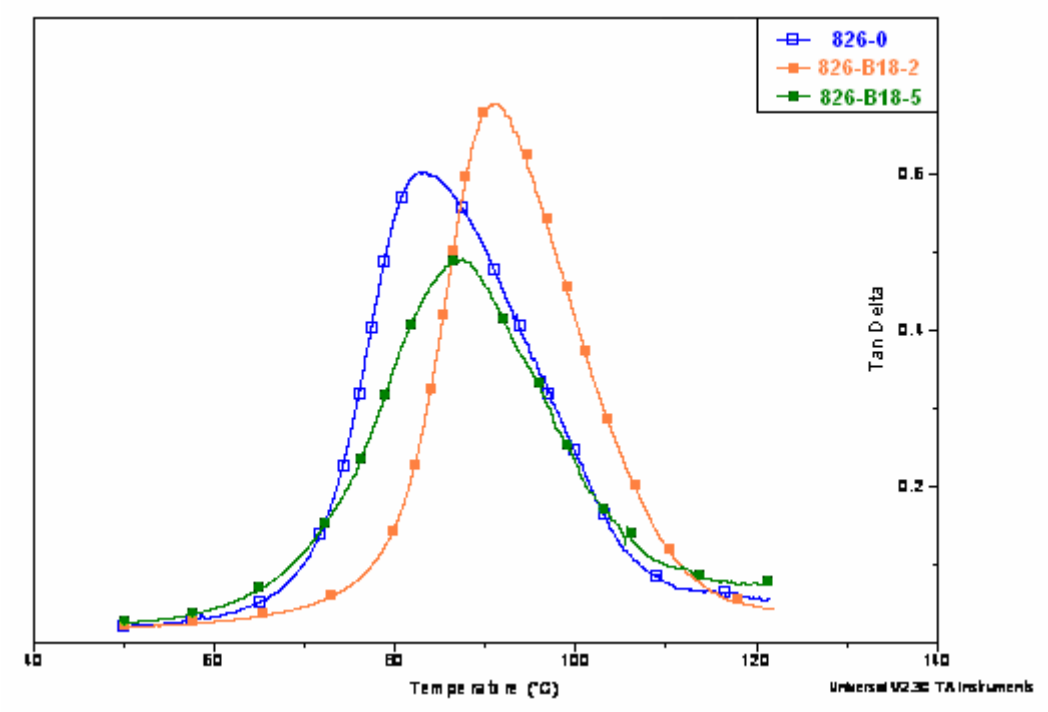

Figure 5.23. Comparison of tan delta for samples of Epon™826 modified with nanoclay B18

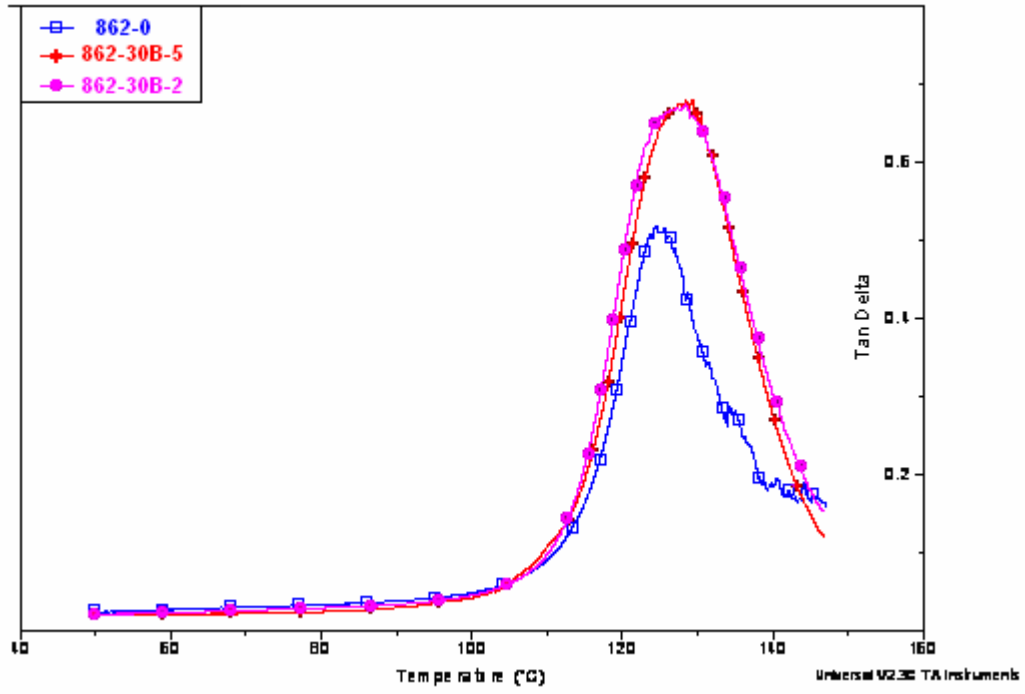

Figure 5.24. Comparison of tan delta for samples of Epon™862 modified with Cloisite®30B

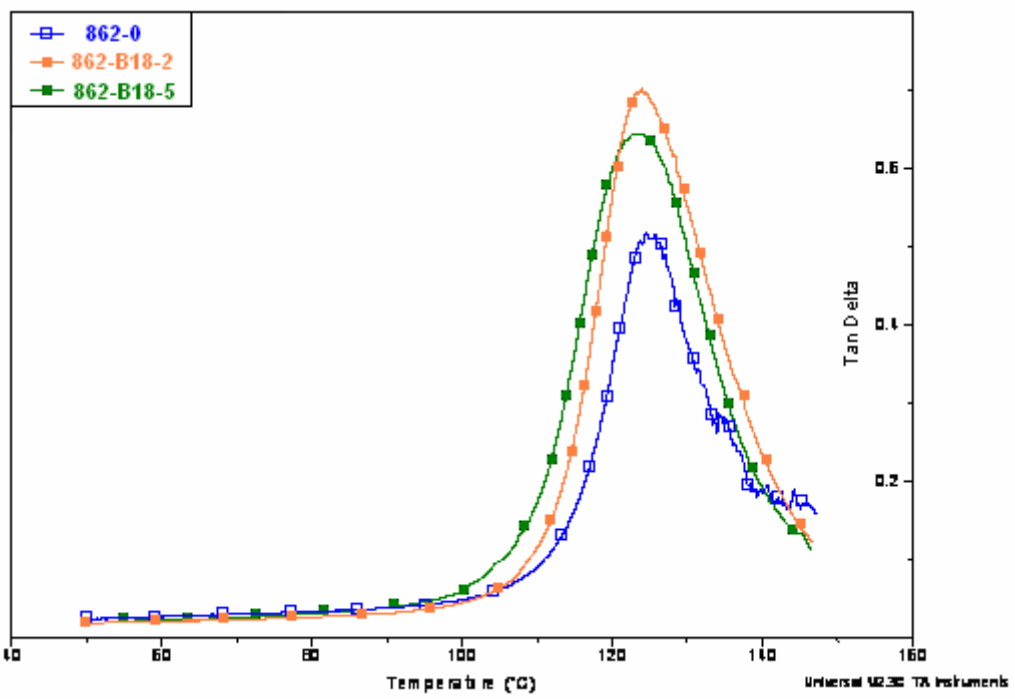

Figure 5.25. Comparison of tan delta for samples of Epon™862 modified with nanoclay B18

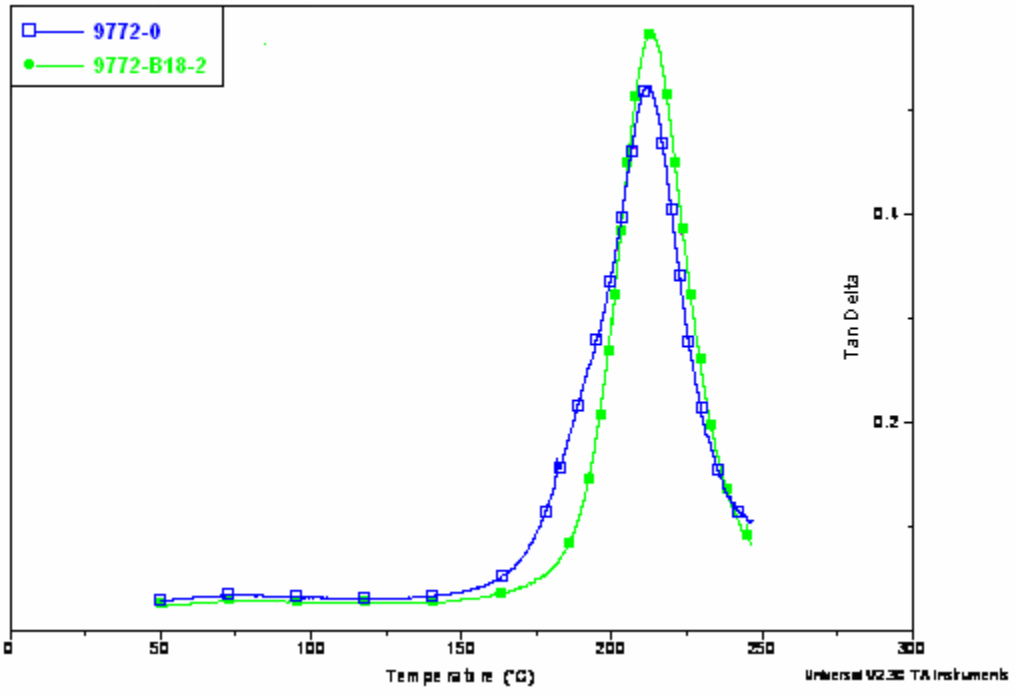

Figure 5.26. Comparison of tan delta for samples of Cycom®977-2

As it can be observed from the graphs above the addition of the nanoclays does not produce a change in the plateau of the storage modulus curves in either case of Epon™826, Epon™862 and Cycom®977-2.

It was noted that below the glass transition the nanocomposites exhibit higher storage modulus than that of the pristine polymer in resins Epon™826 and Epon™862. It was observed that at 50°C, within the glassy region, the storage modulus of the Epon™826 nanocomposite modified with 5wt% of nanoclay B18 was approximately 16% higher compared with the neat epoxy polymer. For Epon™862 modified with 5wt% of Cloisite®30B the increase was of 29% when compared to the pristine polymer.

The fact that there is no variation on the rubbery plateau with the addition of the nanoclays indicates that there are no changes in the mechanical properties of the samples with the addition of the nanoclays.

Another characteristic that can be observed from the DMA graphs is the width of the tan delta curve at the T_g. If the width at the T_g remains the same when the nanoparticles are added into the matrix it is understood that there are no changes in the network structure of the nanocomposite. It can be observed that in the case of samples of Epon™826 and Epon™862 there is a change of the width of the curve when the nanoclays are added and therefore the nanoclay addition modified the network structure of the matrix. There is no change observed in the case of samples manufactured with Cycom®977-2.

5.3. TGA measurements

With the TGA tests the values of the degradation temperature and the residue were obtained for all the samples. Three measurements were done in all the cases and the values averaged. The degradation temperature was obtained from the peak of the derivate curve of the weight (DTG). The corresponding graphs can be observed in Figures 5.27 to 5.34.

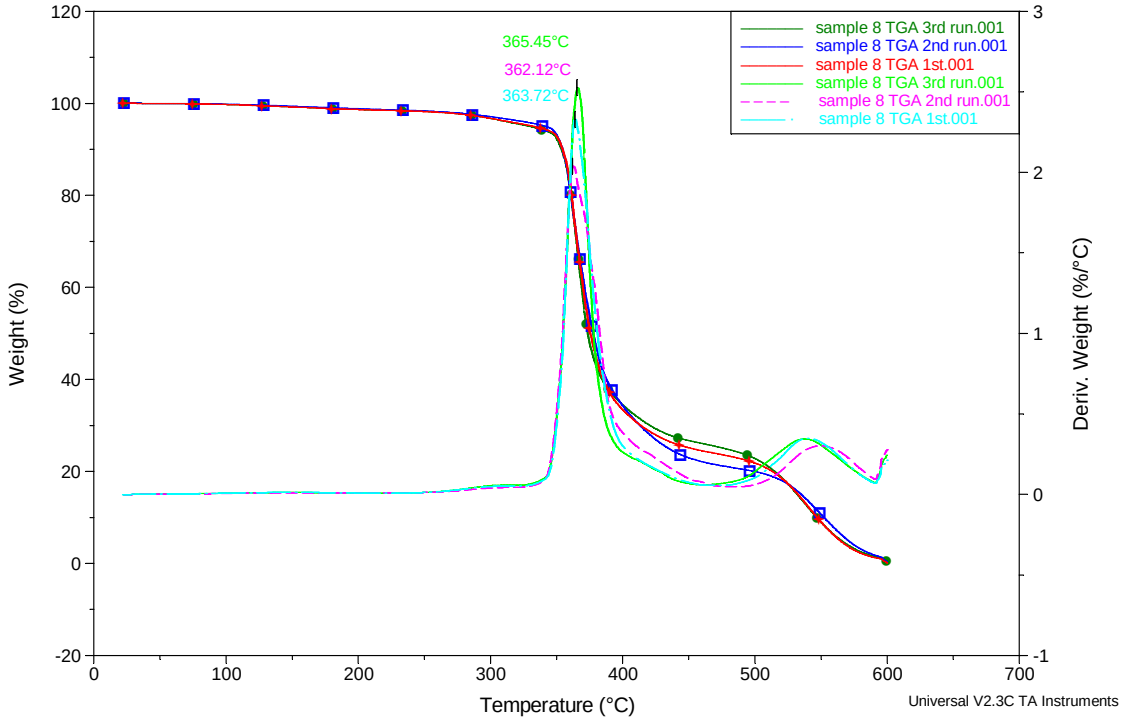

Figure 5.27. TGA graph for Epon™826 non-modified

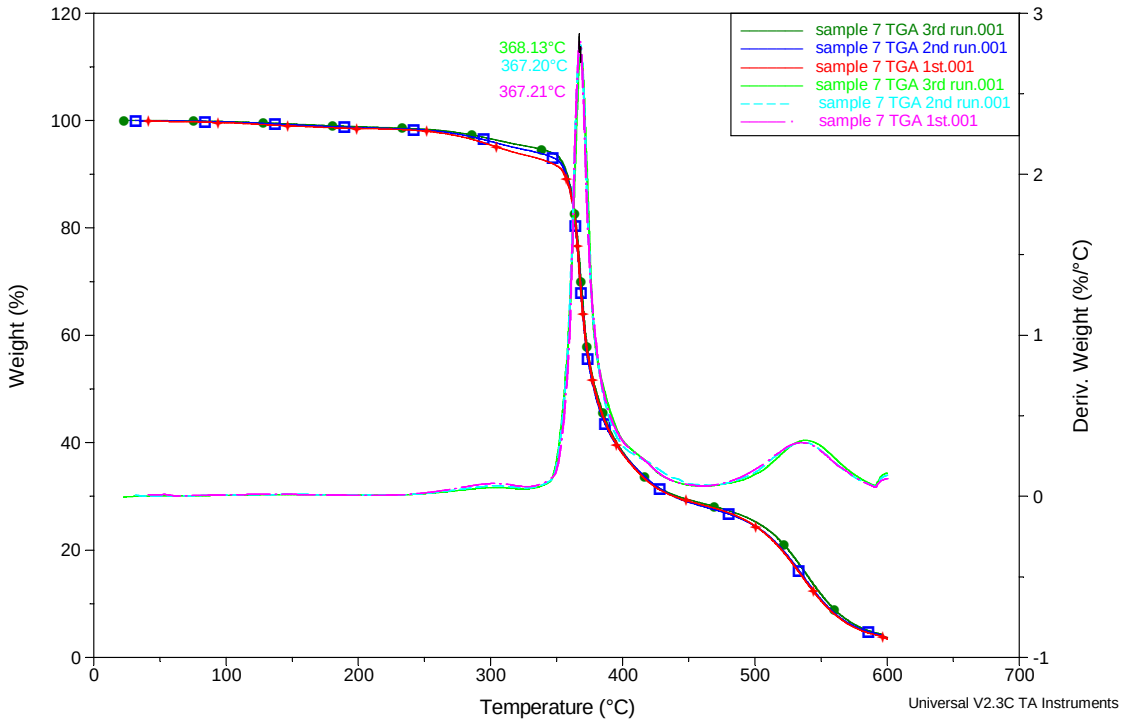

Figure 5.28. TGA graph for Epon™826 modified with 5wt% of Cloisite®30B

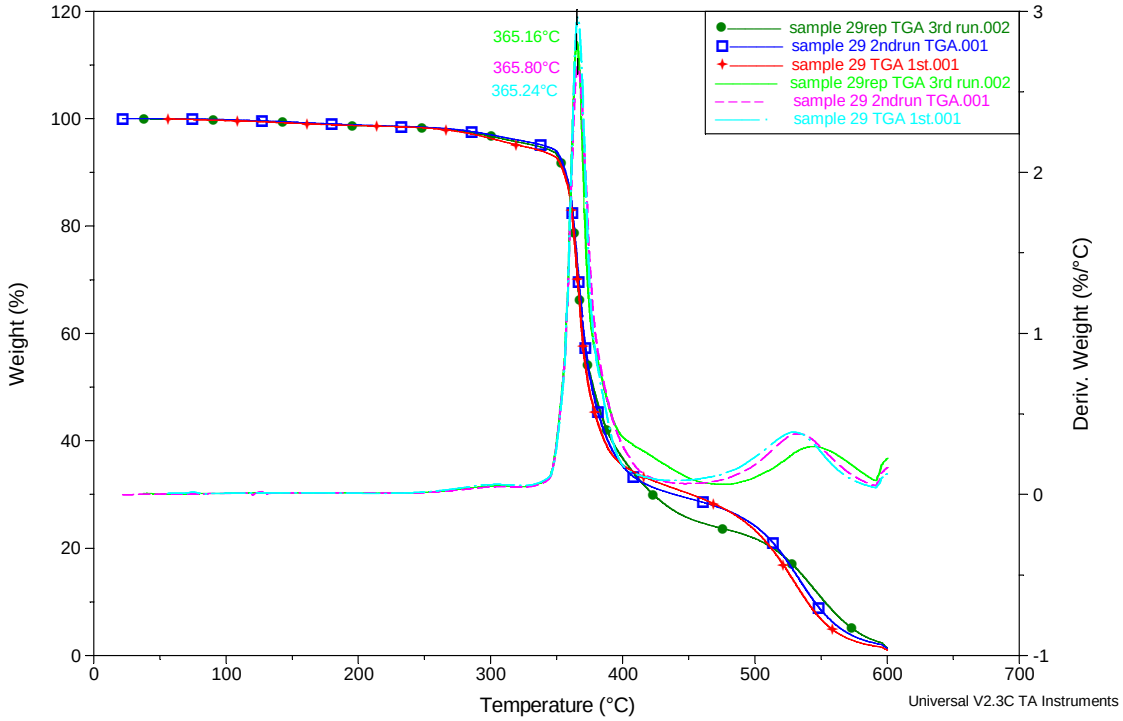

Figure 5.29. TGA graph for Epon™826 modified with 2wt% of nanoclay B18

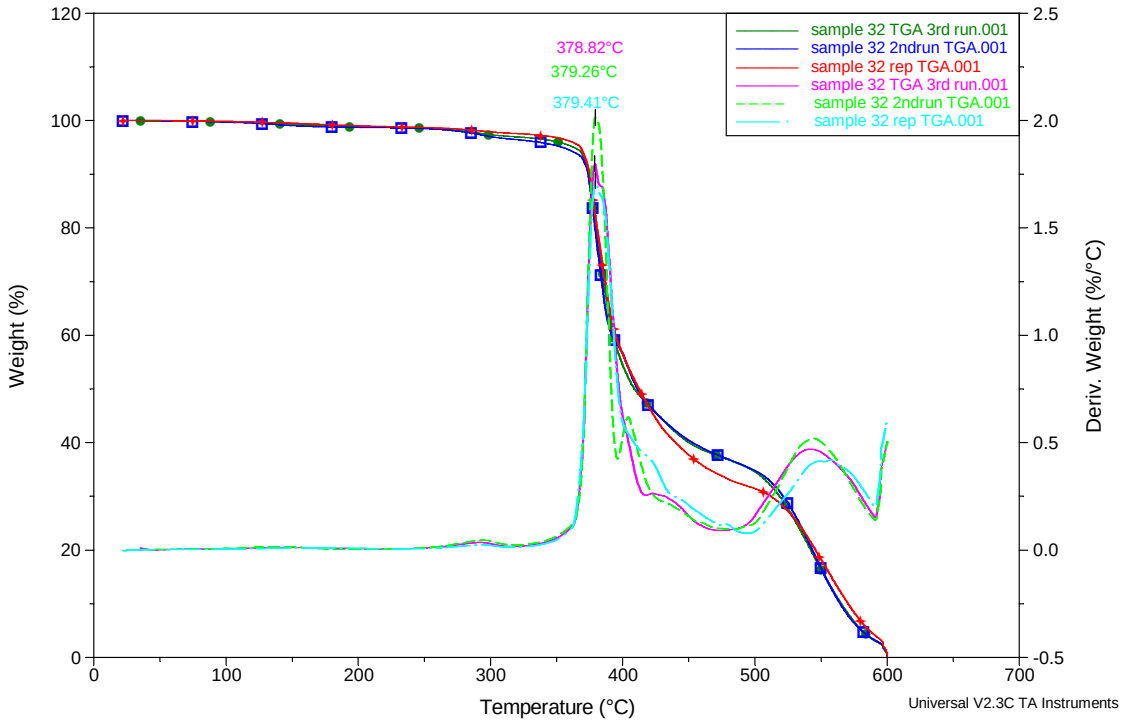

Figure 5.30. TGA graph for Epon™862 non-modified

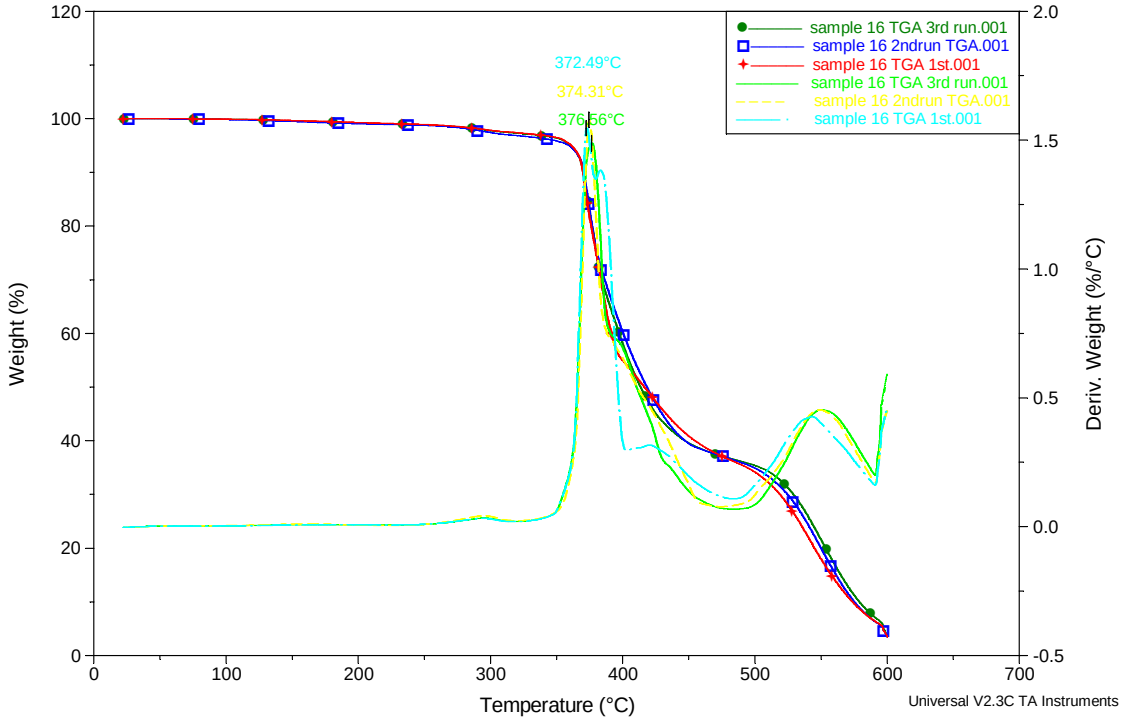

Figure 5.31. TGA graph for Epon™862 modified with 5wt% of Cloisite®30B

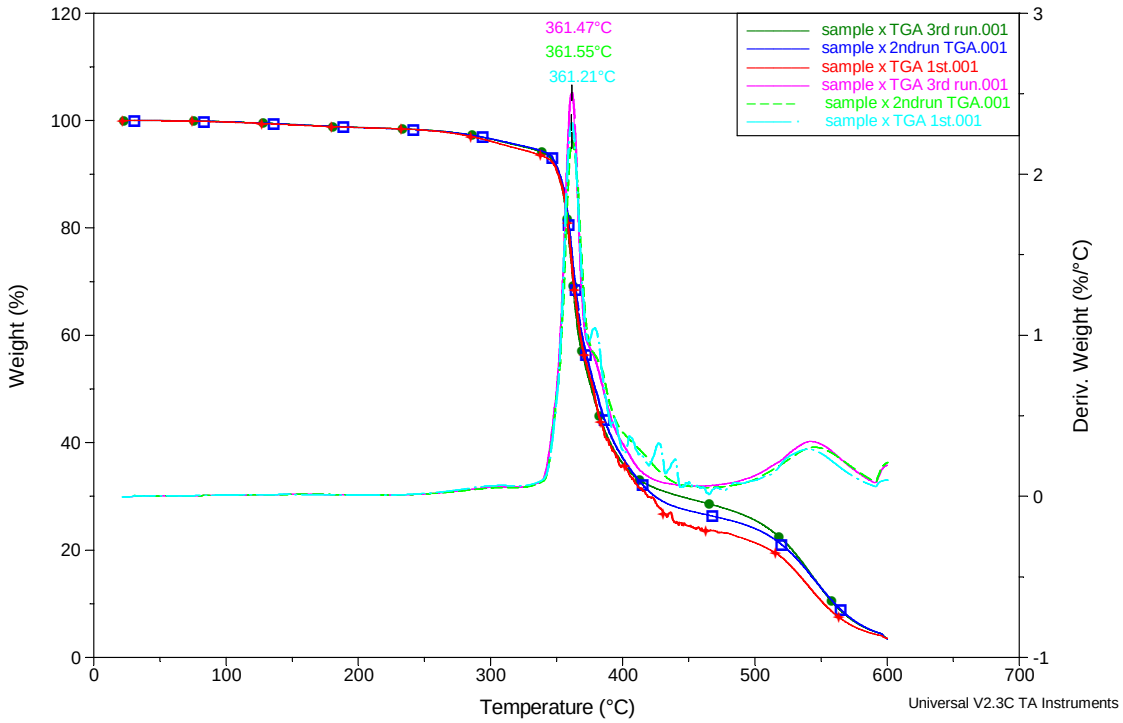

Figure 5.32. TGA graph for Epon™862 modified with 5wt% of nanoclay B18

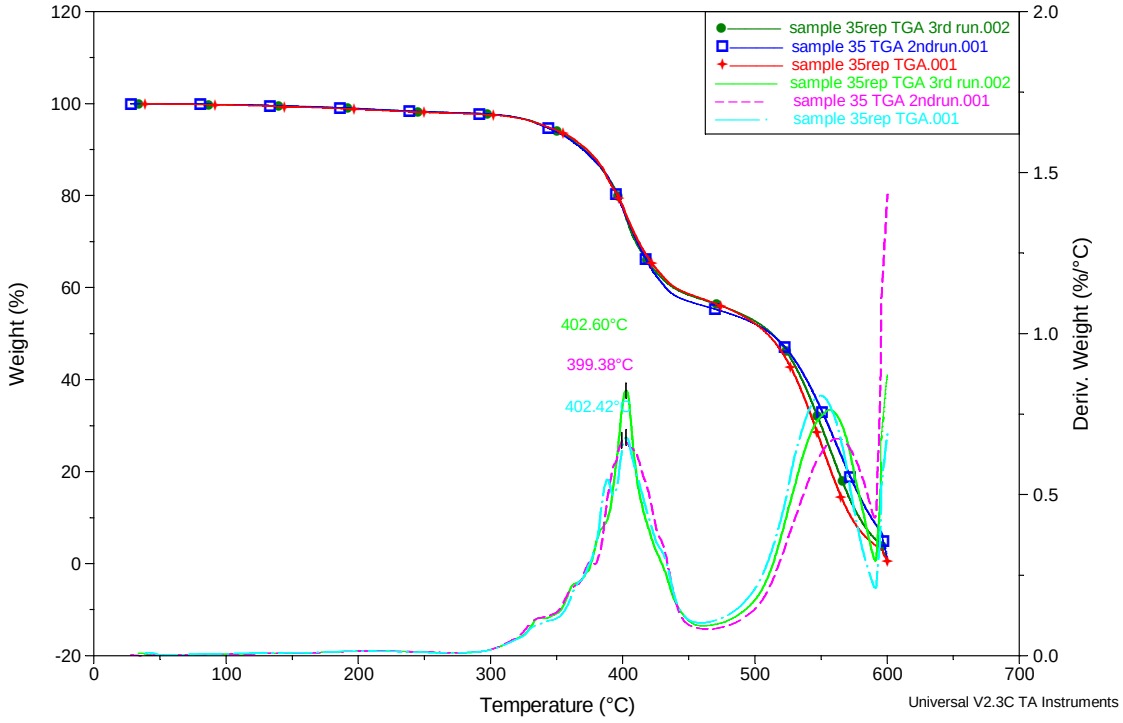

Figure 5.33. TGA graph for Cycom®977-2 non- modified

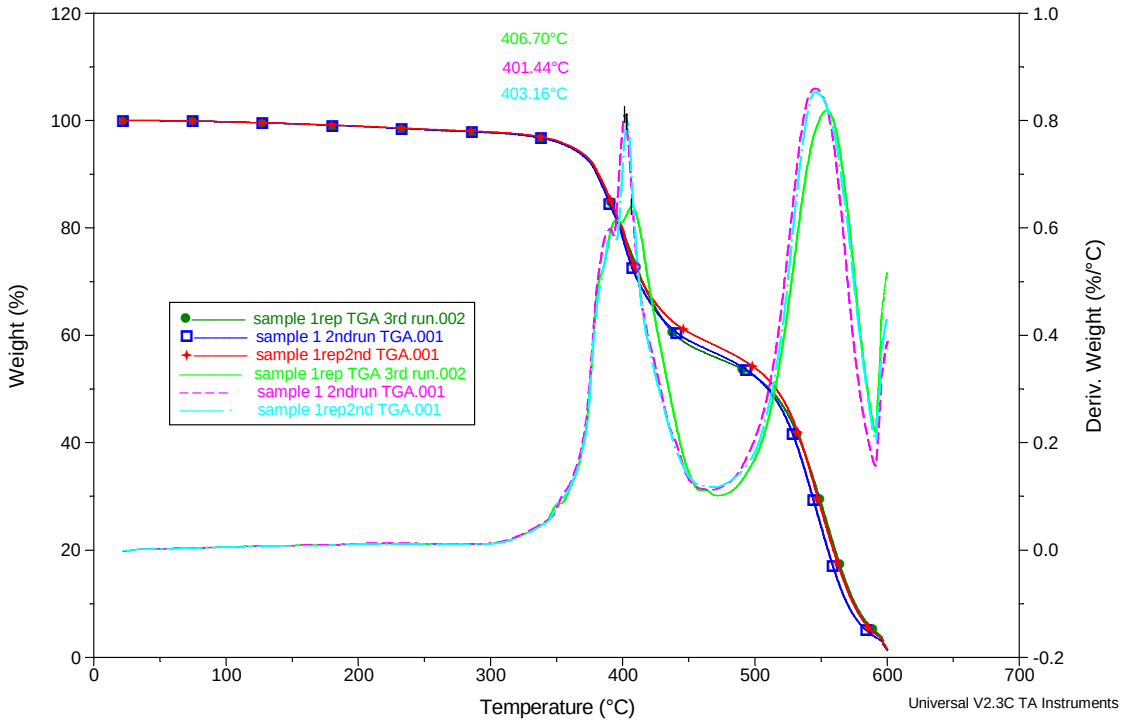

Figure 5.34. TGA graph for Cycom®977-2 modified with 2wt% of nanoclay B18

The results are summarized in the following table.

Table 5.3. Degradation temperature and residue before cycling

		degradation temperature (˚C)		residue	
samples	number	average	stand dev	average	stand dev
826-0	8	363.76	1.67	0.38	0.25
826-30B-2	9	367.57	0.62	1.63	0.15
826-30B-5	7	367.51	0.53	3.55	0.09
826-B18-2	29	365.40	0.35	1.24	0.20
826-B18-5	x	361.41	0.18	3.50	0.06
862-0	32	379.16	0.31	0.74	0.30
862-30B-2	4	380.19	4.02	1.57	0.27
862-30B-5	16	374.45	2.04	3.50	0.02
862-B18-2	6	374.48	0.95	1.44	0.16
862-B18-5	33	369.50	0.43	3.61	0.12
9772-0	35	401.47	1.81	0.24	0.25
9772-B18-2/1	1	403.77	2.68	1.44	0.11

In Epon™826 samples, the thermal stability generally increased upon addition of nanoclay, except for samples modified with 5wt% of B18 nanoclays. For nanocomposites made with Epon™862, the observed trend was opposite, with the thermal stability basically decreasing with the addition of nanoclays. In general it was observed that the samples modified with Cloisite®30B achieve higher degradation temperatures than those samples modified with nanoclays B18.

After the TGA analyses were performed the results of the tests were analyzed with the help of the Polysolver® software.

Typical TGA and DTG traces obtained from these nanocomposites suggested the presence of overlapping reactions, the fact that there are overlapping peaks and peaks with shoulders, and that the DTG curve does not reach a zero value between some peaks are characteristics that indicated that the degradation process may have more than one reaction involved. The existence of overlapping reactions prevented the application of classical kinetic models on the raw data; and therefore a logistic mixture approach was used to separate the overlapping processes in single ones with the help of the mentioned software. Taking advantage on the fact that the logistic functions used in the model correlate very well to the reaction order model, the kinetic parameter values were obtained for each single process.

In order to analyze the curves, the data obtained from the TGA were entered in the software and an estimation of logistic curves was done. The initial single degradation process was separated into five different degradation processes and their activation energy was obtained. In order to evaluate the number of processes that take part in the degradation the estimation of the average squared error (ASE) was done. An initial estimation of four logistic components was performed but while the fitting of the curve was accurate the ASE obtained was high. Therefore, a fifth logistic curve was added obtaining an optimal fitting and improving significantly the value of the ASE. The addition of an additional 6th LC did not improve significantly the ASE or the visual fitting. Once the fitting parameters were optimised for one of the samples, the same components were assumed for all the curves. An example of the curves obtained is shown in the figure below.

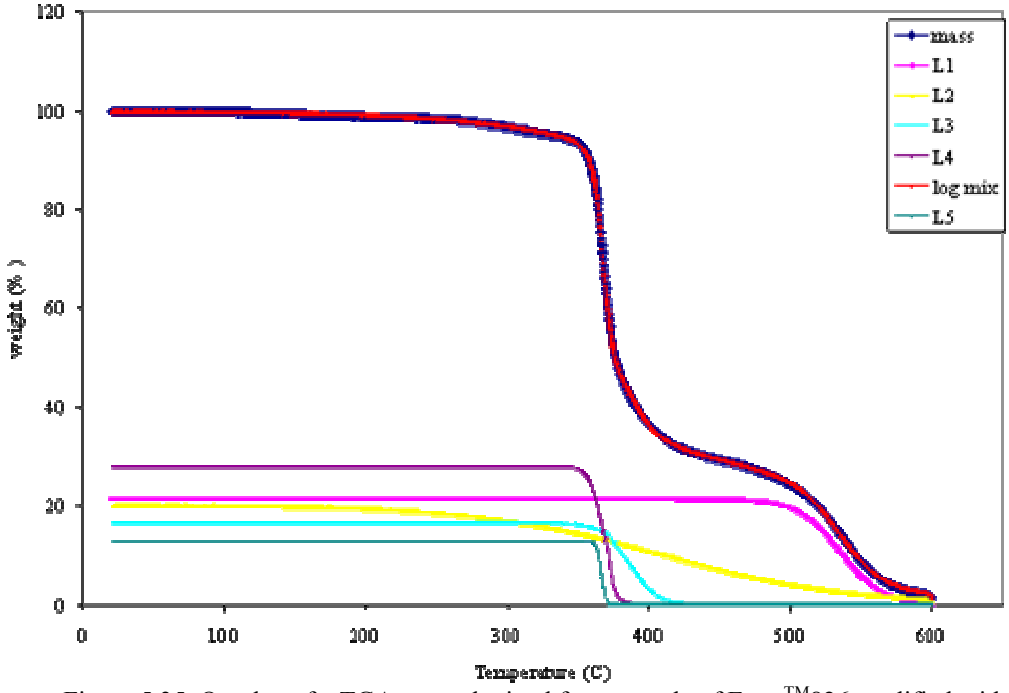

Figure 5.35. Overlay of a TGA trace obtained from sample of Epon^{TM}826 modified with 2wt% of Cloisite$^{®}$30B, the logistic mixture fitting and its component functions

The TGA trace obtained from the test was decomposed into five separate curves that indicated the existence of five degradation processes overlapped instead of only one process. After the five processes were defined the kinetic parameters for each of them was calculated as well as the temperatures were the degradation occurred. The data obtained is summarized for all the samples in the following tables.

Table 5.4. ASE and w_i values for resin Epon^{TM}826

Samples		826-0	826-30B-2	826-30B-5	826-B18-2	826-B18-5
LC1	w_1	5.59	12.75	32.62	0.71	9.99
	T (˚C)	281.45	366.35	367.55	122.17	338.37
LC2	w_2	10.17	28.08	1.03E-05	17.48	11.16
	T (˚C)	364.73	368.36	369.86	366.02	362.51
LC3	w_3	42.90	16.64	21.39	36.15	42.11
	T (˚C)	368.47	386.45	384.38	370.37	367.32
LC4	w_4	18.19	20.11	22.01	21.19	14.77
	T (˚C)	397.99	410.34	387.88	400.43	410.21
LC5	w_5	23.32	21.37	20.60	23.59	18.58
	T (˚C)	541.20	535.10	535.67	527.72	540.69
Constant		3.5E-07	0.89	3.06	0.79	3.38
ASE		0.0790	0.0288	0.0530	0.0272	0.1010

Table 5.5. ASE and w_i values for resin Epon^{TM}862

Samples		862-0	862-30B-2	862-30B-5	862-B18-2	862-B18-5
LC1	w_1	6.27	12.65	4.30	2.63E-03	13.25
	T (˚C)	368.58	373.93	304.31	296.38	369.87
LC2	w_2	35.23	27.75	38.82	12.84	31.72
	T (˚C)	382.65	385.26	379.10	369.07	389.87
LC3	w_3	26.37	7.84	20.12	18.09	25.63
	T (˚C)	417.13	414.32	425.09	379.16	452.11
LC4	w_4	18.15	21.32	31.93	31.19	14.36
	T (˚C)	541.76	425.09	542.64	409.36	542.91
LC5	w_5	14.26	30.22	1.45	34.39	12.28
	T (˚C)	562.02	549.27	584.43	545.34	569.39
Constant		3.37E-04	0.52	3.42	1.21	2.48
ASE		0.0500	0.0534	0.0258	68.7456	0.0396

Table 5.6. Kinetic parameters of each logistic component for Epon^{TM}826 samples

Samples		826-0	826-30B-2	826-30B-5	826-B18-2	826-B18-5
LC1	Ea (KJmol^{-1})	17.56	2504.86	1105.47	64.47	27.23
	n	1.15	2.14	1.85	1.85	1.26
	ln A (min^{-1})	0.91	470.52	205.72	19.14	2.31
LC2	Ea (KJmol^{-1})	1708.85	614.88	2925.58	2593.20	0.00
	n	1.82	1.55	1.85	1.66	0.00
	ln A (min^{-1})	321.93	113.99	559.03	488.33	0.00
LC3	Ea(KJmol^{-1})	448.92	369.14	314.86	469.02	357.57
	n	1.86	1.93	1.87	1.85	1.85
	ln A (min^{-1})	81.17	64.72	54.78	84.89	63.98
LC4	Ea(KJmol^{-1})	158.46	37.64	40.15	50.64	216.56
	n	1.74	1.33	1.36	1.43	1.79
	ln A(min^{-1})	25.36	3.28	3.95	5.68	35.38
LC5	Ea (KJmol^{-1})	295.42	335.86	303.49	292.90	308.87
	n	1.81	1.83	1.82	1.81	1.82
	ln A (min^{-1})	40.40	46.91	42.05	40.78	42.64

Table 5.7. Kinetic parameters of each logistic component for Epon^{TM}862 samples

Samples		862-0	862-30B-2	862-30B-5	862-B18-2	862-B18-5
LC1	Ea (KJmol^{-1})	12.53	1196.71	26.59	949.83	1329.92
	n	0.95	1.63	1.27	0.22	1.75
	ln A(min^{-1})	-0.76	222.07	2.79	-8.69	248.08
LC2	Ea (KJmol^{-1})	612.14	610.84	533.46	1901.86	392.22
	n	1.83	1.98	1.84	1.97	1.90
	ln A (min^{-1})	109.79	108.79	95.66	355.55	68.10
LC3	Ea(KJmol^{-1})	223.47	13.74	209.05	0.00	44.76
	n	1.81	0.89	1.78	0.00	1.30
	ln A (min^{-1})	35.68	-0.66	32.98	0.00	4.10
LC4	Ea(KJmol^{-1})	213.97	165.39	255.08	268.73	455.78
	n	1.66	1.74	1.77	1.83	1.86
	ln A(min^{-1})	28.63	25.29	34.13	44.10	64.65
LC5	Ea (KJmol^{-1})	352.41	350.14	551.35	293.37	485.74
	n	1.70	1.85	1.26	1.81	1.76
	ln A (min^{-1})	48.31	47.81	76.84	39.58	67.17

The peak of the derivative of the TGA curve (DTG) gives a value for the degradation temperatures of the samples, but with the help of the model it was possible to separate the different components in the samples and to understand that in fact one big stage in the TGA trace was the result of several overlapped degradation processes. It was observed for both types of resins that the TGA trace has two main stages, one occurring in the region between 250 °C and

450 ˚C and the second step around 450 ˚C -550 ˚C. In samples from Epon^{TM}826 the main step seems to be the result of four different overlapped processes while the second step corresponds to a single degradation process. In the case of most of the samples made from resin Epon^{TM}862 the main step appears to be formed by three overlapped processes while two processes form the second step. The values obtained for the activation energy show that for the first degradation process the energy required for the neat resin is smaller than in the case of the nanoclay modified resins.

Regarding the mass loss processes it is usually understood that the first process corresponds to the evaporation of water, as water is the major product at that temperatures [4]. Both resins used in the manufacturing of the samples are based on diglycidyl ether of bisphenol A (DGEBA) and Epon^{TM}862 on diglycidyl ether of bisphenol F (DGEBF), and therefore the degradation of the phenolic compound is expected to appear as major products in the degradation process as well.

5.4. DSC measurements

The glass transition was calculated as the inflection point of the DSC trace using the help of the Universal Analysis Software. The results are summarized in the following figures.

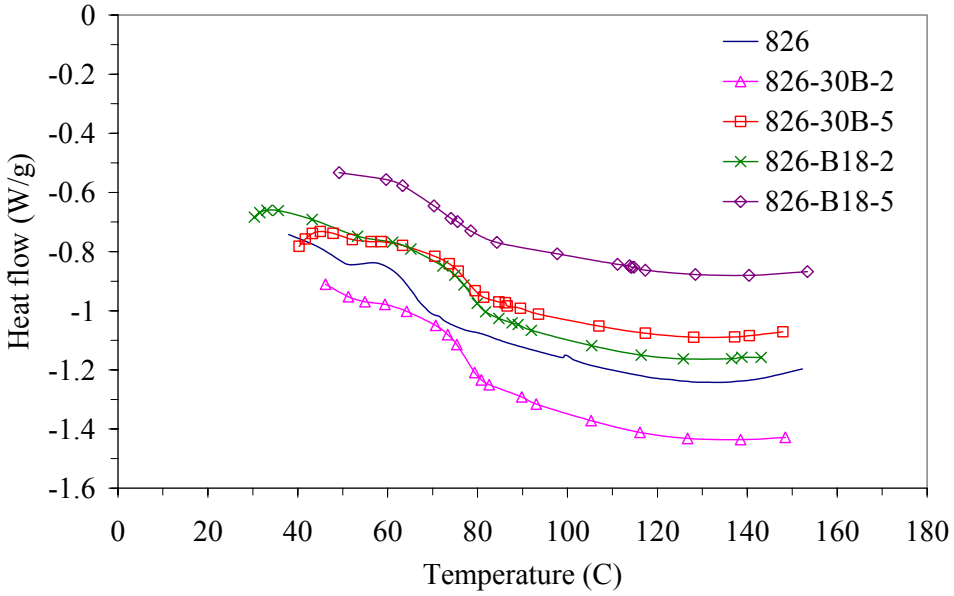

Figure 5.36. DSC curves of Epon^{TM}826 nanocomposites, before thermal cycling.

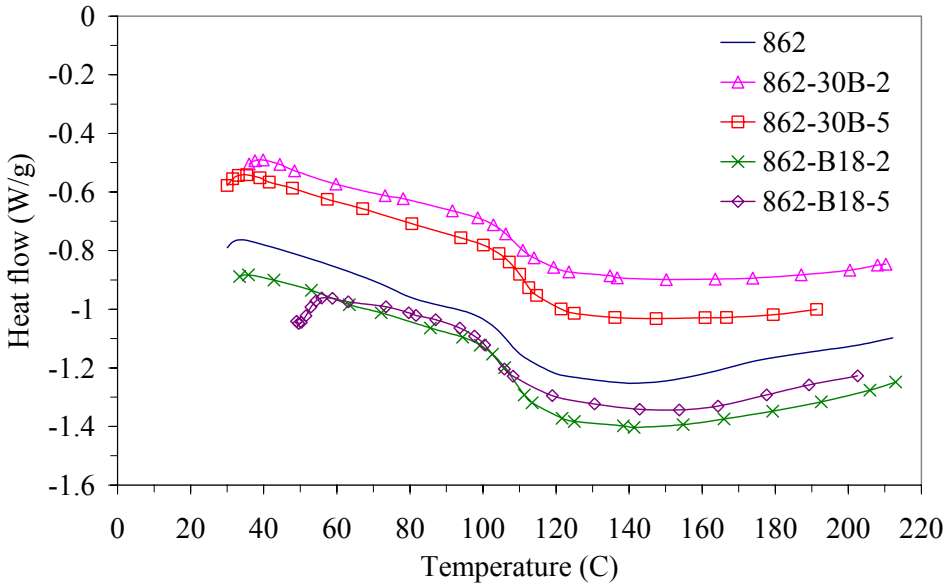

Figure 5.37. DSC curves of Epon™862 nanocomposites, before thermal cycling.

The values of the glass transition temperatures are summarized in the following table.

Table 5.8. Glass transition temperatures for Epon™826 and Epon™862 nanocomposites

samples	T_g(°C)	stand dev.
826-0	65.03	1.92
826-30B-2	77.28	0.13
826-30B-5	77.42	0.24
826-B18-2	77.31	1.58
826-B18-5	71.23	1.36
862-0	107.41	0.29
862-30B-2	108.60	0.04
862-30B-5	109.63	1.62
862-B18-2	109.29	0.91
862-B18-5	104.84	2.36

The values of the glass transition for samples manufactured with resin Cycom®977-2 were not observable in the DSC traces. These values were obtained with the DMA data and are reported in the table below.

Table 5.9. Glass transition temperature for Cycom®977-2 samples obtained with DMA data

samples	T_g(°C)		
	onset E'	peak E''	tan delta
9772-0	153.90	166.31	194.20
9772-B18-2	166.04	179.57	206.86

It is important to notice the fact that the glass transition values obtained from DSC or DMA differ from each other. Results obtained through DMA analyses are usually higher than those from DSC data. It is needed to point that the glass transition is not a specific temperature but rather a temperature range that indicates when the amorphous polymer starts to have increased polymeric chain movements. It is an indication of the range of temperatures where the materials start to lose their mechanical properties.

From the DSC graphs it was also analyzed the extent of curing of the nanocomposites. The DSC plots do not show a residual curing peak after the T_g is reached. An exothermic peak was observed for all the samples, an example of Epon™826 modified with 2 wt% of B18 is shown in Figure 5.38. Here, the peak appears around 300 - 400˚C and it was interpreted as a degradation peak, which was confirmed by TGA, as seen in Figure 5.39.

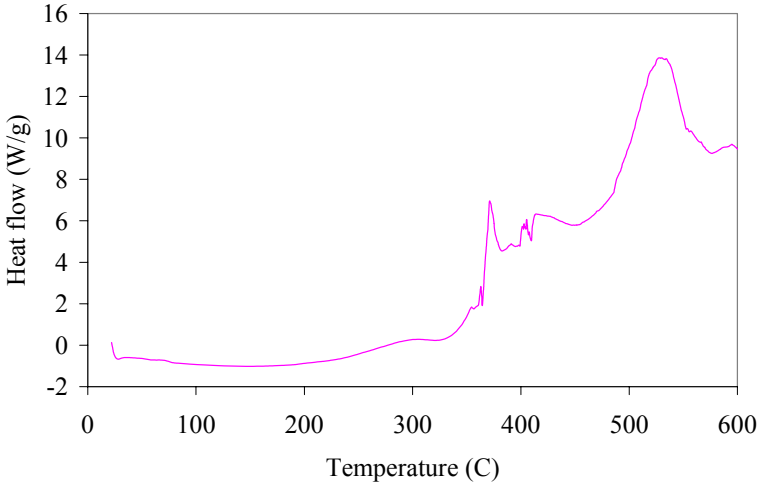

Figure 5.38. A typical DSC plot of Epon™826 modified with 2% of B18 nanoclay

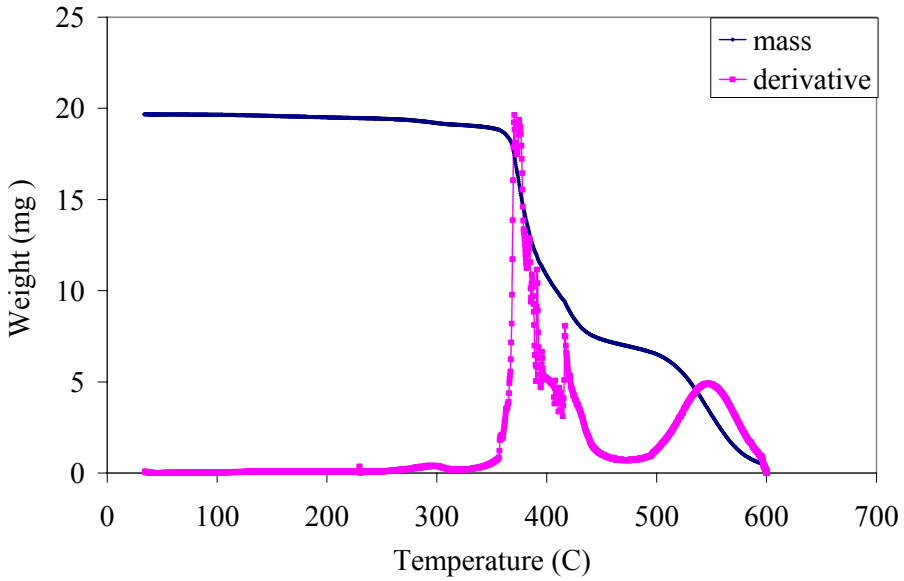

Figure 5.39. A typical TGA plot of Epon^{TM}826 modified with 2% of B18 nanoclay

The fact that there is no residual peak implies that the epoxy system was fully cured and therefore any treatment applied later would not induce chemical changes in the samples [5]. Consequently, it is believed that the applied thermal treatment would not induce any further crosslinking of the polymer chain and any material property changes are only related to segmental mobility and free volume arrangements.

The addition of nanoclays slightly increased the values of the T_g in all cases, when compared to that of the pristine matrix, except for samples of Epon^{TM}862 modified with 5 wt% B18. The relative increase observed in the T_g when compared to the neat matrix, was more noticeable in samples manufactured from Epon^{TM}826, where the general increase observed was about 12°C for all samples except the one modified with 5wt% of B18 which had an increase of 6°C. Nanocomposites manufactured from Epon^{TM}862 did not show a significant increase in the T_g values when compared to the pristine polymer.

The increase observed in the glass transition values when the nanoclays are added to the neat polymer is related to the fact that when the nanoclays are added the possibility of mobilization of the polymer chains decreases and therefore there is an increase of the chain stiffness that is related to the increase of the glass transition.

5.5. Free volume analyses

With the help of positron annihilation lifetime spectroscopy (PALS), the average size of the free volume holes and the relative fractional free volume were obtained.

The purpose of the free volume measurements is to understand how the distribution of the free volume is affected by the presence of the nanoclays and how the free volume distribution varies after the thermal treatment is applied.

The results obtained from the PALS tests are given as intensity and lifetime of the positrons. Usually for polymers, of the three lifetimes, the ortho-positroniums (o-Ps) pickoff lifetime (τ_3) and its intensity (I_3) are of importance since τ_3 is related to the free-volume hole size and I_3 is considered to be a measure of the relative number density of free-volume holes in the material. Since the chain mobility and chain conformations under stress depend on the size and available free-volume content (fractional free volume) of the material, the analysis is focused on these two parameters of positron lifetime. The o-Ps lifetime τ_3 is related to the free-volume hole size by the Tao-Eldrup model discussed recently by Nakanishi et al. [6].

$$\tau_3 = \frac{1}{2}\left[1 - \frac{R}{R_0} + \frac{1}{2\pi}\sin\left(\frac{2\pi R}{R_0}\right)\right]^{-1} \tag{1}$$

By substituting the value of τ_3 obtained from the PALS test and using this relationship, it was obtained the radius of the free volume cavity, R. In the relationship shown in equation (1) R_0 is given as $R_0 = R + \delta R$, where δR=0.1657 nm.

With this value of δR, the value of the free volume radius was calculated and assuming a spherical shape for the free volume holes, their average size, V_f, was calculated with the following expression, $V_f = (4/3)\pi R^3$.

Then the relative fractional free volume can be obtained as:

$$F_v = V_f I_3 \tag{2}$$

The values of the intensity and lifetime of the o-Ps obtained with the PALS experiment are listed below.

Table 5.10. Value of I_3 and τ_3 obtained from PALS experiments

samples	I_3 (%)	Stand dev	τ_3 (ns)	Stand dev
826-0	27	0.31	1.628	0.012
826-30B-2	27.9	0.33	1.69	0.011
826-30B-5	27	0.27	1.714	0.015
826-B18-2	27.3	0.35	1.707	0.012
826-B18-5	26.2	0.22	1.697	0.018
862-0	27.9	0.32	1.614	0.015
862-30B-2	27.3	0.28	1.619	0.011
862-30B-5	26.8	0.32	1.658	0.018
862-B18-2	26.3	0.46	1.626	0.022
862-B18-5	25.7	0.28	1.683	0.02
9772-0	22.6	0.19	1.563	0.017
9772-B18-2	24.2	0.27	1.635	0.015

According to the method described above the values of the average size free volume holes and the relative fractional free volume were obtained and they are summarized in the following table.

Table 5.11. Average size free volume holes (V_f) and relative fractional free volume (F_v)

samples	R (nm)	V_f (nm^3)	V_f (A^3)	F_v (%)
826-0	0.248	0.064	63.999	17.280
826-30B-2	0.255	0.069	69.228	19.315
826-30B-5	0.257	0.071	71.288	19.248
826-B18-2	0.256	0.071	70.686	19.297
826-B18-5	0.255	0.070	69.828	18.295
862-0	0.247	0.063	62.839	17.532
862-30B-2	0.247	0.063	63.252	17.268
862-30B-5	0.251	0.067	66.506	17.823
862-B18-2	0.248	0.064	63.833	16.788
862-B18-5	0.254	0.069	68.630	17.638
9772-0	0.241	0.059	58.660	13.257
9772-B18-2	0.249	0.065	64.581	15.629

It was obtained from the calculations that the radius of the free volume cavity was about R=0.25 nm for all the samples. The average size of the free volume holes increased when the nanoclays were added to the pristine polymer in the three resins Epon™826, Epon™862 and Cycom®977-2. For the resin Epon™826, it was observed a slight increase of the relative fractional free volume when the nanoclays were added, from 17.28% in the neat resin to an average of 19% for the modified samples. In the case of Epon™862 there was no significant change of the relative fractional free volume.

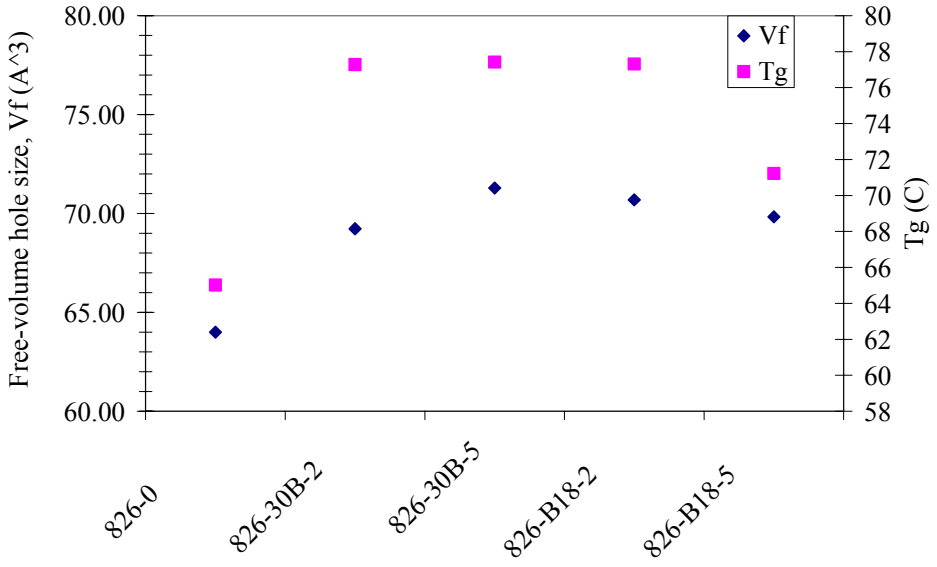

Figure 5.40. Comparison of free volume hole size and T_g values for Epon™826 specimens

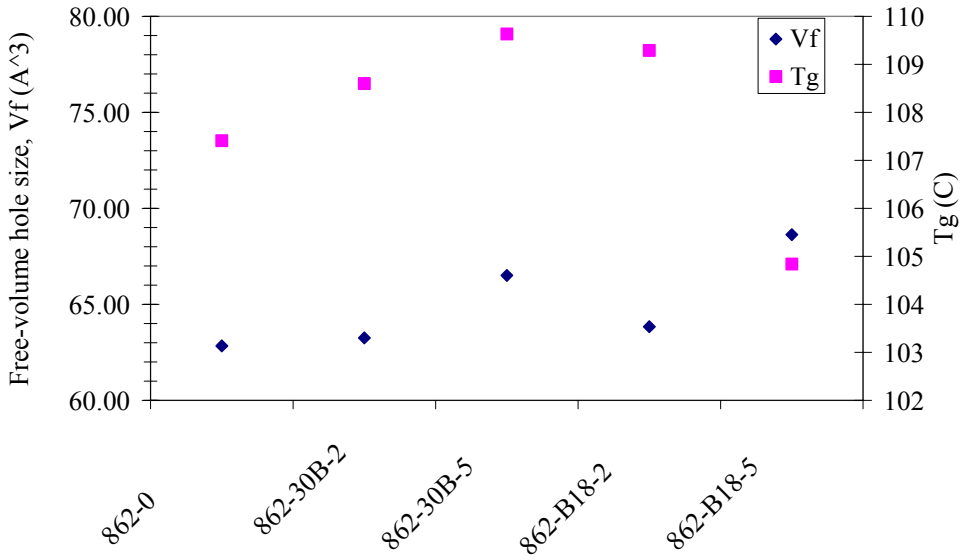

Figure 5.41. Comparison of free volume hole size and T_g values for Epon™862 specimens

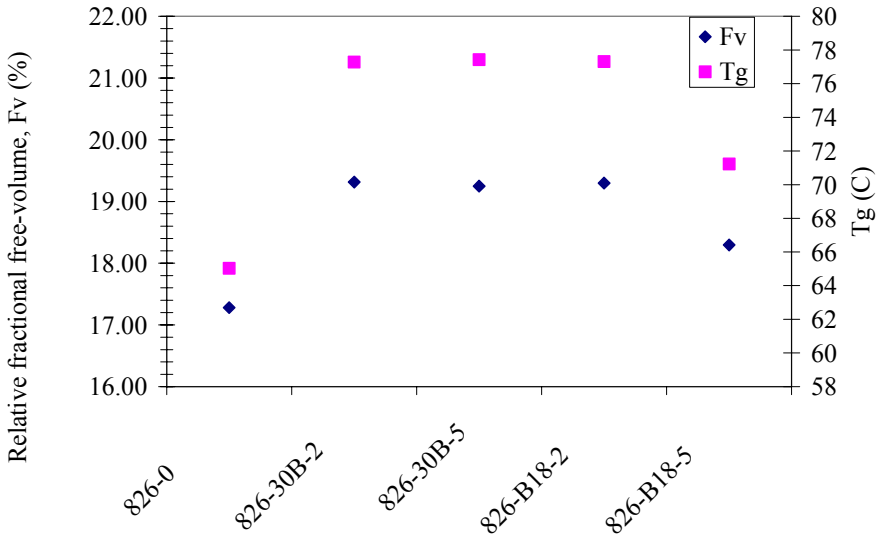

Figure 5.42. Comparison of relative fractional free volume and T_g values for Epon^{TM}826 specimens

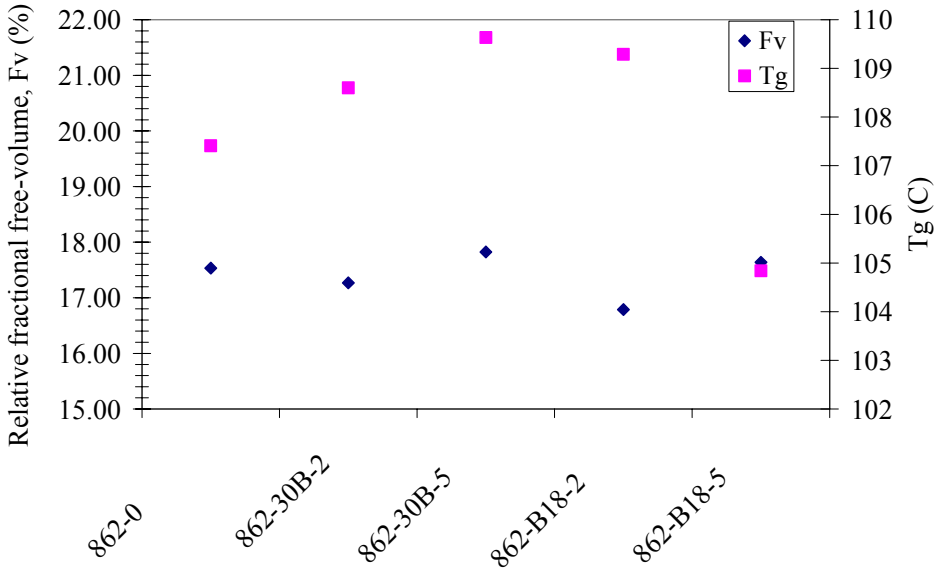

Figure 5.43. Comparison of relative fractional free volume and T_g values for Epon^{TM}862 specimens

According to the results observed in other publications [7] usually the addition of nanofillers produces a restriction in the polymeric chain mobility and therefore this can decrease the free volume concentration. When there is a strong interaction between the nanofillers and the polymer the constraining effect on the polymer chains increases and it is observed that the lifetime of the o-Ps and the intensity decreases with the increase of filler content. In this current

work, the changes observed in the intensity I_3 and lifetime τ_3 of the o-Ps when the nanoclays were added are not very significant.

In general it was noted that the average size of the free volume holes and the relative fractional free volume increased on the nanoclay modified samples when compared to the neat resin in the case of Epon™826. In samples from Epon™862 the relative fractional free volume decreased with the addition of 2wt% of Cloisite®30B and 2wt% of B18 when compared to the pristine samples.

When the values of the glass transition temperature are compared to the free volume data it was noted that it was not followed the expected behavior. Normally, an increase in the glass transition is related with the decrease in the chain mobility of the polymer and the subsequent increase of the polymer chain stiffness. This increase in the chain stiffness is commonly associated with a decrease in free volume.

In the results shown above it was noted that samples with higher T_g had higher average free volume hole sizes and higher relative fractional free volume. This higher value of the free volume could be related with the fact that sometimes in heterogeneous systems with small particles there is an out-diffusion of positrons and o-Ps from the filler particles into the matrix [8]. The out-diffusion of positrons, which later forms o-Ps from the filler particles, into the polymer matrix would result in an increase of the apparent o-Ps formation in the nanocomposite, and this increase would produce a higher value of the free volume.

In the graphs following below it was also done the comparison of the free volume with the permeability values for samples from Epon™826 and Epon™862.

Permeability and free volume are closely related to each other, the higher amount of free volume available in the nanocomposite material would yield to higher permeability values. The molecular level interaction of the matrix polymer with the filler results in changes in the fractional free volume. Physically, reduced permeation in filled polymers is attributed to the increase in diffusion path length and decrease in effective cross-sectional area available for transport [7].

The permeation of gases in the nanocomposite material is not only affected by the relative fractional free volume but also by the distribution of the free volume [9]. Different permeation can occur if the same amount of volume is distributed in large versus small holes, see schematic below for a better understanding. In this example it is assumed that the free volume is

the same for both systems, but the distribution of this free volume varies and this will make the permeability value different for each of the materials. If the gas molecules of the permeant gas are smaller than the average size holes in the case of material (a) but bigger than the average size hole in the case (b) then the material in (a) will have larger permeability than material (b) even though they have the same free volume.

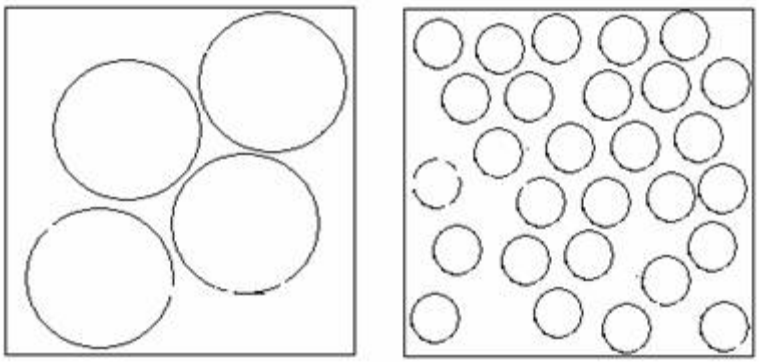

(a) (b)

Figure 5.44. Distribution of free volume

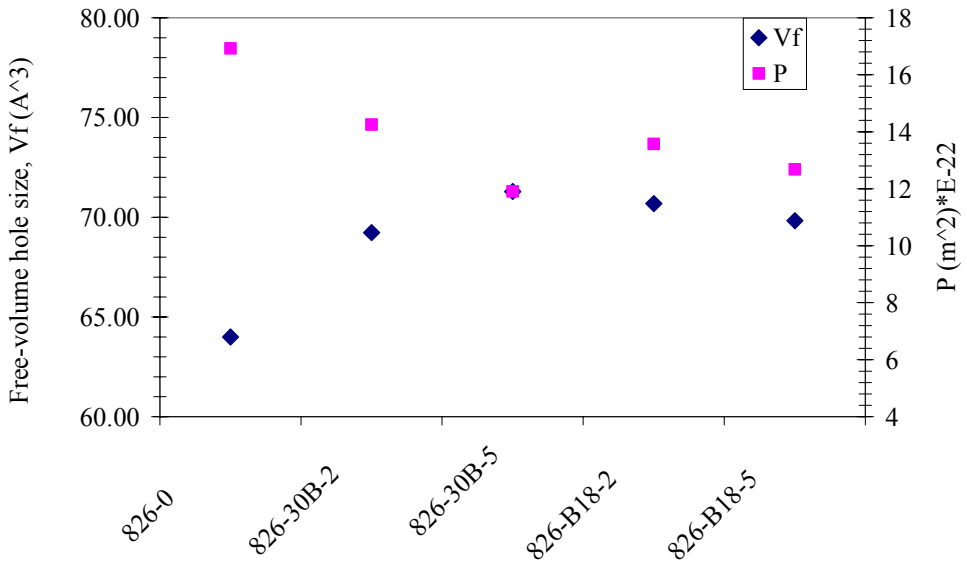

Figure 5.45. Comparison of free volume hole size and permeability values for Epon™826 specimens

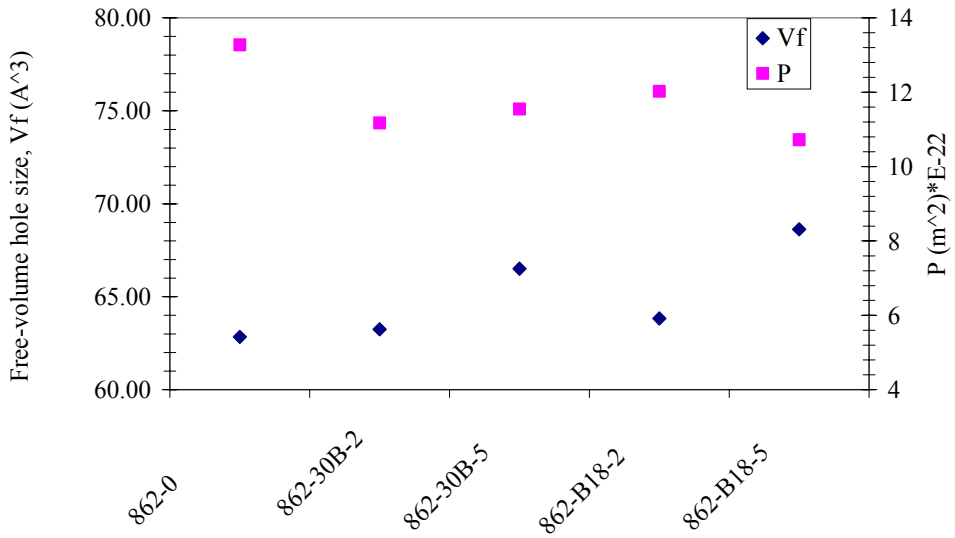

Figure 5.46. Comparison of free volume hole size and permeability values for Epon™862 specimens

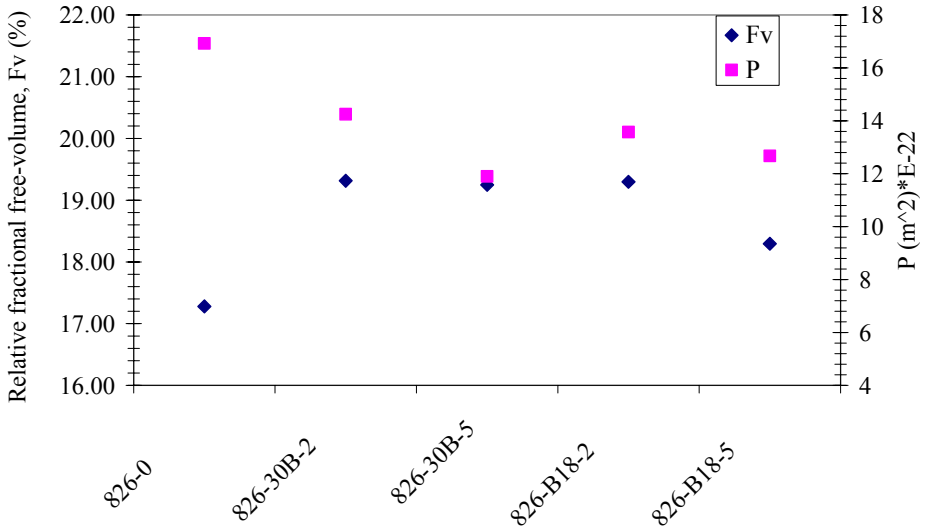

Figure 5.47. Comparison of relative fractional free volume and permeability values for Epon™826 specimens

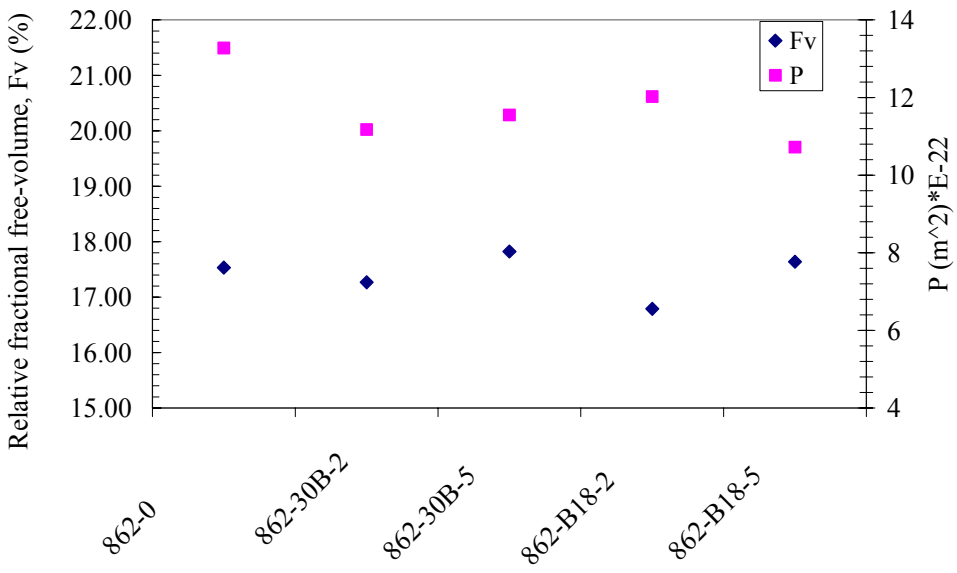

Figure 5.48. Comparison of relative fractional free volume and permeability values for Epon^{TM}862 specimens

After analyzing the results of the graphs shown above it can be observed that, in general, samples that are not modified with nanoclays with higher permeability had the lower value of relative fractional free volume and free holes size. This result can be contradictory with the expected behavior, nevertheless as mentioned above; the higher values of the free volume noticed in the modified samples could be related to the out-diffusion of positrons and o-Ps from the filler particles into the matrix.

Permeability in nanocomposites modified with platelet like particles is affected by two main factors. One is the geometric factor that favors the reduction in permeability by forcing diffusing molecules to take a long way around the platelets and hence depends only on the size of clay nanoparticles and the other factor is related to the molecular level interaction of the matrix polymer with the filler.

It was observed that the samples of Epon^{TM}826 and Epon^{TM}862 with the lowest value of permeability had the highest values of free volume void size. This apparent contradiction could be explained with the theory mentioned before regarding the distribution of the free volume.

5.6. Thermal cycling

It is well known that the addition of nanoclays has positive effects on many properties of the composite materials, such as flame retardance, thermal stability, mechanical properties, and permeability. However, the behavior of the nanoclay modified composite at extreme

temperatures is not yet fully understood. Zhang et al. [10] studied the behavior of a nanoclay modified polyimide material at cryogenic temperatures and discovered that the addition of the clays could increase the composite's strength due to the fact that the interfacial adhesion of the clay and polymer matrix was stronger at cryogenic temperature than at room temperature. Extreme temperatures can cause significant changes in a nanocomposite affecting the material's performance and in order to understand how the properties of the materials are affected, this work was focused in the study of the thermal properties of epoxy-nanoclay composites subjected to extreme thermal cycling. After the samples were thermally cycled, the permeation and all the thermal characterization data were measured again in order to assess how the environmental conditions affect the leakage and the thermal properties of the nanocomposites.

5.6.1. Permeability coefficient

The analyses of the permeability coefficient were done following the same method mentioned above.

The leak rate was obtained from the leak detector after the samples were thermally cycled and some of the results are displayed in the figures 5.49 to 5.55.

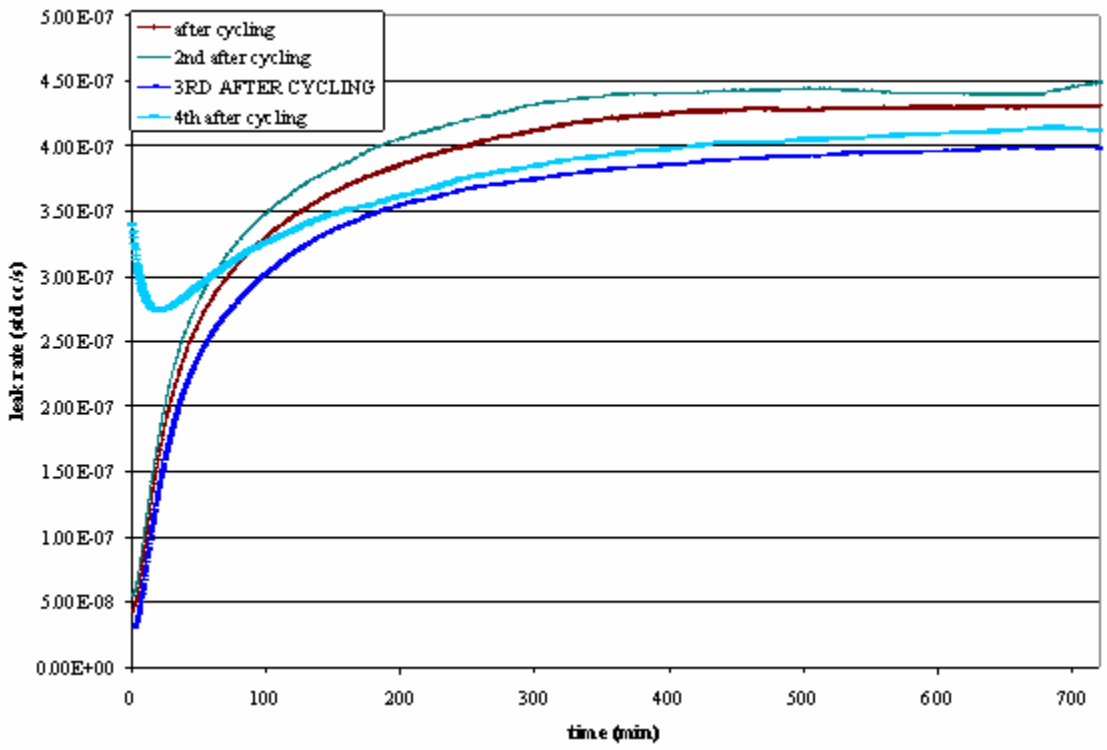

Figure 5.49. Leak rate after thermal cycling of Epon^{TM}826 non-modified

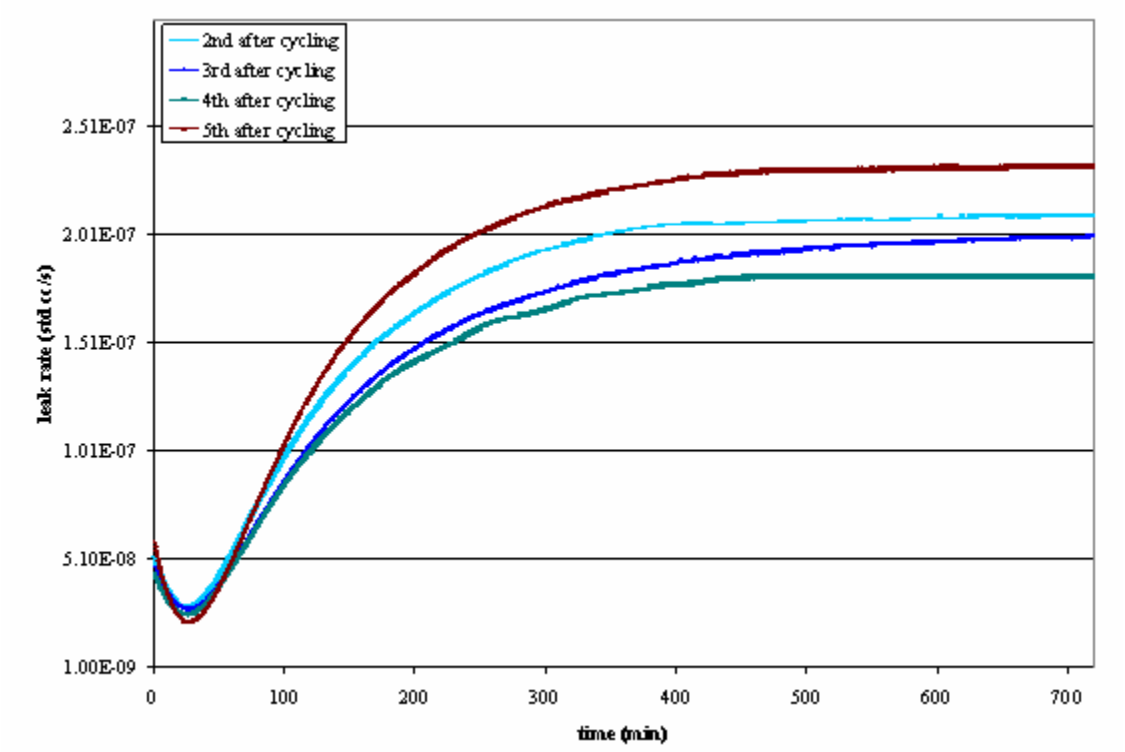

Figure 5.50. Leak rate after thermal cycling of Epon™826 modified with 5wt% of Cloisite®30B

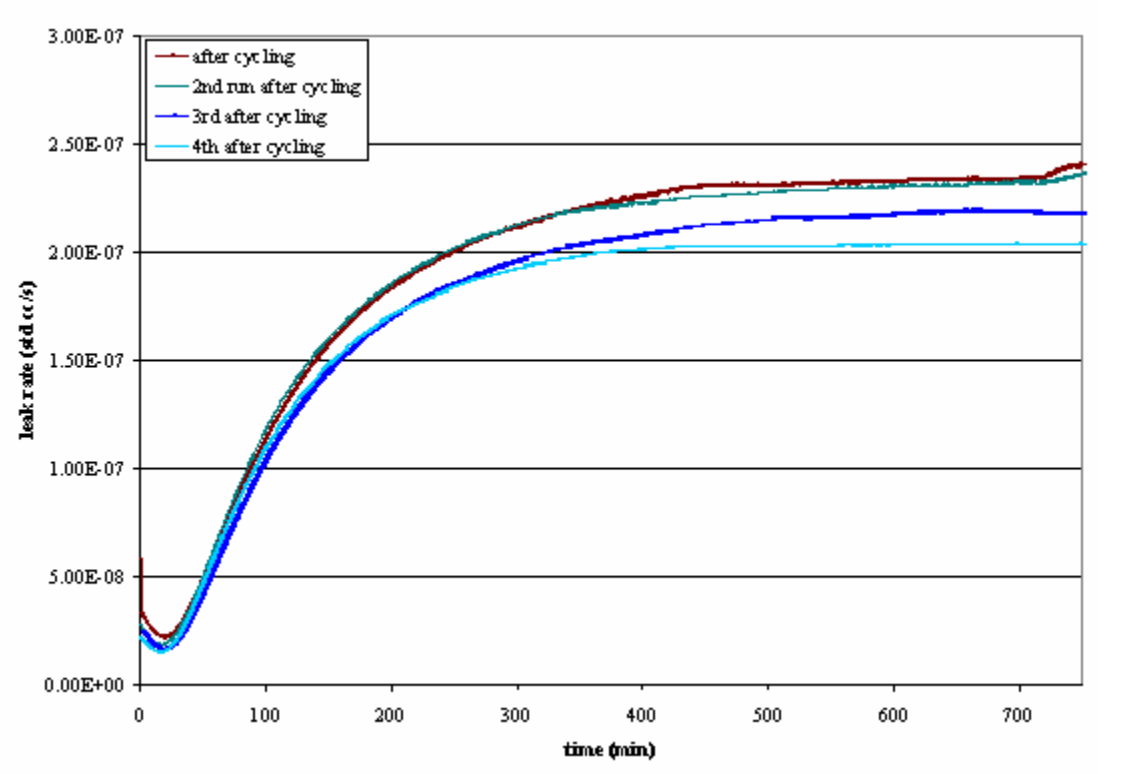

Figure 5.51. Leak rate after thermal cycling of Epon™826 modified with 2wt% of nanoclay B18

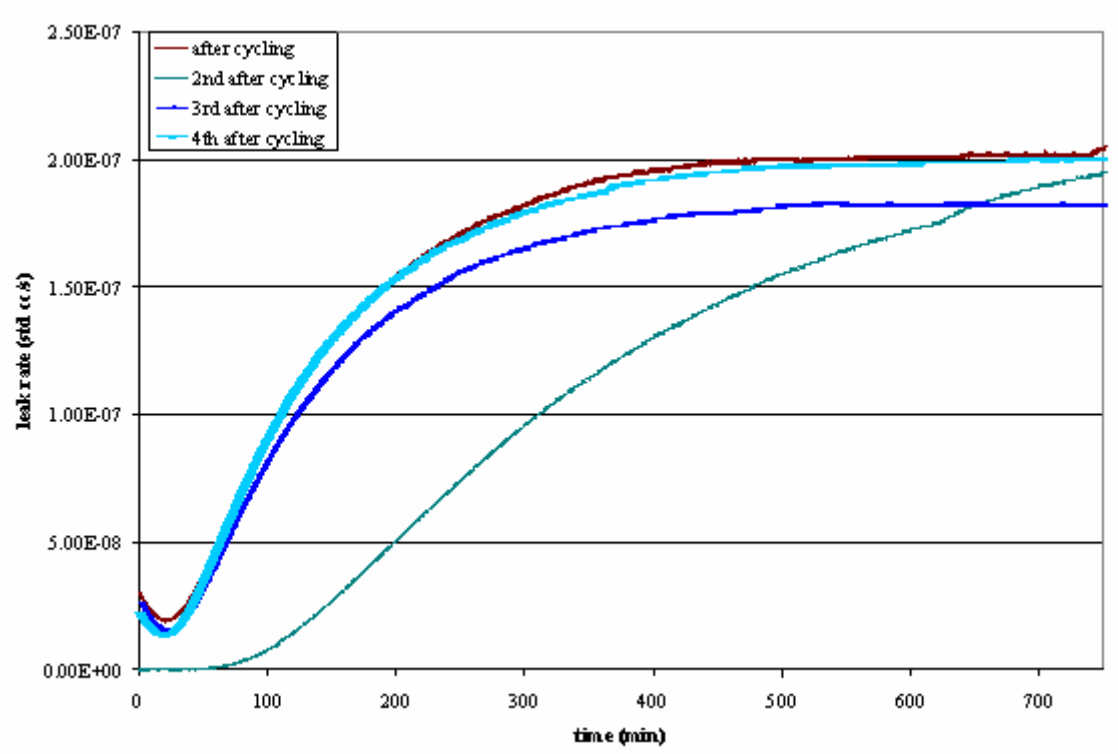

Figure 5.52. Leak rate after thermal cycling of Epon™862 modified with 2wt% of Cloisite®30B

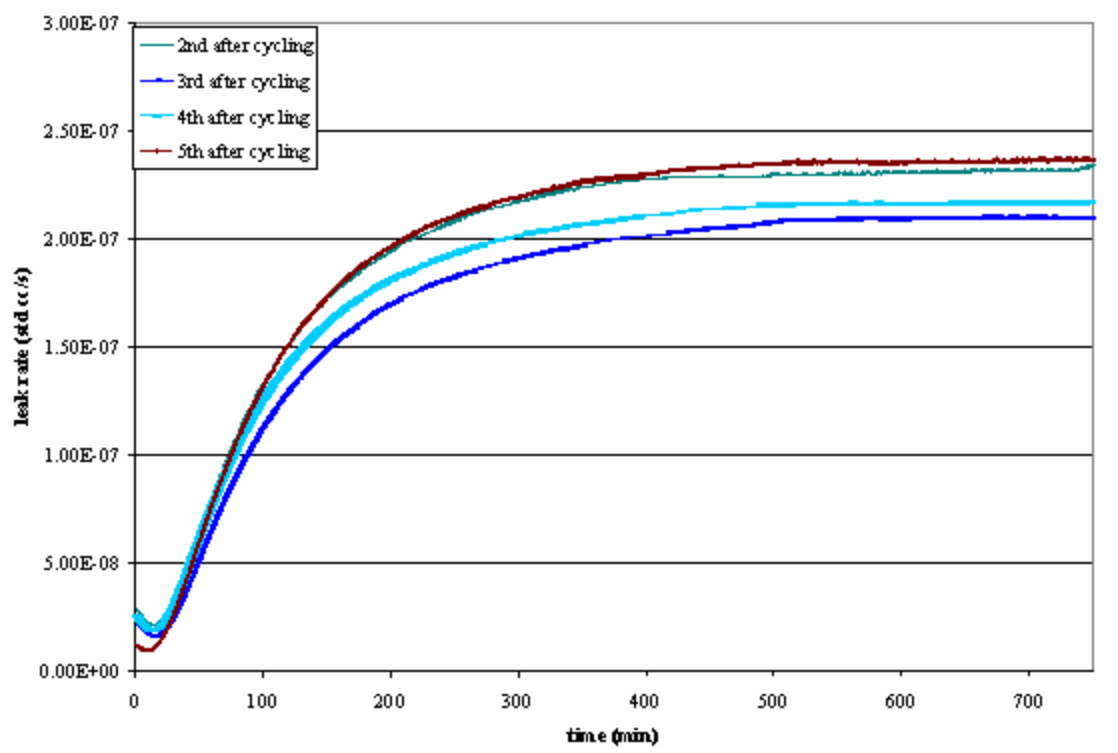

Figure 5.53. Leak rate after thermal cycling of Epon™862 modified with 2wt% of nanoclay B18

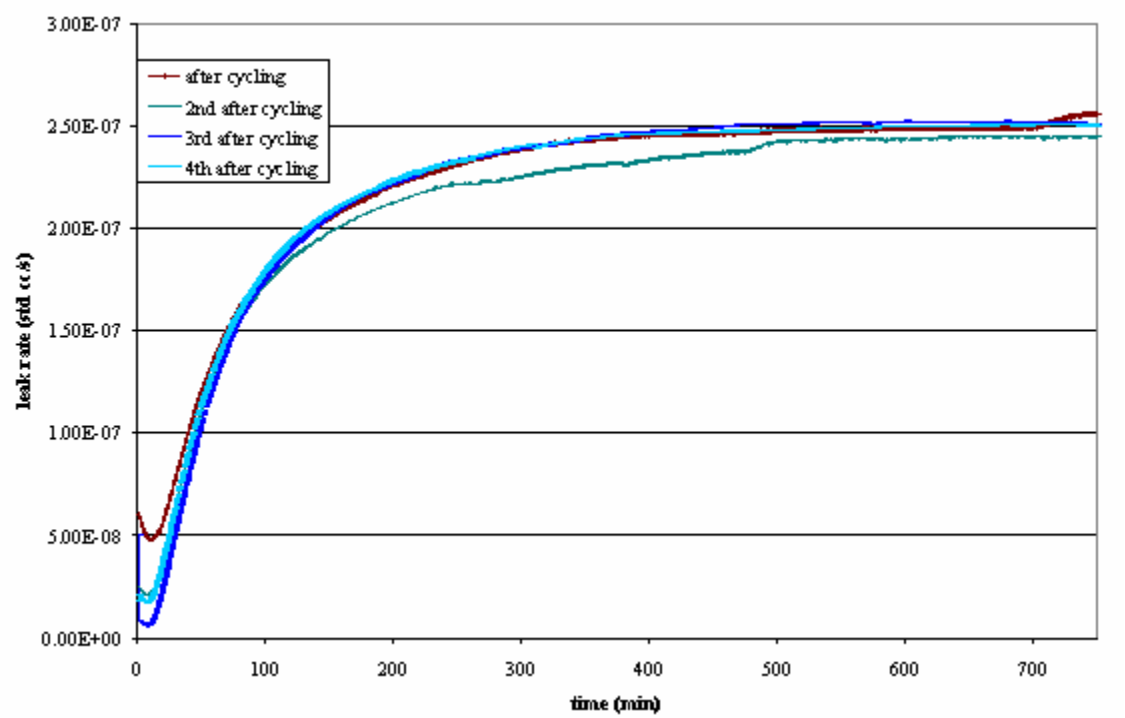

Figure 5.54. Leak rate after thermal cycling of Cycom®977-2 non-modified

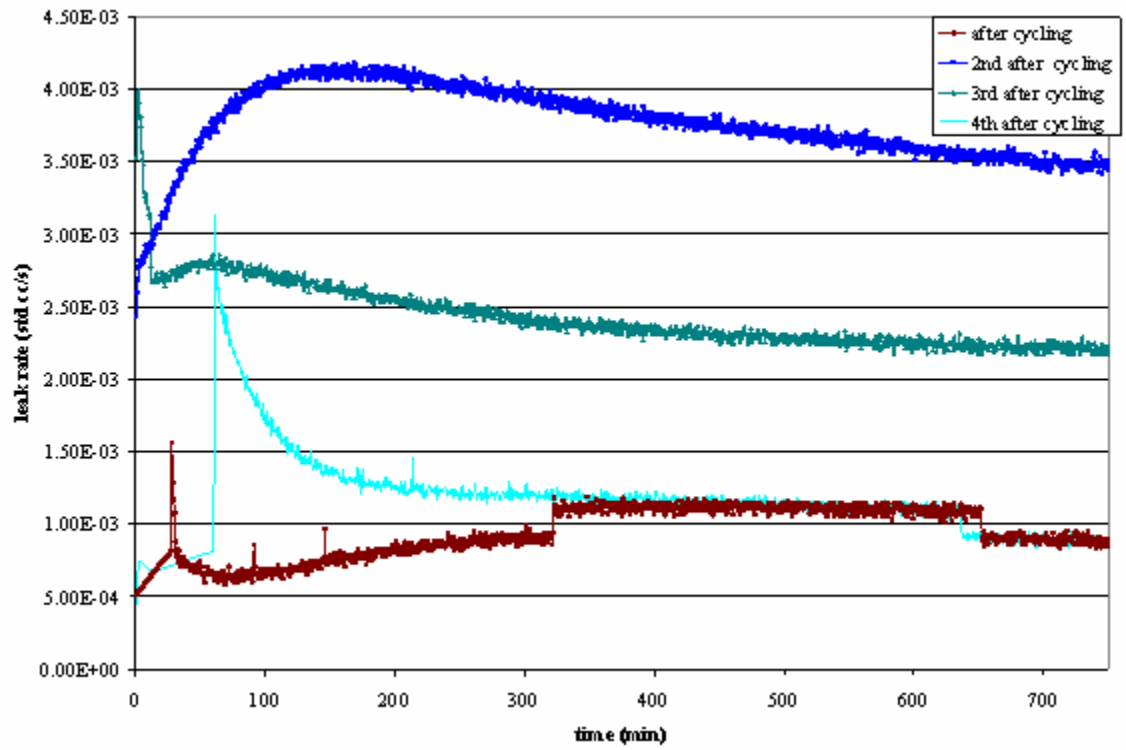

Figure 5.55. Leak rate after thermal cycling of Cycom®977-2 modified with 2wt% of nanoclay B18

The results of the permeability coefficient are summarized in the following graph where they are compared to the results before thermal cycling.

As it is noted there is no value for the coefficient after cycling for samples 862-0 and 862-B18-5, these two samples were cracked during the cycling procedure and their leak rate was too high for the sensitivity of the leak detector. In the case of sample 9772-B18-2 the sample was cracked as well, and although the value of the leak rate was measured, it was four orders of magnitude higher than the rest of the samples and too high to be compared in the same graph. The value of the permeability coefficient after cycling for this sample was found to be $5.81*10^{-18}$ m^2.

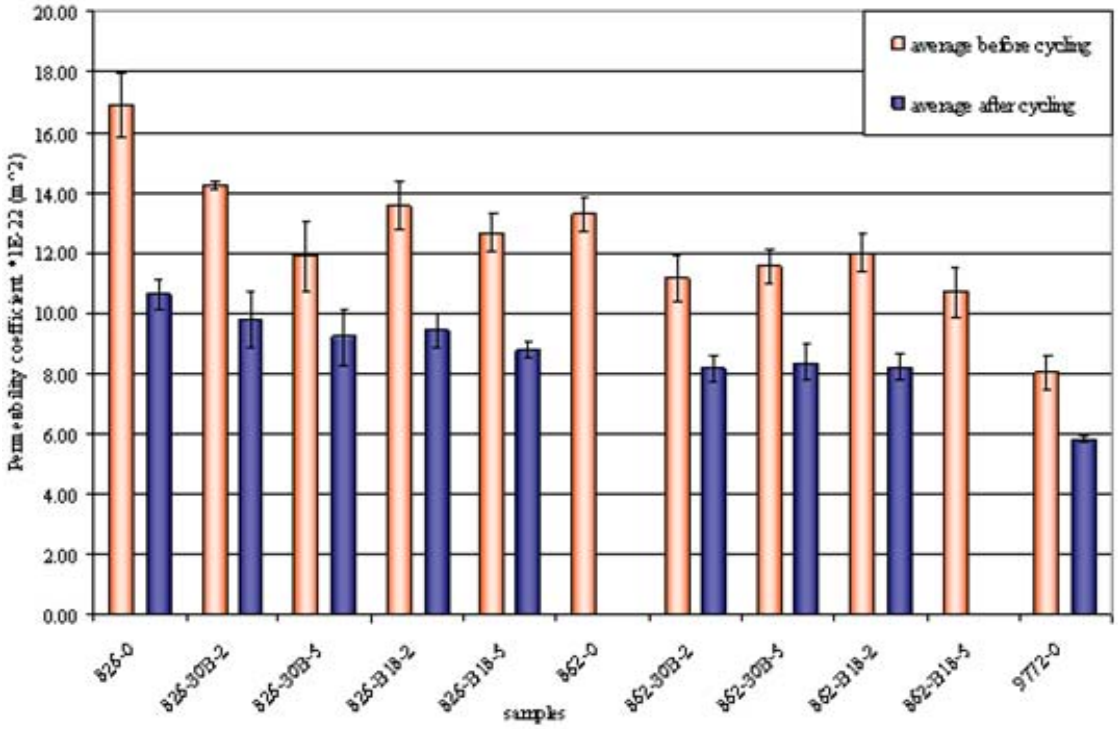

Figure 5.56. Comparison permeability coefficient (m^2) before and after thermal cycling

From the results obtained it was observed that after thermal cycling all the samples improved their permeability to helium under the conditions stated before. For samples from Epon^{TM}826 it was found that the reduction in permeability was up to 37% for samples not modified when compared to the permeability before cycling. In nanoclay modified samples of

Epon^{TM}826 was noted that the average reduction in permeability was about 30%. In the case of Epon^{TM}862 the reduction in permeability was of about 27%.

It was observed that the thermal cycling applied to the samples reduced the permeability values in all the cases including in samples that are not modified with nanoclays. It is believed that the thermal treatment caused an arrangement of the polymeric chains and modifies the free volume distribution of the polymers. The distribution of the free volume is related with the permeability and any changes in the free volume are therefore reflected in the permeability of the diffusing gas.

Table 5.12. Permeability coefficient comparison before and after thermal cycling

sample	Permeability coef. $(m^2)*10^{-22}$ before thermal cycling	std dev	Permeability coef. $(m^2)*10^{-22}$ after thermal cycling	std dev
826-0	16.93	1.05	10.65	0.49
826-30B-2	14.25	0.10	9.80	0.93
826-30B-5	11.90	1.16	9.21	0.94
826-B18-2	13.58	0.79	9.43	0.57
826-B18-5	12.68	0.60	8.80	0.27
862-0	13.28	0.57	-	-
862-30B-2	11.18	0.75	8.15	0.41
862-30B-5	11.55	0.56	8.36	0.58
862-B18-2	12.03	0.65	8.21	0.45
862-B18-5	10.72	0.82	-	-
9772-0	8.03	0.55	5.83	0.08
9772-B18-2	8.76	0.62	58100.00	-

5.6.2. DMA results

The DMA tests were repeated in the samples after they were thermally cycled. The results are shown in the following figures.

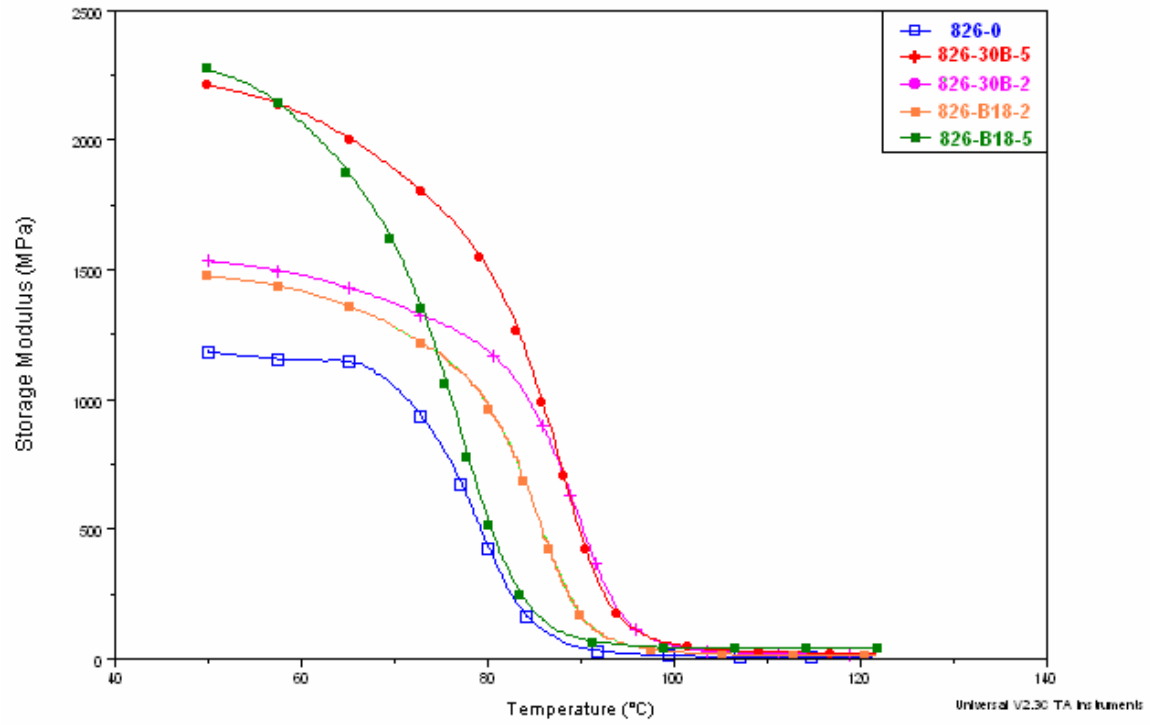

Figure 5.57. Comparison of storage modulus after thermal cycling for samples from Epon™826

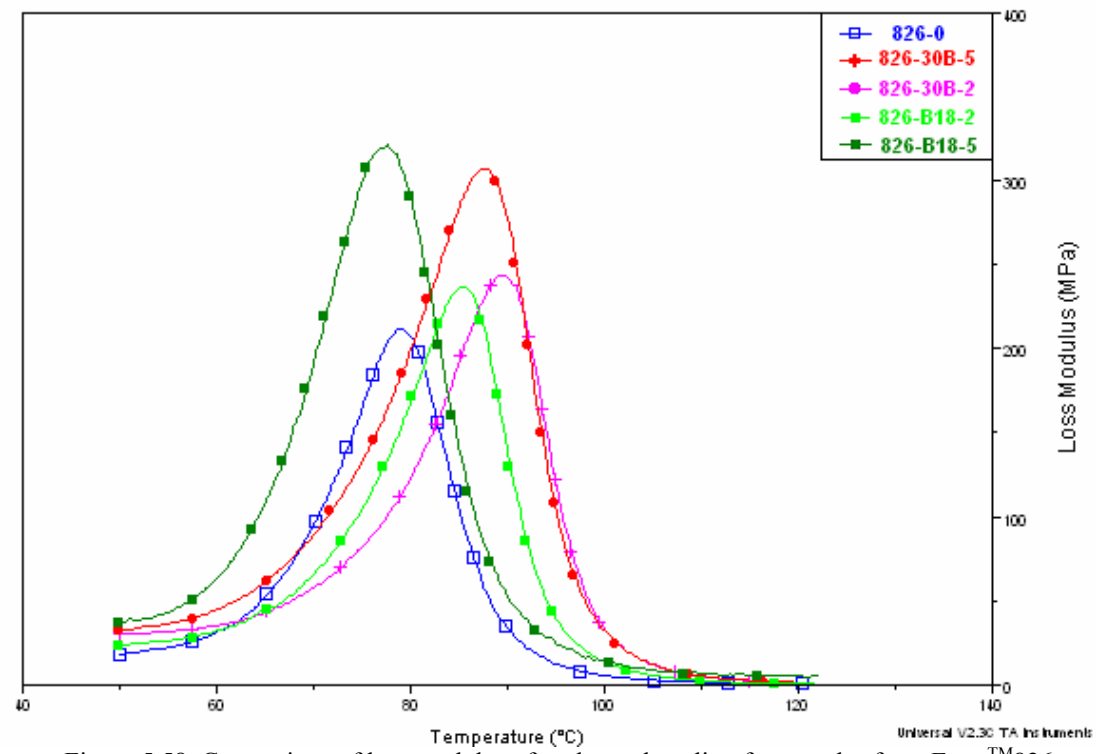

Figure 5.58. Comparison of loss modulus after thermal cycling for samples from Epon™826

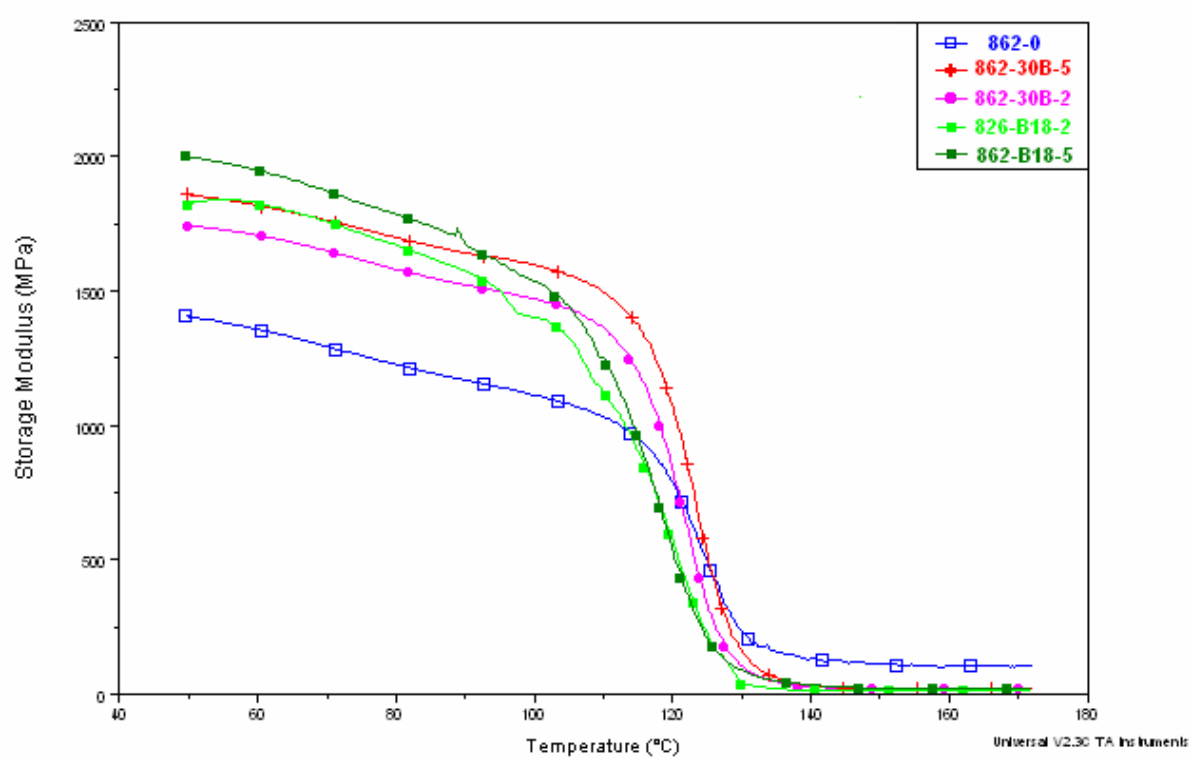

Figure 5.59. Comparison of storage modulus after thermal cycling for samples from Epon™862

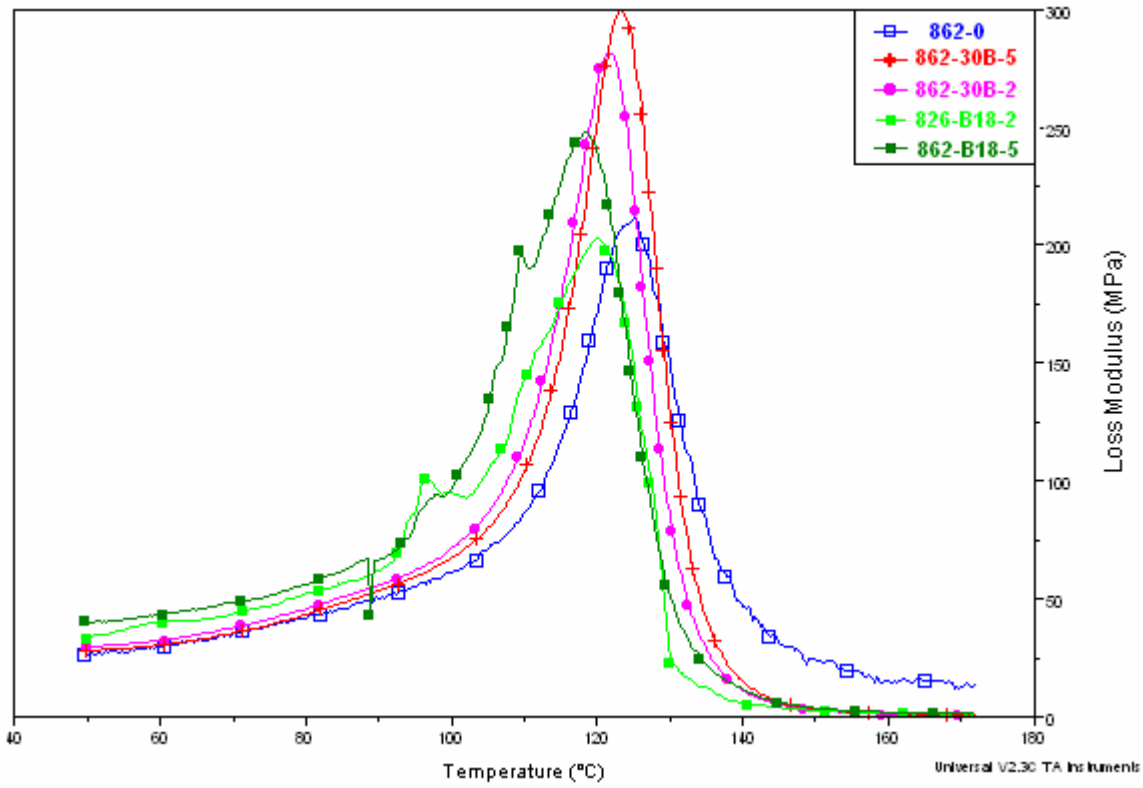

Figure 5.60. Comparison of loss modulus after thermal cycling for samples from Epon™862

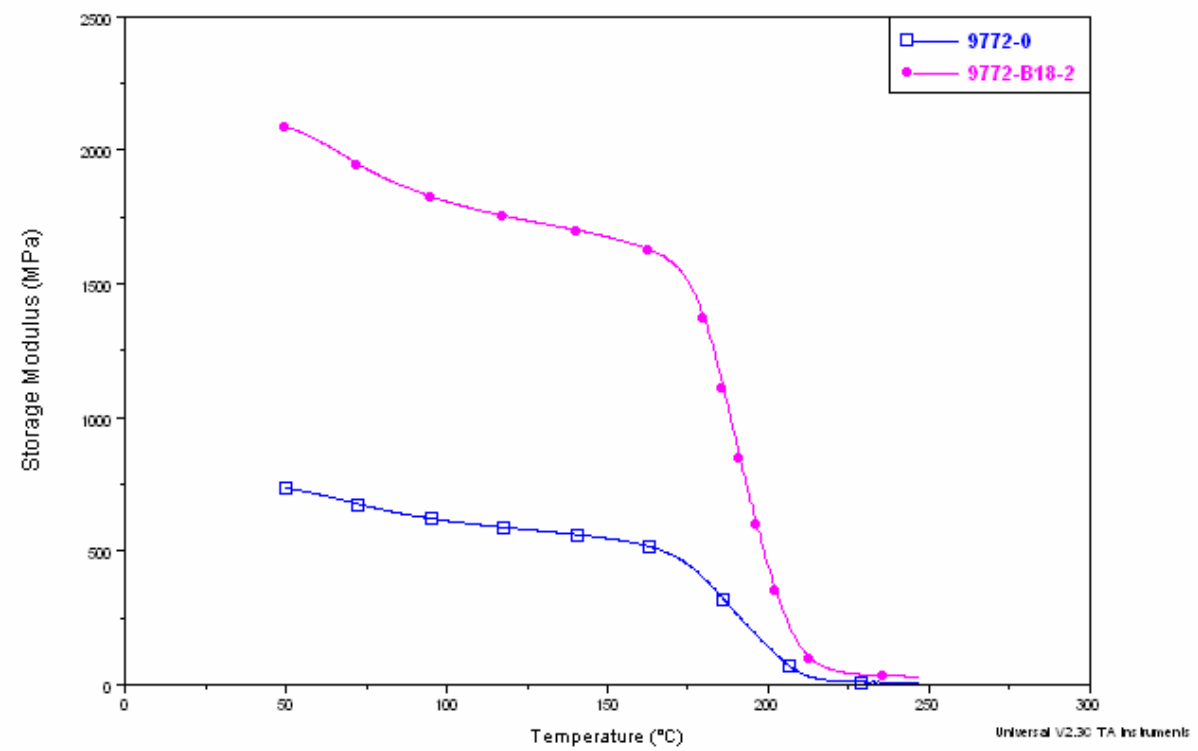

Figure 5.61. Comparison of storage modulus after thermal cycling for samples from Cycom®977-2

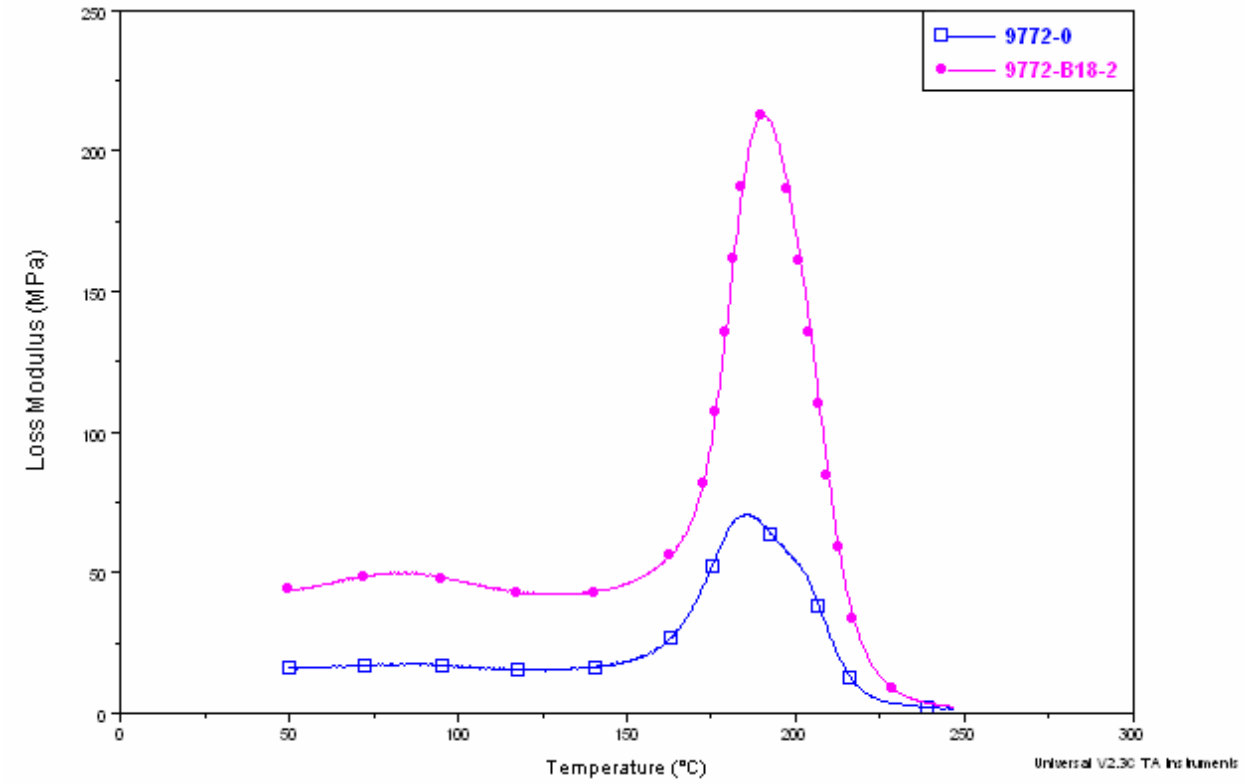

Figure 5.62. Comparison of loss modulus after thermal cycling for samples from Cycom®977-2

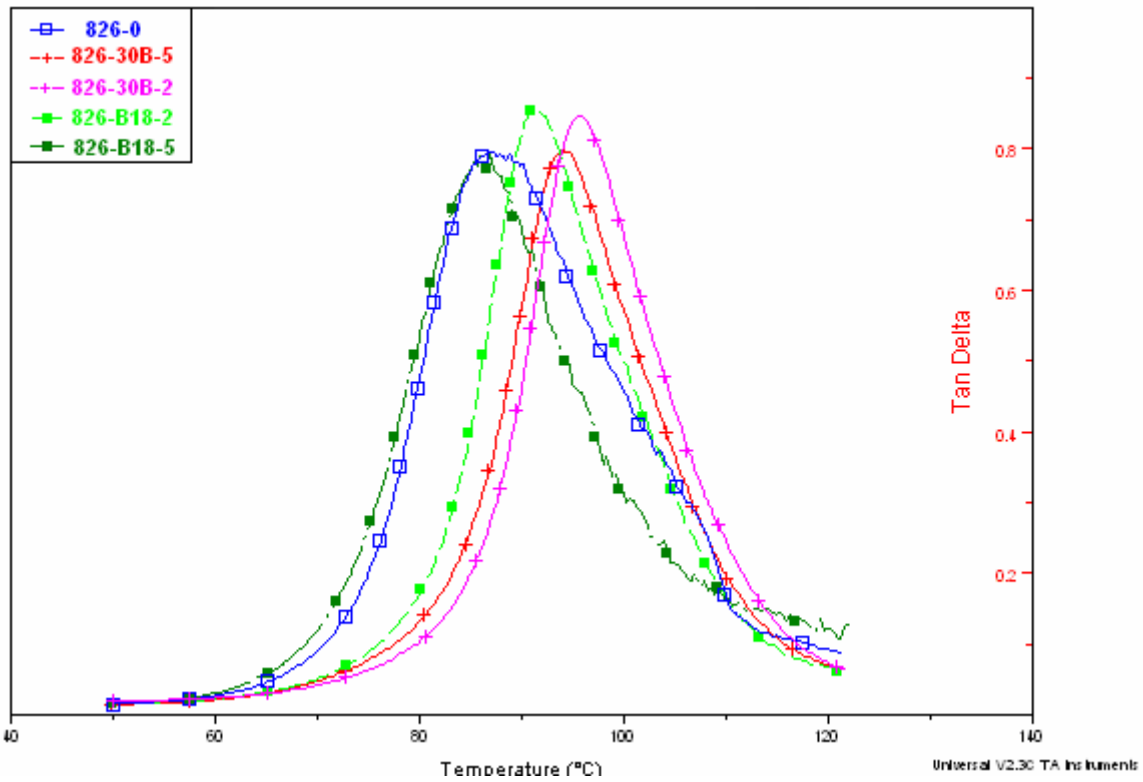

Figure 5.63. Comparison of tan delta after thermal cycling for samples from Epon^{TM}826

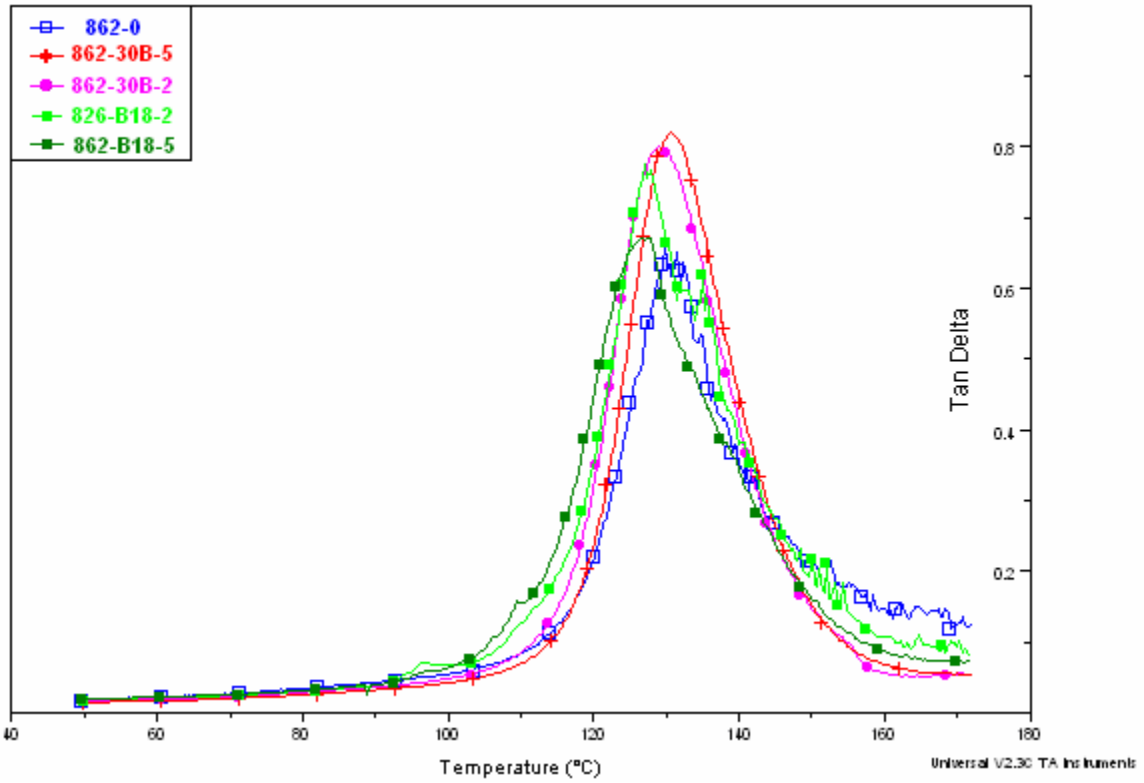

Figure 5.64. Comparison of tan delta after thermal cycling for samples from Epon^{TM}862

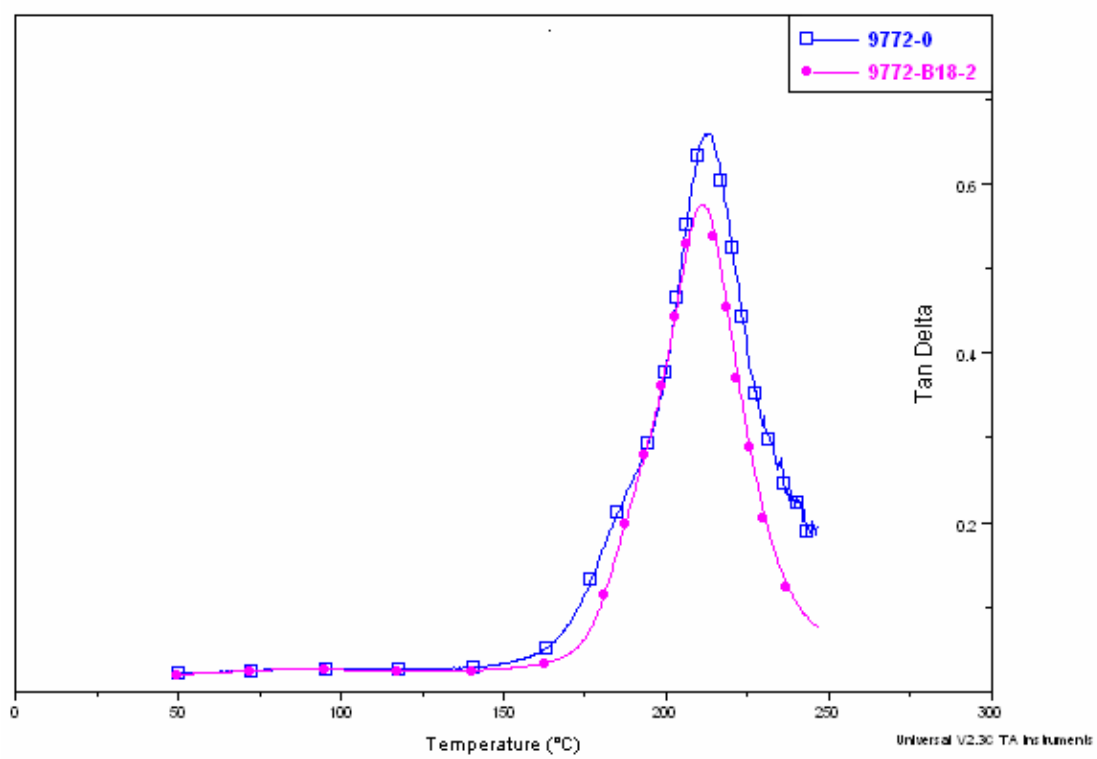

Figure 5.65. Comparison of tan delta after thermal cycling for samples from Cycom®977-2

The results obtained showed that there is no change in the rubbery plateau region after thermal cycling was done. Nevertheless, some changes were observed after the thermal cycling was applied to the samples.

In samples from Epon™826 was observed that at 50°C, within the glassy region, the storage modulus of the neat epoxy decreased about 28% when compared to the same value before thermal cycling and in the case of samples modified with 2wt% of Cloisite®30B the decrease was of 10%. In all the other samples it was noticed an increased value, the highest increase of 28% was observed in samples modified with 5wt% of nanoclay B18.

In samples manufactured with Epon™862 the neat epoxy showed a decrease of 25% in the storage modulus at 50°C after the thermal cycling was applied and samples modified with Cloisite®30B had a decrease in the storage modulus as well. In the case of the specimens modified with nanoclay B18, the value of the storage modulus at 50°C after the thermal treatment was applied showed an increase of 8% when compared to the same value before the cycling.

Specimens made of neat Cycom®977-2 resin had a decrease of 67% in the storage modulus after the thermal treatment and in the case of samples modified with 2wt% of B18; the reduction was of 15%.

5.6.3. TGA data

The results obtained after the thermal cycling was applied to the samples are shown in the following graphs.

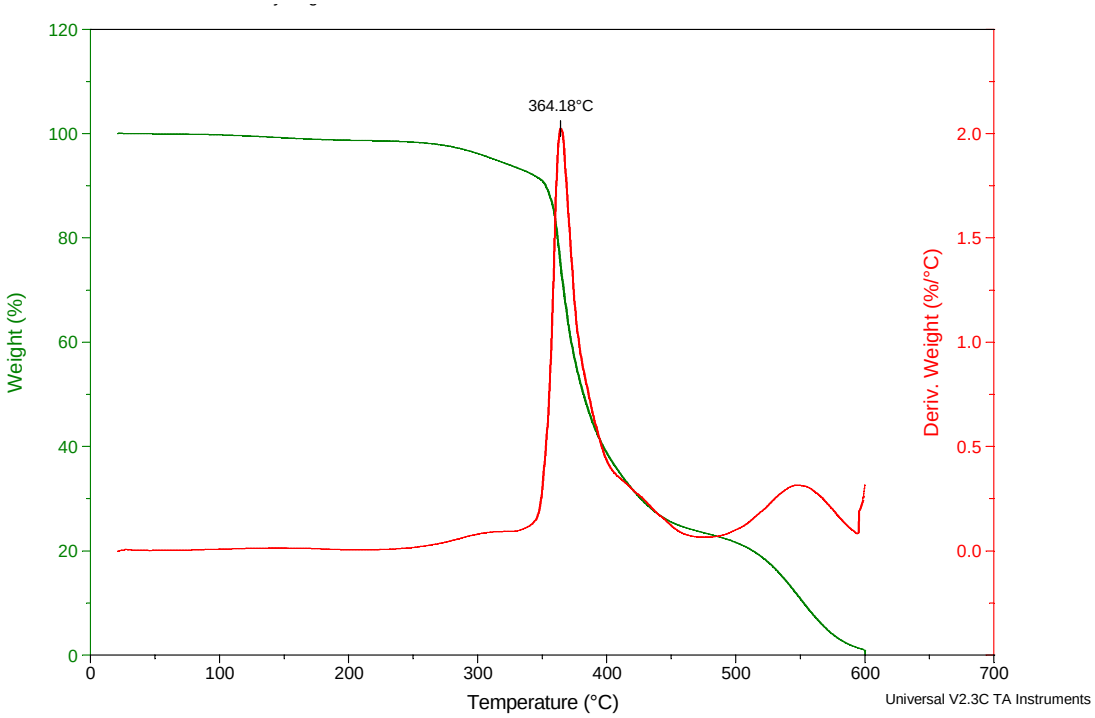

Figure 5.66. TGA curve after thermal cycling for sample of Epon™826 non-modified

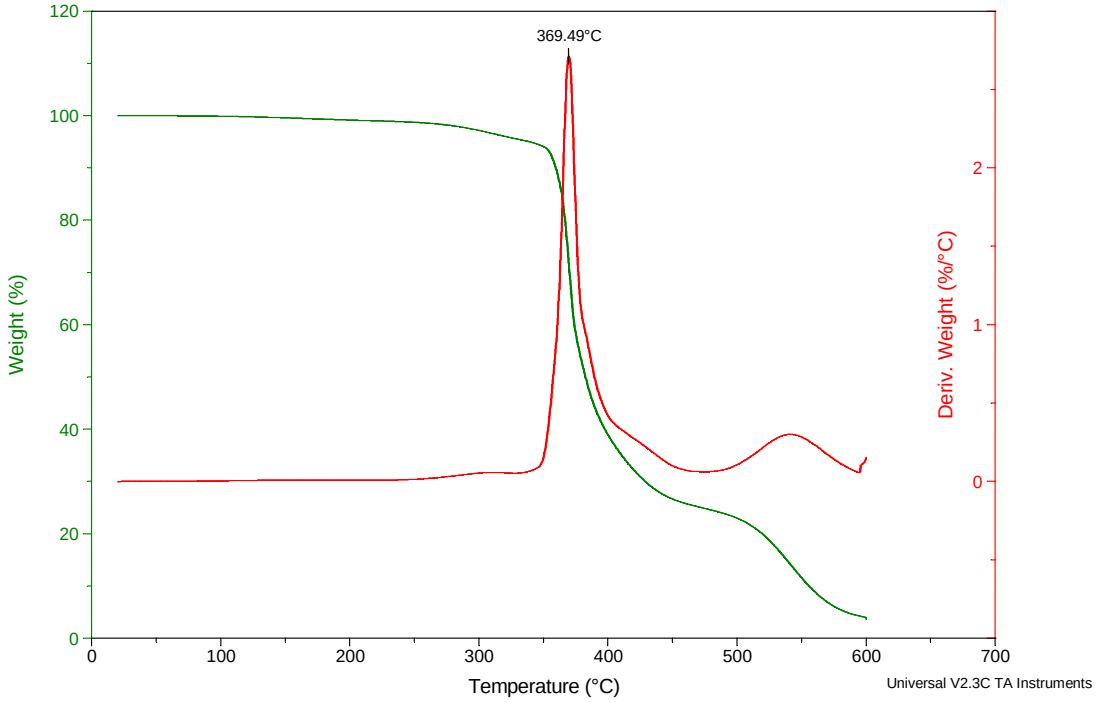

Figure 5.67. TGA curve after thermal cycling for sample of Epon^{TM}826 modified with 5wt% of Cloisite$^{®}$30B

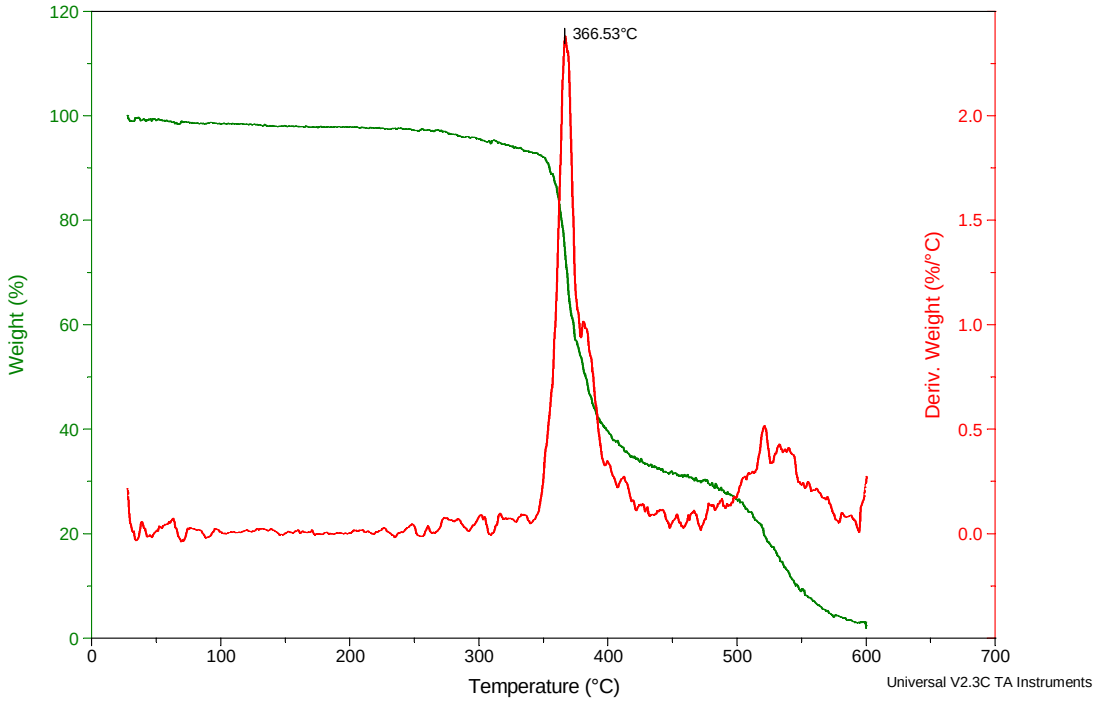

Figure 5.68. TGA curve after thermal cycling for sample of Epon^{TM}826 modified with 2wt% of nanoclay B18

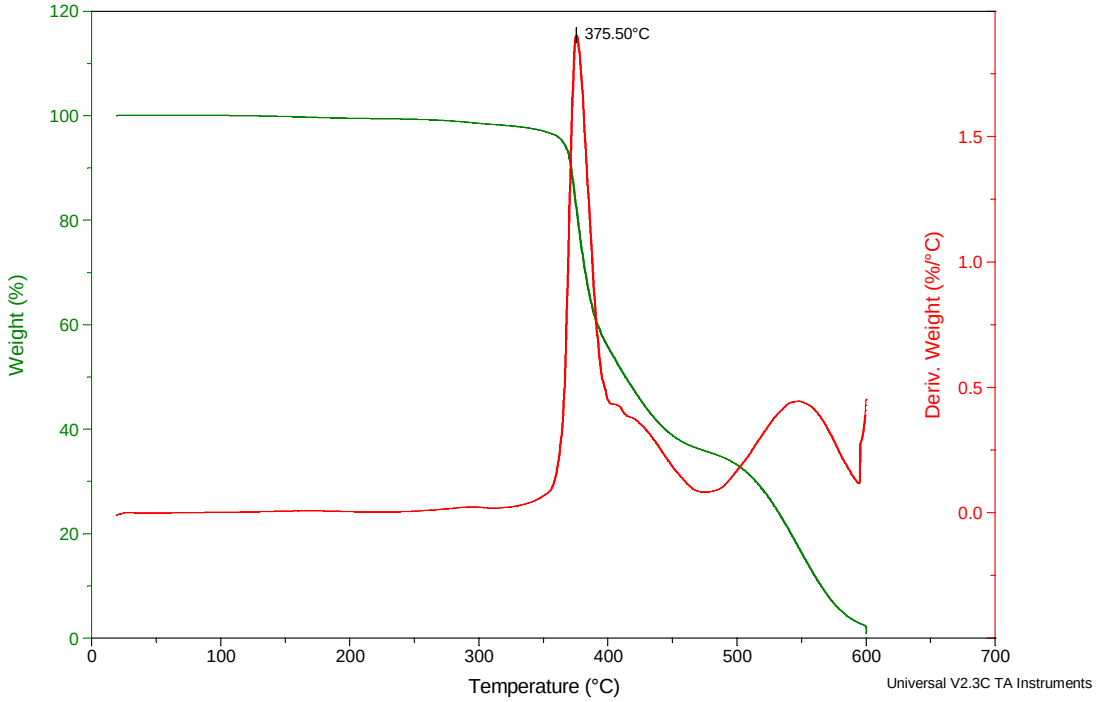

Figure 5.69. TGA curve after thermal cycling for sample of Epon™862 non-modified

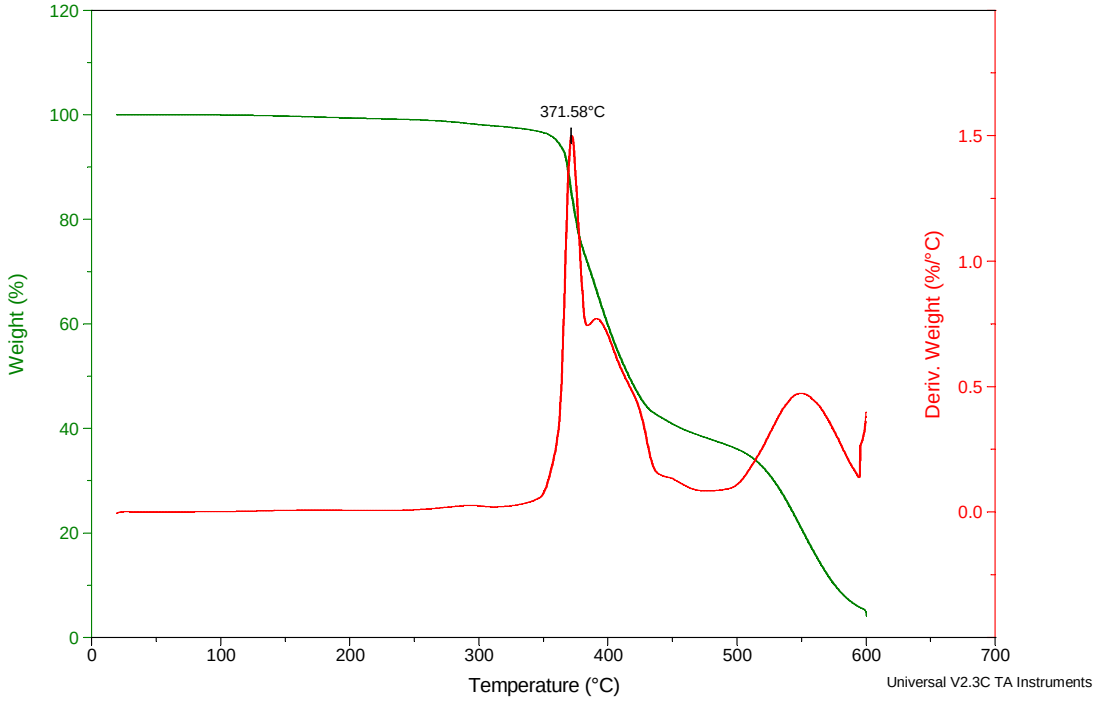

Figure 5.70. TGA curve after thermal cycling for sample of Epon™862 modified with 5wt% of Cloisite®30B

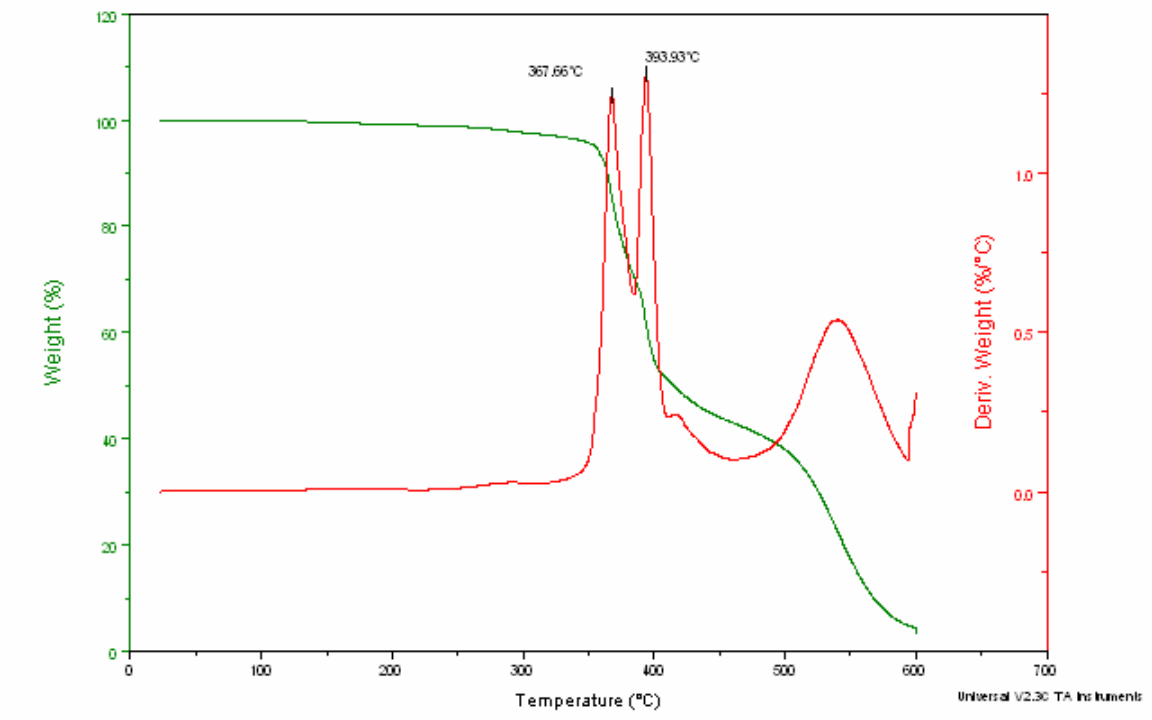

Figure 5.71. TGA curve after thermal cycling for sample of Epon^{TM}862 modified with 5wt% of nanoclay B18

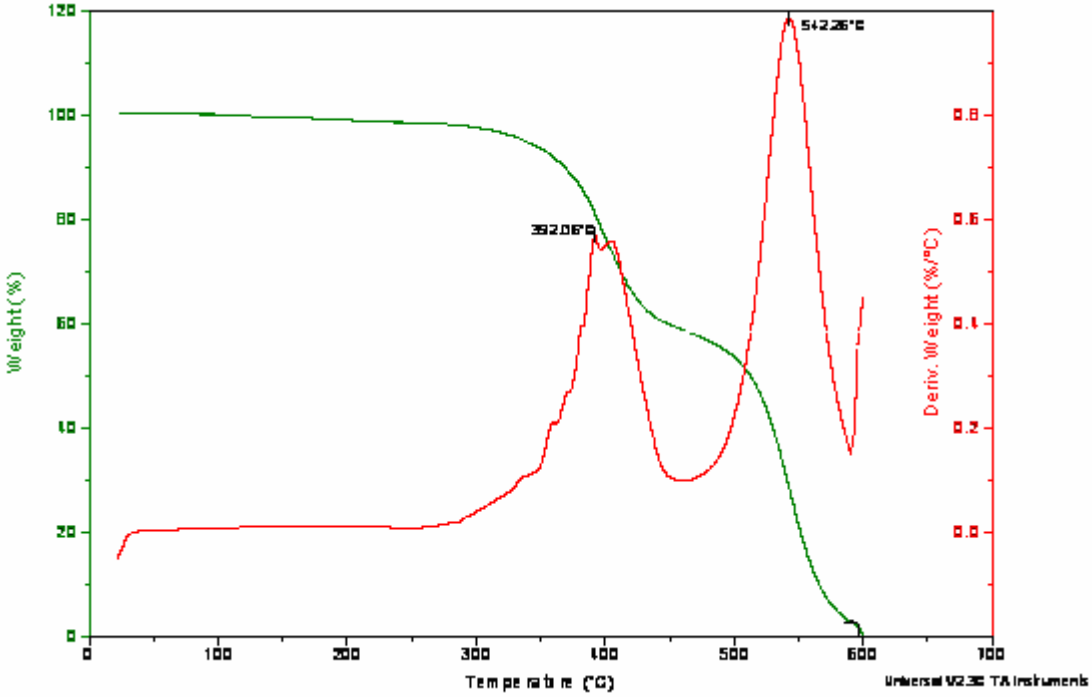

Figure 5.72. TGA curve after thermal cycling for samples from Cycom®977-2 non-modified

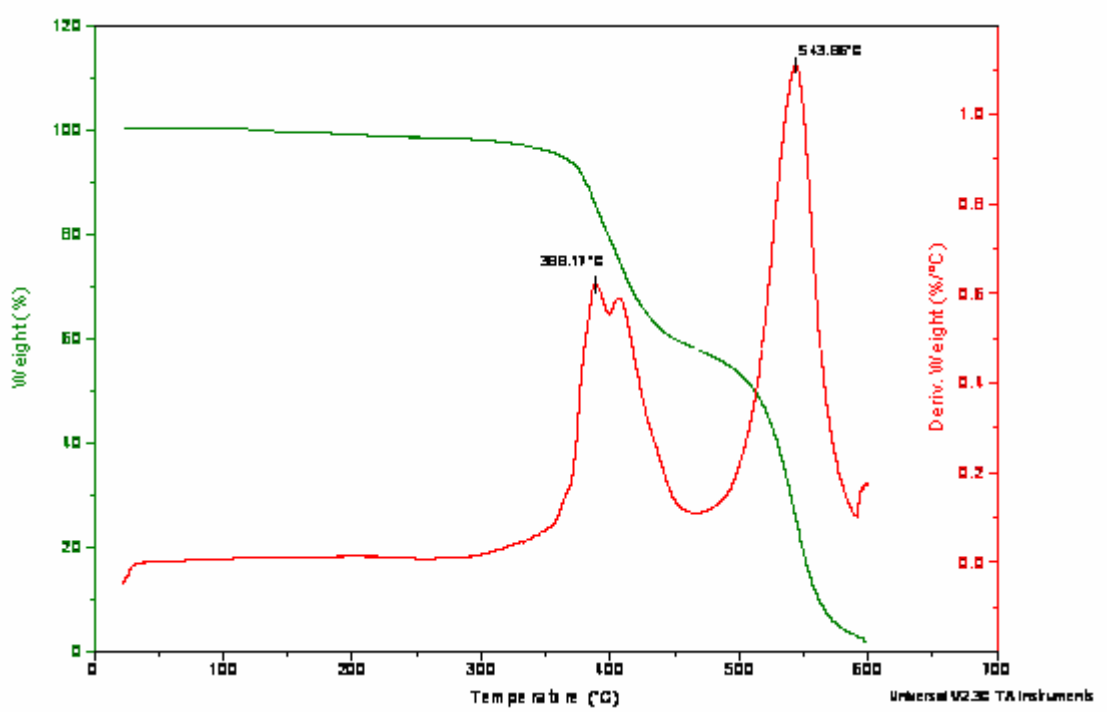

Figure 5.73. TGA curve after thermal cycling for samples from Cycom®977-2 modified with 2wt% of nanoclay B18

After the thermal treatment was applied, the effect of the nanoclays on the thermal stability of the samples was analyzed. The thermal stability of the nanocomposites decreased after the thermal cycling was applied. Regarding the behavior of the samples modified with nanoclays, it was noted that the tendency observed before thermal aging was maintained, i.e., the nanocomposites manufactured from Epon^{TM}826 modified with nanoclays showed a general increasing trend in thermal stability when compared to the neat epoxy, while those made with Epon^{TM}862 the observed behavior was a reduction in thermal stability when the nanoclays were added and compared to the values of the pristine polymer. The summary of the values obtained before and after cycling is reported in the table below.

Table 5.13. Comparison of TGA results before and after thermal cycling

samples	Before cycling				After cycling			
	Degradation temperature (˚C)	Std dev	Residue (%)	Std dev	Degradation temperature (˚C)	Std dev	Residue (%)	Std dev
826-0	363.76	1.67	0.38	0.26	360.37	0.97	0.39	0.03
826-30B-2	367.57	0.62	1.63	0.15	364.48	0.63	1.62	0.22
826-30B-5	367.51	0.53	3.55	0.09	366.26	0.86	3.62	0.49
826-B18-2	365.40	0.35	1.24	0.20	363.25	0.92	1.28	0.39
826-B18-5	361.41	0.18	3.50	0.06	359.53	0.66	3.39	0.18
862-0	379.16	0.31	0.74	0.30	376.05	0.59	0.77	0.28
862-30B-2	380.19	2.02	1.57	0.27	375.42	0.95	1.54	0.01
862-30B-5	374.45	2.04	3.50	0.02	370.19	1.39	3.46	0.07
862-B18-2	374.48	0.95	1.44	0.16	371.52	0.99	1.72	0.13
862-B18-5	369.50	0.43	3.61	0.13	368.31	1.02	3.45	0.09
9772-0	401.47	1.81	0.24	0.25	394.95	4.08	0.54	0.05
9772-B18-2	403.77	2.68	1.44	0.11	388.20	0.04	1.59	0.10

5.6.4. DSC measurements

The DSC tests were repeated after thermal cycling and the results are displayed in the following graphs.

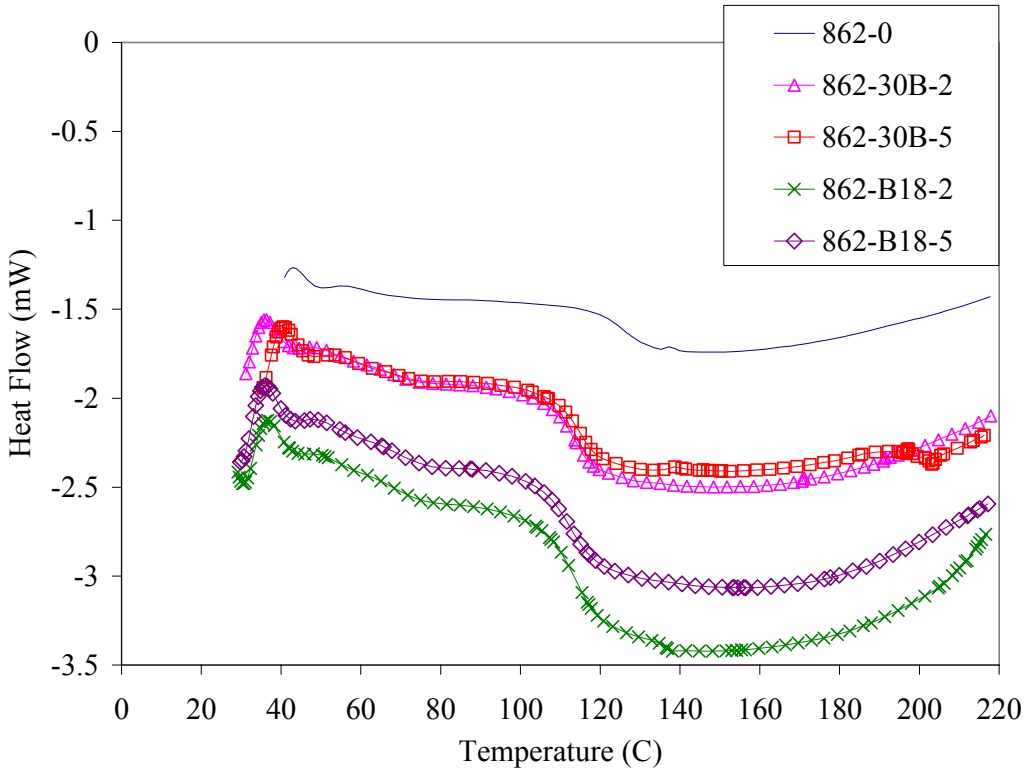

Figure 5.74. DSC plots after thermal cycling for samples from Epon™862

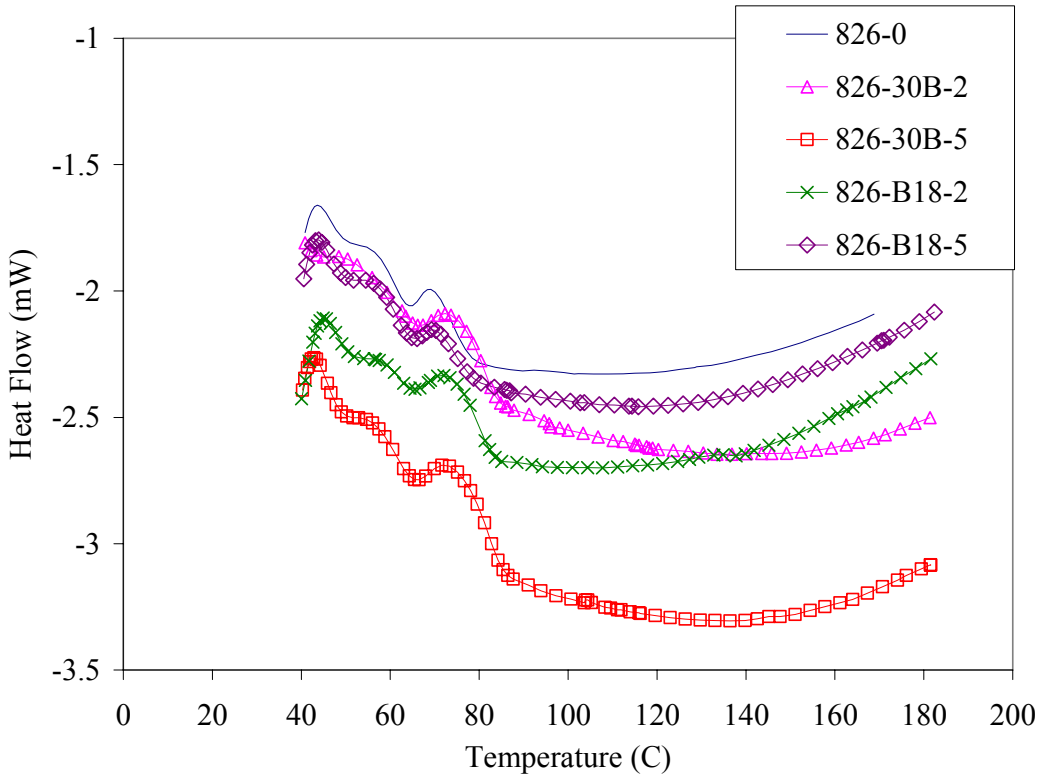

Figure 5.75. DSC plots after thermal cycling for samples from Epon^{TM}826

The comparison of the results for the glass transition before and after thermal cycling is listed in the following table and in figure 5.76.

Table 5.14. Glass transition values comparison before and after thermal cycling

samples	Glass transition T_g (˚C)			
	Before cycling	Std dev	After cycling	Std dev
826-0	65.03	1.92	83.17	0.53
826-30B-2	77.28	0.13	80.86	0.76
826-30B-5	77.42	0.24	80.96	1.14
826-B18-2	77.31	1.58	79.79	0.72
826-B18-5	71.23	1.36	79.00	1.16
862-0	107.41	0.29	117.21	0.79
862-30B-2	108.60	0.04	114.49	0.38
862-30B-5	109.63	1.62	115.51	1.29
862-B18-2	109.29	0.91	113.72	0.38
862-B18-5	104.84	2.36	112.26	0.46

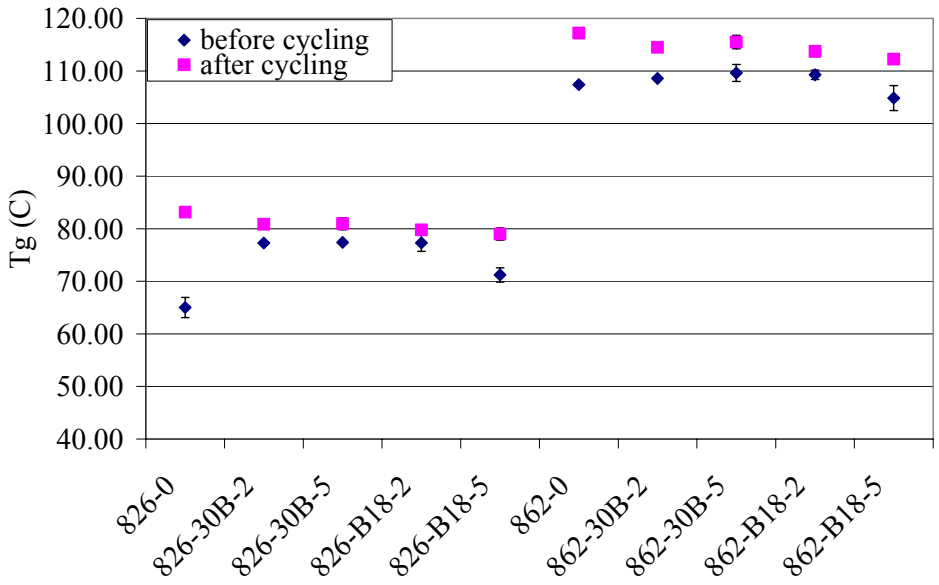

Figure 5.76. Comparison of values of T_g before and after thermal cycling

Thermal cycling increased the glass transition temperatures of the nanoclay modified composites, compared to those that were not thermally cycled. It is noticed that thermal cycling induced a higher increase in the T_g of both neat polymer resins, Epon^{TM}826 and Epon^{TM}862, over their nanoclay modified composites. Here the neat samples showed an increase of 27% in the T_g value for Epon^{TM}826 and 9% increase for Epon^{TM}862. For the nanocomposite samples the average increase in T_g values after thermal treatment was about 4% - 5%. It was also observed that samples modified with 5wt% of B18 showed a higher T_g increase in both Epon^{TM}826 and Epon^{TM}862 nanocomposites.

During the cycling process, the material first entered a cryogenic stage of -196 ˚C where the polymer chains were in a "frozen" state with decreased segmental motions. Then they were placed in an elevated temperature environment of 177 ˚C, which was above the T_g of the materials, leading to higher segmental motions. The cycle was repeated 140 times. Lastly the samples were cooled from the high temperature stage to room temperature. During this final cooling process the materials had more time to approach the equilibrium state and therefore a lower free volume was achieved. This resulted in an increased T_g.

The movement of the polymer chains in the nanoclay modified samples was hindered by the presence of the nanoclay particles. When the material was subjected to cooling from the elevated temperature stage, the rearrangement of the polymer chains was restricted, resulting in

the polymer chains being obstructed by the nanoclays while trying to approach an equilibrium state. Consequently the decrease in their free volume was not as high as that of the pristine polymer. A smaller decrease in the free volume thus is reflected in the lower values of the T_g.

After thermally cycled, the samples of both Epon^{TM}826 and Epon^{TM}862 modified with 5wt% of nanoclay B18 behaved differently from the rest of all other samples. Modification of the epoxy resin with 5wt% B18 yielded an increase in T_g which was small when compared with other nanoclay modified composites. After thermal aging the relative increase in the T_g was higher than all other samples with respect to the values before thermal cycling. X-ray diffraction results, which will be summarized in a separate paragraph, showed that these two samples had a more exfoliated structure than the other samples.

The higher nanoclay exfoliation observed in these samples could be the reason for the difference of their glass transition temperatures from those of the rest of the samples. It was reported by Xu et al. that the T_g of exfoliated nanoclay composites decreased when the content of nanoclays increased [11]. The relative lower increase in the glass transition temperature value of these samples may be associated with the mobility of the host matrix. In highly exfoliated samples the molecular mobility of the host matrix is less reduced than in the case of intercalated structures where the polymer is confined between the galleries of the clay platelets. This difference in the segmental mobility of the polymer chains results in a difference in the glass transition temperature values.

The same reasoning can be applied to the samples that underwent thermal treatment. The exfoliation of the nanoclays in the polymer matrix influences the arrangement of the polymer chains in the nanocomposite but the spatial confinement of the chains is not as restricted as in the case of intercalated structures. Therefore the increase in the T_g is higher than in the case of mixed intercalated-exfoliated structures.

5.6.5. Free volume analyses

The same procedure explained before was used to analyze the results of the PALS experiments after the samples underwent thermal cycling.

The results of the intensity and lifetime of the ortho-positroniums (o-Ps) are shown below and in the graph are compared to the values obtained before the thermal cycling was applied.

Table 5.15. Value of I_3 and τ_3 obtained from PALS experiments after thermal cycling

samples	I_3 (%)	Stand dev	τ_3 (ns)	Stand dev
826-0	10.82	0.83	1.895	0.06
826-30B-2	15.88	0.6	1.706	0.02
826-30B-5	12.28	0.8	1.862	0.05
826-B18-2	13.8	0.71	1.776	0.039
826-B18-5	13.88	0.66	1.731	0.034
862-0	12.13	0.8	1.746	0.044
862-30B-2	10.88	0.85	1.922	0.062
862-30B-5	12.76	0.74	1.829	0.045
862-B18-2	15.13	0.77	1.729	0.035
862-B18-5	13.66	0.88	1.775	0.044
9772-0	9.48	1.01	1.789	0.069
9772-B18-2	9.42	1.67	1.828	0.109

It was observed that after thermal cycling the intensity of the o-Ps decreased significantly, an average of 47% reduction when compared to the values before thermal cycling. The intensity is related to the relative number density of free volume holes in the material and therefore after thermal cycling it seems that the concentration of the largest voids is significantly reduced, this result agrees with the fact that the permeability decreased after thermal cycling. The reduction on the concentration of voids leads to a decrease in the permeability since there is less available free volume for the diffusing gas to permeate through the nanocomposite.

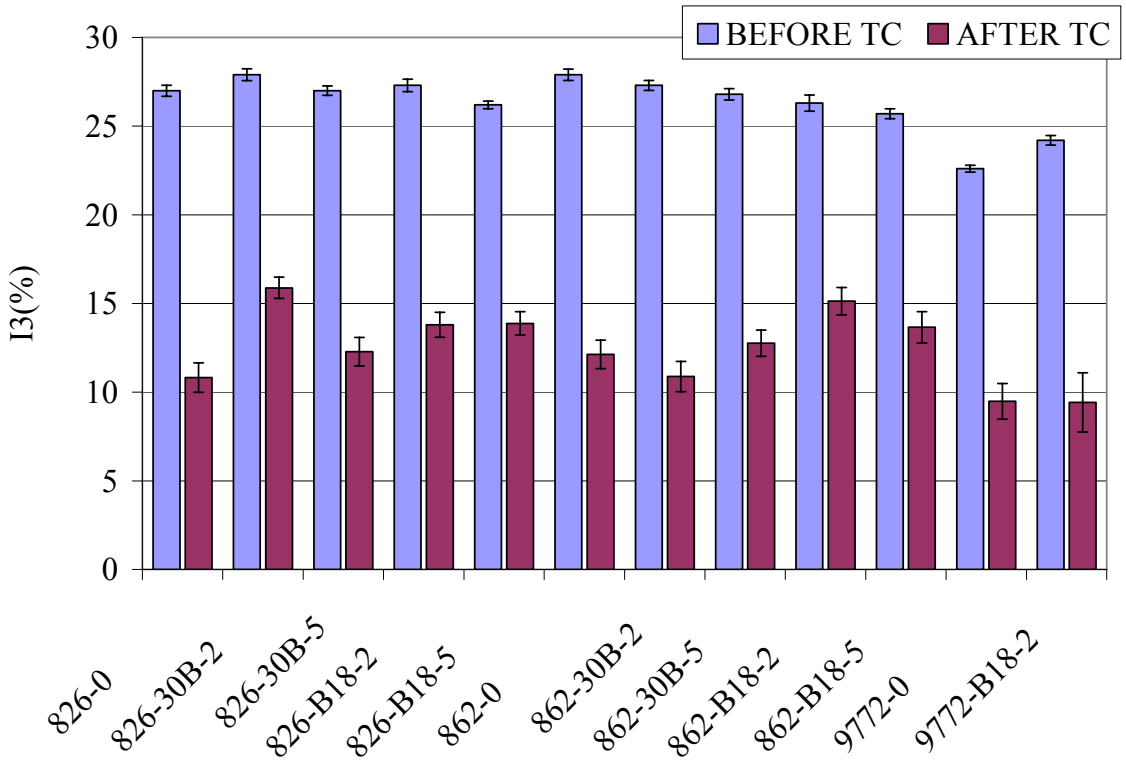

Figure 5.77. Comparison of the I_3 values before and after thermal cycling

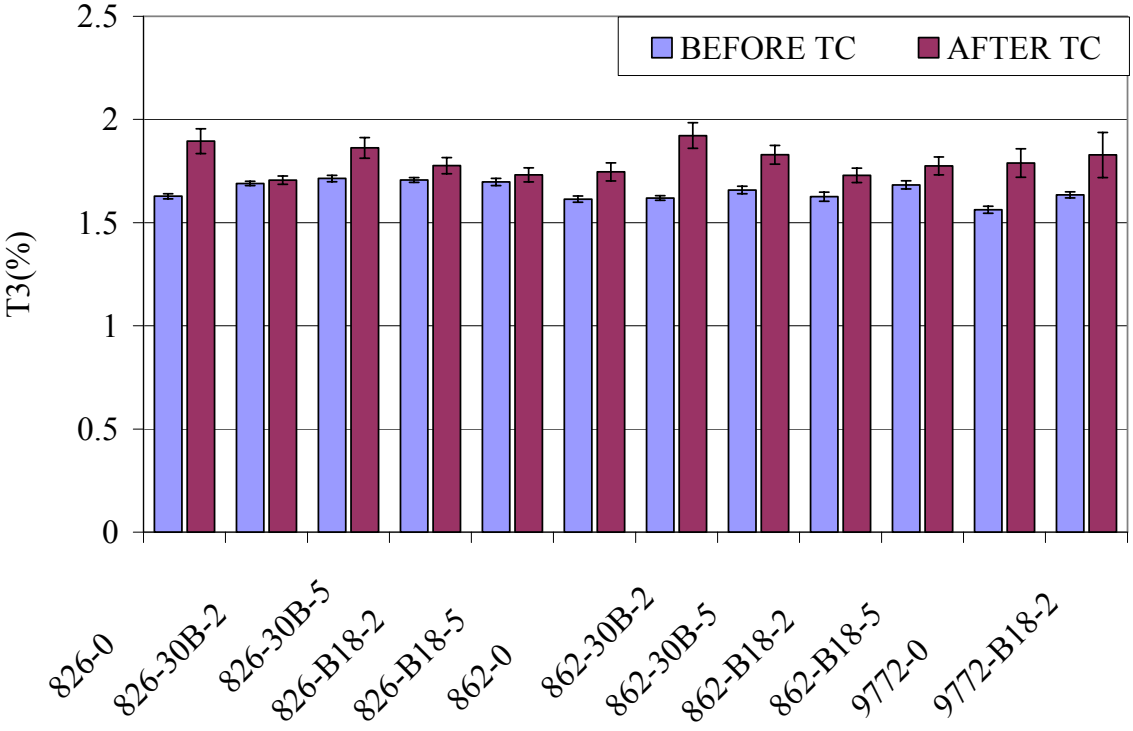

Figure 5.78. Comparison of the τ_3 values before and after thermal cycling

Regarding the values of the lifetime τ_3 it was noticed that there was a slight increase after thermal cycling. According to the PALS results, as a result of thermal cycling, the concentration of the largest voids, probably microscopic pores in the epoxy, was significantly reduced while the average size of the pores becomes slightly larger. Overall, this is related to the reduction in permeability observed with the leak detector results.

Table 5.16. Comparison of average size free volume holes (V_f) and relative fractional free volume (F_v) before and after thermal cycling

samples	Before Thermal cycling				After thermal cycling			
	R (nm)	V_f (nm^3)	V_f (A^3)	F_v (%)	R (nm)	V_f (nm^3)	V_f (A^3)	F_v (%)
826-0	0.248	0.064	63.999	17.280	0.275	0.087	87.194	9.434
826-30B-2	0.255	0.069	69.228	19.315	0.256	0.071	70.600	11.211
826-30B-5	0.257	0.071	71.288	19.248	0.272	0.084	84.057	10.322
826-B18-2	0.256	0.071	70.686	19.297	0.264	0.077	76.680	10.582
826-B18-5	0.255	0.070	69.828	18.295	0.259	0.073	72.757	10.099
862-0	0.247	0.063	62.839	17.532	0.261	0.074	74.059	8.983
862-30B-2	0.247	0.063	63.252	17.268	0.278	0.090	89.736	9.763
862-30B-5	0.251	0.067	66.506	17.823	0.269	0.081	81.370	10.383
862-B18-2	0.248	0.064	63.833	16.788	0.259	0.073	72.584	10.982
862-B18-5	0.254	0.069	68.630	17.638	0.263	0.077	76.593	10.463
9772-0	0.241	0.059	58.660	13.257	0.265	0.078	77.824	7.378
9772-B18-2	0.249	0.065	64.581	15.629	0.269	0.081	81.281	7.657

As it is observed in the above table, after thermal cycling was applied there was a slight increase of the radius of the free volume cavity and therefore the average size of the free volume holes varied as well. The increase noticed in the average size of free holes of Epon™826 non modified specimens was of 36% after the thermal cycling was applied, for modified samples of the same resin the increase reported was smaller, of about 2% for Epon™826 modified with 2wt% of Cloisite®30B and 18% in the case of the same resin but modified with 5wt% of Cloisite®30B.

For samples manufactured with Epon™862 it was found that the highest increase occurred on specimens modified with 2wt% of Cloisite®30B with a change of 42%. Samples non-modified had an increase of 18% with respect to the values before thermal cycling.

Samples from Cycom®977-2 also showed an increase of V_f, of 33% for the neat resin and 26% increase for samples modified with 2wt% of nanoclays B18.

Regarding the relative fractional free volume it was observed that it decreased after the thermal cycling was applied to the samples. On Epon™826 nanocomposites the average

decrease was about 45% when compared to values before thermal cycling while in samples from Epon^{TM}862 was of the order of 42% decrease.

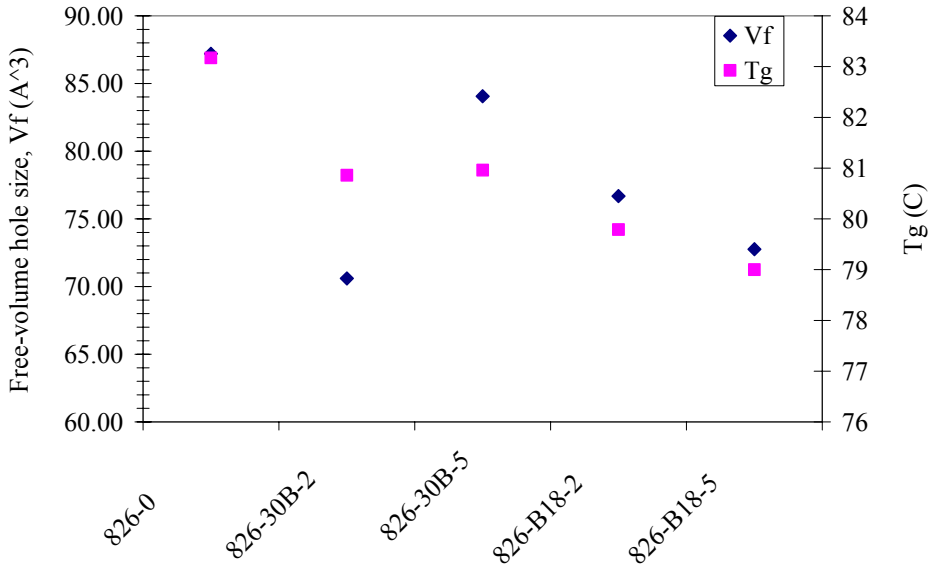

Figure 5.79. Comparison of free volume hole size and T_g for Epon^{TM}826 specimens after thermal cycling

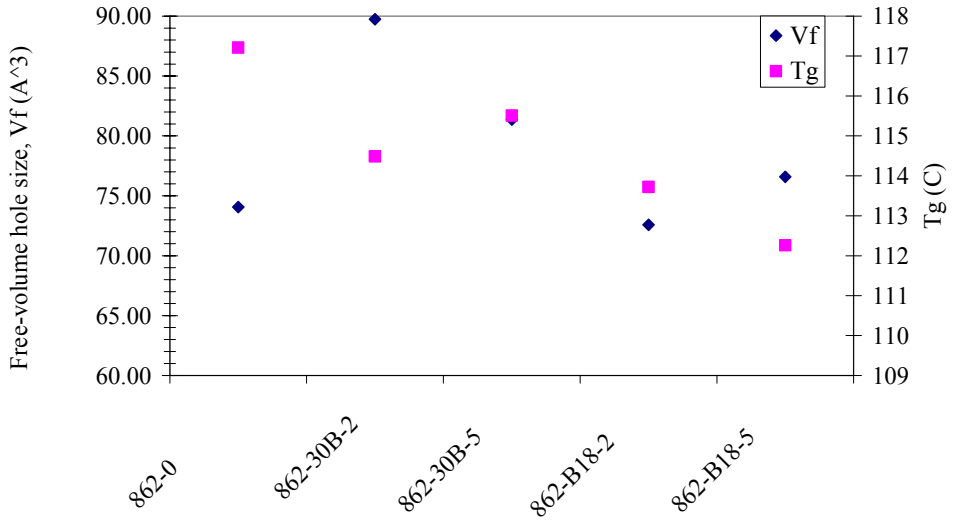

Figure 5.80. Comparison of free volume hole size and T_g for Epon^{TM}862 specimens after thermal cycling

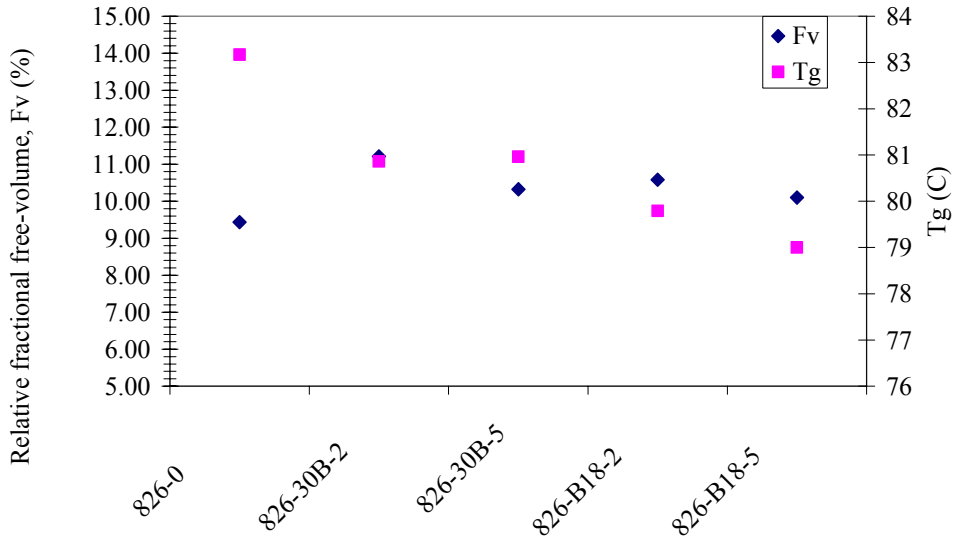

Figure 5.81. Comparison of relative fractional free volume and T_g for Epon^{TM}826 specimens after thermal cycling

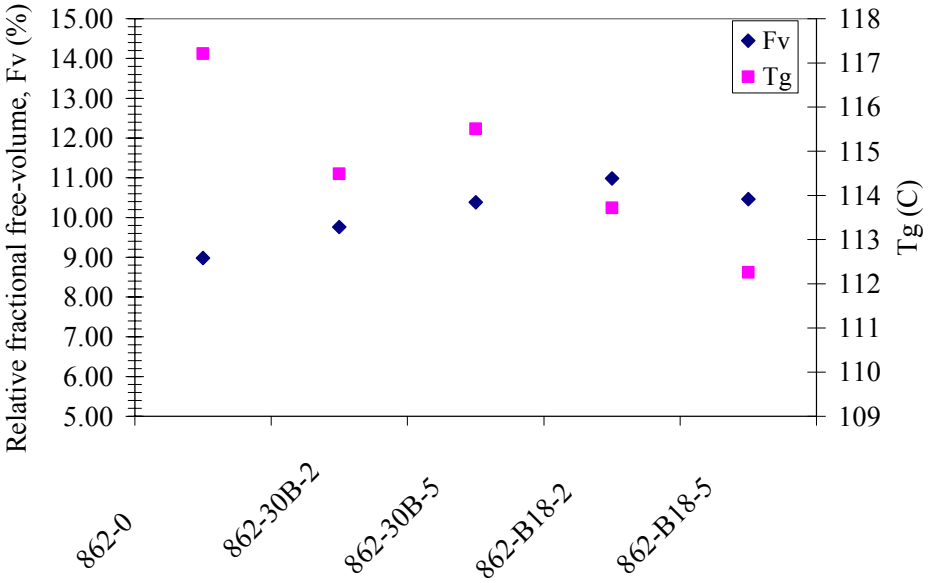

Figure 5.82. Comparison of relative fractional free volume and T_g for Epon^{TM}862 specimens after thermal cycling

With respect to the behavior observed in the glass transition and the free volume it was noted that samples with the highest glass transition had the lowest free volume values. The thermal treatment increased the polymeric chain stiffness, reflected in a higher T_g and, therefore, the decrease in the chain mobilization caused a decrease in the free volume.

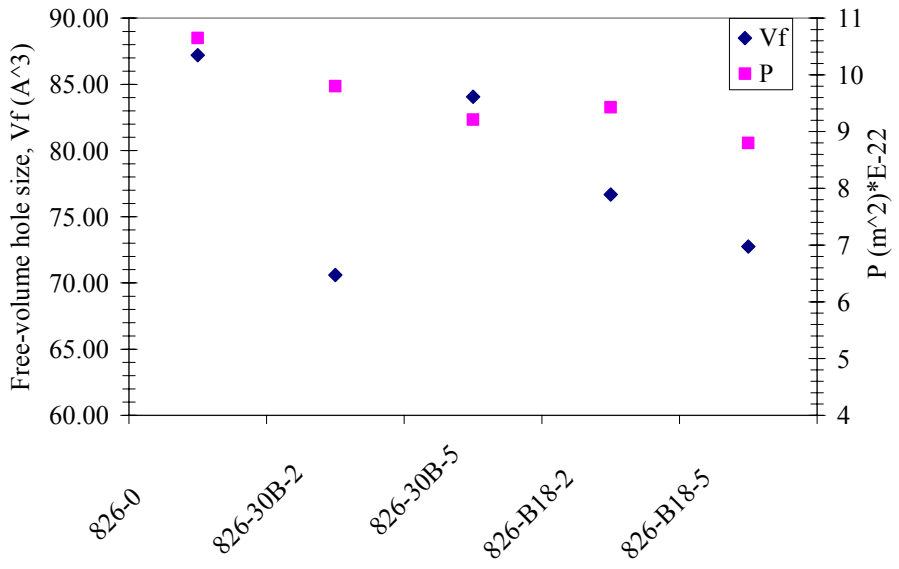

Figure 5.83. Comparison of free volume hole size and permeability for Epon^{TM}826 specimens after thermal cycling

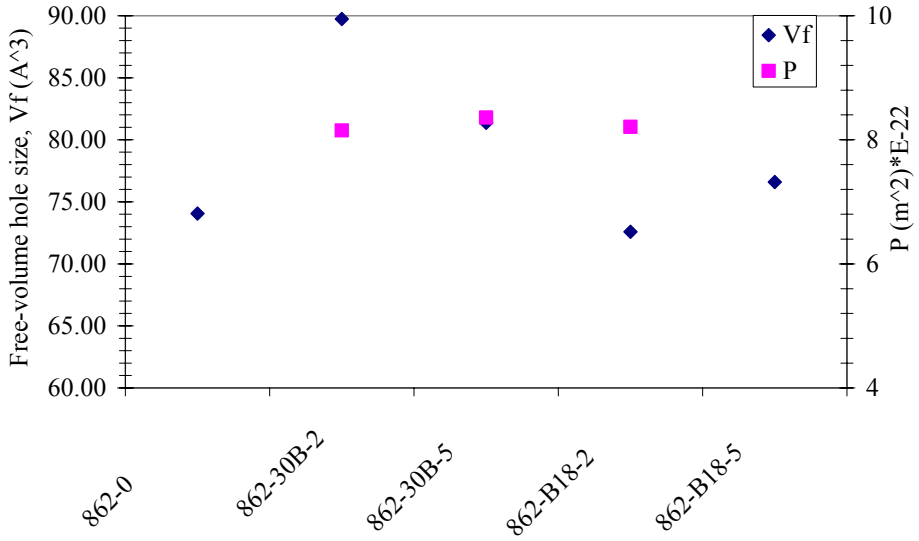

Figure 5.84. Comparison of free volume hole size and permeability for Epon^{TM}862 specimens after thermal cycling

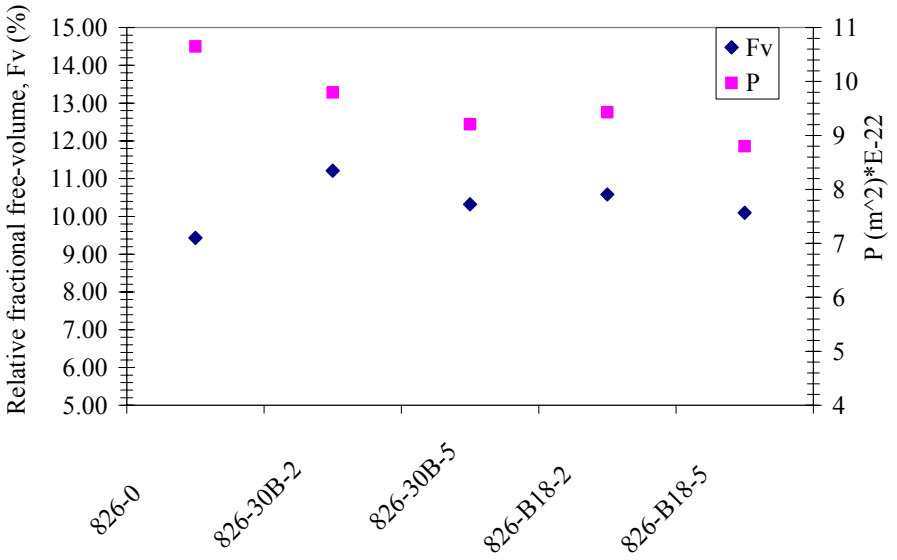

Figure 5.85. Comparison of relative fractional free volume and permeability for Epon^{TM}826 specimens after thermal cycling

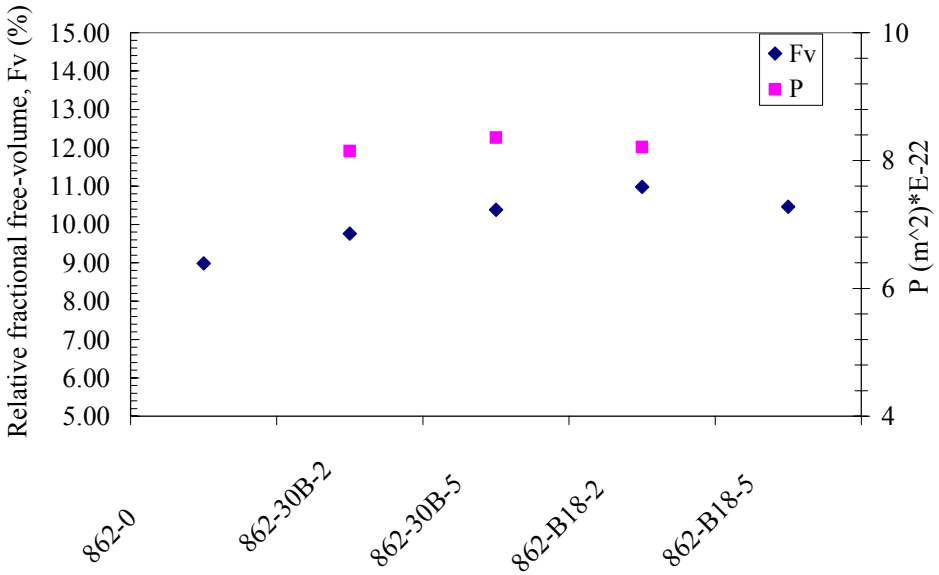

Figure 5.86. Comparison of relative fractional free volume and permeability for Epon^{TM}862 specimens after thermal cycling

After the thermal cycling was applied to the samples, the overall result was a reduction of the relative fractional free volume. This reduction in the free volume was also reflected in the decrease of the permeability values obtained after the specimens underwent thermal cycling. It was observed that nanoclay modified samples had in general higher free volume values than those of the pristine matrixes, while the permeability values were lower in these samples. This contradictory behavior is again explained with the theory mentioned before regarding the

distribution of the free volume in the nanocomposite. Also the fact that the introduction of nanoclays in the material could cause an apparent increase of the o-Ps formation causing an increase of the free volume in nanoclay modified samples.

5.7. Microscopic evaluation

After thermal cycling various of the samples presented a crack that was observed with the help of an optical microscope. The samples are shown in the figures below.

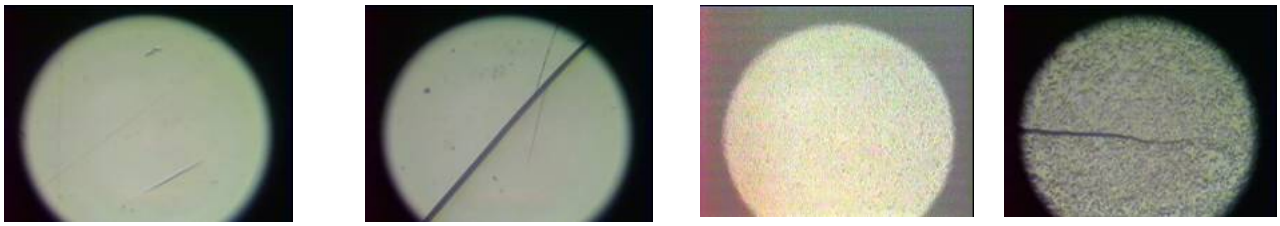

(a) (b) (c) (d)

Figure 5.87. (a) sample 862-0 before cycling (b) sample 862-0 after 140 cycles (c) sample 862-B18-5 before cycling (d) sample 862-B18-5 after 140 cycles

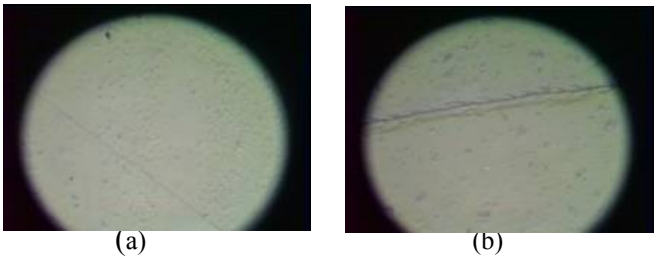

(a) (b)

Figure 5.88. Sample 9772-B18-2 (a) before cycling (b) after 140 cycles

5.8. X-Ray diffraction and TEM

In order to understand the possible mechanisms involved, the structure of all samples were characterized by the Polymers Branch, Materials Division at NASA John H. Glenn Research Center, using X-ray diffraction (XRD) and transmission electron microscopy (TEM) to identify intercalated or exfoliated structures of the nanocomposites. It was observed, as shown in Figures 5.89 and 5.90, that the XRD spectra were similar for all the samples, except for samples modified with 5wt% of B18 nanoclay. Wide angle XRD did show a peak corresponding to an expanded d_{001} spacing of the silicate layers, as well as a reduction in peak intensity, suggesting combined intercalated and exfoliated nanocomposite morphology. In the particular case of samples modified with 5 wt% of B18, the XRD pattern showed a much smaller peak, suggesting a more exfoliated structure, which was supported by the TEM micrograph, shown below.

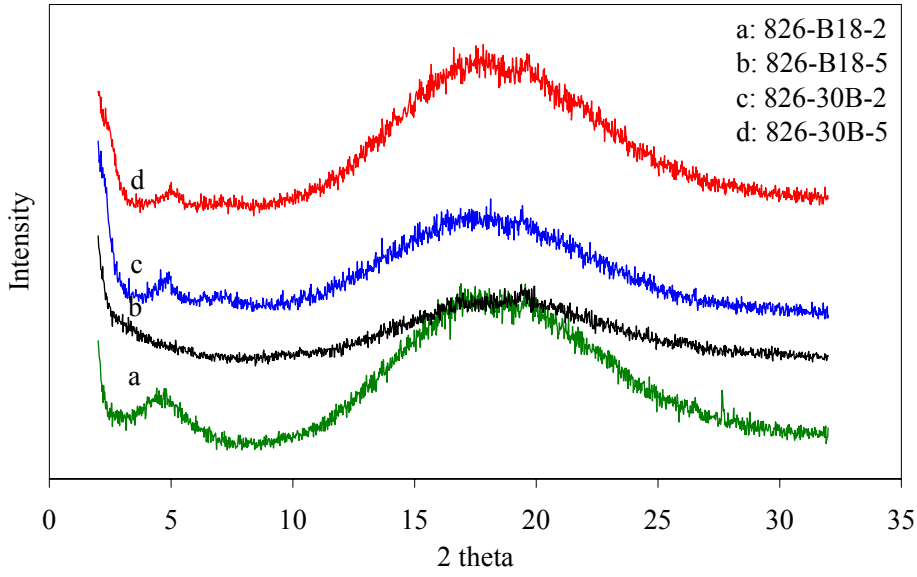

Figure 5.89. XRD spectra of Epon^{TM}826 modified with nanoclays

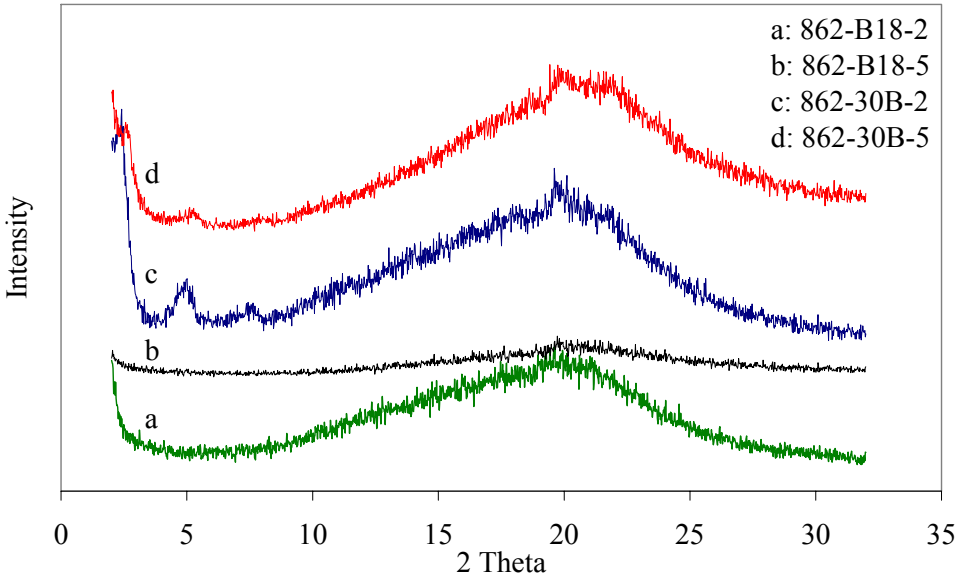

Figure 5.90. XRD spectra of Epon^{TM}862 modified with nanoclays

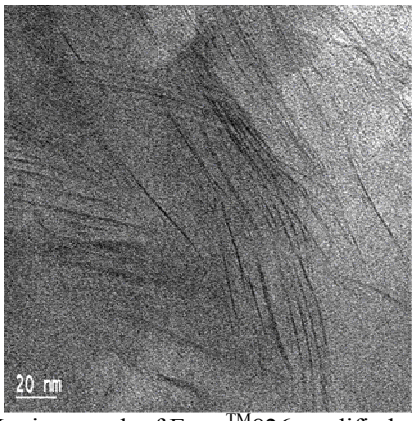

Figure 5.91. TEM micrograph of Epon^{TM}826 modified with 5wt% of B18 nanoclay

The results obtained from the TEM micrograph were used to obtain the aspect ratio of the nanoclay particles which resulted in an approximate value of a=*L/W*=100. This value corresponds with the value that the manufactured suggested for the nanoclays particles (70-150).

Meanwhile, the higher nanoclay exfoliation observed in these samples could be the reason for the difference of their glass transition temperatures from those of the rest of the samples. It was reported by Xu et al. that the T_g of exfoliated nanoclay composites decreased when the content of nanoclays increased [11]. The relative lower increase in the glass transition temperature value of these samples may be associated with the mobility of the host matrix. In highly exfoliated samples the molecular mobility of the host matrix is less reduced than in the case of intercalated structures where the polymer is confined between the galleries of the clay platelets. This difference in the segmental mobility of the polymer chains results in a difference in the glass transition temperature values.

The same reasoning can be applied to the samples that underwent thermal treatment. The exfoliation of the nanoclays in the polymer matrix influences the arrangement of the polymer chains in the nanocomposite but the spatial confinement of the chains is not as restricted as in the case of intercalated structures. Therefore the increase in the T_g is higher than in the case of mixed intercalated-exfoliated structures.

5.9. Density measurements

The density of all the specimens was determined using Archimedes' principle.

The samples were weighted (m_{sample}) and then submerged in distilled water to calculate the volume of the displaced water, which is equal to the volume of the samples ($V_{sample}=m_L/\rho_{water}$). With the volume and the mass the density was calculated.

The results are summarized below.

Table 5.17. Density values for all the specimens

Samples	before cycling		after cycling		rule of mixtures		
	density	Std dev	density	Std dev	theoretical	experimental before cycling	experimental after cycling
826-0	1.009	0.000	1.004	0.025	1.160	1.009	1.004
826-30B-2	1.015	0.008	1.010	0.032	1.176	1.029	1.024
826-30B-5	0.998	0.000	0.986	0.017	1.201	1.058	1.053
826-B18-2	1.004	0.009	0.986	0.000			
826-B18-5	1.017	0.000	0.989	0.013			
862-0	0.998	0.000	0.962	0.001	1.170	0.998	0.962
862-30B-2	1.022	0.018	0.998	0.000	1.186	1.018	0.982
862-30B-5	1.015	0.008	0.976	0.000	1.211	1.047	1.013
862-B18-2	0.998	0.000	0.979	0.009			
862-B18-5	1.005	0.010	0.991	0.010			
9772-0	1.016	0.000	0.998	0.000	1.310	1.016	0.998
9772-B18-2	0.998	0.000	0.986	0.017			

The rule of mixtures was applied with the data obtained from the manufacturers and the theoretical density was obtained and then compared to the experimental values, as reported in the table above.

Table 5.18. Manufacturer's data

manufacturers data	
Material	density (g/cc)
Epon™826	1.16
Epon™862	1.17
Cycom®9972	1.31
Cloisite®30B	1.98

The density of ideal mixture was calculated as

$$\langle \rho \rangle = \rho_1 c_1 + \rho_2 c_2 + \rho_3 c_3 + \ldots; \quad c_1 + c_2 + c_3 + \ldots = 1;$$

where $c_i = \frac{V_i}{V}$ - is the concentration of the constituent, in this case it would be two components, polymer and nanoclays. It was observed from the data that the density of the ideal mixture is higher than the density of the experimental data. This suggested that in the samples there are pores. Thereby, the real concentration of nanoparticles differs from the theoretical value. The real concentrations $c_{p;real}$ and $c_{n;real}$ are lower than the ones calculated with the rule of mixtures with the experimental data in the two-component system:

$$c_{p;real} = c_p \frac{\rho_{\exp}}{\rho_{two}}; \quad c_{n;real} = c_n \frac{\rho_{\exp}}{\rho_{two}};$$

Consequently the total concentration of pores will be

$$c_{pores} = 1 - c_{p;real} - c_{n;real}$$

This concentration was calculated and the results are summarized in the table below. The data was only obtained for samples manufactured with Cloisite®30B since the density of the nanoclays B18 was not available.

Table 5.19. Pores concentration in the specimens

Samples	Pores concentration before thermal cycling (%)	Pores concentration after thermal cycling (%)
826-0	13.0	13.4
826-30B-2	11.2	11.7
826-30B-5	8.6	9.1
862-0	14.7	17.8
862-30B-2	13.0	16.1
862-30B-5	10.4	13.6

5.10. Statistical studies

In order to determine the effect of the different variables in the permeability a factorial design with three factors was used:

- Type of resin, three levels (Epon™862, Epon™826 and Cycom ®977-2);
- Type of nanoclays, three levels (no nanoclay added, B18 and Cloisite®30B);
- Percentage of nanoclays, three levels (0%, 2%, and 5%).

In this case the dependent variable was the permeability of the samples to helium gas at temperature of 23.8±0.5˚C. Each measurement of the dependent variable was repeated four times. Analyses were done for all data obtained before and after the thermal cycling of the specimens.

5.10.1. Multifactor analysis of the variance for permeability

With this analysis, various tests were conducted to determine which factors had a statistically significant effect on the permeability and which the significant interactions amongst the factors were. The tests were conducted on the permeability results before and after thermal cycling.

The results from the analysis of variance are shown on Table 5.20. The variance of the permeability was divided into three components, one accounting for the type of resin, another one for the percentage of nanoclays and the last one for the type of nanoclays added. Each factor after the first was nested in the one above. The goal of such analysis was to estimate the amount of variability contributed by each of the factors, called the variance components. In this case, the factor contributing the most variance was the type of resin, whose contribution represented 54.86% of the total variation in permeability. The less significant factor is the type of nanoclays added, with a contribution of 1.91%.

Table 5.20. Analysis of variance for samples before thermal cycling

Source	*Sum of Squares*	*Mean Square*	*Var. Comp.*	*Percent*
type resin	127.202	63.601	4.47959	54.86
percent nano	57.3872	19.1291	2.96855	36.36
type nano	3.5575	1.18583	0.156213	1.91
ERROR	15.1465	0.560981	0.560981	6.87

The same analysis was done on the population of samples after thermal cycling was applied, and the results are presented on Table 5.21. In this case it is observed that the resin still plays a major role in to the variation of the permeability, with a total contribution of 76.58% and the type of nanoclays does not influence the variability of the permeability.

Table 5.21. Analysis of variance for samples after thermal cycling

Source	*Sum of Squares*	*Mean Square*	*Var. Comp.*	*Percent*
type resin	50.8513	25.4256	2.2632	76.58
percent nano	7.33547	2.44516	0.347486	11.76
type nano	0.617513	0.205838	0.0	0.00
ERROR	9.3096	0.3448	0.3448	11.67

In Figure 5.92(a) and (b) three box-and-whisker plots are presented for the results before and after thermal cycling, each plot represents each level of the type of resin: level 1, Epon™862; level two, Epon™826; and level 3, Cycom®977-2. With the help of this test it is determined if there is a significant difference between the three levels studied.

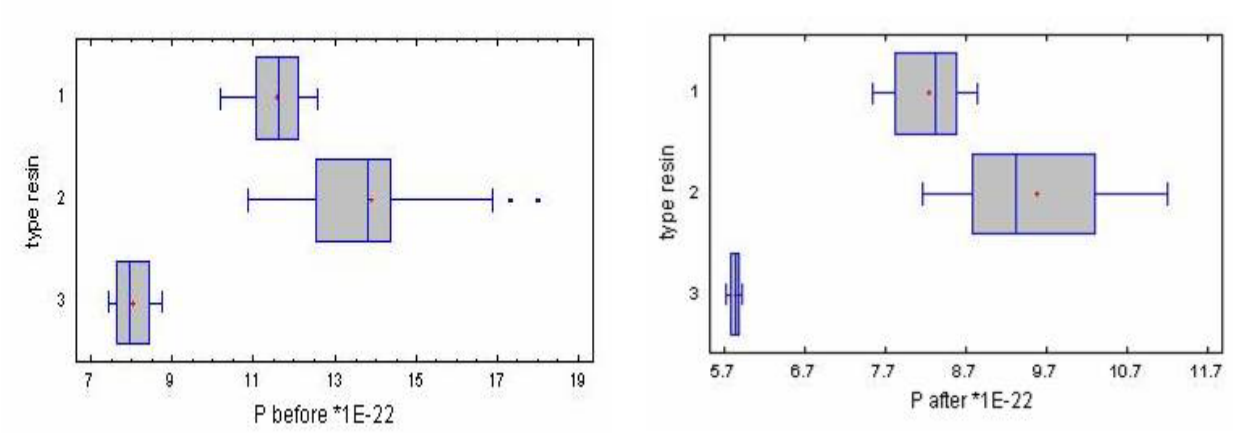

(a) (b)

Figure 5.92. Box-and-whisker plot for type of resin: (a) before thermal cycling; and (b) after thermal cycling

The box-and-whisker plot for the three levels of percentage of nanoclays, 0%, 2% and 5%, for the cases of before and after thermal cycling is represented in Figure 5.93 (a) and (b). The rectangular part of the plot extends from the lower quartile to the upper one, covering the center half of each sample. The center lines within each box show the location of the sample medians. By analyzing the boxes, an overlap for the medians is observed, indicating that there was not a statistically significant difference between the medians at the 95% confidence level.

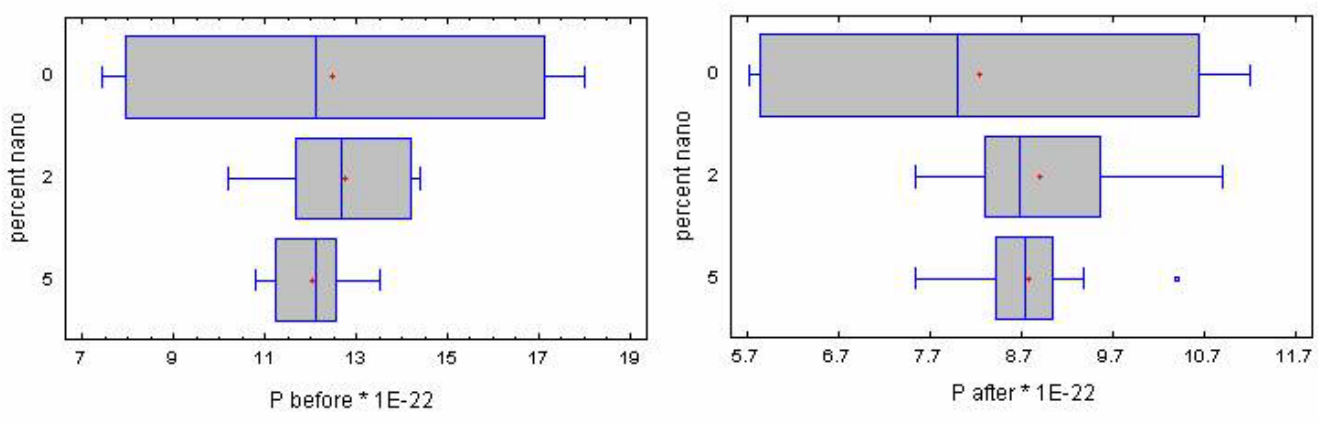

(a) (b)

Figure 5.93. Box-and-whisker plot for percentage of nano: (a) before thermal cycling; and (b) after thermal cycling

The same analysis was repeated for the type of nanoclays added to the resin in Figure 5.94 (a) and (b). The three levels of nanoclays are represented by 0, no nanoclay added; 1, where the type of nanoclay is B18 and level 2, which symbolizes Cloisite®30B. An overlap for the medians is observed, indicating that there was not a statistically significant difference between the medians at the 95% confidence level.

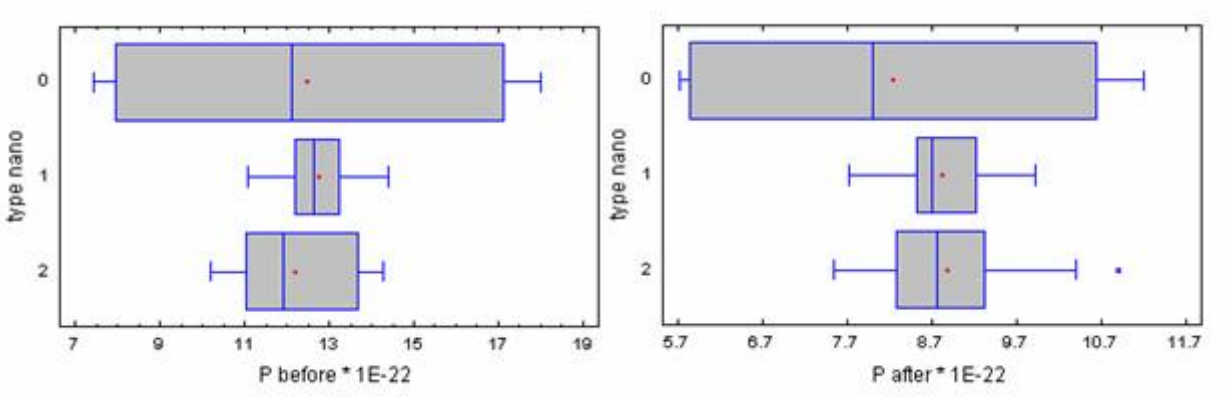

(a) (b)

Figure 5.94. Box-and-whisker plot for type of nano: (a) before thermal cycling; and (b) after thermal cycling

5.10.2. Model

With the help of the ANOVA analysis a mathematical model was generated, which related the helium permeability of the samples with the type of resins used and the amount of nanoclays added into the composite. Two different models have been obtained, one related to the data before the thermal cycle is applied and the second one with the data after thermal cycling. Table 5.22 shows the estimated values for the coefficients of the model at a confidence level of 95% for the date before thermal cycling and Table 5.23 shows the coefficients for the data after the thermal cycle.

Table 5.22. Estimated parameters for permeability model at a confidence level of 95% before thermal cycling

Parameter	Estimated error	Standard error	Lower limit	Upper limit	V.I.F.
constant	11.6142	0.305026	10.9912	12.2371	
type of nano	1.79167	0.419411	0.935112	2.64822	5.1869
type of nano	-0.845833	0.253489	-1.36353	-0.328139	2.34945
type of resin	1.85667	0.306927	1.22984	2.4835	1.77778
type of resin	3.51917	0.234419	3.04040	3.99792	1.23148
percentage nano	-0.325	0.114385	-0.558606	-0.0913943	2.23765

Table 5.23. Estimated parameters for permeability model at a confidence level of 95% after thermal cycling

Parameter	Estimated error	Standard error	Lower limit	Upper limit	V.I.F.
constant	8.03542	0.20546	7.61581	8.45502	
type of nano	0.614167	0.282508	0.0372077	1.19113	5.1869
type of nano	-0.469583	0.170745	-0.818293	-0.120874	2.34945
type of resin	0.816667	0.20674	0.394446	1.23889	1.77778
type of resin	2.00042	0.157901	1.67794	2.32289	1.23148
percentage nano	-0.12	0.0770476	-0.277352	0.0373525	2.23765

The equations of the obtained models are as follows:

P_{before} = 11.6142 + 1.79167*I1 (1) – 0.845833*I1 (2) + 1.85667*I2 (1)
+ 3.51917*I2 (2) – 0.325*percent nano

P_{after} = 8.03542 + 0.614167*I1 (1) – 0.469583*I1 (2) + 0.816667*I2 (1)
+ 2.00042*I2 (2) – 0.12*percent nano

where, P is the permeability and:

I1 (1) = 1, if type nano is zero;
-1, if type nano is 30B;
0, otherwise.

I1 (2) = 1, if type nano is B18;
-1, if type nano is 30B;
0, otherwise.

I2 (1) = 1, if type resin is Epon™862;
-1, if type resin is Cycom®977-2;
0, otherwise.

I2 (2) = 1, if type resin is Epon™826;
-1, if type resin is Cycom®977-2;
0, otherwise.

The models are represented in Figures 5.95 and 5.96

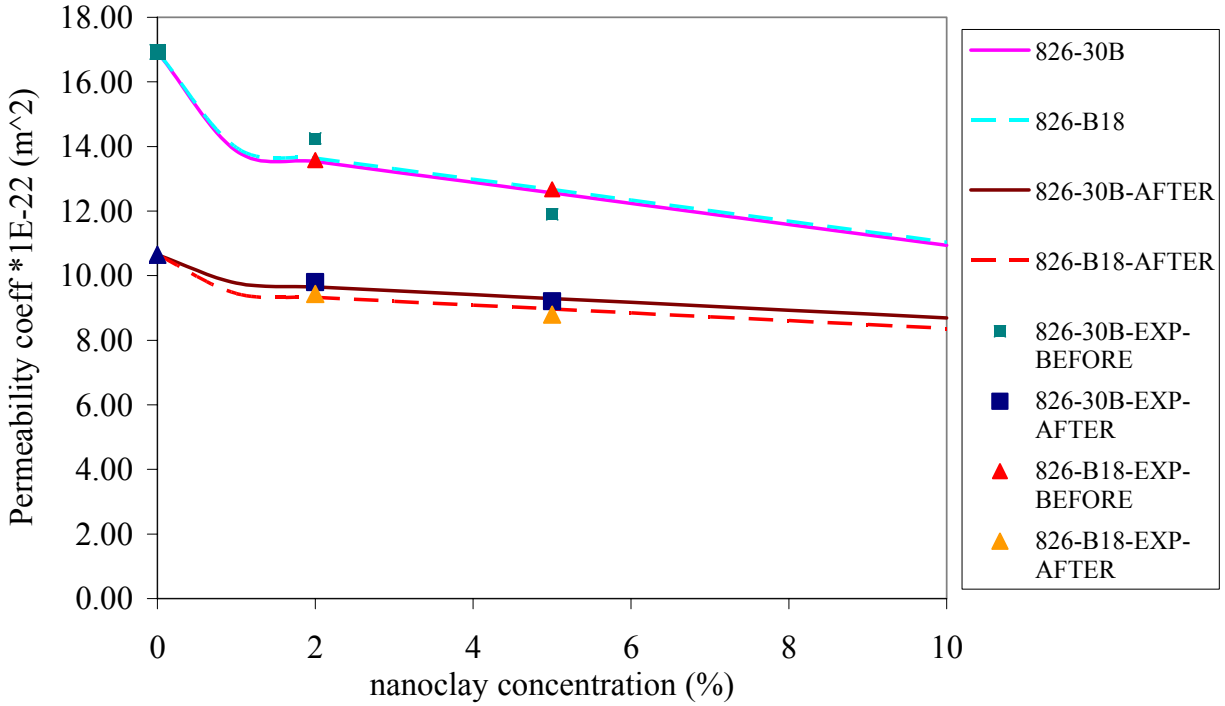

Figure 5.95. Model obtained for samples from resin Epon™862 before and after cycling data

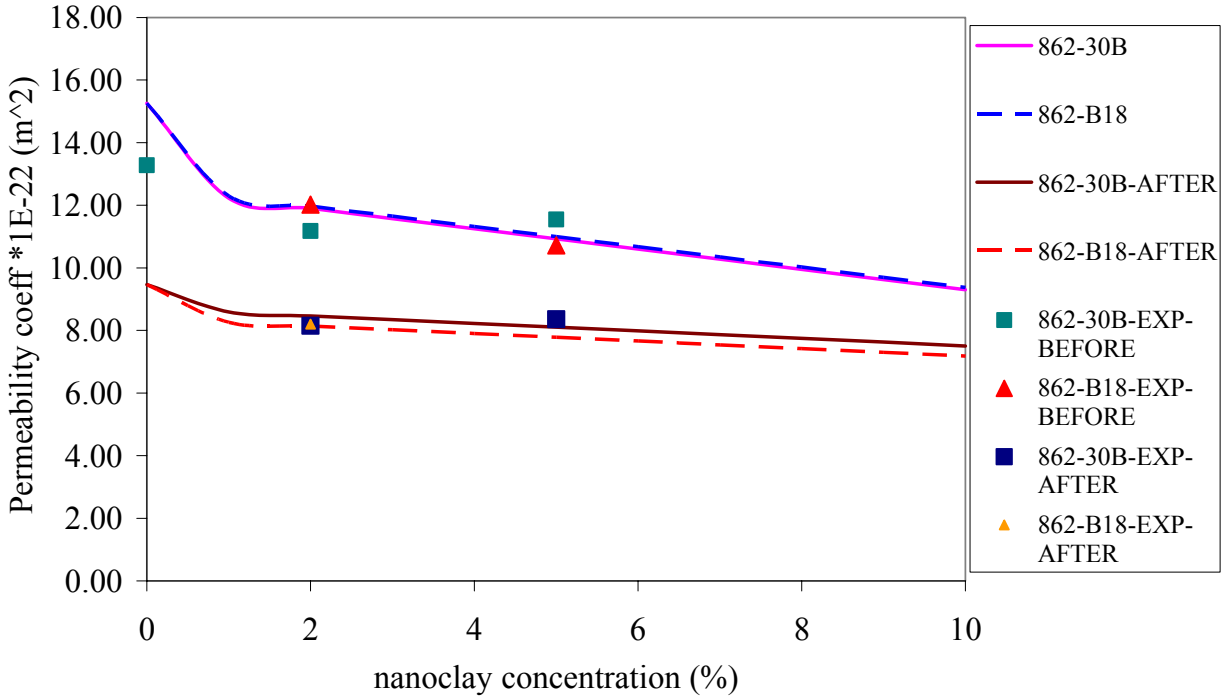

Figure 5.96. Model obtained for samples from resin Epon™826 before and after cycling data

5.11. Mathematical models

The experimental results were validated with several models available in the literature. Nielsen [12], Fredrickson and Bicerano [13], Cussler et al. [14], Gusev and Lusti [15] developed models which take into consideration the geometric factors that affect the permeability of platelet modified nanocomposites. According to the formulas mentioned in the previous chapter the calculated results are shown below.

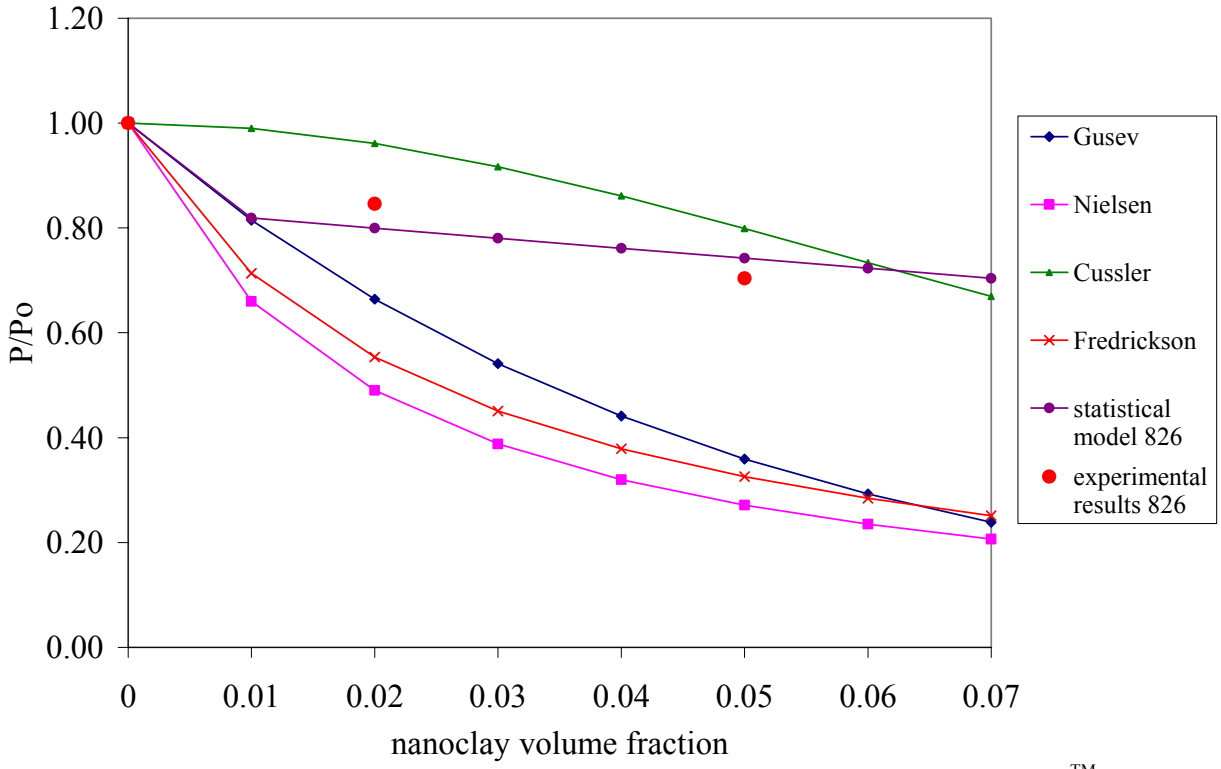

Figure 5.97. Comparison of experimental results and literature models for resin Epon^{TM}826

In the calculation of the models the platelet was taken having lateral dimensions of 100 nm in two directions and a thickness of 1 nm. Therefore the aspect ratio of the nanoclays was equal to $\alpha = 100$. This value was taken from the TEM micrographs and is in accordance with the values suggested by the manufacturer. In this particular case, of $\alpha = 100$, the nanoclay volume fraction and the nanoclay weight concentration are the same.

As it is observed in the graph shown above three of the models predict lower permeability values as the concentration of the nanoclays increases while the model suggested by Cussler is more conservative. It was noted that the experimental values in the case of both resins, Epon^{TM}826 and Epon^{TM}862 followed better Cussler's model.

In the graph plotted below it can be observed the values obtained in the case of Epon^{TM}862.

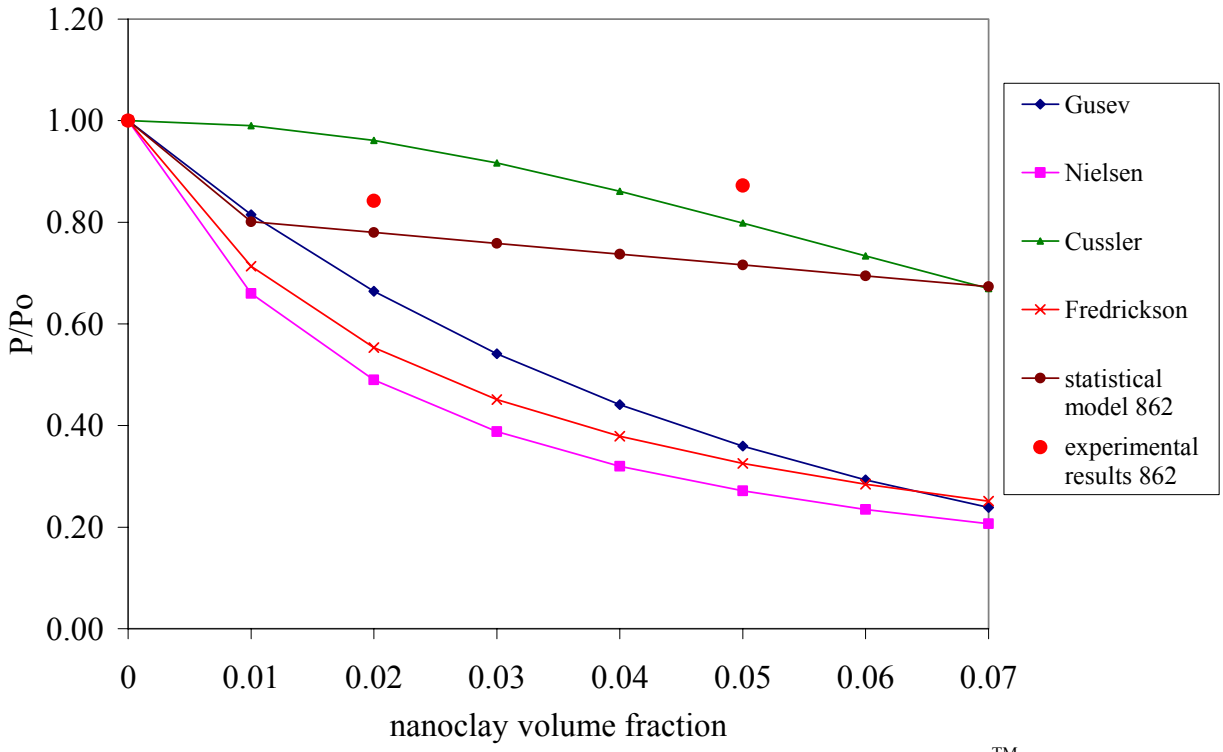

Figure 5.98. Comparison of experimental results and literature models for resin Epon^{TM}862

All the models take into consideration only geometric factors that are related with the tortuosity and the reduction in permeability by increasing the path that the gas needs to go through to diffuse into the material. But in the diffusion phenomenon in nanoclay modified nanocomposites it needs to be consider the fact that inclusions produce molecular level modifications in the surrounding polymer that affect the overall permeability. This effect cannot be taken in account in the prediction of the permeability. This is why experimental values don't completely agreed with the models.

The fact that models cannot predict the molecular level modifications that happen when nanoclays are added and that will affect the permeability is observed when the data after thermal cycling is plotted against the models.

When the samples were subjected to thermal cycling, modifications at the molecular level took place arranging the polymeric chains in a different fashion. This was confirmed by the T_g

data and the free volume measurements. The values of permeability decreased after thermal cycling but the geometric factors never changed, therefore the changes were related to the rearrangement of the polymeric chains around the nanoclays.

As it was established by DSC, all the samples were completely cured and therefore the thermal cycling did not induce any further crosslinking of the polymer chain and any material property changes were only related to segmental mobility and free volume arrangements.

The models comparison with the values after thermal cycling is shown below for the case of Epon^{TM}826 samples.

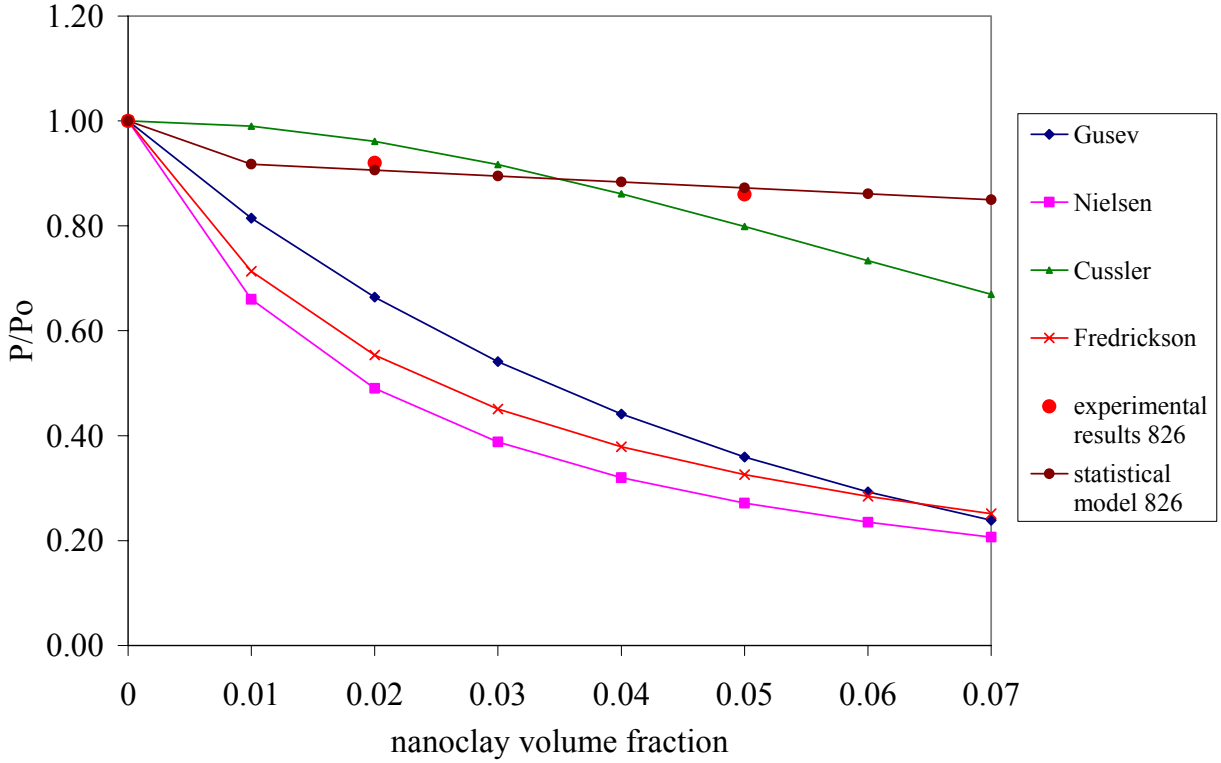

Figure 5.99. Comparison of experimental results and literature models for resin Epon^{TM}826 after thermal cycling

Cussler's model gives the better fit to the samples but as mentioned before the molecular changes induced with the thermal cycling cannot be predicted in the final permeability values.

The degenerated Maxwell's formula, the modified version using Fricke's assumptions and the influence of the platelet's orientation were plotted against the experimental data. The results are shown below.

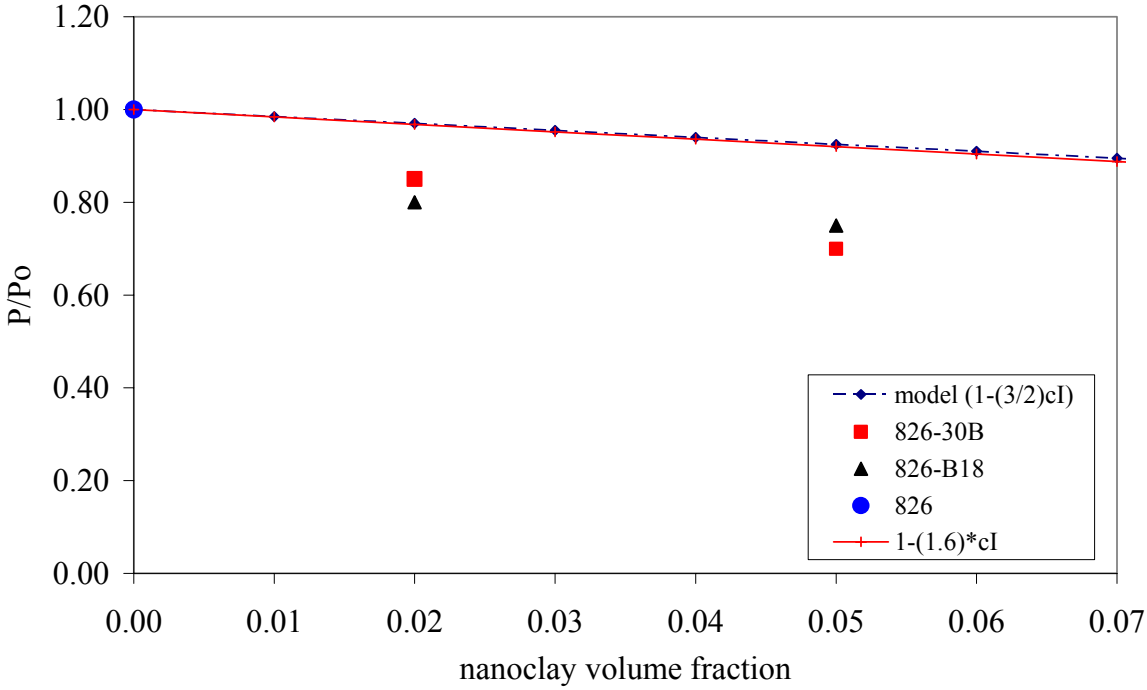

Figure 5.100. Comparison of experimental results and modified Maxwell's models for resin Epon™826

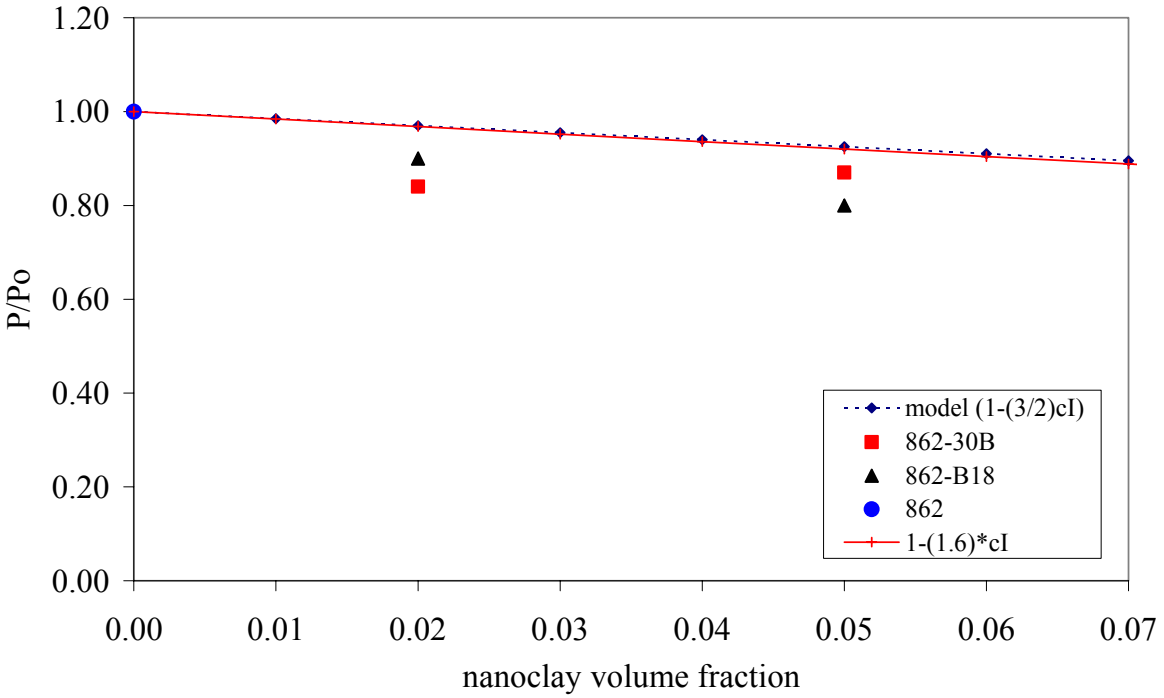

Figure 5.101. Comparison of experimental results and modified Maxwell's models for resin Epon™862

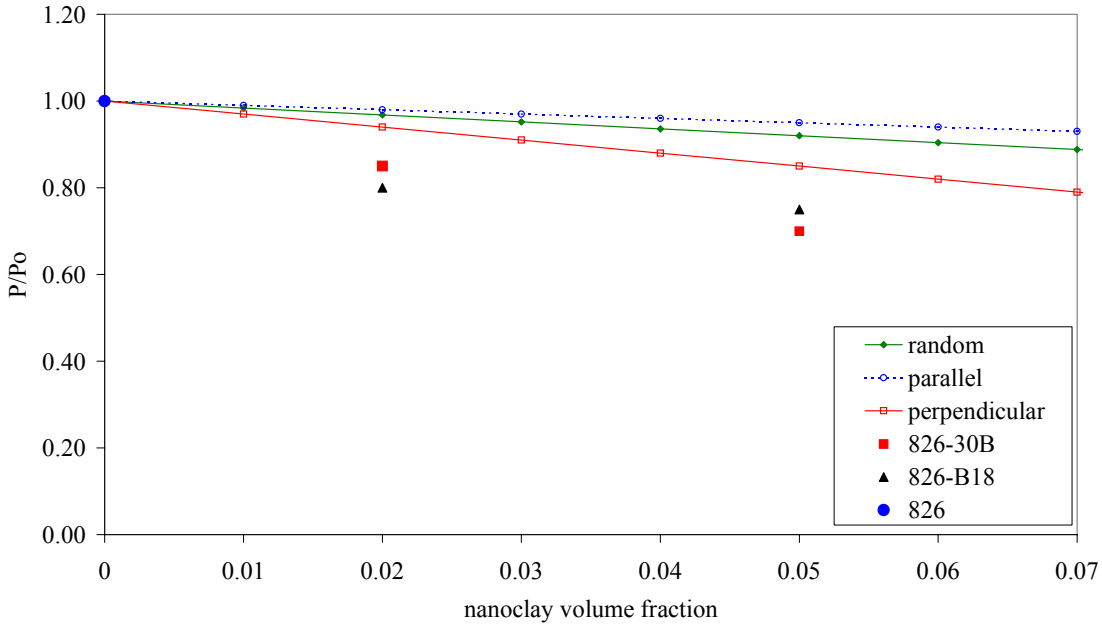

Figure 5.102. Effect of the orientation of the platelets in the permeability for Epon^{TM}826

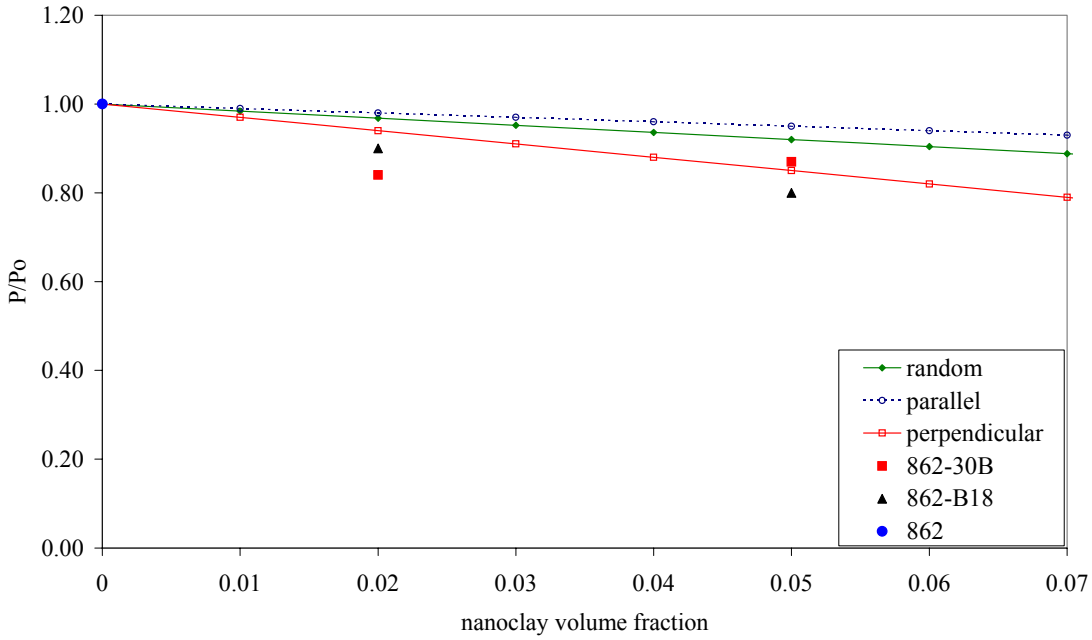

Figure 5.103. Effect of the orientation of the platelets in the permeability for Epon^{TM}862

As it is noted above the experimental results are closer to the model for an orientation of the platelets perpendicular to the flow.

Using the model explained in the previous chapter, the relative permeability was calculated considering the existence of an interface around the nanoclay with lower permeability than that of the pristine polymer. The results were obtained with the following formula, where the porosity values, Ψ, where taken from the calculation done in part 5.9:

$$\frac{P}{P_0} = \frac{1-\phi_f}{1+\frac{1}{2}\sqrt{1-\Psi}}$$

The graphs obtained are represented below. It is noted that the relative permeability predicted by the model is lower than that obtained in the other models. The interlayer with lower permeability than the neat polymer is affecting the tortuous path followed by the permeant and affecting the permeability as well.

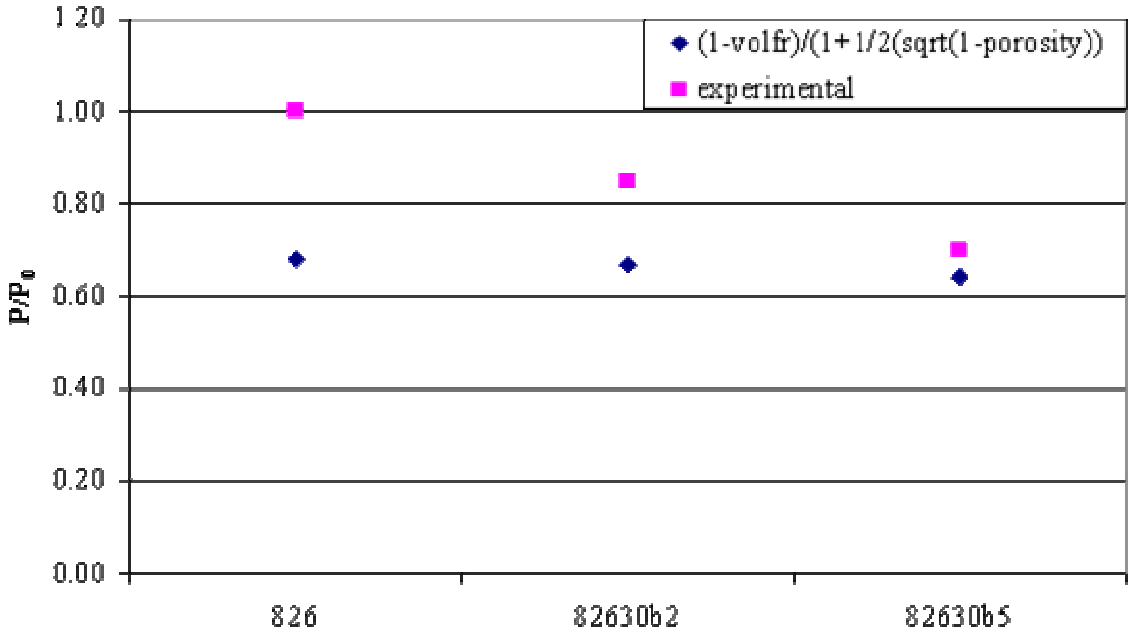

Figure 5.104. Effect of interface clay-polymer in the relative permeability, Epon™826

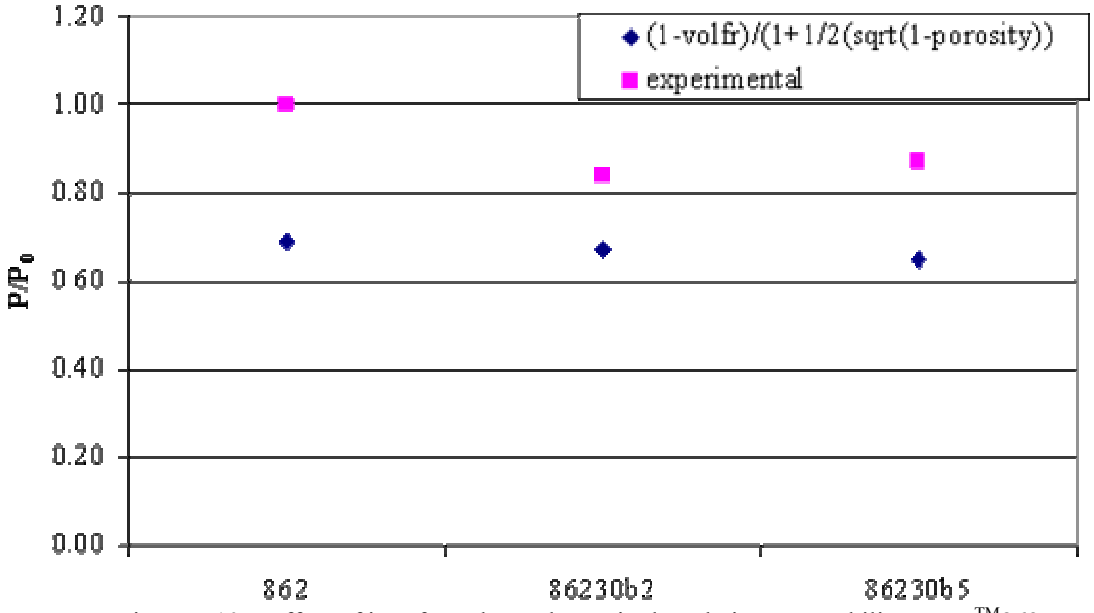

Figure 5.105. Effect of interface clay-polymer in the relative permeability, Epon^{TM}862

5.12. References

[1] Final Report of the X-33 Liquid Hydrogen Tank Test Investigation Team, George C. Marshall Space Flight Center, Huntsville, NASA Report, May, 2000

[2] NetMBA Business Knowledge Center, http://www.netmba.com/statistics/plot/box/

[3] Engineering Statistics Handbook, http://www.itl.nist.gov/div898/handbook/eda/section3/qqplot.htm

[4] J.C. Paterson-Jones. Journal of Applied Polymer Science 1975; 19:1539-1547

[5] D. Colombini, J.J. Martinez-Vega, G. Merle. Polymer 2002; 43: 4479–4485

[6] H. Nakanishi, S.J. Wang, Y.C. Jean. Positron annihilation in fluids. Ed. Sharma S.C. World Scientific, Singapore, 1998.

[7] Z.F. Wang, B. Wang, N. Qi, H.F. Zhang, L.Q. Zhang. Polymer 2005; 46: 719–724

[8] P. Winberg, M.Eldrup, F. H.J. Maurer. Polymer 2004; 45: 8253–8264

[9] Y. C. Jean, J.-P. Yuan, J. Liu, Q. Deng, H. Yang. Journal of Polymer Science: Part B: Polymer Physics 1995; 33: 2365-2371

[10] Y.-H. Zhang, J.-T. Wu, S.-Y. Fu, S.-Y. Yang, Y. Li, L. Fan, R. K.-Y. Li, L.-F. Li, Q. Yan. Polymer 2004; 45: 7579–7587

[11] W.-B Xu., S.-P. Bao, P.-S He. Journal of Applied Polymer Science 2002; 84, 4: 842-849

[12] Nielsen, L. E. J. Macromol. Sci., Chem. 1967, A1, 929

[13] G. H. Fredrickson, J. Bicerano. Journal of Chemical Physics 1999; 110: 4

[14] E.L. Cussler, S.E. Hughes, W. J. Ward, III, R. Aris. Journal of Membrane Science 1988; 38: 161-174

[15] A. A. Gusev, H.R. Lusti. Adv. Mater. 2001; 13: 21

CHAPTER 6

DISCUSSION AND CONCLUSIONS

The main purpose of this work was to study the permeability to helium of different systems of nanocomposites in order to correlate the type of polymer and nanoclays with their effects on the permeability. Another important aspect of the research work was to analyze the effect of extreme thermal cycling on the nanocomposites and examine the influence of the different compositions of the nanocomposites in the thermal properties.

Using a statistical approach the optimal duration of the leak rate experiments was found to be 12 hours. The leak rate was measured and after the necessary calculations it was obtained the permeability coefficient for all the samples.

Nanoclays were proven to be effective in the reduction to the permeability to helium. It was noted that samples manufactured from Epon™826 showed in general higher reduction of the permeability to helium than samples from Epon™862. Specimens modified with 5wt% of Cloisite®30B had a decrease of 29% on the permeability coefficient when compared to the neat Epon™826. It was observed in general that the addition of 5wt% of nanoclays was more effective in the reduction of the permeability than the addition of 2wt%.

With the addition of nanoclays an increase in the storage modulus below the glass transition was observed. The storage modulus in the glassy region was increased by 16% in nanocomposite Epon™826 modified with 5wt% of nanoclay B18 when compared to the pristine polymer. In Epon™862 modified with 5wt% of Cloisite®30B the increase was of 29% when compared to the neat epoxy.

The thermal stability measured with TGA was increased with the addition of nanoclays in samples manufactured from Epon™826, except for samples modified with 5wt% of B18 nanoclays. In nanocomposites made with Epon™862 the thermal stability decreased with the addition of nanoclays. Samples modified with Cloisite®30B achieve higher degradation temperatures than those samples modified with nanoclays B18.

The TGA curves were separated into five different decomposition processes. It was observed for both types of resins that the TGA trace had two main stages, one occurring in the region between 250 ˚C and 450 ˚C and the second step around 450 ˚C - 550 ˚C. In samples

from Epon™826 the main step seemed to be the result of four different overlapped processes while the second step corresponded to a single degradation process. The values obtained for the activation energy of the degradation process showed that in the first degradation process the degradation energy required for the neat resin was smaller than in the case of nanoclay modified resins.

The extent of curing of the nanocomposites was studied by DSC and it was observed that DSC plots do not show a residual curing peak after the T_g is reached. An exothermic peak was observed for all the samples around 300˚C - 400˚C and it was interpreted as a degradation peak, which was confirmed by TGA. This fact implied that the epoxy system was fully cured and therefore any treatment applied later would not induce chemical changes in the samples. Consequently, it was believed that the applied thermal treatment would not induce any further crosslinking of the polymer chain and any material property changes were only related to segmental mobility and free volume arrangements.

The glass transition temperature was obtained for all samples and it was reported that the addition of nanoclays slightly increased the values of the T_g in all cases, when compared to that of the pristine matrix, except for samples of Epon™862 modified with 5wt% B18. The relative increase observed in the T_g when compared to the neat matrix, was more noticeable in samples manufactured from Epon™826, where the general increase observed was about 12°C for all samples except the one modified with 5wt% of B18 which had an increase of 6°C. Nanocomposites manufactured from Epon™862 did not show a significant increase in the T_g values when compared to the pristine polymer.

Free volume measurements were done with the help of PALS. From this tests the radius of the free volume cavity was obtained and had a value of R=0.25 nm for all the samples. The average size of the free volume holes increased when the nanoclays were added to the pristine polymer in the three resins Epon™826, Epon™862 and Cycom®977-2. For the resin Epon™826, it was observed a slight increase of the relative fractional free volume when the nanoclays were added, from 17.28% in the neat resin to an average of 19% for the modified samples. In the case of Epon™862 there was no significant change of the relative fractional free volume.

In general it was noted that the average size of the free volume holes and the relative fractional free volume increased on the nanoclay modified samples when compared to the neat resin in the case of Epon™826. In samples from Epon™862 the relative fractional free volume

decreased with the addition of 2wt% of Cloisite®30B and 2wt% of B18 when compared to the pristine samples.

When the values of the glass transition temperature were compared to the free volume data it was noted that it did not follow the expected behavior. Normally, an increase in the glass transition is related with the decrease in the chain mobility of the polymer and the subsequent increase of the polymer chain stiffness. This increase in the chain stiffness is commonly associated with a decrease in free volume.

In the results obtained it was noticed that samples with higher T_g had higher average free volume hole sizes and higher relative fractional free volume. This higher value of the free volume could be related with the fact that sometimes in heterogeneous systems with small particles there is an out-diffusion of positrons and o-Ps from the filler particles into the matrix. The out-diffusion of positrons, which later forms o-Ps from the filler particles, into the polymer matrix would result in an increase of the apparent o-Ps formation in the nanocomposite, and this increase would produce a higher value of the free volume.

In general, samples that are not modified with nanoclays with higher permeability had lower value of relative fractional free volume and free holes size when compared to modified samples. This result can be contradictory with the expected behavior, nevertheless as mentioned above; the higher values of the free volume noticed in the modified samples could be related to the out-diffusion of positrons and o-Ps from the filler particles into the matrix.

All the specimens were subjected to thermal cycling between temperatures of -196°C to 177°C in order to study the performance of the nanocomposites under extreme thermal environments.

The leak rate was evaluated and it was reported a decrease in the permeability to helium after thermal cycling of all the samples. Samples from Epon™826 had a reduction in permeability up to 37% for neat samples when compared to the permeability before cycling. In nanoclay modified samples of Epon™826 the average reduction in permeability was about 30%. In the case of Epon™862 the reduction in permeability was of about 27%.

It is believed that the thermal treatment caused an arrangement of the polymeric chains and modified the free volume distribution of the polymers. The distribution of the free volume is related with the permeability and any changes in the free volume are therefore reflected in the permeability of the diffusing gas.

The storage modulus below the glass transition temperature in neat samples from Epon™826 decreased about 28% when compared to the same value before thermal cycling and in the case of samples modified with 2wt% of Cloisite®30B the decrease was of 10%. The rest of the Epon™826 samples increased their storage modulus value, the highest increase of 28% was observed in samples modified with 5wt% of nanoclay B18.

In nanocomposites manufactured with Epon™862 the neat epoxy decreased 25% in the storage modulus after the thermal cycling was applied and samples modified with Cloisite®30B had a decrease in the storage modulus as well. Specimens modified with nanoclay B18 had an increase of 8% in their storage modulus when compared to the same value before the cycling.

Specimens made of neat Cycom®977-2 resin had a decrease of 67% in the storage modulus after the thermal treatment and in the case of samples modified with 2wt% of B18; the reduction was of 15%.

The thermal stability of the nanocomposites decreased after the thermal cycling was applied when compared to the values before thermal cycling.

The thermal treatment increased the glass transition temperatures of the nanoclay modified composites, compared to those that were not thermally cycled. It was noticed that thermal cycling induced a higher increase in the T_g of both neat polymer resins, Epon™826 and Epon™862, over their nanoclay modified composites. Here the neat samples showed an increase of 18˚C in the T_g value for Epon™826 and 9˚C increase for Epon™862 when compared to values before thermal cycling. For the nanocomposite samples the average increase compared to T_g values before the thermal treatment was about 3-5˚C. It was also observed that samples modified with 5wt% of B18 showed a higher T_g increase in both Epon™826 and Epon™862 nanocomposites of about 7˚C.

After thermal treatment the free volume was analyzed again and it was observed that the intensity of the o-Ps decreased significantly, an average of 47% reduction when compared to the values before thermal cycling. The intensity is related to the relative number density of free volume holes in the material and therefore after thermal cycling it seems that the concentration of the largest voids is significantly reduced, this result agrees with the fact that the permeability decreased after thermal cycling. The reduction on the concentration of voids led to a decrease in the permeability since there is less available free volume for the diffusing gas to permeate through the nanocomposite.

After thermal cycling was applied there was a slight increase of the radius of the free volume cavity and therefore the average size of the free volume holes varied as well. The relative fractional free volume decreased after the thermal cycling was applied to the samples. On Epon^{TM}826 nanocomposites the average decrease was about 45% when compared to values before thermal cycling while in samples from Epon^{TM}862 was of the order of 42% decrease.

The morphology of the samples was studied with XRD and found that the spectra were similar for all the samples, except for samples modified with 5wt% of B18 nanoclay. All the samples had a combined intercalated-exfoliated structure except on samples modified with 5wt% of B18 which showed a more exfoliated structure.

The experimental results were validated with several models available in the literature. Three of the models predicted lower permeability values as the concentration of the nanoclays increases while the model suggested by Cussler is more conservative. The experimental values in the case of both resins, Epon^{TM}826 and Epon^{TM}862 followed better Cussler's model.

All the models take into consideration only geometric factors that are related with the tortuosity and the reduction in permeability by increasing the path that the gas needs to go through to diffuse into the material. But the diffusion phenomenon in nanoclay modified nanocomposites is affected by the fact that inclusions produce molecular level modifications in the surrounding polymer that affect the overall permeability. This effect cannot be taken in account in the model prediction of the permeability. This is why experimental values don't completely agreed with the models.

The fact that models cannot predict the molecular level modifications that happen when nanoclays are added and that will affect the permeability is observed when the data after thermal cycling is plotted against the models.

When the samples were subjected to thermal cycling, modifications at the molecular level took place arranging the polymeric chains in a different fashion. This was confirmed by the T_g data and the free volume measurements. The values of permeability decreased after thermal cycling but the geometric factors never changed, therefore the changes were related to the rearrangement of the polymeric chains around the nanoclays.

Overall, it was observed that samples subjected to the specified thermal cycling had improved permeability and higher glass transition. The nanoclay addition decreased the chain mobility of the polymer increasing the glass transition values. The increase in the glass transition

temperature is related with a lower development of microcracks and also with a decrease of the free volume, which in turn, decreased the permeability to helium.

By comparing the experimental values with the permeability models, it was observed that the data was better approximated by the modified Fricke's equation. It was concluded that the diffusion properties of the epoxy-clay nanocomposites studied were more sensitive to the molecular changes induced in the polymer than to the tortuosity factor.

The effect of the molecular changes induced in the matrix when the nanoclays are added and their influence in the permeability needs further consideration. Molecular modeling studies are being conducted with the help of Materials Studio software from Accelrys© to simulate these changes.

Previous research was published in the following journals and conferences:

1. S. Martínez Vilariño, S. Miller, J. Zhou, S. Naya, R.Artiaga, D. Hui. Thermal characterization of layered silicate nanocomposites subjected to thermal cycling. Composites Science and Technology (submitted for publication)
2. S. Naya, S. Martinez-Vilariño, R.Artiaga, D. Hui, J. Zhou. Factorial design applied to nanoclay-epoxy permeability. Materials Science Forum (submitted for publication)
3. S. Martínez Vilariño, S. Naya, R. Artiaga, R. Cao, A. García, J. Zhou, D. Hui. Study of thermal degradation of epoxy-clay nanocomposites through a logistic mixture model. Polymer degradation and stability (prepared for submission)
4. J. Zhou, J. Moore, V. Calvin, R.Wilkins, S. Martinez Vilarino, B. Gersey, Y. Zhong, S. Thibeault. Effects of extreme radiation environment on composite materials. In Materials in Extreme Environments, edited by Daryush ILA, Christian Mailhiot, Premkumar B. Saganti (Mater. Res. Soc. Symp. Proc. 929, Warrendale, PA, 2006), paper#: 0929-II06-06
5. J. Zhou, T. Song, S.M. Vilariño, R. Wilkins. Characterizations of carbon nanotubes upon radiation exposures. SAMPE 38th International Technical Conference, November 6-9, Dallas, TX
6. S.M. Vilariño, J. Zhou, S. Naya, R. Artiaga, D. Hui. Statistical Tools Applied on the Design of Nanocomposite Permeability Experiments. SAMPE 38th International Technical Conference, November 6-9, Dallas, TX

7. E. Hawkins, M. Benard, T. Ford, R. Wilkins, S. Martinez Vilarino, J. Zhou. Development of in-Situ Composites for Lunar/Martian Missions. Proceedings of the 14th International Conference on Composites/Nano Engineering, Boulder, Colorado, July 3-7, 2006
8. S. Martinez Vilarino, S. Naya, R. Artiaga, J. Zhou, D. Hui. Statistical tools applied on the design of experiments of nanoclay-epoxy composites. Proceedings of the 14th International Conference on Composites/Nano Engineering, Boulder, Colorado, July 3-7, 2006
9. T. Song, S. Martinez Vilarino, J. Zhou, R. Wilkins. TGA and Raman analyses of irradiated carbon nanotubes. Proceedings of the 14th International Conference on Composites/Nano Engineering, Boulder, Colorado, July 3-7, 2006
10. S. Naya, R. Artiaga, R. Cao, A. García, S. Martínez Vilarino. Some applications of parametric and nonparametric curve estimation to thermal degradation of materials. Proceedings of the 14th International Conference on Composites/Nano Engineering, Boulder, Colorado, July 3-7, 2006
11. S. Martínez Vilariño, D. Hui, L. Daniel. Permeability measurements in epoxy-nanoclay modified composites. SAMPE 37th International Technical Conference, Seattle, October 31-November 3, 2005
12. S.Martínez Vilariño, D. Hui, L. Daniel, S. Campbell. Study of permeability in candidate materials for cryogenic tanks. International Astronautical Congress proceedings, Fukuoka, Japan, October 17-21, 2005
13. S. Martínez Vilariño, D. Hui, S. G. Miller, L. Daniel. Helium permeability in nanoclay modified polymers. Proceedings of the 12th International Conference on Composites/Nano Engineering, Tenerife, Spain, August 1-7, 2005
14. S. Campbell, M. Meador, J. C. Johnston, D. Hui, S. Martinez. Evaluation of epoxy/clay nanocomposites for use in cryogenic storage tanks. Poster on the 12th International Conference on Composites/Nano Engineering, Tenerife, Spain, August 1-7, 2005
15. S. Martínez Vilariño, D. Hui, L. Daniel. Overview of corrosion issues in ships. Proceedings of the 12th International Conference on Composites/Nano Engineering, Tenerife, Spain, August 1-7, 2005
16. M. Bubacz, S. Martinez-Vilarino, D. Hui, L. Daniel. Problem of corrosion in spacecraft. Proceedings of the 12th International Conference on Composites/Nano Engineering, Tenerife, Spain, August 1-7, 2005

17. S. Naya, R. Artiaga, I. López de Ullibarri, A. García, S. Martínez Vilariño. Statistical tools used in experiments designed for epoxy resin fatigue. Proceedings of the 12th International Conference on Composites/Nano Engineering, Tenerife, Spain, August 1-7, 2005
18. S. M. Vilarino, M. Chipara, D. Hui, D. L. Pelecky, R. Skomski, A. Lau, J. Zhou, M. Bubacz, R. Artiaga, D. J. Sellmyer. Magnetic investigations on barium ferrite nanoparticles dispersed in block copolymers. Poster on TNT2003 Salamanca, Spain, September 15-19, 2003
19. S. Martinez, M. Chipara, D.Hui. Liquid Crystal Polymers. Proceedings of the 10th International Conference on Composites/Nano Engineering, New Orleans, LA, July 20-26, 2003
20. S. Martinez, D. Hui, R. Artiaga, A. Varela, A. Garcia, L. Garcia. Effect of the curing conditions on a carbon/epoxy composite. Proceedings of the 9th International Conference on Composites/Nano Engineering, San Diego, CA, July 1-6, 2002

VITA

Sofía Martínez Vilariño was born in Marin, a small city in the south of Galicia, Spain on March 16, 1974. Third of the fourth daughters of Ramón and Purificación, she finished high school with honors at "Instituto Saturnino Montojo" in 1992 and then graduated with a M.S. degree in Industrial Engineering, concentration on Materials Science in the Escuela Politécnica Superior de Ferrol, Universidad de la Coruña, obtaining a special distinction for her master thesis. After meeting her current supervisor in a conference in Spain, she joined the Ph.D. program in Engineering and Applied Science at the University of New Orleans in May of 2002. She worked as a Graduate Research Assistant at the Mechanical Engineering Department at this university until fall 2005 and then moved to Houston, TX and joined Prairie View A&M University as a Graduate Research Assistant in the Mechanical Engineering Department. Currently she continues her collaboration with PVAMU in addition to her work as a Research Engineer for Clarkson Aerospace in Houston.